N° d'ordre : 4594

THÈSE

PRÉSENTÉE A

L'UNIVERSITÉ BORDEAUX 1

ÉCOLE DOCTORALE DES SCIENCES SCIMIQUES

Par Yifeng LEI

Pour obtenir le grade de

DOCTEUR

SPÉCIALITÉ: POLYMÈRES

BioChemical and Microscale Modification of Polymer for Endothelial Cell Angiogenesis

Directeur de thèse : Mme Marie-Christine DURRIEU

Soutenue le : **10 octobre 2012**

Devant la commission d'examen formée de :

M. Alain M. JONAS	Professeur d'Université catholique de Louvain, Belgique	Rapporteur
M. Matthieu PIEL	Chargé de Recherche CNRS, Paris	Rapporteur
M. Thibaud CORADIN	Directeur de Recherche CNRS, Paris	Examinateur
M. Thierry COLIN	Professeur d'Université Bordeaux 1, Bordeaux	Examinateur
M. Cédric AYELA	Chargé de Recherche CNRS, Bordeaux	Examinateur
Mme Marie-Christine DURRIEU	Chargée de Recherche INSERM, Bordeaux	Directeur

This thesis work was carried out in:

Unité de recherché mixte:
Université de Bordeaux I-CNRS, CBMN UMR5248,
Institut Européen de Chimie et Biologie,
2 Rue Robert Escarpit,
33607 Pessac Cedex, France

and

Unité de recherché mixte:
Université de Bordeaux II-INSERM, U1026,
Bioingénierie Tissulaire,
146 Rue Léo-Saignat,
33076 Bordeaux Cedex, France

Under the supervising of:

Marie-Christine Durrieu (CR1 INSERM / HDR)

Acknowledgements

This three-year thesis work was carried out in the Lab of INSERM U1026 in University of Bordeaux II for the first two years, and then continued in the Lab of CBMN UMR 5248 in “Institut Européen de Chimie et Biologie” (IECB) for the third year.

First and foremost, I would like to express my sincerest appreciation to my thesis advisor, Dr. Marie-Christine Durrieu. Thank her to accept me as a foreign student so that I have this opportunity to do my Ph.d in France. Thank for her supports on administrative work and human relationship which were difficult for a foreign student like me. I greatly thank her for her patience, tolerance and encouragements that carried me on through the tough times. She always encouraged me no matter how the experiment result was. And she left me great freedom in my work so that I could have opportunities to develop new techniques and learn new things.

I own my great gratitude to my co-advisor, Dr. Omar F. Zouani. Thank for his endless help and kindness to me, no matter from the cell culture, the biological evaluation to the discussion and writing of the papers. Without his help, I can’t imagine how I can finish my thesis work. His comments and advices not only helped me to improve my research skills but also led me to go deeper insights into further research.

In INSERM U1026, I thank Mme Joëlle Amédée, the director of the labs, for accepting me to work there. I would like also to pronounce my sincere appreciation to Dr. Murielle Rémy, she kindly prepared the endothelial cells for my experiments, and she taught me the culture of endothelial cells. Lila Rami, she is so friendly and helped me a lot on confocal microscopy. I would like to thank Céline Chollet, Jérôme Kalisky, Christel Chanseau for their technical assistances. I would also thank Patrick Guitton for explaining French to me when we lunched together in “Restaurant Universitaire”.

It is my great pleasure to joint and work in ODA group in IECB for the third year. IECB is an international institute and I feel more freely to work here. I would like to express my sincere gratitude to Dr. Reiko Oda, she accepts me to work in her group, and I thank for her coordination with different groups so that I can continue my work after our move into IECB. I thank Annie Zhe Cheng for English assistance of every manuscript. Loïc Pichavant, thank for his explanation of chemistry. Rajat Das, thank for his optimist attitude and the constructive discussion about the future career. And I am thankful to all other group members for their great helps and friendship throughout my work.

Thank Jochen Lang’s lab for their sharing of cell culture room and material, thank Elizabelle Génot’s lab for allowing me to do acquisition on their confocal microscopy.

I thank Professor Thierry Colin and Dr. Julie Joie (Institut de Mathématiques de Bordeaux, IMB) for their cooperation on mathematical modeling. And thank Dr. Cédric Ayela (Laboratoire de l'Integration du Materiau au Systeme, IMS) for sharing of equipment and his assistance in photolithography.

Thank Sébastien Marais (Bordeaux Imaging Center, BIC) for his assistance in image analysis, and thank Christine Labrugère (Institut de Chimie de la matière condensée de Bordeaux, ICMCB) for her help in analysis of XPS and AFM.

Last but not least, I would like to thank my family in China for their remote but spiritual support. My special thanks go to my boyfriend Wubin Dai, he is always there to accompany me and encourage me to overcome each trouble during my thesis, without his love and support, this thesis in France would have been more difficult.

Summary

The creation of a functional vascular network is a major concern to ensure the perfect vitality of tissue engineered products. Understanding the mechanisms of angiogenesis is essential for the vascularization in tissue engineering. In this work, we aimed to characterize the microenvironment responsible for angiogenesis of endothelial cells (ECs). To achieve this request, we developed bioactive biomaterials (polymers functionalized mainly with peptides, and controlled their distribution at micrometer scale) to mimic a physiological microenvironment of ECs.

First, we developed the biochemical functionalization of polymer materials (polyethylene terephthalate, PET) using endothelial cell specific peptides. The peptide immobilization ensured the bioactivity onto material surfaces, and enhanced endothelial cell functions such as cell adhesion, spreading and migration.

Second, we introduced photolithographical technique to control geometrical distribution of peptides on material surfaces, and studied the effects of peptide micropatterning onto EC angiogenesis. ECs were adhered and aligned onto peptides micropatterns whatever the size of peptide micropatterns (from 10, 50 to 100 µm). However, EC behaviors (cell spreading, orientation and migration) were significantly more regulated on smaller peptide micropatterns (10 and 50 µm) than on larger peptide stripes (100 µm). EC morphogenesis into tube formation can also switch onto the smaller micropatterns (10 and 50 µm) with either RGD or SVVYGLR peptides. The central lumen of tubular structures can be formed by single-to-four cells due to geometrical constraints applied on the micropatterns. Sprouting angiogenesis of ECs and vascular network formation can be induced on surfaces micropatterned with angiogenic SVVYGLR peptides. Our overall results revealed that the induction of angiogenesis is multi-parametric. This is dependent on biochemical constituents and their micro-distribution.

Third, we employed mathematical modeling to understand the impact of bioactive micropatterns on endothelial cell migration. A continuous Patlak-Keller-Segel type model was used, and the numerical results were in well accordance with our experimental results.

Furthermore, we also developed the study of stabilization of tubular structures of ECs in this thesis. The results showed that the co-cultures of endothelial cells with pericytes, as

well as the recruitment of basement membrane components (Matrigel) can stabilize the vascular tubular structures.

In general conclusion, our work in this thesis proved that bioactive micropatterning of polymer is effective to stimulate angiogenesis and to construct functional vascularization. This work helps us to understand the fundamental biology of angiogenesis, and has great potential for application in tissue engineering.

Keywords: functionalization; peptides; micropatterning; endothelial cells; angiogenesis; tissue engineering

Résumé

La création d'un réseau vasculaire fonctionnel est une préoccupation importante afin d'assurer la parfaite vitalité des produits d'ingénierie tissulaire (IT). La compréhension des mécanismes de l'angiogenèse est essentielle pour la synthèse de produits d'ingénierie tissulaire vascularisés. Dans ce travail, nous avons visé à caractériser le microenvironnement responsable de l'angiogenèse des cellules endothéliales (CEs). Pour cela, nous avons élaboré des biomatériaux bioactifs (polymères fonctionnalisés par des peptides, et contrôlé leur distribution à l'échelle micrométrique) afin de mimer une situation physiologique des CEs.

Dans un premier temps, nous avons mis au point une stratégie de fonctionnalisation biochimique d'un matériau polymère (le polyéthylène téréphtalate, PET) en utilisant des peptides spécifiques des CEs. L'immobilisation de ces peptides a permi d'assurer une bioactivité de ces surfaces, et l'amélioration des fonctions des CEs comme l'adhésion, l'étalement et la migration cellulaire.

Ensuite, notre travail s'est inscrit dans l'évaluation de l'impact d'une distribution contrôlée de peptides en surface de matériaux (acquise par photolithographie) sur le comportement des CEs et sur l'angiogenèse. Nos résultats ont montré que les CEs adhèrent et sont alignés sur les « micropatterns » peptidiques quelle que soit la taille de ces « micropatterns » (lignes de largeurs comprises entre 10 et 100 µm). Nous avons mis en évidence que la taille des « micropatterns » bioactifs a un réel impact sur le comportement des CEs (l'étalement, l'orientation et la migration cellulaire). La morphogenèse des CEs (la formation d'un « tube-like ») a été mise en évidence sur des matériaux microstructurés par des lignes peptidiques de 10 et 50 µm de largeur, quels que soient les peptides RGD ou SVVYGLR immobilisés en surface. Nous avons montré que la lumière de structures tubulaires peut être constituée d'une à quatre cellules selon la contrainte géométrique appliquée sur les « micropatterns ». Nos travaux ont montré que le « sprouting » ainsi que la formation du réseau vasculaire peuvent être induits seulement sur des surfaces « micropatternés » par des peptides SVVYGLR. Nos résultats démontrent que l'induction de l'angiogenèse est multiparamétrique. Celle-ci est dépendante de constituants biochimiques ainsi que de leur micro-distribution.

Troisièmement, nous avons utilisé la modélisation mathématique pour comprendre l'impact de « micropatterns » bioactifs sur la migration des CEs. Un modèle de type continu

Patlak-Keller-Segel a été utilisé, et les résultats numériques sont bien conformes avec nos résultats expérimentaux.

Pour finir, nos travaux se sont focalisés sur l'étude de la stabilisation de ces structures tubulaires. Les résultats ont montré que les co-cultures de CEs avec les péricytes, ainsi que le recrutement de composant de membrane basale (Matrigel) peuvent stabiliser ces structures vasculaires.

En conclusion générale, le travail réalisé dans cette thèse a prouvé que le « micropatterning » des principes bioactifs sur polymères est efficace pour stimuler l'angiogenèse et pour construire une vascularisation fonctionnelle. Enfin, ce travail a permis de comprendre la biologie de l'angiogenèse et pourra aider indéniablement tous les travaux en cours s'inscrivant dans l'ingénierie tissulaire.

Mots clés : fonctionnalisation; peptides; micropatterning; cellules endothéliales; angiogenèse; ingénierie tissulaire.

Table of contents

General Introduction 1

Literature Review 7

1. Tissue engineering & current challenges 9

2. Endothelium and blood vessel structures 12

2.1. Blood vessel structure 12

2.2. Function of endothelium 13

2.3. Vasculogenesis and angiogenesis 14

3. State of art of vascularization in tissue engineering 18

3.1. Scaffold design 18

3.2. Angiogenic factor therapy 21

3.3. Cell-based therapy 23

3.4. *In vitro* prevascularization 28

3.5. *In vivo* prevascularization 30

4. Biochemical modification of biomaterials for vascularization 31

4.1. Material modifications with proteins 31

4.2. Material modifications with peptides 33

4.3. How to immobilize biomolecules onto materials 35

5. Micropatterning of biomolecules to induce vascularization 37

5.1. Photolithography 37

5.2. Soft lithography 40

5.3. 3D microfabrication to generate vascularization 46

Problems and Objectives 51

Results and Discussions 55

1. Biochemical Modification for Endothelial Cell Functions 57

Introduction 59

Paper I. Surface functionalization of polyethylene terephthalate by peptides to study specific endothelial cell adhesion, spreading and migration 61

2. Microscale Modification for Induction of Endothelial Cell Angiogenesis 63
Introduction.....65
Paper II. Modulation of lumen formation by microgeometrical bioactive cues and migration mode of actin machinery.....67
Paper III. Geometrical microfeature cues for directing tubulogenesis of endothelial cells.....69
Paper IV. Modeling of the migration of endothelial cells on bioactive micropatterned polymers.....71
Discussion.....73
3. Stabilization of Tubulogenesis by Co-culture of Cells.....79
Paper V. Pericytes, stem cell-like cells, but not mesenchymal stem cells are recruited to support vasculogenic tube stabilization.....81
Conclusions and Perspectives.....83
Annexes.....89
Scientific Communications.....91
References.....93

General Introduction

The failure or loss of organ or tissue is one of the most serious health problems faced by developed nations. Tissue engineering addresses this issue by restoring, maintaining or enhancing their functions for clinical application. However, the lack of vascularization remains a key challenge for development of complex tissue/organs in the field of tissue engineering (Literature Review).

Angiogenesis, the formation of new blood vessels, is essential for the development of vascularized tissues. However, the process of angiogenesis is intricate and the details of conditions that govern angiogenesis are yet to be delineated. To simplify the complexity of numerous variables typical of endothelial cells' (ECs) native microenvironment, advanced synthetic systems in this thesis were development to facilitate the study of angiogenesis process.

In this study, we aim to address the aforementioned challenge by guiding and promoting angiogenesis based on two dimensional synthetic polymer materials: (i) we focus on the research on the interaction of endothelial cells with specific peptides on polymer surfaces; (ii) we aim to induce angiogenesis by surface micropatterning conjugated with peptide functionalization.

In the first stage, we functionalized the polymer (polyethylene terephthalate, PET) surfaces with different peptides in a homogenous way. The investigated peptides are cell adhesive RGD, endothelial cell specific REDV, YIGSR and angiogenic SVVYGLR peptides (Paper I). We studied the specific effects of each or combination of peptides onto endothelial cell functions, and examined what EC morphological and functional changes can be correlated to these specific bioactive motifs (Paper I). The surface functionalization by peptides was validated by physical-chemical characterization (X-ray photoelectron spectroscopy, atomic force microscopy, fluorescence microscopy, contact angle measurement). The biological evaluation revealed that these peptides can give bioactivity to polymer surfaces, and induced endothelial cell responses due to integrin interaction, and consequently resulted in different levels in cell adhesion, spreading and migration (Paper I).

Subsequent and the most important studies in this thesis were focused on the elaboration of polymer surface micropatterning conjugated with peptide functionnalization (Paper II, III and IV). It's related to the development of the polymer surface characteristic by micro-geometrical distribution of peptides. The different geometrical domains were synthesized by photolithographic technique, and characterized by optical microscopy, profilometer and fluorescence microscopy. The influence of peptide micropatterning onto endothelial cell behaviors as well as the induction of angiogenesis was addressed.

At the first step, we started by the micropatterning of RGD peptides, which are the most investigated adhesive sequences in biomaterial research (Paper II). In this study, firstly, we are interested in guiding tubulogenesis by the micropatterning of RGD peptides onto polymer surfaces. Photolithography was employed to fabricate peptide micropatterns onto PET surfaces (with peptide stripe widths varying from 10, 50 to 100 μm). Human umbilical vein endothelial cells (HUVECs) were seeded onto the surfaces for studying their effects onto EC orientation and morphogenesis. After cell culture, ECs were aligned on the RGD peptide stripes whatever the pattern geometry. The cell alignment and elongation were enhanced on smaller RGD micropatterns (10-50 μm) as compared with cells on unpatterned surfaces and on larger micropatters (100 μm). Confocal images revealed that small RGD micropatterns (10-50 μm) elicited a collective cell organization and induced EC lumen formation, whereas large RGD micropatterns (100 μm) promoted EC orientation without lumen formation. These results proved that EC tube-like formation can be regulated by the geometrical factor of bioactive principles. However, are there only geometrical cues that regulate the lumen formation of ECs? To make it clear, we addressed the correlation between EC actin machinery expression and EC self-assembly into lumen formation. Adhesion molecule (RGD peptides) and inductor molecule (BMP-2 mimetic peptides) were micropatterned onto PET surfaces to induce filopodial and lamellipodial migration mode of ECs, respectively. No matter the geometrical distribution of peptide micropatterns, lumen formation cannot be detected in the microenvironment promoting lamellipodial migration mode of ECs (BMP-2). We demonstrated that only filopodial migration mode (mimicked by RGD), but not lamellipodial migration mode (mimicked by BMP-2), promoted EC lumen formation. This work may give a new concept for the design of biomaterials for tissue engineering.

Systematic and more detailed works were carried out using angiogenic SVVYGLR peptide micropatterning (Paper III). Angiogenesis is usually triggered by soluble growth factors such as VEGF. In fact, geometrical cues also play an important role in this process. In this section of thesis, we report the induction of angiogenesis solely by angiogenic SVVYGLR peptide micropatterning on polymer surfaces. SVVYGLR peptide stripes were micropatterned onto polymer surfaces by photolithography. Our results showed that the EC behaviors (cell spreading, orientation and migration) were more significantly guided and regulated on narrower SVVYGLR micropatterns (10 and 50 μm) than on larger stripes (100 μm). Furthermore, EC morphogenesis into tube formation was switched onto the smaller patterns. We illustrated that the central lumen of tubular structures can be formed by only single-to-four cells due to geometrical constraints applied on the micropatterns which

mediated cell-substrate adhesion and cell-cell adhesion. In addition, sprouting of ECs and vascular networks were also induced by surfaces micropatterning with SVVYGLR peptides. These micropatterned surfaces provide opportunities for mimicking angiogenesis by peptide modification instead of exogenous growth factors. The organization of ECs into tubular structures and induction of sprouting angiogenesis are very important for the fabrication of vascularized tissues.

Simultaneously, mathematic modeling was developed to investigate the endothelial cell migration on micropatterned surfaces (cooperative work with "Institut de Mathématiques de Bordeaux") (Paper IV). A continuous Patlak-Keller-Segel type model was adopted to describe endothelial cell migration on bioactive micropatterned polymer. The mathematical studies reveal that the numerical results were in good agreement with our experimental results.

The understanding of mechanism of EC angiogenesis on peptide micropatterned surfaces was carried out in the "Discussion" section. It concluded that the induction of angiogenesis is multi-parametric: geometrical cues of peptides, effects of different peptide motifs as well as peptide densities were all considered important to the process of angiogenesis (Discussion).

After obtaining of ECs' tubular structures on peptide micropatterned surfaces, we then carried out the research of stabilization of blood vessels (Paper V). Co-culture of endothelial cells with pericytes/mesenchymal stem cells (MSCs) as well as the recruitment of basement membrane components (type IV collagen and Matrigel) was developed for this purpose. The newly formed tubular structures on micropatterned surfaces were not stable, and ECs proliferated rapidly to form a homogeneous monolayer of cells. Interestingly, the integration of pericytes as well as the recruitment of Matrigel in co-culture system can stabilize the primitive tubular structures (Paper V).

Our works in the thesis highlights that bioactive micropatterning of polymer is effective to stimulate angiogenesis and construct functional vascularization. This work helps us to understand the fundamental biology of angiogenesis, and has great potentials for application in tissue engineering.

Literature Review

1. Tissue engineering & current challenges

The failure or loss of organ or tissue is one of the most serious health problems faced by the healthcare industry in developed nations. Each year, only in the United States, millions of people suffer from end-stage organ failure and tissue loss, resulting in more than $ 400 billion in healthcare costs [1]. The number of people in the waiting list for organ transplantation overpasses the number of organ donation [2], only 10% of these patients benefit from organ transplantation, whereas the majority of patients perish due to the severe shortage of available organ donors [2], and this situation was predicted to get even more serious as the population ages.

Tissue engineering provides a promising alternative to organ and tissue transplantation [1]. Tissue engineering applies the principles of engineering and the life science to replace, restore, maintain, enhance the functions of tissues or organs [1, 3]. It has been attracted attentions and had been developed since the beginning of 1990s.

Tissue engineering is an interdisciplinary research field, which advantages both engineering approaches and biological understanding. Tissue engineering uses the combination of cells, engineering, materials, suitable biochemical and physical-chemical factors to improve or replace tissue/organ functions [1, 4]. Commonly-adopted tissue engineering approaches incorporate (i) isolated cells or cell substitutes, (ii) biocompatible materials for cellular support and regeneration, or (iii) cell-biomaterial / scaffold composites [5]. Isolated cells are cultured on biocompatible scaffolds, which could provide chemical and physical supports and guide the cell growth and organization into three dimensional (3D) tissues *in vivo*, as one can see in Figure 1.

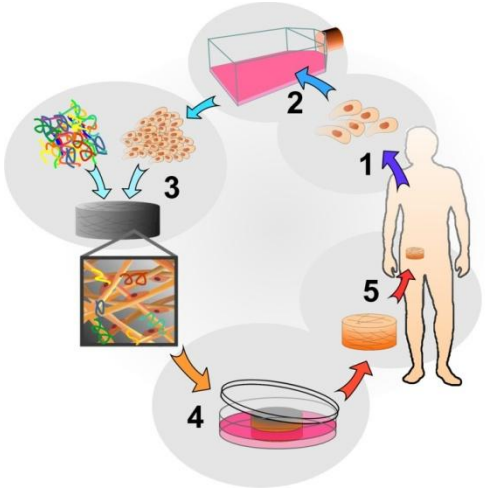

Figure 1. Basic principles of tissue engineering [6].

Ever since the Food and Drug Administration (FDA) first approval of tissue engineered skin in 1998 [7], there have been tremendous efforts using tissue engineering to replace and restore various parts of the body [8]. Despite of the enormous advances in tissue engineering, several challenges still prevent the widespread clinical application of tissue engineered products. These challenges include a number of business, regulatory and ethical issues as well as scientific barriers. These scientific issues include (i) how to acquire adequate source of cells, (ii) how to engineer complex vascularized tissues that mimic the complexity of native tissue architecture, and (iii) how to generate tissue *in vivo* with the biomechanical and metabolic functions that mimic normal tissues. Among all these scientific issues, one critical challenge of engineering tissues is the lack of a proper and functional vascularization [2, 9, 10].

In fact, most tissues in human bodies rely on blood vessels to supply the individual cells with nutrients and oxygen. Capillaries and vascular systems are required to supply nutrients and oxygen and to remove metabolic waste products and CO_2 (as one can see in Figure 2) [11]. *In vivo*, most cells don't survive more than a few hundred micrometers away from the nearest capillary because of the diffusion limitation (Figure 2) [11]. Without an intrinsic capillary network, the maximal thickness of engineered tissue is limited to approximately 100-200 μm, whereas cells and tissues located more than a few hundred microns away from nearest capillaries suffer from hypoxia and apoptosis (Figure 2) [11].

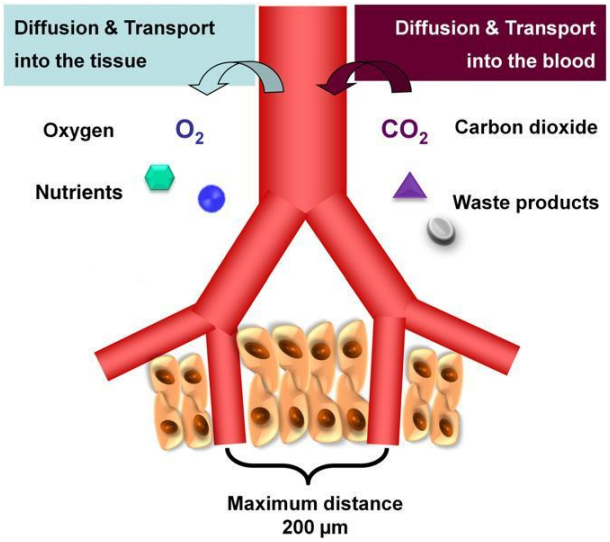

Figure 2. Schematic description of diffusion and transport process in vascularized tissues *in vivo*. The surrounding tissue is supplied with oxygen and nutrients via the vasculature. Waste products and CO_2 are moved away from the tissue into the blood vessels [11].

To date, the most successful tissue engineering application in clinic has been limited to thin tissues (such as skin and cartilage) or avascular tissues (such as bladder) [2, 8, 12]. For these thin tissues, oxygen and nutrients can diffuse into the implants and sustain cellular viability [2]. However, for the development of more complex and functional tissues/organs, such as liver, kidney, heart or bone, vascularization remains a great challenge.

As mentioned above, the major challenge in tissue engineering has been identified as functional vascularization of tissue engineered products [2, 9, 10]. To success in the application of large and complex tissue engineered constructs, the understanding and development of an artificial microvasculature are critical to move engineered products into clinical application.

2. Endothelium and blood vessel structures

2.1. Blood vessel structure

The formation of blood vessels is essential for establishment and maintenance of engineered tissues. All blood vessels *in vivo* begin from an inner coating of endothelial cells (ECs), as one can see in Figure 3. These endothelial-lined tubes arisen during vasculogenesis and angiogenesis can subsequently differentiate into capillaries (after association with pericytes) or into larger diameter vessels such as arteries and veins (after association with smooth muscle cells (SMC)) (Figure 3). Blood circulation occurs from arterial to venous system with capillary beds interconnecting the two systems (Figure 3).

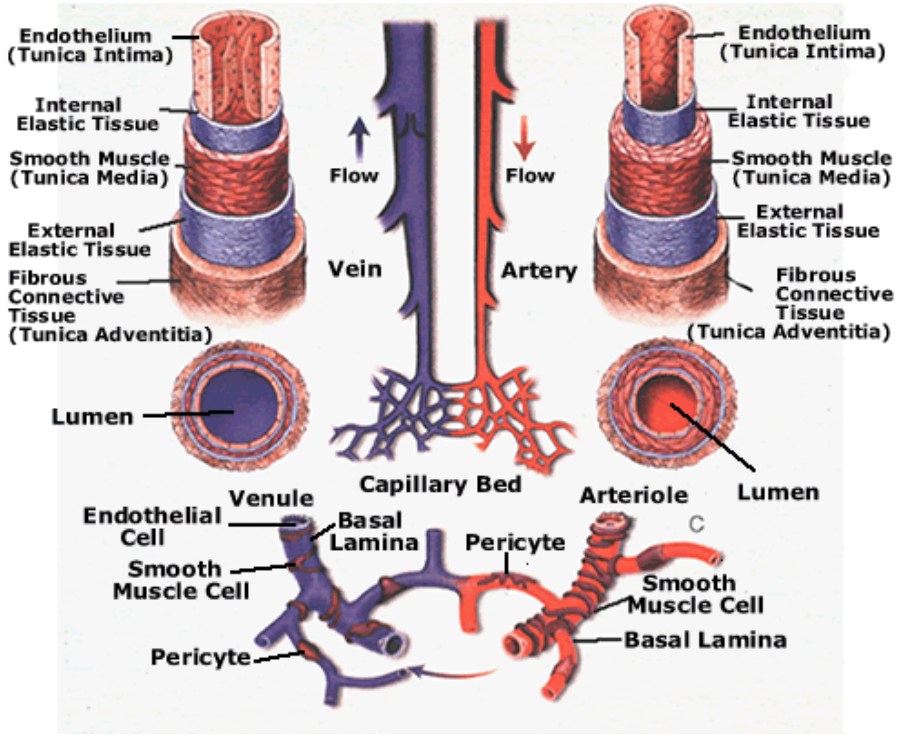

Figure 3. Schmatic of arteries, veins and capillaries and blood circulation [13].

Arterial system is responsible for transporting oxygenated blood from heart to every part of the body (see above Figure 3). Arteries are composed of three distinct layers: intima, media and adventitia (as shown in Figure 4A). Intima, the innermost layer of an artery (or vein), is made up of one layer of ECs connected to basement membrane. The media is mainly composed of vascular SMCs and the extracellular matrix (ECM) proteins secreted by the

SMCs, such as collagen, elastin, and proteoglycans. Collagen (type I and III) and elastin are the major ECM in the media layer and provide the mechanical properties of the blood vessel walls [14]. Collagen in its cross-linked formation contributes high tensile strength to maintain structural integrity of the vessel wall, and elastin provides elastic properties [15]. The adventitia, the outermost layer of arteries, contains fibroblasts and collagen fibers, the later one serves to anchor the blood vessel to nearby organs [15].

The veins have similar structure with arteries, venous system returns deoxygenated blood from tissues back towards to the heart (Figure 3).

Capillaries are the smallest diameter vessels, which consist of a layer of ECs, basement membrane and pericytes (Figure 4B). Exchange of gas and nutrients between the blood and the tissues occurs in the capillary beds.

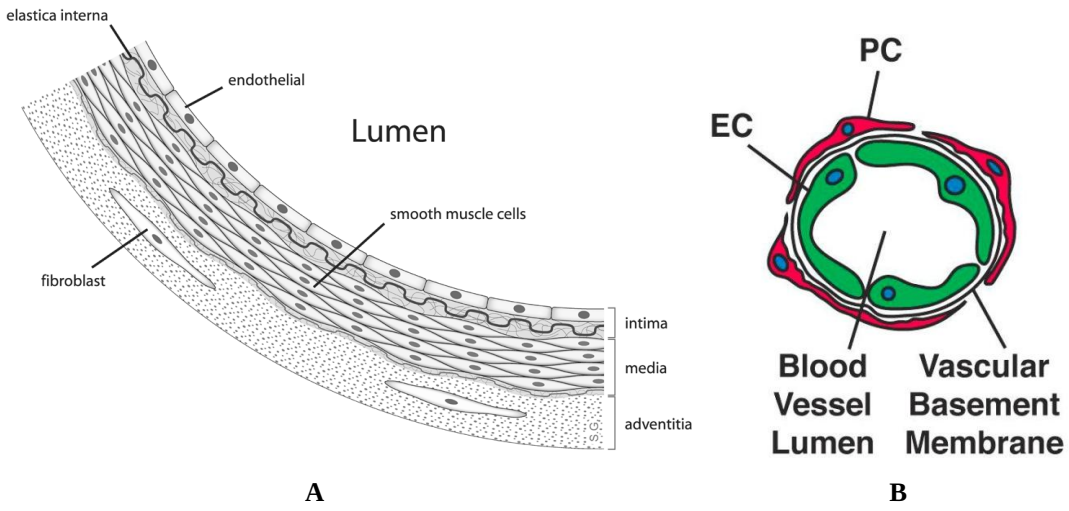

Figure 4. (A) Aanatomy of artery [16]. (B) Capillary structure. Capillary are composed of endothelial cells (ECs) that form the inner lining of wall with a surrounding basal membrane and pericytes (PCs) [17].

2.2. Function of endothelium

All blood vessels *in vivo* have an inner lined layer of endothelial cells in the interior surfaces. This layer of endothelial cells is defined as endothelium.

Morphologically, endothelial cells are very flat cells, have a central nucleus and show cobblestone morphology in culture [18]. ECs are about 25-50 μm in length, 10-15 μm in width and 1-2 μm thick according to different origin sources [18]. ECs present the specific

markers expressed on their surfaces or localized inside their cytoplasm, a long but non-exhaustive list of endothelial cell specific markers were used to identify ECs in cell culture: such as CD31, VE-cadherin (or CD144), VEGF-R2, E-selectin, vWF, etc… [19].

The layer of endothelial cells, i.e. endothelium, is key determinant of health in blood vessels, and thus involved in many aspects of vascular biology [20], as shown in Figure 5. Endothelium provides thrombo-resistant barrier between circulating blood and the vascular walls. A complete endothelium is necessary for an optimal blood flow without thrombogenicity [20]. Fibrin clots formed during thrombosis are degradable by tissue-type plasminogen activator (t-PA) secreted by ECs [20, 21]. Platelet adhesion and aggregation are actively inhibited by release of nitric oxide and prostacyclin by ECs [20]. Endothelium also represents a selective permeable barrier which must be penetrated in order to exchange molecules and gas between the vessel lumen and the surrounding tissue [11]. Endothelium controls both blood flow and blood pressure [22]. Intact endothelium also suppresses SMC migration and proliferation to maintain vascular homeostasis [20].

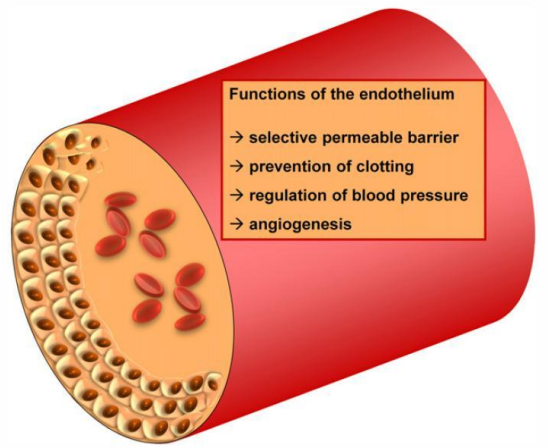

Figure 5. The endothelium inside the vessels accomplishes numerous functions: selective permeable barrier, prevention of clotting, regulation of blood pressure and angiogenesis ([11])

2.3. Vasculogenesis and angiogenesis

The process of neovascularization (i.e. blood vessel formation) can be categorized into two general processes: vasculogenesis and angiogenesis [23, 24]. Vasculogenesis, refers to the *in situ* assembly of angioblasts, the precursor cells, into the formation of blood vessels

(Figure 6A); whereas angiogenesis refers to a morphogenic process involving the formation of new blood vessels by sprouting from pre-existing blood vessels (Figure 6B). Although the previously held belief was that vasculogenesis occurred exclusively during embryogenesis, it is now recognized that neovascularization is most likely a more complex process involving both angiogenesis and vasculogenesis simultaneously [24]. Adult blood vessel formation may be a combination of the two processes [24].

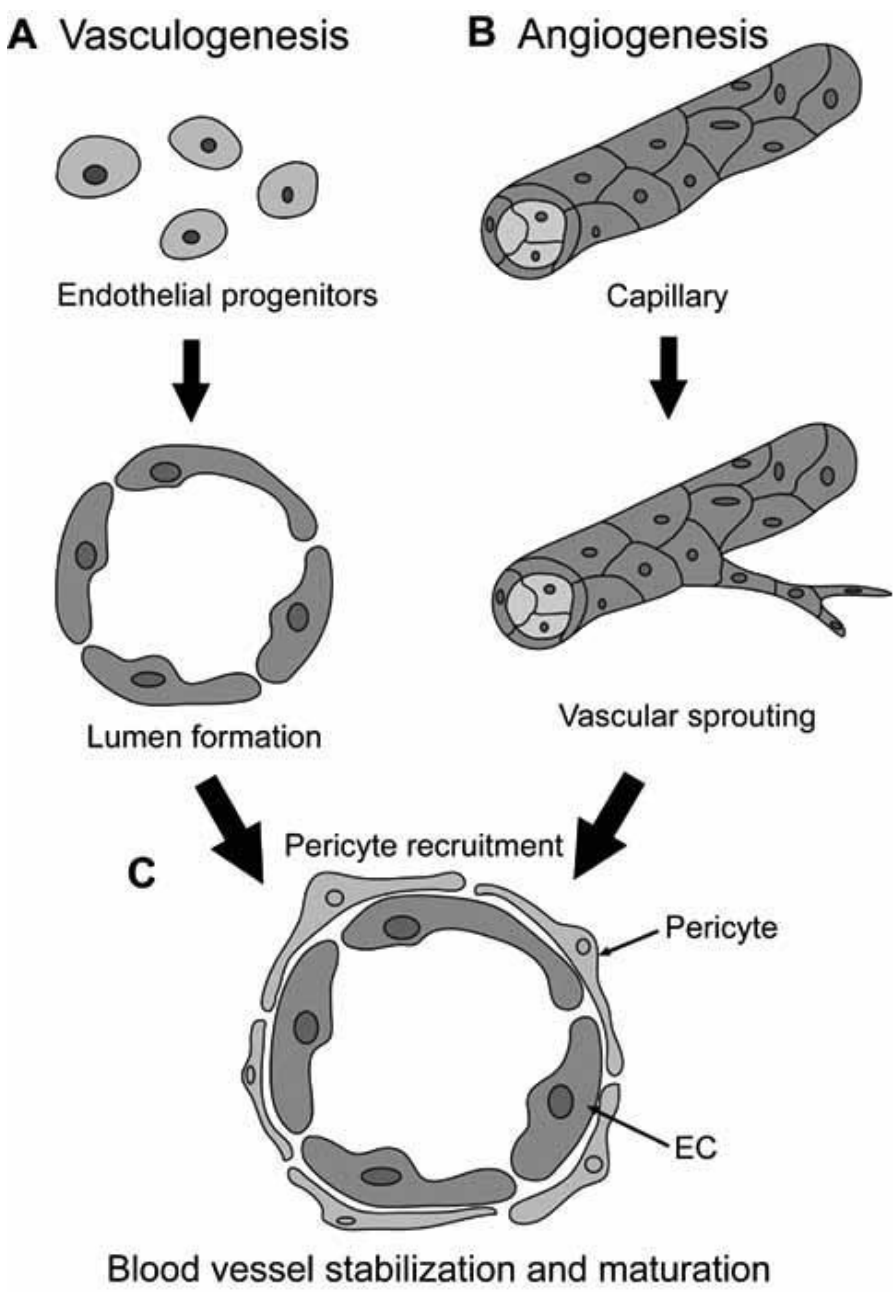

Figure 6. Endothelial tube formation are generated by (A) vasculogenesis and (B) angiogenesis, and at the end stabilized by recruitment of pericytes to form (C) capillary structures [25].

In principle, the vasculogenesis describes a *de novo* assembly of undifferentiated ECs to capillaries, and involves in different steps [23]:

a. The *in situ* differentiation of mesodermal cells into angioblasts or hemangioblasts.
b. Differentiation of precursor cells (angioblasts or hemangioblasts) into ECs.
c. ECs form the vessel primordial and aggregates that establish cell-cell contact but have no lumen.
d. A nascent endothelial tube is formed.
e. Primary vascular network is formed from an array of nascent endothelial tubes.
f. Pericytes are recruited to stabilize the network.

For angiogenesis, it refers to the sprouting of capillaries from pre-existing blood vessels, the process can be described into different steps [24, 26, 27] (also as shown in an example in Figure 7):

a. Vascular endothelial cells are stimulated by angiogenic stimulus (collagenase, plasminogen activators, angiogenic factors (VEGF, FGF, angiopoietin-1, etc…).
b. The basement membranes close to the angiogenic stimulus are locally degraded.
c. Vascular spouts grow form the pre-existing vessels. Endothelial tip cells [28] lead the cell migration via filopodia mode towards the angiogenic stimulus. Endothelial stalk cells [28] highly proliferate behind tip cells.
d. Formation of a capillary lumen in stalk cells (with intra-cellular or intercellular vacuoles).
e. Synthesis of new basement membrane.
f. Recruitment of pericytes to aid in tube stabilization and maintenance.

The event of angiogenesis requires complex interaction and crosstalk between vascular endothelial cells, adhesion proteins, junctional molecules and growth factors [29]. It's critical to develop better understanding of mechanisms associated with angiogenesis and apply that knowledge to guide vessel growth and to promote vascularization in engineered constructs.

In this study, endothelial cell tube formation together with sprouting angiogensis on synthetic polymer (polyethylene terephthalate, PET) were guided and regulated by culturing Human Umbilical Vein Endothelial Cells (HUVECs) on functionalized PET surfaces.

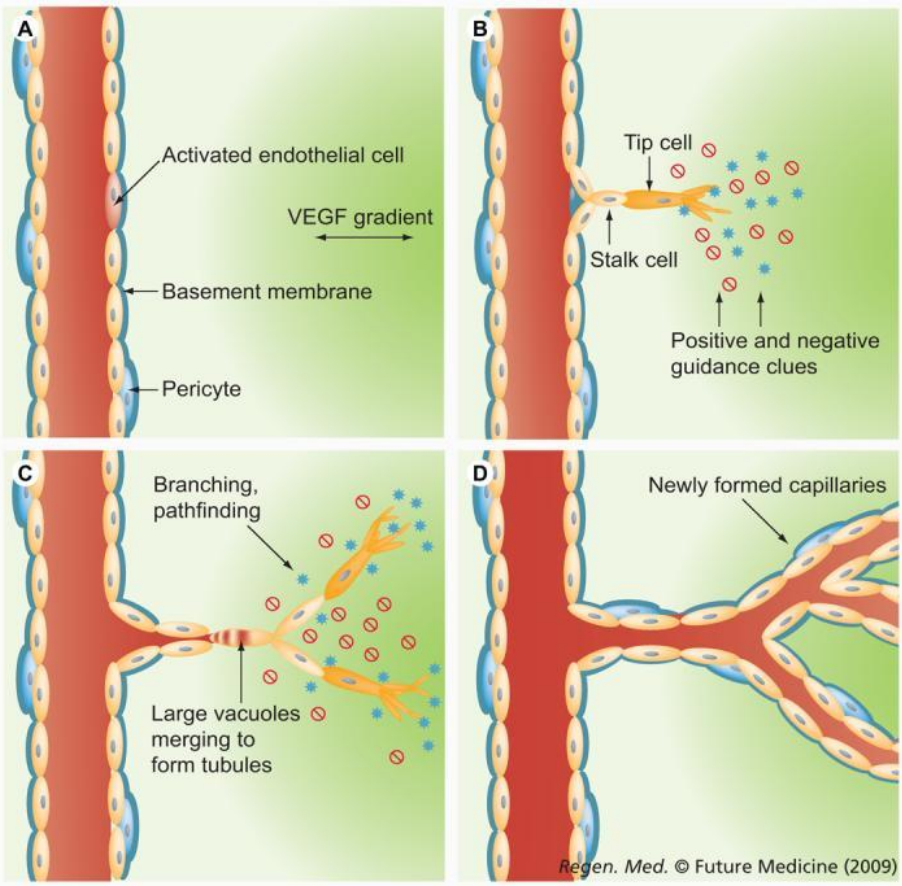

Figure 7. An example of sprouting angiogenesis induced by VEGF ([30]). (A) Endothelial cells are activated in response to a growth factor gradient. (B) Tip cell degrades basement membrane and migrates towards gradient; stalk cells are formed behind leading tip cell. (C) Vacuoles form in stalk cells and merge to make tubules. (D) Deposition of basement membrane and recruitment of pericytes stabilize newly formed endothelial tubules.

3. State of art of vascularization in tissue engineering

There are a large number of attempts to induce vascularization of engineered tissues. Numerous researchers have undertaken a variety of approaches to study vascularization, including material functionalization, scaffold design, bioreactor development, microelectronmechanical systems (MEMS)-related approaches, endothelial cell growth factor delivery , cell-based thechniques, *in vitro* vascularization, *in vivo* vascularization, etc… [11, 31, 32]. Of course, these strategies can't be separated clearly and there are overlaps in various approaches. In this section, the state-of-art of main strategies for vascularization was reviewed.

3.1. Scaffold design

Effective vascularization of tissue engineering is inherently linked to scaffold design. Beside storage and release function of compounds and the providing an appropriate surface for all involved cell types, the scaffold itself should contain certain architecture to promote vascularization. Important scaffold designs include surface topography, structure quality, biocompatibility and bioactivity, porosity, biodegradation property, etc... This section will give an insight into the scaffold porosity and degradation property onto vascularization.

Porosity

As confirmed, the pore size of the scaffold is a critical parameter for blood-vessel ingrowth . Druecke *et al.* showed that vessel ingrowth was significantly faster in scaffold with pores greater than 250 μm than those with smaller pores [33]. However, it is not only the pore size important for vascularization, but also the interconnectivity of the pores. Cao *et al.* described in both *in vitro* and *in vivo* studies that the pore size and pore interconnections superior than 300 μm are recommended for sufficient vascularization of the tissue-engineered grafts [34, 35], the cell migration and thus vascularization will be inhibited if pores are not interconnected [35].

Suitable fabrication techniques are eagerly required to achieve the scaffold porosity. Conventional scaffold fabrication techniques include solvent leaching, gas foaming, freeze drying, and phase separation in combination with salt leaching to produce form-like scaffold structure [36]. The shape and the pore sizes can be varied by changing the parameter of these techniques. However, the organization of the pore obtained by above techniques is random, the pore pathways are only partially connected (as shown in Figure 8A&C), which in turn could hamper the supply of nutrients and the ingrowth of vessels into the scaffolds.

Nowadays, there is an increasing interest of using new techniques to design interconnective scaffold for tissue engineering. Among them, advanced manufacturing technologies, known as rapid prototyping or solid freeform fabrication systems, are now being explored by investigators [35]. These techniques offer better control and the ability to produce complex scaffolds with well-defined architecture and optimized pore interconnectivity [35]. An example of solid freeform fabrication technology is shown in Figure 8B&D [35]. This method uses computer-aided design (CAD) data sets, and deposit molten polymer, hydrogels or biomaterials on a stage to form a layer of the scaffold [35]. Subsequently, layer-by-layer deposition of scaffold are used to achieve an entire freeform three-dimensional scaffold [37].

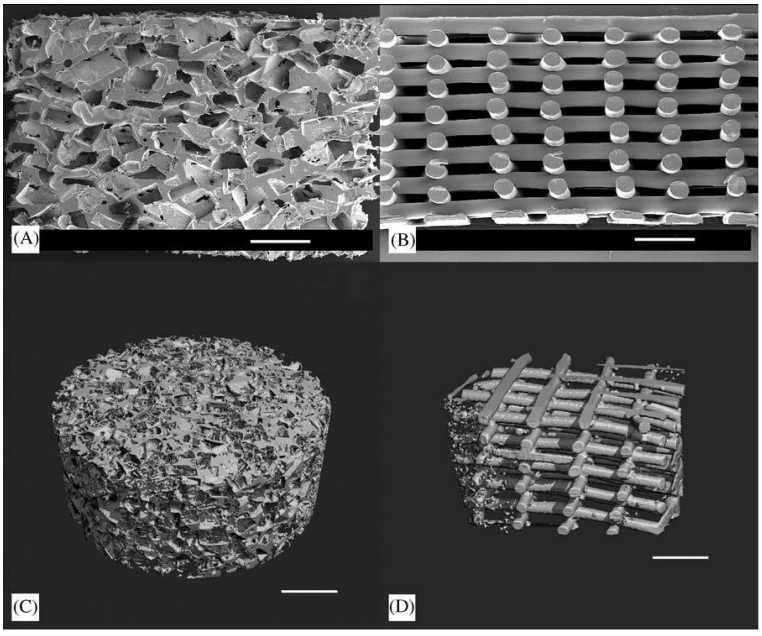

Figure 8. Scaffold design. (A) A scaffold was prepared by conventional scaffold fabrication technique via salt leaching. (B) 3D fiber scaffold deposited by solid freeform fabrication technology. (C) and (D) are 3D reconstruction of (A) and (B), respectively (modification after [38]).

Biodegradability

Aside from the scaffold porosity which favors tissue and vessel in growth, another important aspect in scaffold design is the material biodegradability. The degradation process of a material can be correlated to the colonization progresses of endothelial cells into the matrix [39]. West and Hubbell' groups used protease-sensitive biomaterials with degradation sites for proteases [40, 41]. By introducing matrix metalloproteinase (MMP) sensitive peptide sequences into the backbone of PEG, the biodegradation rate and, therefore, the ability to increase angiogenesis performances, could be examined *in vitro* as well as *in vivo* [42]. Gafni *et al.* designed a system in which a highly degradable biomaterial was adopted to create a filamentous scaffold. This scaffold was then seeded with endothelial cells *in vitro*, resulting in a monolayer of endothelial cells on the filaments. After implantation *in vivo*, the filaments were degraded, but the tubular structures of endothelial cells remained. After two weeks of implantation, these tubular structures had become perfused [43].

3.2. Angiogenic factor therapy

Angiogenic factors are powerful to stimulate different stages of vascularization. It's a common approach to delivery angiogenic factors for promoting the vascularization of a tissue-engineered graft.

Factors charged for regulating angiogenic processes of endothelial cells include the vascular endothelial growth factor (VEGF, or VEGF-A), the basic fibroblast growth factor (bFGF), platelet-derived growth factor (PDGF), transforming growth factor-β (TGF-β) and angiopoietins, etc... (Review in Table 1). To date, the most extensively tested factors are VEGF and b-FGF [44-46].

Table 1. Summary of current used vascular growth/signal factors

Growth/signaling factors	Functions	Reference
Vascular endothelial growth factor-A	The most potent pro-angiogenic cytokines; initiator of endothelial capillary formation	[47-52]
Fibroblast growth factor	Heparin-binding protein mitogens; stimulates EC proliferation and migration; induces sprouting of blood vessels; supports role in angiogenesis	[45, 53, 54]
Platelet-derived growth factor	Mitogen for connective tissue cells, released from platelet; recruits SMCs to endothelial cells, promotes vessel maturation	[55, 56]
Transforming growth factor β (TGF-β)	Low dose of TGF-β contributes to angiogenic switch, high dose of TGF-β contributes to stabilization of new vessels	[46, 57]
Angiopoietin 1 (Ang-1)	Key regulatory in vessel homeostatis; promotes stabilization of newly formed vessels	[58, 59]

SMCs, smooth muscle cells; ECs: endothelial cells.

The delivery of growth factors generally can result in effective angiogenesis in different stages. However, the design of growth factor therapy is normally expensive, moreover, the most critical problem during this therapy is the uncontrollable dose of factor delivered [60]. The bolus injection of angiogenic factors associates with negative side effects (hyperpermeable vessels, hypotension, stimulation of tumor growth and uncontrolled neovascularization, etc...) [61].

Many strategies have been developed for delivery of angiogenic factors. Coating or loading the biomaterial scaffold with growth factors is the easiest method and has been most widely used [62]. The delivery of growth factors with biomaterial matrices is either driven by passive diffusion or can be coupled to the rate of biomaterial degradation [62]. Both processes are not often in tune with the actual healing process [62]. The kinetics of factor releases can be mediated by varying the degradation rate of the material. However, these measures are often insufficient to synchronize the growth factor levels with actual cellular demands.

A novel approach solved this problem is using a specific chemical linkage of growth factors to a material matrix. The endothelial cells of blood vessels secrete MMPs that are able to degrade the matrix. By degrading the matrix, the cells thus release the growth factors locally in response to cellular demand. These neovasculatures induced by cell-demanded release of growth factors showed a higher degree of organization than those arose from an uncontrolled growth factor release, as one can see in Figure 9 [63, 64].

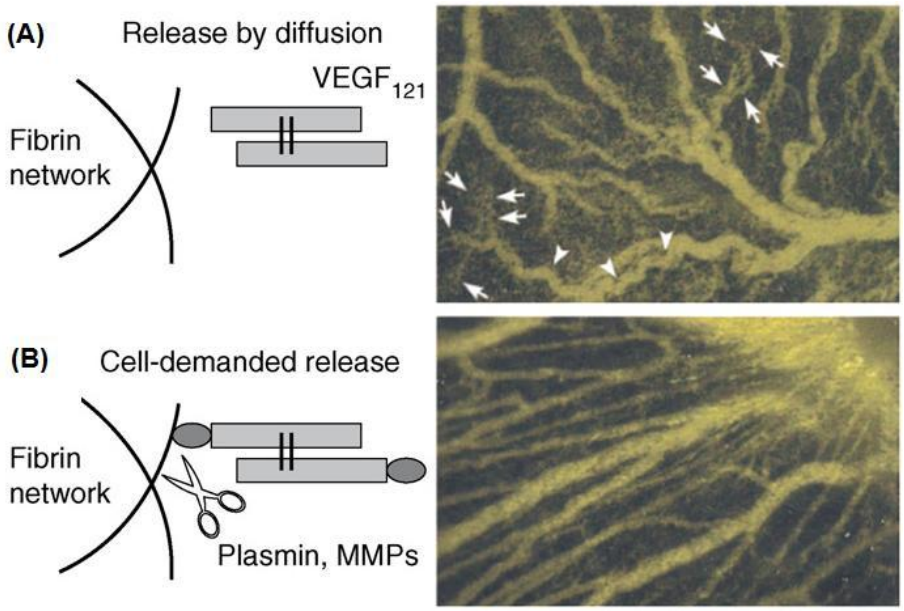

Figure 9. Angiogenic factor delivery. Fibrin gel matrices were placed on a chicken egg membrane. Panel (A) shows the effects of freely diffusible $VEGF_{121}$, which resulted in the formation of vessels with a disturbed morphology. Many of the newly formed vessel branches were characterized by malformed, corkscrew-like structures (arrowheads) and irregular capillary enlargement and growth (arrows). In panel (B), $VEGF_{121}$ was enzymatically released by MMPs in a cell-demanded release. A much more regular organization of the vascular structures can be observed upon cell-demanded release [63].

3.3. Cell-based therapy

Regardless of the approaches adopted to accelerate vascularization, all of the strategies directly or indirectly consist of ECs. Incorporation of ECs with/into materials is important to enhance neovascularization in engineered tissue.

Cell sources

Mature ECs can be isolated form a great variety of sources such as the umbilical cord, skin, fat tissue, and saphenous vein [18]. The ECs can be derived either as autologous (from humain) or xenografts (from different species, such as bovine, rat, etc…) [18].

The investigations of EC tube formation in/on biomaterials are summarized in Table 2. The cell sources for *in vitro* models of angiogenesis and vasculogenesis are versatile [65, 66]. Variation among experimental protocols, differences in cell types, cell seeding density, serum content and supplemented growth factors, could all be responsible for some different properties in tube formation.

Comparing to mature ECs, endothelial progenitor cells (EPCs) are alternative source of ECs to support pro-angiogenic therapy in tissue engineering. These cells are present in bone marrow, fat tissue and peripheral blood, and are able to differentiate into mature ECs and participate in both angiogenesis and vasculogenesis [67, 68]. EPCs have been widely used for tissue engineering applications [69-72]. The EPCs adhered on polysaccharide hydrogels and made it suitable for vascular tissue engineering [73]. Furthermore, the applicability of EPCs was demonstrated in bone tissue engineering and fracture healing processes [74-76].

Co-culture

The interaction of ECs with other cell types has also been employed to promote and maintain vascularization. The aim of using co-culture of endothelial cell with other cells is to mimic the complex interactions between cells. However, the optimal combination of cells, their ratio and culture condition are still critical challenge [77]. The co-culture of ECs (or EPCs) with different cell types such as SMCs, fibroblasts, adipocytes or osteoblasts, were employed to supporting angiogenic process [78-81].

Table 2. Summary of endothelial cell tube formation on/in different substrates.

Cell type	Substrate	Time until tubes form	Comments
Two-dimensional culture-plated cells			
HCEC	Gelatin	3-6 weeks	Capillary tubes form in tumor-conditioned medium. First demonstration of angiogenesis *in vitro* [82]
HUVEC	Matrigel	8 h	Tube formation dose dependent on Matrigel (+GF) [83]
HUVEC	Matrigel + thrombin	18 h	Thrombin induces capillary structures in a dose-dependent fashion on Matrigel [84]
HUVEC	FN	4-6 weeks	ECs organized into tubular structures in condition supporting high density survival [85]
BCEC	FN, collagen IV	1-2 d	Tubular network formation on intermediate protein coating density [86]
BCEC	FN	3 d	Tube formation on 10 μm-stripes of FN [87]
BAEC	Alkylated cellulose	10 d	Higher hydrophobicity needed for tubes [88]
RSEC	Collagen I + laminin	1-2 d	Tube length increases with laminin [89]
HMVEC	Gelatin	5d	Capillary tube-like structure on 20 μm line of gelatin [90]
EPC	Nanotopographic PDMS	6 d + 1 d	Capillary tube formation was assessed after Matrigel deposition for 1 d [91]
Sandwich culture-plated cells			
HUVEC	Fibrin I, II	1 d	Maximal tube formation with fibrin II, minimal tube formation with fibrin I [92]
RCEC	Collagen I	2 d	Capillary-like tube formation [93]

Three-dimensional culture-embedded or plated cells			
HUVEC	Hygrogel + EphrinA1	6 h-7 d	Tubulogenesis in hydrogels containing three different concentration of PEG-ephrinA1 [94]
HUVEC	Hydrogel + RGD	1 d, 18 d	Cord-like structure on 50 μm stripes of RGD peptides [95]
HUVEC	Hydrogel + RGDS + VEGF	2 d	Tubules formed on ~ 10 μm lines of RGDS and VEGF [96]
HUVEC,HDMEC	Nano/micro fibrous scaffolds	14 d	Nano-network provide the structure for ECs' organization into capillary-like structures [97]
HMVEC	Fibrin/collagen hydrogel	5-25 d	Only fibrin-based hydrogel allowed the formation of 3D vascular structure [98]
EPC	Patterned FN + fibrin gel	1 d-2 d	Tubular structure are detected at 1-2 d after gel addition, and tube structures diminished at 3-4 d after gel application [99]

EC: Endothelial cell; EPC: endothelial progenitor cells; HUVEC: human umbilical vein EC; HMVEC: human microvascular EC; HDMEC: human dermal microvascular EC; HCEC: human capillary EC; BAEC: bovine aortic EC; BCEC: bovine capillary EC; RCEC: rat capillary EC; RSEC: rat sinusoidal EC. FN: fibronectin; + GF: growth factors supplemented; PDMS: polydimethylsiloxane

The simplest co-culture is the seeding of a mixed suspension of the two (or more) cell types and plated in two-dimentional (2D) surface. In co-culture of ECs and osteoblastic lineage cells on tissue culture flask, this initially 2D system became 3D within 7 days, and the ECs had already self-assembled to yield lumen-containing vessel structures (Figure 10A) [100]. Human EPCs interacted with smooth-muscle-like cells supported and improved cord-like structures *in vitro* [101], providing the potential application for therapeutic vascular tissue engineering.

Naturally, the cells were in connection to nearby organs or tissues, it is evident that the more suitable *in vitro* model would adopt a 3D cellular system. In a tissue engineering strategy, the cells would be seeded in 3D using a biomaterial scaffold or matrix (such as hydrogels). In the cooperative works by research groups of C.J. Kirkpatrick and R.L. Reis, extensive studies have been developed to stimulate vascularization using co-culture of cells on 3D scaffold ([77, 102]). Their works have been performed on 3D microporous scaffold

such as silk fibroin constructs, fiber-mesh scaffold made from a blend of starch with poly(caprolactone) (SPCL), etc… [77, 97, 100, 103-110]. When outgrowth endothelial cells (OECs) co-cultured with primary human osteoblasts (pOBs), these OECs grew well on 3D microfibrous silk fibroin scaffolds and developed a migratory phenotype with cord formation [110]. They also found human dermal microvascular ECs (HDMECs) possess the propensity to form capillary-like structures during co-culturing of HDMECs with pOBs on the 3D scaffolds, these co-cultures gave massive sprouting of vessel-like structures over a period of 6 weeks (Figure 10B) [103].

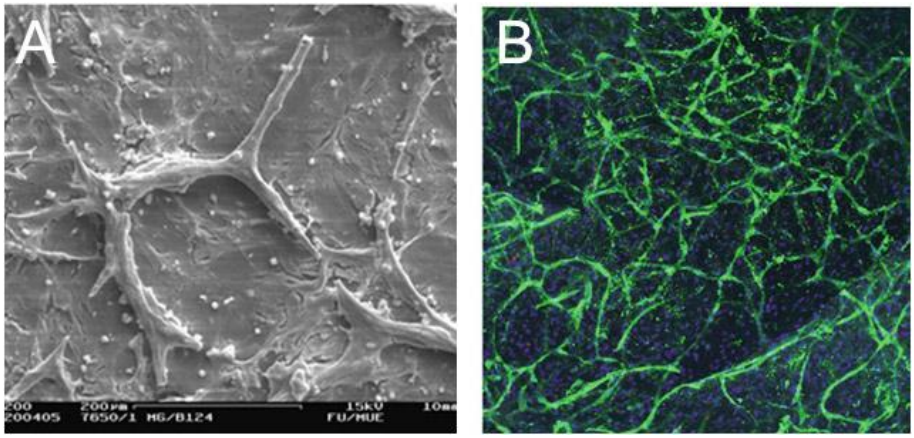

Figure 10. Co-culture of cells to stimulate vascularization. (A) Morphological assessment of endothelial interconnected networks formed by outgrowth endothelial cells (OECs). OECs co-cultured with MG63 cells for 1 week on 2D plates [100]. (B) Confocal images of co-culture of HDMECs with osteoblasts on 3D biomaterials. Endothelial cells were stained with PECAM-1 (green) and formed capillary-like structures, DAPI staining (blue) showing nuclei of both types of cells, it can be seen that many nuclei lie between the capillary-like structures, indicating the presence of osteoblasts [103].

Meanwhile, as proved by Yu *et al.*, an implanted co-culture of EPCs and bone marrow-derived osteoblasts on porous PCL improved not only osteogenesis but also vascularization [111]. Steffens *et al.* also reported the formation of vasculature after implanting sub-cutaneously into mice a co-culture of mature ECs with osteoblasts in fibrin [112]. Specially worth mentioning was the fact that vasculature was stabilized by the recruitment of mural cells and the newly formed vascular networks anastomosed with the mouse vasculature [112].

Regulation and maturation of blood vessels

The blood vessel formation is important for tissue engineering. However, once blood vessels are formed, it is very important that the newly formed capillary structures are stabilized [113]. The stabilization of nascent vessels is usually accompanied by a recruitment of smooth muscle cells or pericytes to the vessels and the subsequent production of an extracellular matrix [114-116].

The nascent vessels only consist of ECs, they are leaky, prone to regression and poorly perfused [52]. To achieve functional blood perfusion, the network must be remodeled into a vascular tree of mature large vessels branching of smaller capillaries, whereby excess immature vessels are pruned [52]. A chronically precise adjustment of vessel growth, vessel maturation and finally suppression of EC growth are then required for the formation of physiologically functional vessels [52].

The recruitment of peri-endothelial cells (PECs) (pericytes in small vessels or SMC in larger vessels) around nascent vessels essentially contribute to the remodeling and maturation of the primitive vascular networks [114-116]. When PECs make contact with ECs, in turn the ECs stop dividing and migrating, and ECs become quiescent, acquire specialized differentiation properties, and survive for longer time [116, 117]. PECs stabilize vessels by producing ECM and tightening junctions, regulate perfusion, establish vascular branches, and make vessels more resistant to regression [118]. PECs help to establish a more functional vascular network and therefore are targets for inducing therapeutic angiogenesis [117]. The currently views state that the initial endothelial tubes form without pericyte contact, and subsequent acquisition of pericyte coverage leads to vessel remodeling, maturation and stabilization [119].

Pericytes, also known as Rouget cells [115], are the perivascular cells which wrap around blood capillaries (peri, around; cyte, cell), as one can see in Figure 11. Molecular markers that are presented in pericytes, albeit not exclusively, are commonly used for their detections: alpha-smooth muscle actin (α-SMA), neuron-gial 2 (NG_2), desmin and platelet-derived growth factor receptor beta (PDGFR-β). Antibodies against these proteins are commonly used to identify pericytes in cell culture or tissue sections [17, 120]. Morphologically, pericytes exhibit an oval cell body extending for some distances along the vessel axis [116]. Pericytes are precisely located adjacent to ECs or over EC junctions of capillary and especially over gaps between ECs during inflammation [116]. Functionally, pericytes stabilize newly formed capillaries and render them to functional structures [17, 115].

The contractile phenotype of pericytes allows contraction and relaxation of EC tubular structure, thus regulating the blood flow through blood vessels [17].

In this study, after obtaining the blood vessel structures on the functionalized polymer surfaces, the investigation of stabilization of blood vessels were performed by recruitment of pericytes in a co-culture system (Paper V).

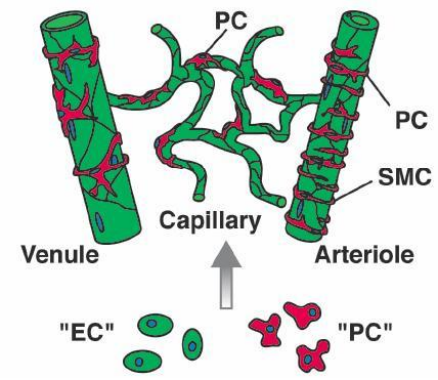

Figure 11. The role of pericytes in blood vessel formation and maintenance. Endothelial cells assemble into a capillary network, and stabilized by pericytes /SMCs. Arterioles exhibit a high density of SMCs and thicker EC walls. Venules have irregularly arranged pericytes and are composed of thinner EC walls. Capillary consists of a layer of ECs surrounding with pericytes. EC: endothelial cell; PC: pericyte (modification after [17]).

3.4. *In vitro* prevascularization

In vitro prevascularization is widely used to enhance vascularization in engineered tissues. In this approach, the scaffolds are seeded with ECs and optionally combined with other cell types. The constructs are cultured *in vitro* with the objective to build 3D pre-vascularized structures. After co-culture of cells in the scaffolding material for a short time (from several hours to few days), the constructs can be subsequently implanted *in vivo.*

Scaffolds sufficiently pre-vascularized *in vitro* would be transplanted *in vivo* and encourage to integrate with the host vasculature (as shown in Figure 12). After implantation, this *in vitro* pre-vascularized network can spontaneously anastomose to the ingrowing vasculature of the host and supply the construct with nutrients (Figure 12). The efficacy of *in vitro* prevascularization has been shown that the prevascular networks formed *in vitro* can connect with the host vascular system after implantation [121, 122]. For instance, Levenberg

et al. reported that prevascularization of a skeletal muscle construct *in vitro* significantly enhanced vascularization, perfusion and survival of the construct after implantation [122].

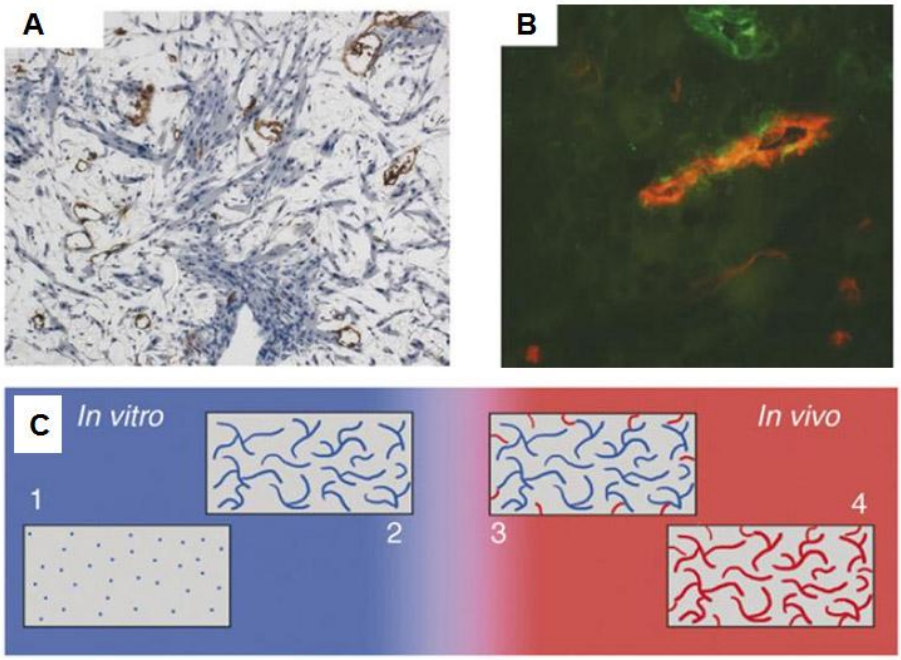

Figure 12. *In vitro* prevascularization. Mouse myoblast cells were combined with HUVECs and mouse embryonic fibroblasts and seeded on a scaffold, resulting in the formation of a 3D prevascular network. After implantation, the network anastomosed to the mouse vasculature. (A) *In vitro* formation of prevascular network. This picture shows a cross section of the scaffold after *in vitro* culture in which ECs are stained brown and muscle cells are stained blue. The presence of cross sections of tubular structures shows that the ECs have organized into vascular structures. (B) The anastomosis of the prevascular network after implantation, which shows a cross section of the scaffold after implantation. The vascular network that was formed *in vitro* was labeled in green and all vessels that were perfused with blood *in vivo* are stained in red. (C) Schematically depicts *in vitro* vascularization. 1: A tissue construct containing endothelial cells is prepared *in vitro*. 2: The endothelial cells organize into a vascular network (blue). 3: The tissue construct is implanted and host vessels (red) grow into the construct. 4: When the host vessels reach the pre-cultured vascular network, the vessels connect and the entire construct becomes perfused (modification after [122]).

3.5. *In vivo* prevascularization

Another promising strategy for enhancing vascularization is *in vivo* prevascularization. In this method, designing and optimization of scaffold materials are employed to promote local angiogenesis directly *in vivo* and encourage infiltration of host vessels into the scaffolds. This method involves two distinct surgical procedures [123-125]. In the first stage, a tissue-engineered construct (scaffolding materials loaded with cells and/or growth factor) is implanted into a site of rich vascularization with an artery-vein loop (or vascular axis) suitable for microsurgical transfer (Figure 13A) [126]. A vascularization period of several weeks at this initial implant site will result in the formation of a microvascular network in the engineered construct (as Figure 13B) [126]. Then, the tissue engineered construct is harvested together with the microvascular network and re-implanted at the defect site. At this site, the vascular axis is connected to the local vasculature using microsurgical vascular anastomosis techniques, which results in instantaneous perfusion of the entire construct [127]. The advantage of this method is that after implantation at the final defect site, the construct becomes immediately perfuse by surgical anastomosis. However, its drawbacks are that two separate surgeries (one to implant the construct at the vascularization site and one to implant the construct at the final defect site) are necessary.

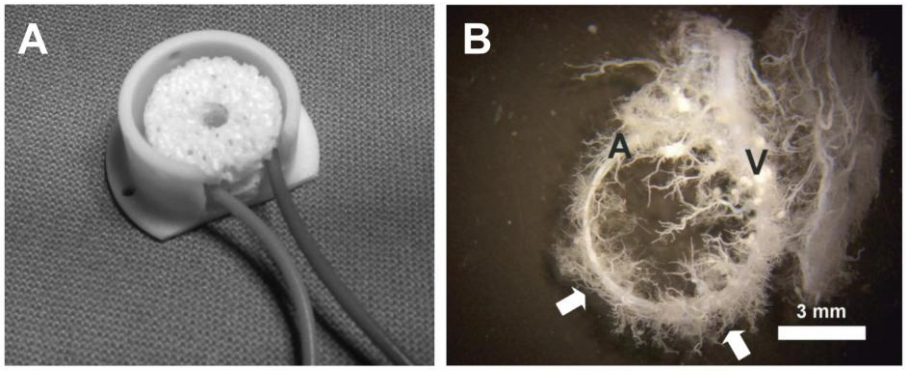

Figure 13. *In vivo* prevascularization. An artery (A) and a vein (V) were joined via a loop, which was then placed around a bone-tissue-engineered scaffold and implanted. (A) The construct before implantation with plastic tubing instead of the AV loop for illustration. (B) The highly vascularized construct that was obtained eight weeks after implantation (after [126]).

4. Biochemical modification of biomaterials for vascularization

The biomaterial plays an important role in tissue engineering strategies [128]. For instance, biomaterials serve as a substrate on which cell population can attach and migrate, and can also serve as biomolecule carrier, can be implanted with a combination of specific cell types as a cell delivery vehicle, etc...

Modification of biomaterials is often required to render them cell-adhesive and conductive to neovascularization. The development of biomaterials for tissue engineering application has focused on the design of biomimetic materials which are able to interact with surrounding tissues by biomolecular recognition. Till up now, different bioactive ligands have been used to study their effect on cell functions for a better understanding of vascularization [129]. This section describes various methods of material modification to promote integration of biomaterials-endothelial cells and consequently to improve angiogenesis responses.

4.1. Material modifications with proteins

In vivo cells are in intimate contact with the ECM, which is formed from a complex connection of proteins, glycoproteins, and proteoglycans [130]. The ECM provides not only structural support but also contains a reservoir of cell signaling motifs and growth factors that guide cellular anchorage and behavior [130]. The organization, density, spatial geometry, and biochemistry of these ECM components determine mechanical strength, cell response, and ultimately, hierarchical tissue organization.

Matrigel™, a basement membrane matrix extracted from Engelbreth-Holm-Swarm (EHS) mouse sarcoma cells [131], has been extensively used as a cell culture substrate to promote both *in vitro* EC tube formation on two dimentional (2D) surfaces and *in vivo* 3D vascularization [132]. However, Matrigel™ is a poorly controlled and uncharacterized environment under the consideration of engineering perspective. Cellular interactions with Matrigel™ are very complex since it contains a mixture of various proteins and growth factors that interact with cell receptors. Therefore, it’s difficult to detect the specific interactions which stimulate angiogenesis. Matrigel™ presents low mechanical strength, with Young’s Modulus 400 Pa and Shear Modulus 180 Pa, which made it difficult for engineered

tissue application. Moreover, the thermal cross linking process of Matrigel shows a reversed characteristic: liquid at low temperature (4 °C) and solid at physiological temperatures (37 °C). Furthermore, because of its tumoral and xenogenic origin, Matrigel is ultimately a sub-optimal choice for the development angiogenic therapies.

For more defined studies, individual ECM proteins, such as collagen, gelatin, fibronectin, laminin and vitronectin, are frequently used to modify the biomaterial surfaces [83, 87, 90]. Biomaterials can be coated or grafted with these proteins, and they have been shown to facilitate cell attachment and promote their interaction with cells. ECs have been cultured successfully on ECM protein coated polymers such as hyaluronic acid [133], poly (L-lysine) [134], poly (caprolactone) [107], and poly (lactic acid) [135]. ECM protein coating on biomaterials can facilitate neovascularization *in vivo*. For instance, expanded poly-tetrafluoroethylene (ePTFE) has been adsorbed with laminin to render the biomaterials cell-adhesive [136]. When these scaffolds were implanted *in vivo*, laminin modification stimulated angiogenesis and accelerated neovascularization in the ePTFE matrices. In the co-work of C.J. Kirkpatrick and R.L. Reis, polymer scaffolds have been systematically pre-coated with fibronectin to promote cell adhesion, co-culture of ECs and osteoblast on these scaffolds enhanced the development of vascularization both *in vitro* and *in vivo* [105, 107].

More recently, several groups have reported the importance of sonic hedgehog (Shh) in vascularization processes [137-139]. Shh is one of three proteins in the mammalian signaling pathway family called hedgehog, the others being desert hedgehog and Indian hedgehog [140]. There is increasing evidence from the literature that the Shh pathway plays a significant role in vasculogenesis [137-139]. Shh promotes both angiogenesis and osteogenesis in a co-culture system consisting of primary osteoblasts and outgrowth endothelial cells [141]. Shh can induce expression of two families of angiogenic cytokines, VEGF-1 and angiopoietins (Ang-1 and Ang-2) [138], these lead to a massive increase in microvessel-like structures in co-culture system with Shh [141]. The findings reveal a novel role for Shh as an indirect angiogenic factor regulating angiogenesis [138, 141].

In fact, a number of membrane-bound proteins are also playing important roles in induction of vascularization and offering opportunities in design of angiogenic biomaterials [46]. Integrins, ephrins, and cadherins are membrane-bound proteins that affect many functions involved in blood vessel assembly [46]. Zisch *et al.* have coupled a cell membrane protein, ephrin-B2, into fibrin matrices and shown to stimulate EC angiogenic responses [142]. In another work, ephrin-A1 was incorporated into PEG hydrogels and found to stimulate EC adhesion and spreading [143]. Interestingly, ECs cultured on these hydrogel

surfaces spontaneously organized into extensive vasculature-like networks with hollow central lumen with diameters ranging 5-30 μm [143].

The ECM proteins were widely employed to improve the material bioactivity. However, the adoption of proteins bears some disadvantages in the view of biomedical applications. At first, the proteins have to be isolated from other organisms and purified. Thus, they may elicit undesirable immune responses and increase infection risks [144]. In addition, proteins are object of proteolytic degradation and needed to be refreshed continuously. Long-time applications of these materials would be impossible. Inflammation and infection can even accelerate protein degradation [144]. Furthermore, only a part of the proteins have proper orientation for cell adhesion because of their stochastic orientation on the surface [145]. In addition, the texture of the surface determined by charge, wettability, and topography may influence the conformation and the orientation of the proteins [146]. This causes the denaturation of proteins or at least a different presentation of cell binding motifs [147].

4.2. Material modifications with peptides

Majority of the protein problems discussed above can be overcome by presenting cell recognition motifs as small peptides [148]. Peptides exhibit higher stability towards sterilization conditions [149], heat treatment and pH-variation [150], storage [151] and conformational shifting, easier characterization and cost effectiveness [149, 152]. Because of lower space requirement, peptides can be packed with higher density on material surfaces. This provides a chance to compensate for possible lower cell adhesion activity [153]. ECM proteins contain normally many different cell recognition motives, whereas small peptides represent normally only one or a few motifs. Therefore, they can selectively address one particular type of cell receptors.

Various ECM peptide sequences have been determined and used for surface modification of materials in numerous studies [149]. Among the peptides investigated, RGD is the most effective peptide sequence to promote cell adhesion in biomaterial studies. The RGD peptide is present in many ECM proteins such as fibronectin, vitronectin, laminin and collagen [154]. Moreover, RGD is able to address more than one integrin receptors [155-157], RGD is recognized by integrin $\alpha_5\beta_1$ and $\alpha_v\beta_3$ which are predominant in cell adhesion [158].

Several studies proved that when exposed to RGD, endothelial cells adhered, spread, and formed focal adhesions and actin stress fibers [159-161]. RGD were conjugated into hydrogels and induced endothelial morphogenesis [95]. RGD also supported the adhesion of many other cell types different from ECs, including fibroblast, SMCs, preosteoblasts, pre-adipocytes and mesenchymal stem cells [155].

In Chollet *et al.*'s study, polymer surfaces (polyethylene terephthalate, PET) presenting different densities of RGD peptides have been developed thanks to the covalent grafting, and the behaviors of different types of cells (ECs and MC3T3 osteoblast cells) were addressed [159]. The results proved that a minimal RGD density of 1 pmol/mm^2 is required to improve MC3T3 and EC responses. Indeed, cells seeded onto a RGD-modified PET surface with a density higher than 1 pmol/mm^2 were able to establish focal adhesion as compared to cells on unmodified PET and RGD-modified PET with density lower than 1 pmol/mm^2. Moreover, the number of cell focal adhesions was enhanced by increasing the RGD peptide density onto the surfaces. With this study, the team proved that the peptide density on the surface is an important parameter influencing the endothelial or osteoblast cell adhesion and focal contact formation [159].

Nowadays, several studies are interesting in peptides which are more specific for endothelial cells in vascular research. The REDV sequence, found within the CS5 domain of fibronectin [162, 163], is essentially recognized by the integrin $\alpha_4\beta_1$ [162, 163]. REDV peptides grafted on synthetic surfaces were known to induce selective adhesion of endothelial cells, while simultaneous binding and spreading of fibroblast or smooth muscle cells were inhibited [162, 164]. The REDV sequence mediates endothelial cell migration via its $\alpha_4\beta_1$ receptors [25, 165].

YIGSR is an sequence derived from B1 chain of laminin [166]. YIGSR motif exerts its cell-adhesive activity through interaction with $\alpha_4\beta_1$ and $\alpha_6\beta_1$ [167]. YIGSR has been used to promote EC-specific adhesion on non-adhesive substrates. Polyurethanes incorporated with YIGSR peptides enhanced EC adhesion, spreading and proliferation while minimizing platelet adhesion [168, 169]. Glass and PEG hydrogels modified with YIGSR also enhanced EC adhesion and migration [170, 171]. It's reported that YIGSR site in the B1 chain of laminin induced endothelial cell-cell interactions and promoted endothelial tube formation [172]; synthetic YIGSR can also induce ECs to form ring-like structures surrounding a hollow lumen, the basic unit in the formation of capillaries [172].

SVVYGLR is a cryptic sequence adjacent to RGD in the osteopontin molecules following thrombin cleavage [173]. It is mainly binds to integrin $\alpha_9\beta_1$ [173]. Hamada *et al.* reported that soluble SVVYGLR had the binding capacity and stimulated the migration of ECs [174]. Furthermore, it induced tube formation of in three-dimensional collagen gel [174]. It also induced angiogenesis in artificial bone marrow scaffold biomaterials [175]. To date, SVVYGLR is the most strong angiogenic peptides as reported, and has much stronger angiogenic activity than VEGF [174, 176]. This small peptide might be expected to stimulate angiogenesis in the future because of its advantages.

Based on the above illustration, it has demonstrated that peptides oftentimes as short as several amino acids long can substitute bulky ECM proteins and enhance cellular adhesion and functions on material surfaces. In this work, we aimed to graft the EC specific peptides onto polymer surfaces, as well as to examine what EC morphological and functional changes can be correlated to these bioactive motifs.

4.3. How to immobilize biomolecules onto materials

Introducing biomolecules onto biomaterials would have beneficial effects in engineered tissues. Biomolecule immobilization onto biomaterials can generally be divided into two catagories, namely, non-covalent and covalent interaction.

Physical absorption

Surface adsorption of biomolecules is widely employed for surface modification and had been shown to mediate cell interactions with biomaterials [177]. Biomolecule absorption by non-covalent interactions are based on hydrophobic, van der Walls interaction, hydrogen bonding or electrostatic forces. An advantage of these concepts is their ease of applications because no chemical modification is required prior to immobilization. However, physical adsorption can induce problems with biomolecule desorption during the assay, which will result in loss of signal [178]. Coating of surfaces with ECM proteins, such as fibronectin or collagen, proves to be less efficient compared with covalent grafting [179], and a poly(carbonate-urea)urethane vascular conduit covalently modified with RGD and heparin showed better retention of ECs as compared with simple coating of the same molecules [179].

Chemical modification

One of more stable biomolecule conjugation is to covalently link the molecules onto surfaces via chemical modifications. Table 3 collected the methods for covalently attaching biomolecules to materials depending on available functional groups, such as hydroxyl-, amino-, or carboxyl groups. In this work, a three step chemical modification was adopted to covalently immobilize peptides onto polymer surfaces for studying the subsequent endothelial cell functions on them.

Table 3. Chemical modifications for covalent binding of biomolecules to biomaterials [180]

reactive groups on proteins/peptides	coupling reagents/ cross-linkers	functional chemical groups on polymer surface
$-NH_2$	cyanogen bromide cyanuric chloride DMT-MM	-OH
$-NH_2$-OH	glutaraldehyde succinate anhydride diisocyanate compounds diisothoncyanate compounds	$-NH_2$
$-NH_2$ -SH -Ph-OH	nitrous acid hydrazine and nitrous acid	$-NH_2$
-COOH	DMT-MM carbodiimide compounds (EDC, DCC)	$-NH_2$
-SH	disulfide compound	-SH
$-NH_2$	thionyl chloride *N*-hydroxysuccinimide *N*-hydroxysulfosuccinimide + EDC	-COOH

DMT-MM, 4(4,6-dimethoxy-1,3,5-triazin-2-yl)-4-methylmorpholinium chloride; EDC, 1-ethyl-3-(3-dimethylaminopropyl) carbodiimide hydrochloride; DCC: dicyclohexylcarbodiimide.

5. Micropatterning of biomolecules to induce vascularization

Aside from biomolecule modification by cell binding ligands (peptides, proteins, growth factors, etc…) and by varying their chemical density [159], another very important approach to manipulate cellular functions on biomaterial surfaces is their spatial micro-distribution.

In situ, cells are highly sensitive to geometrical and mechanical constraints from their microenvironement. Microengineering techniques provide tools to modify the cell culture substrates at cellular scales [181]. The so-called micropatterns [181], can be used to restrict the location and shape of the substrate regions, in which cells can attach and develop their functions.

The microelectromechanical systems (MEMS), which are an extension of the semiconductor and microelectronics industries, have been increasingly used to fabricate micropatterns of proteins or cells for biomedical and biological applications.

Micropatterning technologies combine the knowledge of surface chemistry and material science [182, 183]. They can achieve a resolution of 0.1 μm, which is two orders of magnitude smaller than the dimension of the capillaries, and span of five orders of magnitude ranging from overall dimension of tens of centimeters down to cellular dimension of 5 μm [184]. Consequently, they are able to position the biomolecules on a substrate with control size and spatial arrangement, thus facilitated fundamental studies in cellular research [183].

The micropatterning are not only to impact the cell size and cell shape, but also to interfere with the regulation of cell functions, such as cytoskeleton organization, cell growth, cell differentiation, cell polarity, as well as tissue-like morphogenesis [181, 183, 185].

The aim of this section is to summary the principles, processes, materials, applications (especially in biology and tissue engineering), and limitations of main microfabrication techniques.

5.1. Photolithography

Photolithography is one of the most successful technologies in microfabrication [186]. It has originally been developed for the fabrication of semiconductor devices. Recently, it has

been applied in biomedical applications and used most extensively for cell and protein patterning [185].

Photolithography is the process of transferring geometric shapes on a mask to the surface of a wafer or other substrates (Figure 14). In photolithographic micropatterning, a layer of photoresist (light sensitive organic polymer) is applied to the surface of the substrate and selectively exposed to ultraviolet (UV) light through a mask containing the pattern features. For positive photoresist, the exposed polymer becomes more soluble in a developer solution than the unexposed polymer. Whereas for a negative photoresist, the exposed polymer becomes insoluble in the developer solution. The obtained photoresist pattern after development can then act as a mask for patterning the material of interest (for example, immobilization of peptides in this thesis). Then, the photoresist is removed by dissolution in an organic solvent (so called "lift-off" process) to expose the remaining area. Furthermore, the chip can be incubated with adhesive resistant materials, resulting in a cell adhesive and cell resistant micropattern.

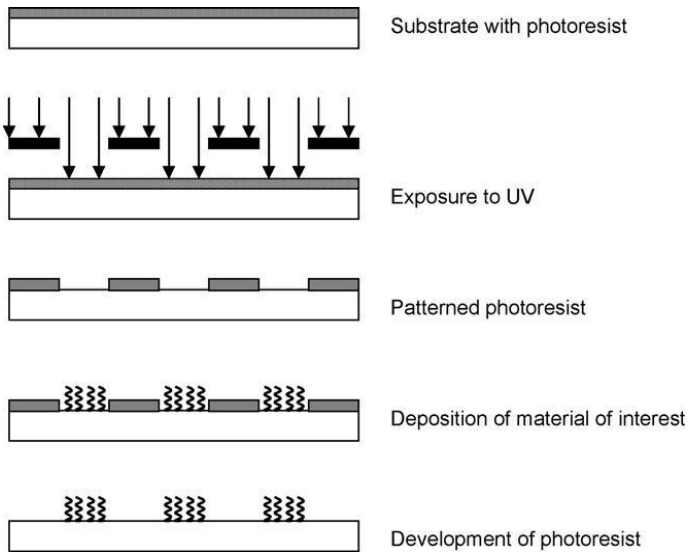

Figure 14. Micropatterning using photoresist lithography [187]

Photolithography had been widely used for patterning biomolecules/cells on hard materials. For instance, a hydrophobic-hydrophilic micropattern of octadecyltrimethoxysilane on silicon substrate was prepared for the selective assembly of carbohydrates [188].

Healy and coworkers produced line patterns of aminosilane/alkylsilane on quartz discs via photolithography [189], cells showed a clear preference for the aminosilane surface. Mineralization was almost exclusively restricted to the aminosilane line patterns after cell culture of 20 days [189].

In previous work of our group, RGD peptide patterns were synthesized on polymer surface by photolithography, the cells culture concluded that osteoblast cells were selectively assembled on peptide patterns [190].

The 2D guiding cues of such micropatterned lines on a flat substrate were shown able to guide 3D morphogenesis. Moon *et al.* conjugated PEG-RGDS patterns on poly(ethylene glycol)-diacrylate (PEGDA) hydrogels via photolithographic technique (photopolymerization) [95]. The EC morphogenesis into capillary-like structures was induced on 50 μm PEG-RGDS stripes (Figure 15), while ECs continued to spread on 200 μm patterns [95]. The concentration of adhesion proteins on the micropatterned lines also affected the self-assembly of endothelial cells into tubular structures [95]. Low concentration of adhesion peptide RGD (<10 $\mu g/cm^2$) is not sufficient to induce cell attachment, whereas high concentration (>100 $\mu g/cm^2$) prevents formation of the tubular structure that only occurs at an intermediate RGD concentration of ~20 $\mu g/cm^2$ [95].

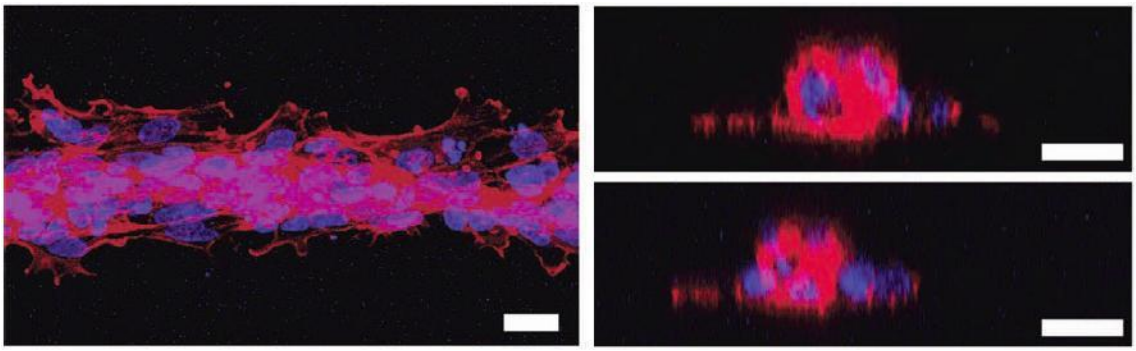

Figure 15. Visualization of EC morphogenesis on hydrogels. Confocal images showed HUVECs underwent cord formation on PEGDA hydrogels micropatterned with 50-μm stripes PEG-RGDS [95].

Photolithography can produce accurate patterns with submicron resolution [185], it will continue as the dominant technology in microfabrication of sophisticated semiconductor devices and systems. In this work, photolithography was used to fabricate peptide micropatterns onto biomaterial surfaces for the purpose of cell culture.

Although photolithography is the dominant technology, it is not always the best and/or the only option for all applications, it has limitations too. For instance, it is poorly suited for patterning non-planar surfaces. It can generate only 2D microstructures. Another major drawback with this approach is that the immobilized biomolecules are always exposed to an organic solvent (acetone is usually used to dissolve the photoresist) and known to be harmful to proteins in a certain degree [185].

5.2. Soft lithography

Alternatively, non-photolithographical set of microfabrication methods have been developed, which is the so-called soft lithography [32]. Because it uses a patterned soft elastomer as the stamp, mold, or mask to generate micropatterns and microstructures [185, 191]. Elastomer is the chosen materials as they can make conformal contact with non-planar surfaces. The stamps is usually prepared by casting the liquid pre-polymer of poly(dimethylsiloxane) (PDMS) against a master which has patterned relief structures (as one can see in Figure 16).

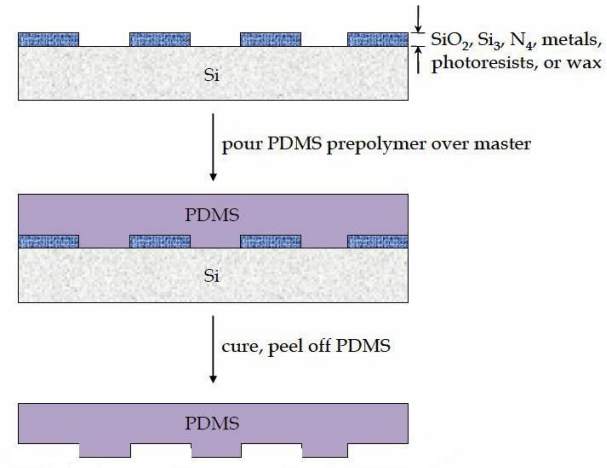

Figure 16. Schematic illustration of the procedure for fabrication of PDMS stamps from a master having relief structures on its surface [191]

Based on this consideration, many soft lithography have been explored [32]: such as microcontact printing (μCP), replica molding (REM), microtransfer molding (μTM), micromolding in capillary (MIMIC), solvent-assisted micromolding (SAMIM) and phase-shift photolithography, etc...

Table 4 compared the advantages and disadvantages of conventional photolithography and soft lithography. Soft lithographic techniques are low in capital cost, easy to learn, straightforward to apply, and accessible to a wide range of users. They can circumvent the limitations of photolithography, which provide access to quasi-three-dimensional structures and generate patterns and structures on non-planar surfaces.

Soft lithography is commonly used to create chemical structures on biomaterial surfaces for controlling cell-substrate interaction [191]. At this stage, we illustrate two soft

lithography techniques which are mainly involved in vascularization application: (i) microcontact printing and (ii) micromolding patterning.

Table 4. Comparison between photolithography and soft lithography (after [32, 192])

	Photolithography	Soft lithography
Definition of patterns	Rigid photomask (patterned Cr supported on a quartz plate)	Elastomeric stamp or mold (a PDMS block patterned with relief features)
Materials that can be patterned directly	Photoresists (polymers with photo-sensitive additives)	Photoresists[a,e]
	SAMs on Au and SiO_2	SAMs on Au, Ag, Cu, GaAs, Al, Pd, and SiO_2[a] Unsensitized polymers[b–e] (epoxy, PU, PMMA, ABS, CA, PS, PE, PVC) Precursor polymers[c,d] (to carbons and ceramics) Polymer beads[d] Conducting polymers[d] Colloidal materials[a,d] Sol-gel materials[c,d] Organic and inorganic salts[d] Biological macromolecules[d]
Surfaces and structures that can be patterned	Planar surfaces 2-D structures	Both planar and nonplanar Both 2-D and 3-D structures
Current limits to resolution	~250 nm (projection) ~100 nm (laboratory)	~30 nm[a,b], ~60 nm[e], ~1 μm[d,e] (laboratory)
Minimum feature size	~100 nm (?)	10 (?) - 100 nm

[a–e]Made by (a) μCP, (b) REM, (c) μTM, (d) MIMIC, (e) SAMIM. PU:polyurethane; PMMA: poly(methyl methacrylate); ABS: poly(acrylonitrile-butadiene-styrene); CA: cellulose acetate; PS: polystyrene; PE: polyethylene; PVC: poly(vinyl chloride) and SAM: self-assembled monolayers

Microcontact printing

Among the soft lithographic techniques, microcontact printing is the most widely used [32]. Originally developed for creating patterns for microelectronics application [193], microcontact printing was soon adapted to produce substrates for cellular patterning [193-195].

Microcontact printing is based on the transfer of the material of interest form a PDMS stamp onto a surface at the areas contacted by stamps (as shown in Figure 17). After fabrication of stamps (see Figure 16), the stamp is inked with a solution and brought into conformal contact with substrate [185]. Upon removing the stamp form the surface, a pattern is left behind on the surface. The final step is generally backfilling of the non-stamped areas with a second molecule.

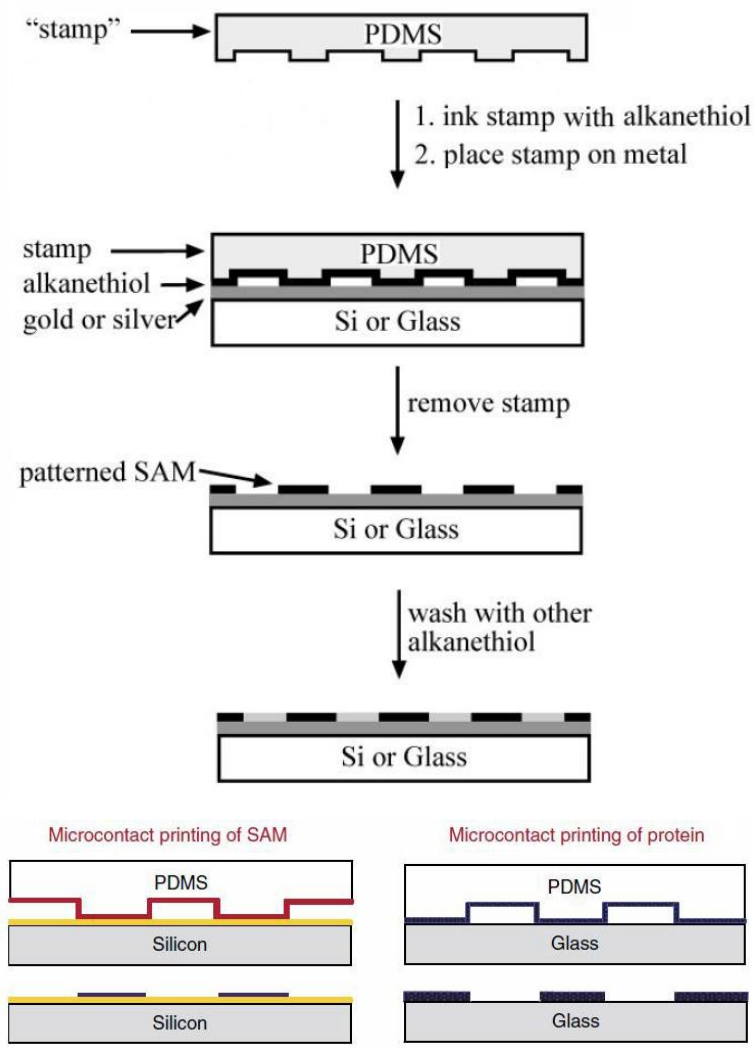

Figure 17. Up: schematic procedures for microcontact printing [185]. Down: microcontact printing of SAM and protein [196]

Microcontact printing is a versatile method for micropatterning since a variety of substrates and molecules are compatible with the technique. In the initial stages, microcontact printing was used to pattern self-assembled monolayers (SAM) of alkanethiols on a surface coated by Au, Ag, Cu, Pd and Pt [185]. Soon, it has been developed to print patterns of molecules (such as proteins) for biological study [185]. Long list of different proteins and peptides have been successfully printed [197].

Mrksich *et al.* used microcontact printing to pattern gold or silver substrates with regions presenting oligo(ethylene glycol) groups and other with methyl groups [198]. After coating the substrates with fibronectin, it adsorbed only on the methyl terminated regions while oligo(ethylene glycol) successfully resisted protein adsorption [199]. Bovine capillary

endothelial cells selectively attached to the fibronectin coated methyl terminated regions, and cells confined to the pattern for at least 5-7 days [199].

In addition to confine cells to specific regions of a substrate, microcontact printing can also be used to change the size and shape of cells and thus to determine the cell fates. Chen *et al.* addressed the cell spreading onto the switching between apoptosis and survival [200].They used microcontact printing to form islands of fibronectin with various geometries on gold, and the substrates were plated with bovine capillary endothelial cells. ECs adhered on fibronectin-coated islands that restricted cell size (mean cell area < 500 μm^2) underwent apoptosis, but ECs on larger islands that permitted spreading (mean cell area > 1500 μm^2) progressed through normal cell cycle [200]. Their study demonstrated that cell shape affects cell growth and cell function. In the subsequent study of the group, ECs were seeded on 10 and 30 μm wide lines of fibronectin [87]. ECs cultured on 30 μm lines spread and proliferated. However, ECs on 10 μm lines of fibronectin initiated capillary morphogenesis and formed tubular structures (Figure 18) [87].

Furthermore, cell-resistant polyelectrolyte was micropatterned on chitosan and gelatin substrates via microcontact printing. Human microvascular ECs formed capillary tube-like structures on 20 μm lines of gelatin after culture for 5 days (Figure 19A-B) [90]. The co-culture of fibroblast and human microvascular ECs on these substrates resulted in the assembly of EC capillary structures wrapping by fibroblast cells (Figure 19C) [90].

For the French colleages, Manuel Théry and co-workers fabricated the ECM (fibronectin) micropatterns on the substrates through microcontact printing [181, 201]. Numerous studies were successfully developped on the spatial distribution of the ECM onto cell artichtecture, cell growth, cell differention, cell division, as well as cell morphogenesis and functions [181, 201]. Micropatterned substrates prepared in their labs have been used successfully with different cells: HeLa-B, RPE1, MCF10A, MCF7, NIH3T3, HepaRG, MDCK, human mesenchymal stem cells, as well as dendritic cells derived from murine bone marrow [181, 202].

Although numerous successes had achieved in various applications, microcontact printing presents problems that need to be solved. For instance, the deformation of the elastomeric stamps or mold [32]. The success of a microcontact printing process highly depends on the mechanical properties of the stamp materials. On one hand, the stamp must be soft enough to enable conformal contact with the substrate, which means it must adapt elastically without leaving voids created by the natural roughness of the substrate. On the

other hand, a precise geometric definition of micropatterns requires a rigid material. These two opposing requirements limit not only the resolution of the technique but also the possible geometries [203, 204].

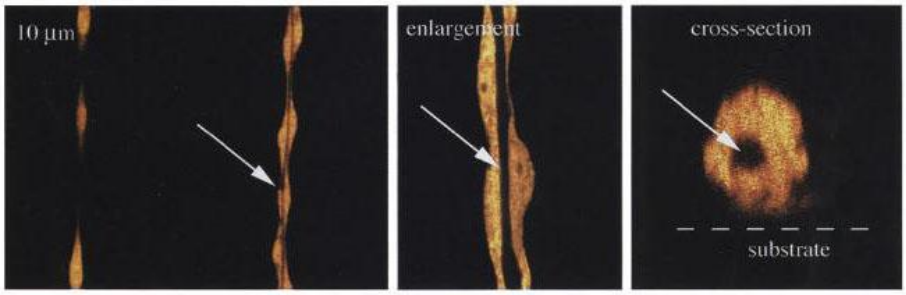

Figure 18. Capillary tube formation by ECs on linear fibronectin patterns. Confocal microscopic images of CMFDA-stained cells cultured on 10 µm lines showed a central cavity extending along several cell lengths (white arrow) when viewed in a horizontal (left and middle) or vertical (right) cross sections (modification after [87]).

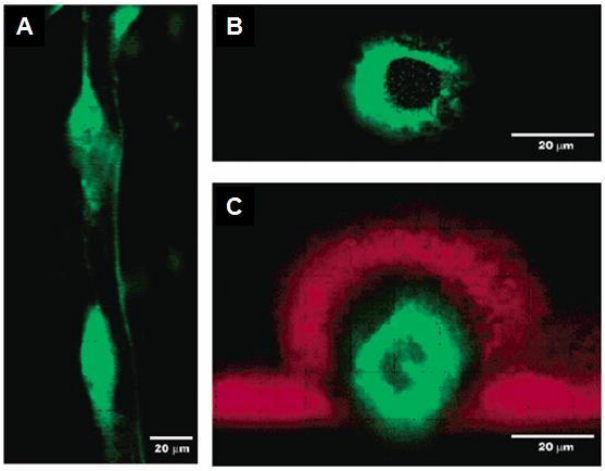

Figure 19. Micropatterning of human microvascular endothelial cells and 3T3 fibroblast cells. ECs and fibroblast cells were prelabeled with Cell Tracker Green and Orange, respectively. Endothelial capillary-like tubes: (A) horizontal and (B) vertical confocal image cross sections of ECs cultured on a 20 µm lines of gelatin show a central cavity extending along cells. (c) Confocal image of the vertical cross section of tube-like structure formed by endothelial cells within a second cell type, fibroblasts ([90]).

Micromolding

Microcontact printing relies on the transfer of material from an "inked" elastomeric stamp to select regions of a substrate. At the same time, patterning can also be carried out by restricting fluid flow to desired regions of a substrate. Kim *et al.* developed a technique which was so-called micromolding in capillary (MIMIC) for fabrication microstructure by allowing solutions to flow into microfluidic channels [205] (also as shown in Figure 20). This method involves in conformal contact a PDMS mold against a substrate to form microchannels [206]. By filling fluids into the microchannels from capillary force, selected areas of the substrate are exposed to the microflow and result in the patterned microstructures on the surfaces of the substrate [206].

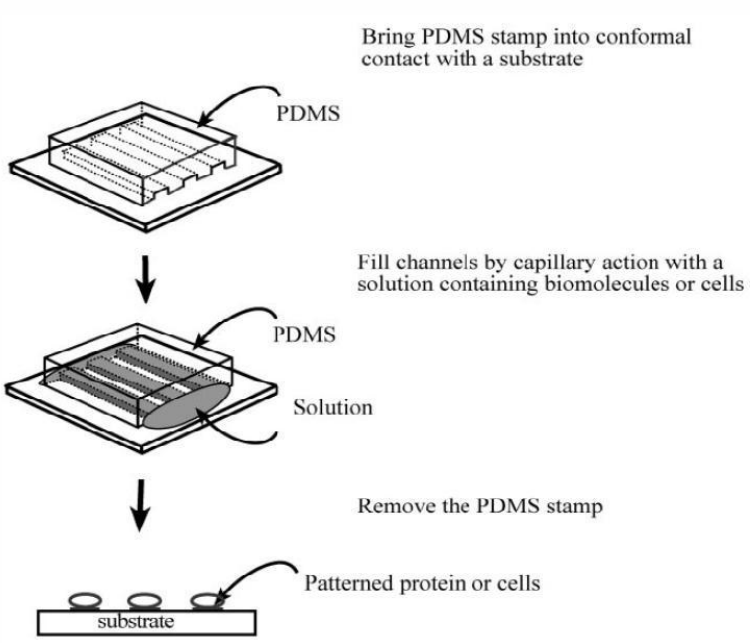

Figure 20. Illustration of the procedure used to pattern proteins and cells using microfluidic channels [185].

Micromolding in capillary is applicable to patterning a broader range of materials, such as polymers, ceramics, sol-gel materials, inorganic salts, colloidal particles and biomolecules [185, 207]. Delamarche *et al.* patterned biomolecules (i.e. immunoglobulin) with submicron resolution on a variety of substrates including gold, glass, and polystyrene, by allowing solutions of the biomolecules to flow through microfluidic channels [208, 209]. Only microliters of reagent were required to cover square millimeter-sized areas. This technique enables simultaneous and highly localized immunoassays for the detection of

different IgGs. Folch *et al.* also used microfluidic channels to produce the patterns of proteins on biocompatible substrates [206, 210]. Micropatterns of collagen or fibronectin were used to cause cells to adhere selectively on various biomedical polymers and on heterogeneous or microtextured substrates [206, 210].

The micromolding patterning has both advantages and disadvantages. Micromolding patterning offers the easiest approach to produce, in a parallel fashion, patterns consisting of many different molecules, which provides a unique opportunity to pattern cells and their environment [208]. It is also possible to produce patterns without the need for drying the surfaces. This is of particular importance for applications of sensitive biomolecules such as labile proteins or enzymes.

Oppositely, this technique is limited by capillary force which is the dominant factor behind the filling of the microchannels. Capillary force driven flow is limited to small areas and channels, thus, the typical length of the device is limited to approximate 1 cm, and it's difficult to form appropriate interconnective networks, which ask for promoting capillary filling. Moreover, it is not suitable for using viscous fluid to do the patterns.

To conquer the above mentioned problems, a range of other microfluidic patterning procedures have been developed, for example, laminar flow patterning [185], pressure filling of molds [32]. Actually, limit to the length, they will not be described here, more details can refer to the review [32].

5.3. 3D microfabrication to generate vascularization

As previously described, most of initial microfabrication techniques tend to generate 2D micropatterning on biomaterial surfaces, thus to study the cell function and cell morphogenesis on them. Although vascularized systems are readily constructed in 2D by photolithographical or soft-lithographical techniques, their construction in 3D remains a challenging problem. Indeed, *in vivo*, cells reside within 3D environments in close proximity to blood vessels. Recently, more complex microfabrication technologies were developed to fabricate 3D scaffold system, thus to trigger 3D physiological environment for cell culture. This section illustrates some pioneer works of 3D microfabrications for application in cell biology, especially for the application in vascularization.

Lee *et al.* [211] conjugated RGDS with fibroblast encapsulated agarose gels via 3D laser lithography, the confocal images clearly revealed cells underwent 3D migration within the Y-shaped RGDS channels.

Raghavan *et al.* presented a novel approach for patterning cells within collagen gels for controlling endothelial tubulogenesis [212]. In their study, endothelial cells cultured within microscaled channels which were filled with collagen gel organized into tubes with lumen within 24-48 h of seeding (Figure 21A). These tubes extended up to 1 cm in length, and exhibited cell–cell junction formation characteristic of early stage of capillary vessels. Tube diameter could be controlled by varying collagen concentrations or channel width [212]. The geometry of the microfabricated template could also be used to guide the development of branches during tube formation, allowing for the generation of more complex capillary architectures [212].

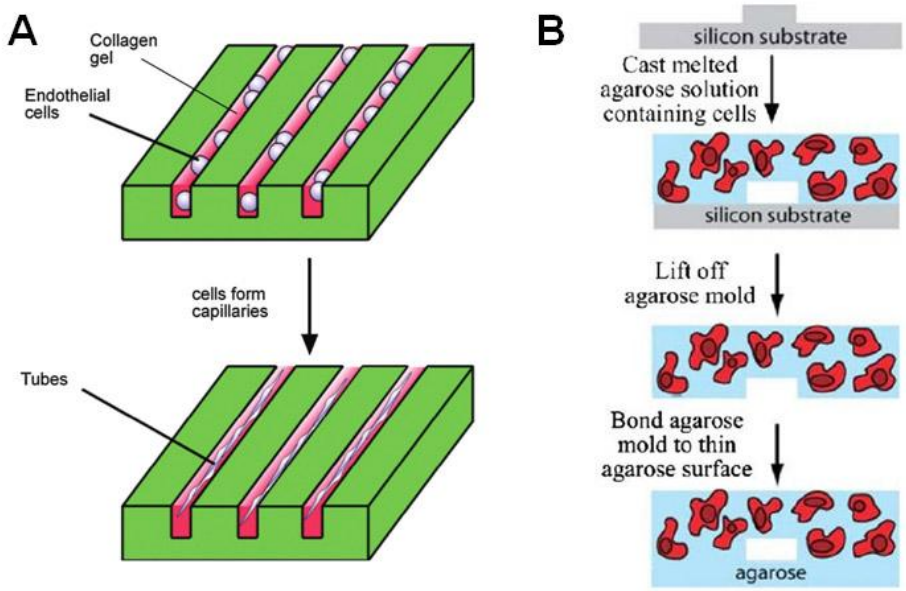

Figure 21. (A) Schematic of method to organize cells and collagen gel in microfabricated channels to form tube structures ([212]). (B) Schematic of the fabrication of agarose microfluidic devices with embedded cells [213]

Ling *et al.* fabricated microfluidic cell-laden agarose hydrogels using soft lithography [213]. Agarose solution suspended with hepatic cells was poured and gelled against templates. The surfaces of the molded agarose and another agarose slab were subsequently heated and sealed together to generate microchannels (Figure 21B). Media pumped through the channels ensured effective delivery of nutrients and removal of waste products. It concluded that hepatic cells were homogeneously distributed in the molded agarose. However, only those

cells in close proximity to the channels remained viable after 3 days' culture, demonstrating the importance of a perfused network in large hydrogel constructs [213].

Build large 3D vascular structures can be obtained by stacking and assembling 2D vascularized layers. King *et al.* developed a scalable fabrication platform for constructing highly branched, multiplayer PLGA microfluidic networks that mimicked tissue microvasculature [214]. In this approach, two or more micro-patterned PLGA networks could be bonded by a pure thermal bonding process to form a 3D biodegradable microfluidic device (Figure 22A). However, this method is a cumbersome process requiring multiple fabrications and masking steps which is difficult to scale-up. Innovative technology was developed to directly fabricate 3D microvascular networks [215]. Lim *et al.*, demonstrated a faster and more flexible method to fabricate multiple-level microfluidic channels using a maskless laser direct micromachining [215], a multi-width and multi-depth microchannel was fabricated to generate biomimetic vasculatures whose channel diameters changed (Figure 22B). These 3D microvascular networks will provide an enabling platform for mimic physiological flow in engineered constructs.

Stroock et al. developed microfluidic scaffolds for 3D tissue engineering [216], and revealed that the approach to control the chemical environment on a micrometre scale within a macroscopic scaffold could aid in engineering complex tissues [216].

The group of Christopher S. Chen recently developed the rapid casting of patterned vascular networks, and demonstrated that the perfused vascular channels sustained the metabolic function of hepatocytes in engineered 3D tissues constructs [217].

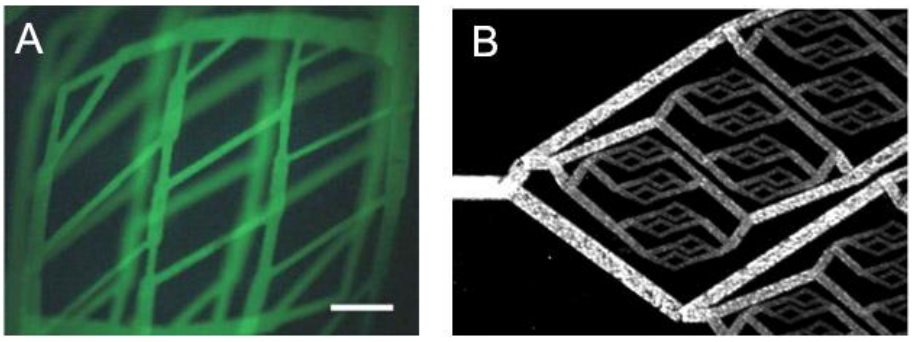

Figure 22. Microfabrication to generate 3D vascularized tissue constructs. (A) A multilayer PLGA microfluidic networks perfused with fluorescein dye [214]; (B) Eight level multi-width and multi-level microvasculature network microchannels fabricated by one-step laser direct writing. Fluorescent image shows the difference in intensity levels corresponding to different channel depths [215]

In general conclusion, the above sections related with technological progress in manipulating cells with micropatterning. The micropatterning methods discussed above have revealed important insights into how the geometry of the microenvironment impacts on cellular physiology, from intracellular organisation to multicellular morphogenesis. The well-defined 2D micropatterned surfaces can provide useful tools to control cell-material interface, to regulate the capillary morphogenesis and to investigate the process of angiogenesis; while the 3D microfabrication techniques are more complex but can construct 3D physiological cellular environment, and offer new opportunities to build vascularized constructs. These techniques enhance our ability to control the cellular environment, and would help increase our understanding of fundamental cell biology.

Organized neovascularization in engineered tissues may allow development of tissues with large mass and complexity. To achieve this requirement, several key issues remain to be addressed. Firstly, we need a better understanding of biology behind neovascularization. Understanding the natural course of angiogenesis and vasculogenesis provides fundamental basis upon which we can build and optimize new vessel growth in biomaterials. Then, we need to optimize fabrication of scaffold-biomolecule hybrids. The performance of biomaterials in conjunction with incorporated bioactive factors (peptides, proteins, growth factors, etc...) needs to be addressed. For instance, organization of biomolecules and cells in biomaterials needs to be optimized to mimic tissue complexity, and micro- and nano-patterning methods may provide solutions. Last but not ended, we need to integrate pre-vascularized tissue constructs with functional cells of interest. To create functional blood vessels, the native cell types have to be either included or recruited into the scaffolds along with vascular cell types. The resulting interaction among multiple cell types has to be carefully examined so that functional tissues are regenerated with complete network of blood vessels.

Problems and Objectives

Vascular engineering remains a key factor in advancing the field of tissue engineering with highly vascularized, complex, metabolic organs.

In this study, we focused on characterizing the microenvironment which was responsible for angiogenesis of endothelial cells. The main objective of this study is control of both the biochemical ligands and micro-geometrical distribution of ligands on biomaterial surfaces to mimic the physiological microenvironment of ECs.

Till now, a wide variety of strategies have been employed to control the formation of organized vascular structures *in vitro* and *in vivo*. Some of these methods include, but are not limited to, controlled growth factor delivery [44, 46], surface bioactivity (nature and density of the ligands on surfaces) [86, 95, 218], biomolecule micropatterning [87], filamentous scaffold geometry [97], enhanced scaffold biomaterials [219]. Majority of these approaches are motivated by bio-mimicking of the *in vivo* microenvironment. Unfortunately, no general consensus (assembling several of these parameters) has been achieved to explain which of these parameters allow the angiogenesis of ECs since all studies proposed different models.

In this study, we developed several models of *in vitro* cell culture combining materials and endothelial cells. Our objective was to understand the process of angiogenesis and explain the involvement of biochemical and microgeometrical properties of the microenvironment in this process. We developed bioactive biomaterials (polymers functionalized with different peptides, and controlled their distribution at the micrometer scale) that may mimic a physiological situation of ECs. We propose in Figure 23 the schematic of the thesis.

Initially, we elaborated the polymer surfaces, which are biochemically modified by peptide ligands to study their specific interaction with endothelial cells (Paper I).

Then, the surfaces micropattening with peptides were developed to modulate the angiogenesis of endothelial cells (Paper II, III, and IV). The peptide micropatterning promoted the organization of ECs into well-defined tubular structures *in vitro*. The mechanism of angiogesis was carried out thereafter (Discussion): the induction of angiogenesis is multiparametric and has strong relationship with biochemical constituents and their micro-distribution.

At last, co-culture of endothelial cells with pericytes/mesenchymal stem cells as well as recruitment of basement membrane components was developed in this study, for the purpose to enhance capillary structures' stabilization (Paper V).

This work helps us understanding the biology of angiogenesis and may help for applications in tissue engineering.

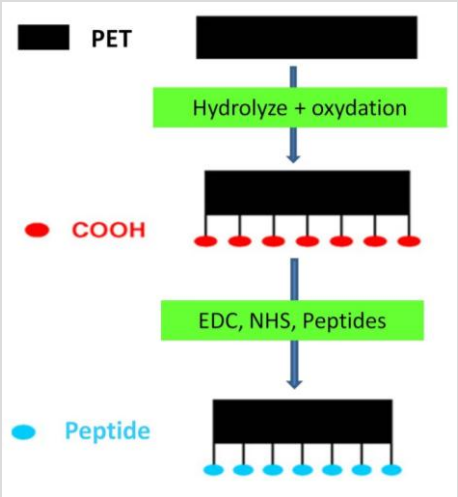

Axis 1:

Biochemiacal modification by peptides for modulating of endothelial cell functions (Paper I)

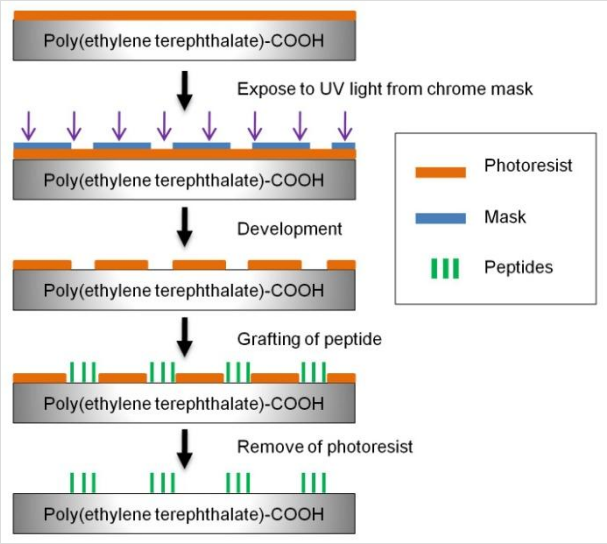

Axis 2:

Microscale modification for inducing endothelial cell angiogenesis and functional vascularization (Papers II-V)

Figure 23. Schematic summary of the objectives of the thesis

Results and Discussions

1. Biochemical Modification for Endothelial Cell Functions

Introduction

Control over endothelial cell (EC) responses at the biomaterial interface is important for endothelialization of vascular prostheses and construction of vascularized tissues [180, 220]. Immobilization of functional peptides onto biomaterial surfaces for modulating cell behavior is scientifically attractive in vascular research [221].

Various peptide sequences have been grafted onto materials to enhance biological properties [159, 221]. Among them, RGD sequence is featured in the largest number of biomaterial studies for promote cell adhesion [149]. Besides RGD, other peptides which are more specifically addressing to ECs were well documented in the literatures to investigate EC functions, such as REDV [162-164], YIGSR [166, 168], and angiogenic SVVYGLR peptides [173-175]. Meanwhile, the combination of peptides was also used to ensure a physiological environment for cell behaviors [222, 223].

In this study, we aimed to covalently immobilize the cell adhesive RGDS, EC specific REDV and YIGSR, angiogenic SVVYGLR sequences as well as combination of peptides onto polyethylene terephthalate (PET) surfaces for the purpose to study specific EC functions. A three step procedure was employed to covalently immobilize these peptides onto PET surfaces. The surface modification was characterized by chemical-physical measurements. Then the surfaces immobilized with peptides were exposed to ECs to study their specific effects onto EC functions.

The main results obtained in this paper are:

(a) The presence of each or combination of peptide onto PET surfaces was confirmed by XPS, AFM, contact angle measurement and fluorescence microscopy observation.

(b) The peptide density on PET surfaces evaluated by fluorescence microscopy was similar on each surface, no significant difference of peptide density was observed between each peptide.

(c) The surface functionalized by these peptides enhanced the EC adhesion, spreading and migration as compared with native PET surfaces. Specifically, the RGDS peptides induced more cell adhesion. Moreover, the YIGSR and SVVYGLR sequences induced more cell spreading and cell migration.

This study indicates that the surface functionalization with peptides specific for ECs has potential applications in promoting endothelialization of vascular prostheses and for construction of vascularized tissues in tissue engineering.

Paper I. Surface functionalization of polyethylene terephthalate by peptides to study specific endothelial cell adhesion, spreading and migration

Journal of Materials Science: Materials in Medicine. 2012. Accepted.

Surface functionalization with endothelial cell specific peptides was used to study their effects onto endothelial cell functions. The peptide functionalization can give bioactivity to polymer surfaces, and induce different levels of cell adhesion, spreading and migration.

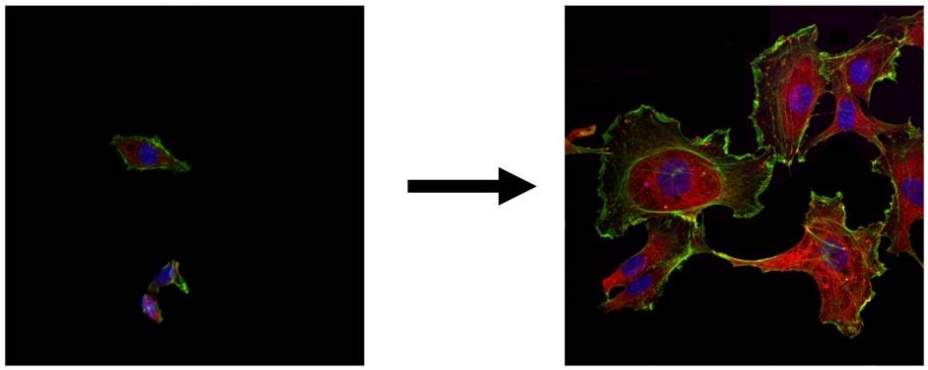

Figure 24. Endothelial cell morphology on native PET surfaces (left) and on surfaces grafted with angiogenic SVVYGLR peptides.

J Mater Sci: Mater Med
DOI 10.1007/s10856-012-4736-x

Peptide immobilization on polyethylene terephthalate surfaces to study specific endothelial cell adhesion, spreading and migration

Yifeng Lei · Murielle Rémy · Christine Labrugère · Marie-Christine Durrieu

Received: 29 March 2012 / Accepted: 26 July 2012
© Springer Science+Business Media, LLC 2012

Abstract To control specific endothelial cell (EC) functions, cell adhesive RGDS, EC specific REDV and YIGSR peptides, and angiogenic SVVYGLR sequences were covalently immobilized onto polyethylene terephthalate (PET) surfaces for the purpose of cell culture. X-ray photoelectron spectroscopy, atomic force microscopy, fluorescence microscopy and contact angle measurement were employed for characterization of surface modifications. The peptide density on PET surfaces was evaluated by fluorescence microscopy. The surfaces immobilized with peptides were exposed to human umbilical vein endothelial cells to study their specific effects onto EC functions. The results showed that the surface functionalized by these peptides enhanced the EC adhesion, spreading and migration as compared with native PET surfaces. Specifically, the RGDS peptides induced more cell adhesion than other peptides. The YIGSR and SVVYGLR sequences induced more cell spreading and cell migration, represented by intense focal adhesion at the leading edges of cell spreading and migration. The bi-functionalization of RGDS and SVVYGLR peptides (MIX) combined the advantages of both peptides and induced significant EC adhesion, spreading and migration. Our study indicates that the surface functionalization by peptides specific for ECs, especially the combination of RGDS with SVVYGLR or YIGSR peptides, has potential applications in promoting endothelialization of vascular prostheses and for construction of vascularized tissues in tissue engineering.

Y. Lei (✉) · M. Rémy · M.-C. Durrieu
Université Bordeaux Segalen, Inserm U1026, Bioingénierie Tissulaire, 146 rue Léo Saignat, 33076 Bordeaux, France
e-mail: yifeng.lei@inserm.fr

Y. Lei · M.-C. Durrieu
Université de Bordeaux 1-CNRS, CBMN UMR 5248, Institut Européen de Chimie et Biologie, 2 rue Robert Escarpit, 33607 Pessac, France

C. Labrugère
Université de Bordeaux-CNRS, ICMCB, 87 avenue du Dr Albert Schweitzer, 33608 Pessac, France

1 Introduction

Endothelialization of vascular prostheses is an active research topic [1]. It's known that vascular prostheses supporting a layer of endothelial cells (ECs) would have better resistance to thrombosis and prostheses stenosis [1, 2]. Control over EC responses at the biomaterial interface is important for endothelialization of vascular prostheses [1].

Synthetic polymers are widely used in biomedical applications. Among them, polyethylene terephthalate (PET) is widely used as a material for surgical suture, vascular grafts (as Darcon®) and anterior cruciate ligament prostheses due to its biocompatibility and mechanical properties such as strength and resistance [3]. Nevertheless, PET surfaces are too hydrophobic for cells to adhere directly, and surface modification is needed in order to improve interaction between the implant and surrounding tissue. A variety of techniques have been explored to modify the biomaterial surface properties to modulate EC adhesion and cell responses: chemical modification by bioactive molecules [1, 4, 5], physical modification by altering the surface mechanical properties [6] and topography [7], etc.

To date, immobilization of biomolecules on biomaterial surfaces remains a center of interest in vascular research. International literature shows an important panel of strategies in order to functionalize biomaterial surfaces using different bioactive principles and thereby assisting specific

Published online: 10 August 2012

cell adhesion and influencing intracellular pathways. Among them, immobilization of functional peptides onto biomaterial surfaces for modulating cell behavior is scientifically attractive [8]. The use of small peptides sequences derived from the extracellular matrix (ECM) proteins has many advantages: chemical definition, stability, controllable density, higher control over the elicited cell response, as well as possibility to be grafted onto a substrate [9, 10].

Various peptide sequences have been isolated and grafted onto materials to enhance biological properties [4, 8]. Among the peptides investigated, RGD is featured perhaps in the largest number of biomaterials studies [9]. RGD is the principal integrin-binding domain presented within many ECM proteins [11]. RGD binds to cell integrin receptors on a wide variety of cell types to impact cell attachment strength, cytoskeletal reorganization, cell spreading and migration [10]. RGD peptides have been grafted onto polymers, metals and ceramics to enhance cell adhesion and focal contact formation [4, 12, 13].

Besides RGD, other peptides which are more specifically addressing to ECs were well documented in the literatures. REDV sequence is a domain derived from fibronectin [14, 15], the immobilized REDV peptides on synthetic surfaces induced attachment and mediated migration of ECs, while simultaneous binding and spreading of fibroblast or smooth muscle cells are inhibited [14, 16]. YIGSR is an active sequence derived from B1 chain of laminin [17]. This peptide promotes adhesion and spreading of ECs [18]. Polyurethanes incorporated with PEG and YIGSR peptides enhanced endothelialization without platelet adhesion [19]. The surfaces of RGD combined with YIGSR peptides were found to enhance the EC migration as compared with RGD alone [20]. SVVYGLR is a novel binding sequence found in osteopontin molecules following thrombin cleavage [21]. SVVYGLR sequences specifically enhance EC migration activity [22], and possess an angiogenic activity as strong as VEGF in its soluble form [23].

In the literatures, the combination of peptides was also used to ensure a physiological environment for cell behaviors [5, 24]. Rezania and Healy [24] developed mimetic peptide surfaces (MPS) by mixing different ratios of RGD and FHRRIKA to study rat calvaria osteoblast-like (RCO) cell function, in the mixtures of the two in the ratio of 25:75 (MPS II) or 50:50 (MPS III), they were more biologically relevant and specific for RCO cells. MPS II and MPS III supported greater cell spreading, promoted the formation of foal contacts and stress fibers, and enhanced mineralization of the ECM compared to homogenous peptide surfaces and controls [24]. Zouani et al. [5] mixed RGD and BMPs mimetic peptides (50:50) to evaluate the state of differentiation of pre-osteoblastic cells, the combination of peptides acted to enhance osteogenic differentiation and mineralization of pre-osteoblastic cells [5].

In this study, we aimed to covalently immobilize the cell adhesive RGDS, EC specific REDV and YIGSR, angiogenic SVVYGLR sequences as well as combination of peptides onto PET surfaces for the purpose of cell culture, and to examine exactly what cellular morphologic changes can be correlated to these specific bioactive motifs. Bi-functionalization of adhesion RGD peptide and angiogenic SVVYGLR peptide was used to mimic physiological microenvironment for endothelial cells. One aim of bi-functionalization is to firstly ensure cell adhesion via RGD peptides, and secondly to allow endothelial cell angiogenic activity (migration, etc.) via SVVYGLR peptides. Human umbilical vein endothelial cells (HUVECs) were cultured to study specific effects of each or combination of peptides onto EC functions. The impact of the biomaterials functionalized by one or several active principles will be investigated at the cellular level (HUVECs). We propose (i) first of all to study cell adhesion (ii) to evaluate the cell spreading level (iii) to measure cell migration, and (iv) to characterize the evolution of cellular cytoskeleton organization and focal adhesion assembly.

2 Materials and methods

2.1 Materials

The PET films were purchased from Goodfellow, France. Inorganic reagents (NaOH, $KMnO_4$, H_2SO_4 and HCl), acetonitrile, dimethylaminopropyl-3-ethylcarbodiimide hydrochloride (EDC), *N*-hydroxy Succinimide (NHS) and 2-(*N*-morpholino)-ethanesulfonic acid (MES) were obtained from Sigma-Aldrich, France. GRGDS, GREDVY, GYIGSR and GDSVVYGLR peptides as well as fluorescent peptides were synthesized by Genecust, France.

2.2 Covalent immobilization of peptides onto PET surfaces

The peptides were covalently immobilized onto PET surfaces according to Chollet et al. [4, 25]. Briefly, PET surfaces were hydrolyzed and oxidized in order to create –COOH function groups on PET surfaces (PET-COOH, referred as "COOH"). Then the samples were immersed in solution of EDC (0.2 M) + NHS (0.1 M) + MES (0.1 M) in MilliQ water for activation (PET-NHS, labeled as "NHS"). Finally, each peptide (GRGDS, GREDVY, GYIGSR and GDSVVYGLR) was dissolved in phosphate-buffered saline (PBS) solution (10^{-3} M for each), and the activated samples were immersed in peptide solution for

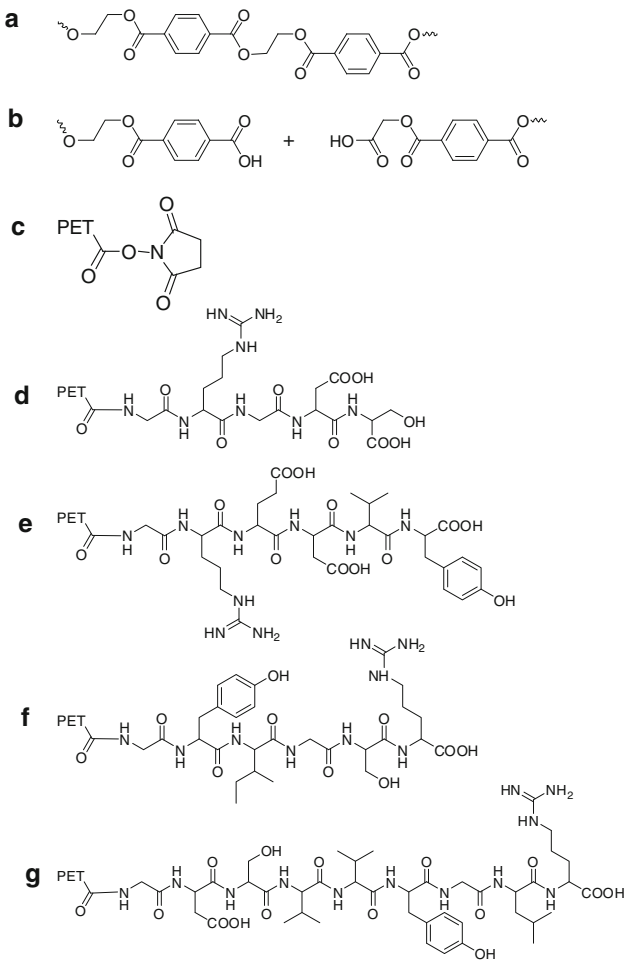

Fig. 1 Schematic of peptide immobilization onto PET surfaces. **a** Native PET; **b** PET hydrolyzed and oxidized to obtain –COOH group (PET-COOH); **c** PET activated with NHS (PET-NHS); PET surfaces immobilized with **d** GRGDS; **e** GREDVY; **f** GYIGSR and **g** GDSVVYGLR peptides

covalent immobilization of peptides for 16 h at room temperature. In another condition, the combination of GRGDS (0.5×10^{-3} M) and GDSVVYGLR (0.5×10^{-3} M) peptides was used. After covalent immobilization, the surfaces were rinsed with MilliQ water for 1 week in order to remove the physically adsorbed peptides. Native PET, PET surfaces grafted with GRGDS, GREDVY, GYIGSR, GDSVVYGLR and the mixture of GRGDS and GDSVVYGLR peptides are named as PET, RGDS, REDV, YIGSR, SVVYGLR and MIX, respectively. A schematic for each peptide immobilization onto PET surfaces is shown in Fig. 1.

2.3 X-ray photoelectron spectroscopy (XPS)

The chemical composition during surface modification was determined by XPS on a VG Scientific ESCALAB photoelectron spectrometer, with an MgK X-ray source (1253.6 eV photons, 100 W). Spectra fitting and determination of atomic composition were realized with software provided by VG Scientific, with each spectrum being referenced by setting carbon pollution at 284.8 eV.

2.4 Atomic force microscopy

Atomic force microscopy (AFM) was used to characterize the surface morphology and surface roughness. AFM (Dimension 3100, Veeco) was performed in tapping mode at a rate of 0.4 Hz at room temperature.

2.5 Contact angle measurement

The surface wettability was evaluated by DIGITROP contact angle meter (GBX Society, France). Static water contact angles were measured by deposing a droplet of distilled water onto the sample. The mean value of contact angle from at least eight measurements was calculated for each surface.

2.6 Evaluation of peptide density by fluorescence microscopy

To determine the peptide density on PET surfaces, PET were immobilized with fluorescent peptides and evaluated by fluorescence microscopy according to Pichavant et al. [26]. Briefly, FITC fluorochrome was covalently linked to the end of each of the peptides via Lysine (K), for instance, GRGDS was linked to FITC fluorochrome via Lysine (labelled as GRGDSK–FITC). Then the fluorescent peptides were immobilized onto PET surfaces as described previously. Quantification of fluorescence intensity on surfaces with FITC-labelled peptides was performed with fluorescence microscopy (Leica DM5500B, Germany) and Leica MMAF software. Firstly, a calibration curve was established: a series of FITC with well-known quantities (from 1.1 to 18.4 nmol) was deposited on native surfaces and photographed with fluorescence microscopy at magnification of 2.5, and the total fluorescence was quantified by Leica MMAF. Then the surfaces grafted with FITC-labelled peptides were observed at the same magnification, and the fluorescence on each surface was quantified by Leica MMAF. Finally, the density of fluorescent peptide was determined according to the calibration curve (in nmol/cm^2). Similarly, we also used TAMRA fluorochrome for the measurement of peptide density on PET surfaces.

2.7 Fluorescent peptide visualization

To furtherly confirm the presence of peptides onto PET surfaces, surfaces were immobilized with different fluorescent peptides and characterized by fluorescence microscopy

as described by Zouani et al. [5]. For instance, GRGDS peptides were linked to FITC fluorochrome via Lysine (K) (labelled as GRGDSK–FITC), and GDSVVYGLR peptides were linked to TAMRA fluorochrome via Lysine (K) (labelled as GDSVVYGLRK–TAMRA), respectively. FITC or TAMRA fluorochromes were linked in a covalent manner at the C-terminal end of the different peptides. Epi-fluorescence microscopy was employed for visualization of fluorescent peptides immobilized onto PET surfaces. Furthermore, the peptide density was calculated according to the calibration curve of FITC or TAMRA fluorochrome as described in the above section.

We used fluorescent peptides for surface visualization and characterization. However, we used normal peptides without fluorochrome to carry out the biological tests.

2.8 Cell culture

HUVECs were obtained from the human umbilical cord vein according to the descriptions previously [27, 28]. HUVECs were isolated and grown on gelatin coated culture flasks in complete HUVEC medium (IMDM (Invitrogen, France) supplemented with 20 % fetal bovine serum (FBS) (PAA, France) and 0.4 % EC growth supplement/heparin kit (Promocell, France)). Cells were subcultured using trypsin/EDTA (Invitrogen, France) and maintained in a humidified atmosphere containing 5 % CO_2 at 37 °C. Cells at passages 3–5 were used for experiments.

2.9 Cell attachment test

Cell attachment was measured by a modified method according to Landegren et al. [29]. The samples (1 × 1 cm) were sterilized with 70 % ethanol and rinsed by PBS, then placed in cell culture plates and fixed by glass rings. HUVECs were seeded onto PET surfaces functionalized with each peptide and on controls (PET, COOH, or gelatin coated culture plates) at a density of 50000 cells/cm^2 in serum-free DMEM medium without phenol red (Invitrogen, France) in 5 % CO_2 at 37 °C. After 4 h, serum-free medium was removed and cells were cultured in DMEM medium containing 10 % FBS till 24 h. After cell attachment for 4 or 24 h, non-adherent cells were removed by PBS rinse. 500 µl chromogenic substrate solution (7.5 mM chromogenic substrate (p-nitrophenyl-*N*-acetyl βD-glucosaminide); 0.1 M Na citrate; 0.5 % Triton-X 100; adjust pH = 5) was added onto each sample and incubated at 37 °C for 2 h. The reaction was stopped with stop solution (5 mM EDTA; 50 mM glycine; adjust pH 10.4). The resulting chromophore was measured using spectrophotometry at 405 nm. Six parallel samples were used for each surface. And data were obtained from two experiments.

2.10 Immunofluorescent staining

Immunofluorescent staining were performed 24 h after cell seeding at a density of 50000 cells/cm^2 (4 h in serum-free IMDM medium, then in IMDM medium supplemented with 10 % FBS till 24 h). The cells were fixed by 4 % paraformaldehyde, permeabilized with 0.5 % Triton-X 100 and blocked with 1 % bovine serum albumin (BSA) in PBS. Samples were then incubated with mouse anti-vinculin primary antibody (Sigma, France) at 37 °C for 1 h, and coupled with Alexa Fluor® 568 rabbit anti-mouse IgG secondary antibody (Invitrogen, France) for 30 min at room temperature. Subsequently F-actin filament was stained with Alexa Fluor® 488 phalloidin (Invitrogen, France) for 1 h at 37 °C. Nuclei were counterstained by DAPI (Sigma, France) for 10 min at room temperature. The samples were mounted and observed with fluorescence microscopy.

2.11 Quantification of cell adhesion and spreading

Fluorescent images of cell staining at low magnification (10×) were randomly photographed and ImageJ (NIH, http://rsb.info.nih.gov/ij/) was used for image analyses. Cell nuclei were counted for evaluation of adherent cell number. The cell areas were determined by tracing the cell edges from F-actin cytoskeleton. At least 20 fields on each surface were analyzed. Data were obtained from three experiments.

2.12 Organization of actin cytoskeleton and focal contact assembly

For characterization of actin organization and focal contact assembly of ECs on each surface, fluorescent images at high magnification (40×) were analyzed by ImageJ. At least 50 cells were analyzed for each surface.

2.13 Cell migration

To analyze EC motility on different surfaces, tomato-labeled HUVECs (red) were seeded in complete HUVEC medium at lower density of 30000 cells/cm^2 in order to get individual cells on each surface. Cells were allowed to adhere in incubator for 4 h, then the samples were transferred to time-lapse microscopy (Leica DM5500B) in a humidified atmosphere containing 5 % CO_2 at 37 °C, and the cell migration was monitored by Leica MMAF software and automated stages. The images were photographed in intervals of every 6 min during 12 h. Then the videos were analyzed using free software "Time Lapse Analyser" (TLA: http://www.informatik.uni-ulm.de/ni/staff/HKestler/tla/). For quantification of cell motility, cell trajectories, total distance traveled

by cells and migration rate of ECs (μm/min) were calculated. A minimum of 30 cells on each surface were analyzed. And experiments were done in duplicate for each surface.

2.14 Statistical analysis

Data were represented as mean values ± standard deviation (SD). Statistical analysis was performed using Student's paired *t* test. A *P* value less than 0.05 was considered to be statistically significant.

3 Results

3.1 Characterization of peptide immobilization by XPS and AFM

XPS was employed to determine the surface chemical composition during surface modification. The XPS spectra during different steps of chemical modifications are shown in Fig. 2. The native PET surfaces exhibit only C and O elements as expected (Fig. 2a). The O/C experimental ratio on PET surfaces is 0.380 (Table 1), which is different from the theoretical ratio of 0.533. The differences between experimental and theoretical ratio are due to semi-quantification property of XPS and the surface contamination like adsorption of CO_2 in air. As compared with PET surfaces, COOH surfaces (Fig. 2b) showed an increased O/C ratio to 0.431 (Table 1), confirming the expected surface modification of oxidation. After NHS activation, new N1s peaks appeared at about 399.85 eV as expected (Fig. 2c), corresponding to the successful grafting of NHS onto the surfaces. After peptides immobilization, XPS atomic analysis confirms the increase of nitrogen due to the presence of peptides onto the surfaces, which was represented by the increased N/C ratio as compared with NHS surfaces (Table 1). As peptide is longer (Fig. 1), the N/C ratio trended to be more significant (Table 1). These results indicated the successful immobilization of peptides onto PET surfaces by covalent interaction. However, no significant difference in XPS spectra appeared after co-immobilization of MIX as compared with single immobilization with RGDS or SVVYGLR alone. It is difficult to distinguish between the two peptides by XPS due to the overlapping of N1s elements for both peptide sequences.

The surface topography during surface modification was shown in Fig. 3. Commonly, the hydrolysis and oxidation step caused a rough PET surface, AFM analysis revealed a significant change of surface roughness from PET surfaces (1.3 ± 0.2 nm) to PET-COOH surfaces (6.4 ± 0.6 nm). However, the roughness of surfaces grafted with peptides was similar to PET-COOH surfaces (for instance,

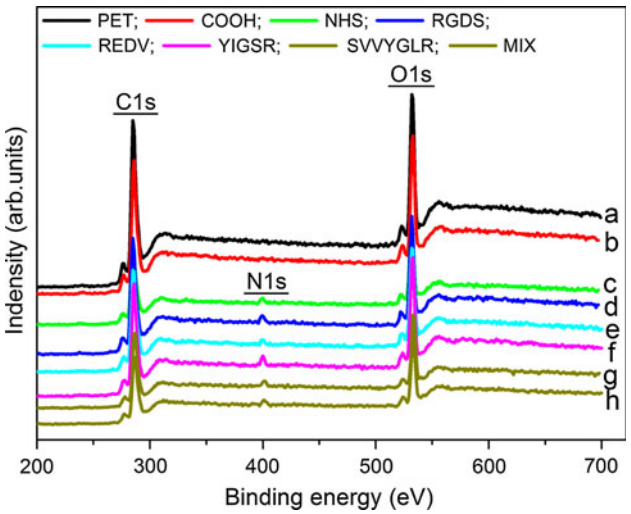

Fig. 2 XPS spectrum of *a* PET; *b* PET-COOH; *c* PET-NHS; and PET surfaces grafted with *d* GRGDS; *e* GREDVY; *f* GYIGSR; *g* GDSVVYGLR and *h* MIX peptides

6.6 ± 0.5 nm for surfaces grafted with RGD, Fig. 3b). No significant difference was observed between PET-COOH and surfaces grafted with different peptides (Fig. 3c). Previous results showed that the thickness of grafted RGD layer onto polymer was very small (1.5 nm determined by Brewster angle microscopy measurements, data not published), this may explain why there was no significant difference of surface roughness of different peptide surfaces by AFM observation.

3.2 Contact angle measurement

The water contact angles were measured during different steps of surface modification (Fig. 4). PET surfaces were hydrophobic and presented the contact angles of 80.8 ± 3.2°. The water contact angle significantly decreased to 52.6 ± 3.6° on COOH surfaces. Surface roughness and chemical composition on material surfaces are two of the key factors to determine the surface wettability. The hydrolysis and oxidation process changed not only the surface chemical composition, but also significantly modified the surface roughness (1.3 ± 0.2 nm of PET surfaces to 6.4 ± 0.6 nm of COOH surfaces, Fig. 3), thus resulting in the significant decrease of water contact angles from PET to COOH surfaces. The surface activation with NHS reduced the contact angle to 46.4 ± 2.3°, mainly due to the chemical changes on the surfaces. After peptide grafting, whatever the type of peptides, the peptide immobilization involved in a reduction in contact angles as compared with PET and COOH surfaces (Fig. 4), indicating an increase in surface hydrophilicity after peptide immobilization. The peptide immobilization introduced a lot of hydrophilic groups such as –OH, –COOH (Fig. 1) and thus improved the surface hydrophilicity. RGDS

Table 1 Experimental atomic composition (%) obtained by XPS analysis in case of native and modified PETsurfaces

	C	O	N	O/C	N/C
PET	72.5	27.5	–	0.380	–
COOH	69.9	30.1	–	0.431	–
NHS	68.4	29.0	2.6	0.424	0.038
RGDS	69.4	27.7	2.9	0.399	0.042
REDV	69.5	27.3	3.1	0.392	0.044
YIGSR	68.2	27.2	3.8	0.400	0.056
SVVYGLR	66.4	29.2	3.9	0.440	0.059
MIX	67.9	28.1	3.2	0.414	0.047

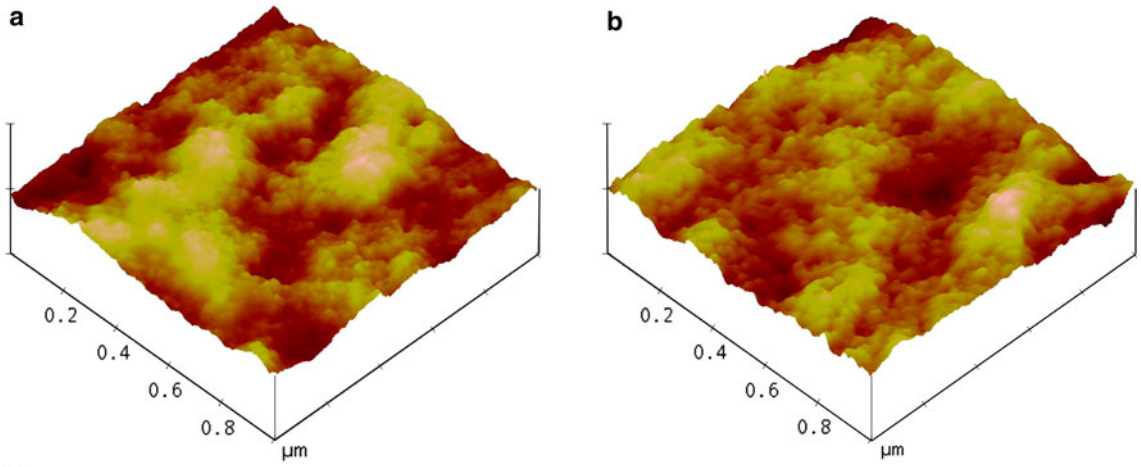

c

PET	COOH	RGDS	REDV	YIGSR	SVVYGLR	MIX
1.3 ± 0.2	6.4 ± 0.6	6.6 ± 0.5	6.5 ± 0.7	6.5 ± 0.4	6.7 ± 0.5	6.7 ± 0.8

Fig. 3 AFM images of the surface morphology of: **a** PET-COOH surfaces; **b** PET surfaces grafted with GRGDS peptides and **c** surface roughness (*Ra*, nm) of different surfaces by AFM analysis

surfaces were the most hydrophilic as indicated by the smallest contact angles (Fig. 4), this enhancement in hydrophilicity may be associated with the –OH group at the end of RGDS sequences as compared with other peptide sequences (Fig. 1).

3.3 Peptide density

Peptide density on each surface was estimated by grafting fluorescent peptides with FITC fluorochrome and hence measuring fluorescent activity by fluorescence microscopy. The peptide density was evaluated at 22.5 ± 3.8, 24.9 ± 5.1, 21.7 ± 5.8, 21.2 ± 4.7 and 25.5 ± 5.7 nmol/cm^2 for PET surfaces grafted with RGDS, REDV, YIGSR, SVVYGLR and MIX peptides, respectively. The peptide density on PET surfaces evaluated in the present study was much more significant as compared with RGD peptide density on PET surfaces of 1.7 ± 0.3 pmol/mm^2 evaluated by Chollet et al. [25] with high resolution micro-imager.

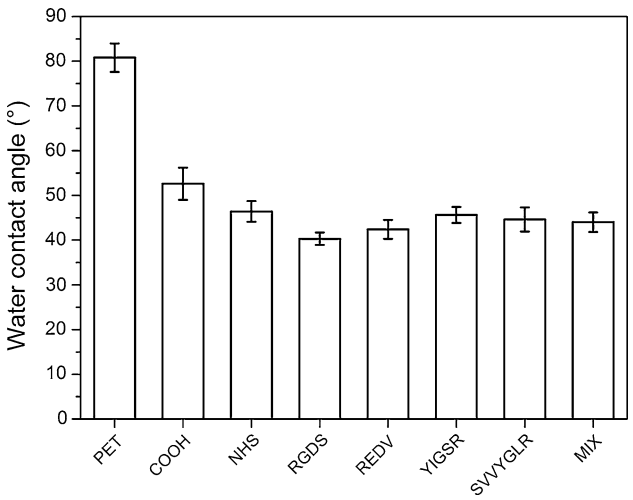

Fig. 4 Water contact angles on native and modified PET surfaces

The peptide densities in these two studies are different due to the different techniques used. However, using the same measuring approach, in this study we obtained similar

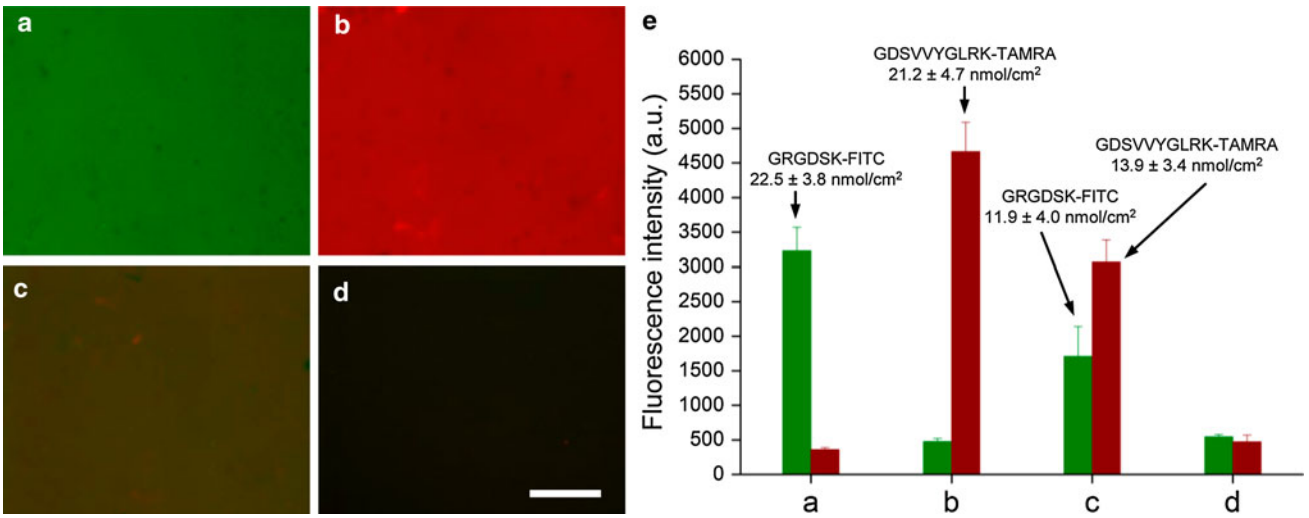

Fig. 5 Fluorescent images of surface grafted with fluorescent peptides: **a** GRGDSK–FITC, 10^{-3} M in solution; **b** GDSVVYGLRK–TAMRA, 10^{-3} M in solution; **c** mixture of GRGDSK–FITC and GDSVVYGLRK–TAMRA, 0.5×10^{-3} M for each in solution; **d** Control of PET-COOH surfaces, scale bar is 50 μm; **e** fluorescence intensity and calculated density of fluorescent peptides on surfaces (a–d)

levels of peptide density on surfaces grafted with each different peptide, and statistical analysis of the data showed no significant differences in peptide density between each other.

3.4 Presence of peptides on polymer surfaces

The surfaces functionalized by different fluorescent peptides were characterized by fluorescence microscopy. We observed the fluorescence changes depending on peptide solution used (Fig. 5). As shown, the surfaces grafted with GRGDSK–FITC showed only green fluorescence (Fig. 5a, e), surfaces grafted with GDSVVYGLRK–TAMRA showed only red fluorescence (Fig. 5b, e). The mixture of previous two peptides (MIX) presented the fluorescence of both GRGDSK–FITC and GDSVVYGLRK–TAMRA peptides (Fig. 5c, e). However, PET-COOH surfaces presented no fluorescence (Fig. 5d, e). These results revealed that the peptides were successfully grafted onto PET surfaces and presented in a homogeneous way. The surface MIX was actually bifunctionalized with both peptides in a homogeneous way. According to the calibration curves, peptide density on these surfaces was calculated: 11.9 ± 4.0 nmol/cm^2 of RGD and 13.9 ± 3.4 nmol/cm^2 of SVVYGLR peptides were presented on "MIX" surfaces. However, the total peptide density on MIX surfaces was similar to the surfaces grafted with each of the peptides as compared with the results in the previous section.

3.5 Cell attachment test

For biological evaluation, firstly, the potential of the peptides to promote EC adhesion was investigated. The results of cell attachment test revealed that peptides constituted good ligands to increase cell adhesion after 4 h of cell culture (Fig. 6a). The results of cell attachment after 24 h of cell culture showed similar tendency (data not shown here). The EC attachment was enhanced on all peptides immobilized surfaces as compared with controls (PET and COOH surfaces). However, more ECs attached on RGDS surfaces as compared with other peptides grafted surfaces, and cell attachment was slightly increased on MIX surfaces (Fig. 6a).

3.6 Quantification of cell adhesion and spreading

The adherent cell number after 24 h of cell culture was represented in Fig. 6b. Cell adhesion on peptides grafted surfaces was greatly improved as compared with PET and COOH surfaces. Moreover, the surfaces with RGDS and MIX peptides induced more cell adhesion (Fig. 6b). These results were in well accordance with cell attachment test (Fig. 6a).

In vitro, initial cell attachment results in cell spreading. Projected cell areas were measured to evaluate EC spreading level on each surface and the results were shown in Fig. 7a. ECs on peptides grafted surfaces showed an increase in cell spreading level as compared with that on PET and COOH surfaces. However, the cell spreading levels were slightly different from one peptide to another; statistical analysis revealed that cell spreading levels on YIGSR and SVVYGLR surfaces were more significant than those on RGDS and REDV surfaces. MIX peptides also showed more significant cell spreading level than on RGDS and REDV surfaces.

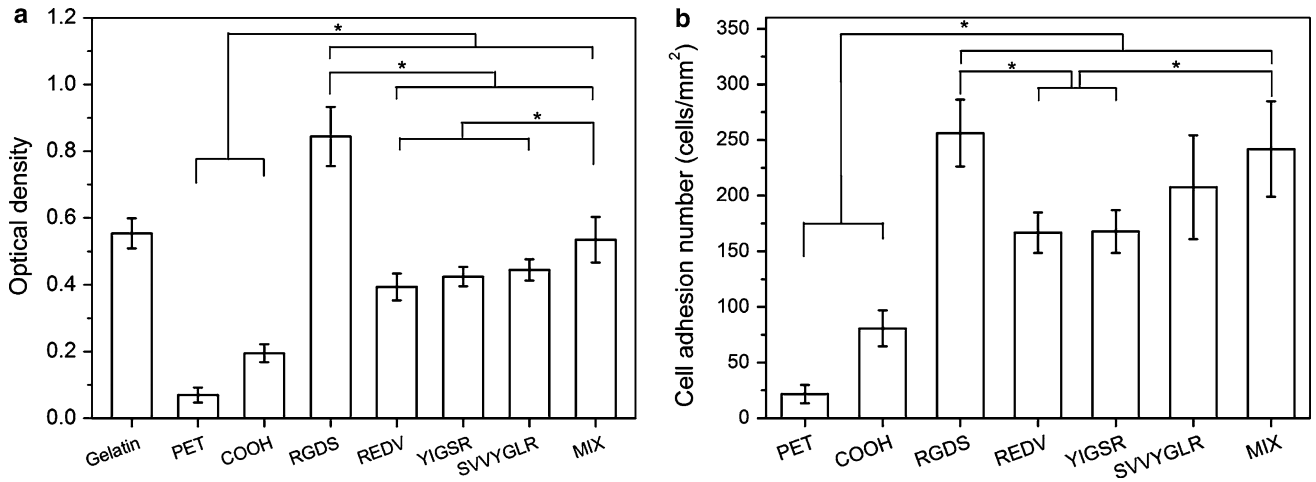

Fig. 6 **a** EC attachment for 4 h onto gelatin, native and modified PET surfaces. **b** Adherent EC number on different surfaces after 24 h of cell culture (*$P < 0.01$)

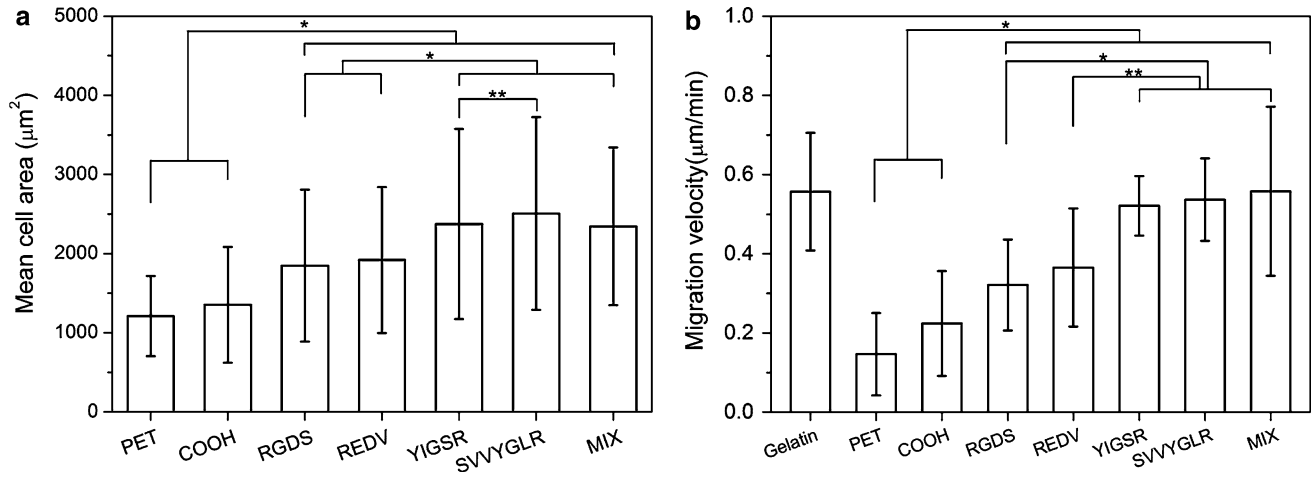

Fig. 7 **a** Cell areas on different surfaces after 24 h of cell culture. **b** Migration rates of ECs on different surfaces (*$P < 0.01$, **$0.01 < P < 0.05$)

3.7 Cell migration

To assess cell motility on peptides grafted surfaces, cell migration was monitored by time-lapse video microscopy. The results in Fig. 7b indicated that EC migration was strongly enhanced on peptides functionalized surfaces as compared with PET and COOH surfaces. Video microscopy revealed that ECs rapidly extended and retracted filopodia on peptide grafted surfaces, indicating an attempt to migrate, but in fact ECs were round and almost did not move on PET surfaces. The quantitative results revealed that EC motility was greater on YIGSR and SVVYGLR surfaces, whereas the cell motility was less significant on RGDS and REDV surfaces. The bi-functionalization of MIX also induced a significant cell velocity.

3.8 Actin organization and focal adhesion assembly

Immunofluorescent staining results showed ECs' cytoskeleton and focal adhesion organization on different surfaces (Fig. 8). Whatever the type of peptides, the cells on the peptide surfaces were evidently large with developing cell processes, whereas the cells on PET surfaces were small and almost round, showing unclear cellular configuration (Fig. 8a, b). ECs on RGDS (Fig. 8c, d) and REDV (Fig. 8e, f) surfaces displayed actin organized into thin filaments, few actin stress fibers and small focal contacts were observed. However, ECs adhered on YIGSR (Fig. 8g, h) and SVVYGLR (Fig. 8i, j) surfaces displayed a well-organized actin cytoskeleton with actin stress fibers, the actin filaments were rather organized into cortical networks

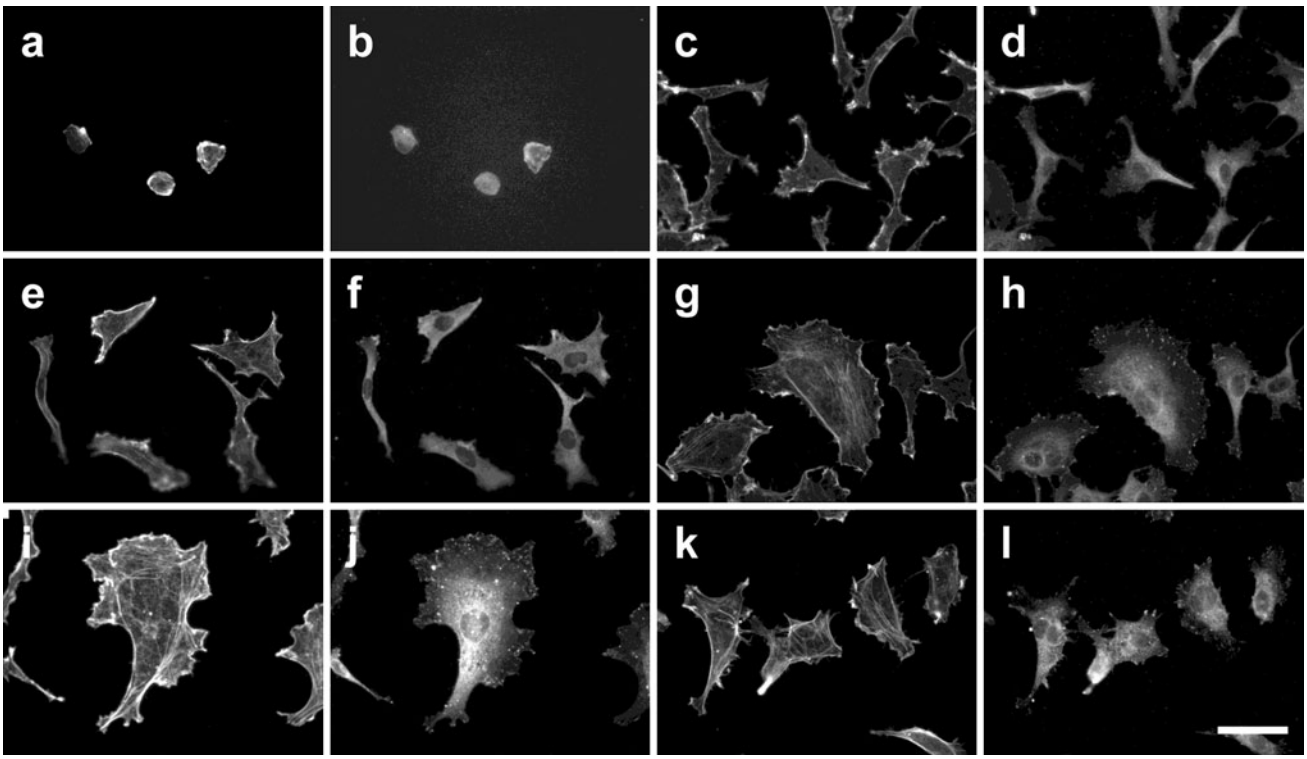

Fig. 8 Representative images of actin filament labeled with phalloidin (**a**, **c**, **e**, **g**, **i**, **k**) and focal adhesion labeled with vinculin (**b**, **d**, **f**, **h**, **j**, **l**) in ECs on PET (**a**, **b**); RGDS (**c**, **d**); REDV (**e**, **f**); YIGSR (**g**, **h**); SVVYGLR (**i**, **j**) and MIX (**k**, **l**) surfaces after 24 h of cell culture. *Scale bar* corresponds to 50 μm

associated with membrane ruffling (Fig. 8g, i), the intensive and extensive localization of the focal adhesion protein vinculin was detected in the leading edge of cell spreading and migration (Fig. 8h, j). ECs adhered on MIX peptides also showed strong actin filament organized into stress fibers, and presented focal adhesion at the leading edges of cell spreading and migration (Fig. 8k, l).

4 Discussion

Endothelialization is an increasing need for development of vascular materials [1]. Control over specific interaction of ECs-materials are important for vascular prostheses endothelialization [1]. In this study, we aim to modify the PET surfaces with different peptide sequences by covalent immobilization, in order to study specific EC functions on peptides grafted surfaces. Four peptide sequences were investigated in this study, including cell adhesive RGDS, EC specific REDV and YIGLR, and angiogenic SVVYGLR peptides.

In previous works, ECs adhered and formed focal contacts on PET surfaces grafted with RGD peptides, whereas no focal adhesion were formed on PET surfaces grafted with its inactive control RGE peptides [4]. The absence of cell focal adhesion on the inactive RGE peptides proves that EC adhesion was mediated by specific interactions between grafted RGD peptides and cell receptors [4]. It's then hypothesized that immobilization of peptides which are more specific for ECs (REDV, YIGSR and SVVYGLR sequences) may be a way to control elicited signals and EC responses.

A three step procedure was employed to covalently immobilize these peptides (RGDS, REDV, YIGSR, SVVYGLR sequences and MIX (mixture of RGDS and SVVYGLR)) onto PET surfaces. The presence of each peptide onto PET surfaces was characterized by XPS, AFM, contact angle measurement and fluorescence microscopy observation (Sects. 3.1–3.4). The peptide density on PET surfaces evaluated by fluorescence microscopy was similar on each surface, and statistical analysis showed no significant differences of peptide density between each peptide (Sect. 3.3). Since each peptide was immobilized onto PET surfaces by the same approach and represented in similar density, we can focus on comparing the specific effects of each peptide onto EC behaviors. Differences in EC attachment, spreading, migration and organization of actin filament and focal adhesion were assessed at various time points (4 h, 24 h).

The statistical analysis of the data showed that the surfaces functionalized by these different peptides enhanced

the EC adhesion, spreading and migration as compared with PET as well as COOH surfaces (Figs. 6, 7). These results revealed that the surface functionalization by bioactive peptides was effective in modifying the PET surfaces. However, EC attachment, spreading, migration, actin cytoskeleton organization and focal adhesion assembly were different on surfaces grafted with different peptides. In more details, RGDS surfaces induced more cell adhesion than other peptides (Fig. 6). And YIGSR and SVVYGLR peptides seemed to improve more cell spreading and migration (Fig. 7). The bi-functionalization of MIX combined the advantages of both peptides, and induced significant EC adhesion, spreading and migration (Figs. 6, 7).

The functionalization of biomaterials by peptides mediates cell-materials interaction mainly via cell adhesion receptors such as integrins [30], thus directing cell functions. Integrins are a family of heterodimeric transmembrane adhesion receptors consisting of α- and β- subunits [31]. They integrate the cell's exterior to the cell's interior (cytoskeleton) [31] and mediate cell functions onto material surfaces.

The RGD sequence is one of the most abundant cell integrin recognition sequences [10]. RGD can address to many integrin receptors such as $\alpha_3\beta_1$, $\alpha_5\beta_1$, $\alpha_8\beta_1$, $\alpha_v\beta_1$, $\alpha_v\beta_3$, $\alpha_v\beta_5$, $\alpha_v\beta_6$, $\alpha_{IIb}\beta_3$ [30, 32], particularly $\alpha_5\beta_1$ and $\alpha_v\beta_3$ are predominant in cell adhesion [33]. REDV sequence binds essentially to the $\alpha_4\beta_1$ integrin receptor [14, 15]. YIGSR motif exerts its cell-adhesive activity through interaction with $\alpha_4\beta_1$ [34], it also interacts with the 67 kDa lamilin binding protein (LBP) receptors [18]. SVVYGLR motif specially binds to $\alpha_4\beta_1$ [35], $\alpha_4\beta_7$ [36], $\alpha_9\beta_1$ [21] and $\alpha_v\beta_3$ [37] integrin receptors.

Since RGDS sequence could be recognized by more integrins of ECs than other peptides, this may be the reason that RGDS surfaces induced more cell adhesion (Fig. 6). This result is in accordance with the results of Boateng et al. [17]: they reported more cellular attachment on silicone surfaces with RGD than that with YIGSR peptides. The RGDS surfaces induced more EC adhesion may also due to the surface hydrophilicity (Sect. 3.2). In the case of MIX peptides, RGDS in association with SVVYGLR would be expected to activate more subtypes of adhesive receptors than either peptide alone, and therefore regulate the cell behavior in more complex ways. However, when RGDS and SVVYGLR were co-immobilized, there might be a competition for $\alpha_v\beta_3$ ligands, thereby attenuating the overall strength of integrin signaling, which may explain MIX resulted in less adhesion than RGDS peptide alone.

In addition to cell adhesion, integrins make transmembrane connections to the cytoskeleton and activate various intercellular signaling pathway [30], thus modulating many aspects of cell functions including proliferation, polarity, spreading, motility, actin cytoskeleton organization and focal adhesion formation [30].

Our findings suggest that these peptides didn't mediate the same cell signaling pathways. The cellular attachment is different between each surface, and resulted in different spreading and migration level as well as difference in actin cytoskeleton organization and focal adhesion assembly. Cell migration requires constant reorganization of the actin cytoskeleton and focal adhesions: extension of filopodia and lamellipodia is followed by attachment to the matrix via focal adhesions and stress fiber formation, which are able to contract the cell body to move forwards [38]. The repeated assembly and disassembly of focal adhesions at the leading edge, and the cytoskeletal contraction and detachment at the tailing edge of the cells result in the migration of the cells [38].

In the case of ECs on RGDS and REDV surfaces, the cells were less spread and less migrated (Fig. 7), in these relatively sessile cells, focal adhesions were small and quite stable (Fig. 8d, f). For the cells on YIGSR and SVVYGLR surfaces, the cells were more spread and more migrated (Fig. 7), YIGSR and SVVYGLR peptides lead to an increase in stress fibers associated with membrane ruffling (Fig. 8g, i) and focal adhesion rearrangement into peripheral ones (Fig. 8h, j). On these surfaces, the focal contacts were dynamically assembled and disassembled, and represented intense focal adhesion at the leading edges of the cell spreading and migration. The observed morphology of ECs on YIGSR and SVVYGLR indicated these peptides induce more cell migration rather than a strong anchorage to the surfaces. The MIX peptides combined the advantages of both peptides, inducing more cell attachment, stronger actin filament organization into stress fibers and focal adhesion assembly presented at the front edge of spreading and migration.

As previously reported, the REDV peptide is essentially recognized by integrin $\alpha_4\beta_1$ [14, 15]. Integrin α_4 subunits bind to paxillin, inducing inhibition of cell spreading [39]. Moreover, paxillin binding to the α_4 cytoplasmic domains leads to focal adhesion disassembly and stress fiber disappearance [39]. The YIGSR peptides were reported to involve in the adhesion, spreading and stress fiber formation of ECs [18]. The YIGSR peptides have been found to co-localize LBP with α-actinin and vinculin, two crucial components of focal adhesion sites [18]. YIGSR has also been shown to cause the phosphorylation of a range of proteins of molecular mass 115–130 kDa. The phosphorylation of cytoplasmic focal adhesion kinase is believed to be central to the regulation of cell motility [40]. The SVVYGLR peptides have important ability to promote EC migration [22]. The expression and activation of integrin $\alpha_v\beta_3$ by SVVYGLR plays a key role in vascular cell migration [30]. On the other hand, integrin α_4 and α_9

subunits share functional similarities as they both enhance cell migration [39, 41].

EC adhesion and migration are required for in situ endothelialization of vascular prostheses and EC invasion into a scaffold is important for construction of vascularized tissues in tissue engineering [1, 42]. Our work proves that the EC specific responses could be optimized through a combinatory approach using biomimetic peptides on polymer surfaces. It's known the geometric arrangement of ligands, orientation as well as conformation can all affect the specificity of cell behaviors. In perspective work, these peptides specific for ECs would be incorporated into a microengineered surfaces [43], to enhance EC morphogenesis and to support invasion of ECs into a scaffold for construction of vascularized tissue. RGDS combined with SVVYGLR or YIGRS peptides could be chosen as candidates for these applications.

5 Conclusions

In this study, the potential use of cell adhesive RGDS, EC specific REDV and YIGSR, and angiogenic SVVYGLR peptides to enhance EC functions on polymer surfaces was assessed. Covalent immobilization of each peptide alone is sufficient to facilitate EC attachment as compared with native PET surfaces. The PET surfaces grafted with RGDS induced the most cell adhesion, and YIGSR and SVVYGLR induced more cell spreading and migration, represented by stronger actin filament reorganization into stress fibers and focal adhesion assembly at the leading edges of cell spreading and migration. The MIX peptides of RGDS and SVVYGLR combine the advantages of both, inducing more cell attachment, spreading and migration. This study indicates that immobilization of EC specific peptides, especially the combination of cell adhesive RGDS peptides with SVVYGLR or YIGSR peptides has potential applications in promoting endothelialization of vascular prostheses and for construction of vascularized tissues in tissue engineering.

Acknowledgment The authors gratefully acknowledge the "Région Aquitaine", the GIS "Advanced Materials in Aquitaine", the "Agence nationale pour la Recherche" (ANR) for their financial supports. The authors gratefully thank Sophia Ziane for providing tomato-labeled HUVECs, thank Annie Zhe Cheng for English assistance, and thank Omar F. Zouani, Loïc Pichavant and Céline Chollet for their technical assistances.

References

1. de Mel A, Jell G, Stevens MM, Seifalian AM. Biofunctionalization of biomaterials for accelerated in situ endothelialization: a review. Biomacromolecules. 2008;9(11):2969–79.
2. Pfisterer M, Brunner-La Rocca HP, Buser PT, Rickenbacher P, Hunziker P, Mueller C, et al. Late clinical events after clopidogrel discontinuation may limit the benefit of drug-eluting stents: an observational study of drug-eluting versus bare-metal stents. J Am Coll Cardiol. 2006;48(12):2584–91.
3. Brun JL, Bordenave L, Lefebvre F, Bareille R, Barbie C, Rouais F, et al. Physical and biological characteristics of the main biomaterials used in pelvic surgery. Biomed Mater Eng. 1992;2(4):203–25.
4. Chollet C, Chanseau C, Remy M, Guignandon A, Bareille R, Labrugere C, et al. The effect of RGD density on osteoblast and endothelial cell behavior on RGD-grafted polyethylene terephthalate surfaces. Biomaterials. 2009;30(5):711–20.
5. Zouani OF, Chollet C, Guillotin B, Durrieu MC. Differentiation of pre-osteoblast cells on poly(ethylene terephthalate) grafted with RGD and/or BMPs mimetic peptides. Biomaterials. 2010;31(32):8245–53.
6. Engler AJ, Sen S, Sweeney HL, Discher DE. Matrix elasticity directs stem cell lineage specification. Cell. 2006;126(4):677–89.
7. Park J, Bauer S, Schmuki P, von der Mark K. Narrow window in nanoscale dependent activation of endothelial cell growth and differentiation on TiO_2 nanotube surfaces. Nano Lett. 2009;9(9):3157–64.
8. Chow D, Nunalee ML, Lim DW, Simnick AJ, Chilkoti A. Peptide-based biopolymers in biomedicine and biotechnology. Mater Sci Eng R Rep. 2008;62(4):125–55.
9. Collier JH, Segura T. Evolving the use of peptides as components of biomaterials. Biomaterials. 2011;32(18):4198–204.
10. Bellis SL. Advantages of RGD peptides for directing cell association with biomaterials. Biomaterials. 2011;32(18):4205–10.
11. Arnaout MA, Mahalingam B, Xiong JP. Integrin structure, allostery, and bidirectional signaling. Annu Rev Cell Dev Biol. 2005;21:381–410.
12. Porte-Durrieu MC, Guillemot F, Pallu S, Labrugere C, Brouillaud B, Bareille R, et al. Cyclo-(DfKRG) peptide grafting onto Ti-6Al-4 V: physical characterization and interest towards human osteoprogenitor cells adhesion. Biomaterials. 2004;25(19):4837–46.
13. Durrieu MC, Pallu S, Guillemot F, Bareille R, Amedee J, Baquey CH, et al. Grafting RGD containing peptides onto hydroxyapatite to promote osteoblastic cells adhesion. J Mater Sci Mater Med. 2004;15(7):779–86.
14. Hubbell JA, Massia SP, Desai NP, Drumheller PD. Endothelial cell-selective materials for tissue engineering in the vascular graft via a new receptor. Biotechnology (N Y). 1991;9(6):568–72.
15. Massia SP, Hubbell JA. Vascular endothelial cell adhesion and spreading promoted by the peptide REDV of the IIICS region of plasma fibronectin is mediated by integrin alpha 4 beta 1. J Biol Chem. 1992;267(20):14019–26.
16. Plouffe BD, Njoka DN, Harris J, Liao J, Horick NK, Radisic M, et al. Peptide-mediated selective adhesion of smooth muscle and endothelial cells in microfluidic shear flow. Langmuir. 2007;23(9):5050–5.
17. Boateng SY, Lateef SS, Mosley W, Hartman TJ, Hanley L, Russell B. RGD and YIGSR synthetic peptides facilitate cellular adhesion identical to that of laminin and fibronectin but alter the physiology of neonatal cardiac myocytes. Am J Physiol Cell Physiol. 2005;288(1):C30–8.
18. Massia SP, Rao SS, Hubbell JA. Covalently immobilized laminin peptide Tyr-Ile-Gly-Ser-Arg (YIGSR) supports cell spreading and co-localization of the 67 kilodalton laminin receptor with alpha-actinin and vinculin. J Biol Chem. 1993;268(11):8053–9.
19. Jun HW, West JL. Modification of polyurethaneurea with PEG and YIGSR peptide to enhance endothelialization without platelet adhesion. J Biomed Mater Res B Appl Biomater. 2005;72(1):131–9.

20. Fittkau MH, Zilla P, Bezuidenhout D, Lutolf MP, Human P, Hubbell JA, et al. The selective modulation of endothelial cell mobility on RGD peptide containing surfaces by YIGSR peptides. Biomaterials. 2005;26(2):167–74.
21. Yokosaki Y, Matsuura N, Sasaki T, Murakami I, Schneider H, Higashiyama S, et al. The integrin alpha(9)beta(1) binds to a novel recognition sequence (SVVYGLR) in the thrombin-cleaved amino-terminal fragment of osteopontin. J Biol Chem. 1999; 274(51):36328–34.
22. Hamada Y, Nokihara K, Okazaki M, Fujitani W, Matsumoto T, Matsuo M, et al. Angiogenic activity of osteopontin-derived peptide SVVYGLR. Biochem Biophys Res Commun. 2003;310 (1):153–7.
23. Hamada Y, Yuki K, Okazaki M, Fujitani W, Matsumoto T, Hashida MK, et al. Osteopontin-derived peptide SVVYGLR induces angiogenesis in vivo. Dent Mater J. 2004;23(4):650–5.
24. Rezania A, Healy KE. Biomimetic peptide surfaces that regulate adhesion, spreading, cytoskeletal organization, and mineralization of the matrix deposited by osteoblast-like cells. Biotechnol Prog. 1999;15(1):19–32.
25. Chollet C, Chanseau C, Brouillaud B, Durrieu MC. RGD peptides grafting onto poly(ethylene terephthalate) with well controlled densities. Biomol Eng. 2007;24(5):477–82.
26. Pichavant L, Amador G, Jacqueline C, Brouillaud B, Héroguez V, Durrieu M-C. pH-Controlled delivery of gentamicin sulfate from orthopedic devices preventing nosocomial infections. J Control Release. doi:10.1016/j.jconrel.2012.06.033.
27. Jaffe EA, Nachman RL, Becker CG, Minick CR. Culture of human endothelial cells derived from umbilical veins. Identification by morphologic and immunologic criteria. J Clin Invest. 1973;52(11):2745–56.
28. Li H, Daculsi R, Grellier M, Bareille R, Bourget C, Amedee J. Role of neural-cadherin in early osteoblastic differentiation of human bone marrow stromal cells cocultured with human umbilical vein endothelial cells. Am J Physiol Cell Physiol. 2010; 299(2):C422–30.
29. Landegren U. Measurement of cell numbers by means of the endogenous enzyme hexosaminidase. Applications to detection of lymphokines and cell surface antigens. J Immunol Methods. 1984;67(2):379–88.
30. Hynes RO. Integrins: bidirectional, allosteric signaling machines. Cell. 2002;110(6):673–87.
31. van der Flier A, Sonnenberg A. Function and interactions of integrins. Cell Tissue Res. 2001;305(3):285–98.
32. Plow EF, Haas TA, Zhang L, Loftus J, Smith JW. Ligand binding to integrins. J Biol Chem. 2000;275(29):21785–8.
33. Zamir E, Geiger B. Molecular complexity and dynamics of cell-matrix adhesions. J Cell Sci. 2001;114(Pt 20):3583–90.
34. Maeda T, Titani K, Sekiguchi K. Cell-adhesive activity and receptor-binding specificity of the laminin-derived YIGSR sequence grafted onto Staphylococcal protein A. J Biochem. 1994;115(2):182–9.
35. Barry ST, Ludbrook SB, Murrison E, Horgan CM. Analysis of the alpha4beta1 integrin-osteopontin interaction. Exp Cell Res. 2000;258(2):342–51.
36. Green PM, Ludbrook SB, Miller DD, Horgan CM, Barry ST. Structural elements of the osteopontin SVVYGLR motif important for the interaction with alpha(4) integrins. FEBS Lett. 2001;503(1):75–9.
37. Egusa H, Kaneda Y, Akashi Y, Hamada Y, Matsumoto T, Saeki M, et al. Enhanced bone regeneration via multimodal actions of synthetic peptide SVVYGLR on osteoprogenitors and osteoclasts. Biomaterials. 2009;30(27):4676–86.
38. Pollard TD, Borisy GG. Cellular motility driven by assembly and disassembly of actin filaments. Cell. 2003;112(4):453–65.
39. Liu S, Thomas SM, Woodside DG, Rose DM, Kiosses WB, Pfaff M, et al. Binding of paxillin to alpha4 integrins modifies integrin-dependent biological responses. Nature. 1999;402(6762):676–81.
40. Hauck CR, Hsia DA, Schlaepfer DD. The focal adhesion kinase–a regulator of cell migration and invasion. IUBMB Life. 2002;53(2):115–9.
41. Young BA, Taooka Y, Liu S, Askins KJ, Yokosaki Y, Thomas SM, et al. The cytoplasmic domain of the integrin alpha9 subunit requires the adaptor protein paxillin to inhibit cell spreading but promotes cell migration in a paxillin-independent manner. Mol Biol Cell. 2001;12(10):3214–25.
42. Bouhadir KH, Mooney DJ. Promoting angiogenesis in engineered tissues. J Drug Target. 2001;9(6):397–406.
43. Falconnet D, Csucs G, Grandin HM, Textor M. Surface engineering approaches to micropattern surfaces for cell-based assays. Biomaterials. 2006;27(16):3044–63.

2. Microscale Modification for Induction of Endothelial Cell Angiogenesis

Introduction

Angiogenesis, the formation of new blood vessels by sprouting from pre-existing ones, is critical for establishment and maintenance of complex engineered tissues. *In vitro*, angiogenesis is often studied by stimulating a monolayer of endothelial cells to assemble into tubes and sprouting [224]. Angiogenesis is usually triggered by extracellular matrix (ECM) proteins (laminin, collagen, etc…) [225] and growth factors (VEGF, bFGF, etc…) [46, 226]. Meanwhile, relative short peptides were also used for triggering angiogenesis [95, 174].

In order to better control the morphogenetic process during angiogenesis, an interesting concept is the inclusion of a network with a vascular geometry. Geometrical cues play an important role in this process. Many studies have adopted microengineering tools to generate materials micropatterned with molecules on their surface [181-183]. Dike *et al.* created stripes of fibronectin onto gold surface by using microcontact printing, and induced EC tube formation on 10 μm-stripes of fibronectin [87].

In this study, our strategy is employing microengineering tools to generate peptide micropatterns on polymer surfaces and thus to control the EC behaviors and angiogenesis. The main results obtained in this part (Paper II, III and IV) are:

(a) Photolithographical technique can be used to prepare peptide micropatterns on polymer surfaces. Peptide micropatterns with different shapes and sizes were revealed by fluorescence microscopy.

(b) ECs were adhered and aligned onto peptides micropatterns after cell culture.

(c) EC behaviors (cell spreading, orientation and migration) were significantly more guided and regulated on narrower micropatterns (10 and 50 μm) than on larger stripes (100 μm).

(d) EC morphogenesis into tube formation was switched onto the smaller micropatterns (10 and 50 μm), with either RGD or SVVYGLR peptides.

(e) The central lumen of tubular structures can be formed by single-to-four cells due to geometrical constraints on the micropatterns which mediated cell-substrate and cell-cell adhesion.

(f) The angiogenesis on micropatterned surfaces also dependent on the peptide motifs themselves. RGD adhesion peptides and BMP-2 mimetic peptides were used to induce filopodial migration and lamellipodial migration of ECs, respectively. However, only filopodial migration mode promotes EC lumen formation. Specifically, sprouting angiogenesis of ECs and vascular network formation were

induced on surfaces micropatterned with angiogenic SVVYGLR peptides, but not with RGD peptides.

(g) Endothelial cell migration on micropatterned surfaces was simulated by mathematical modeling (Paper IV). The results of numerical studies were in good accordance with our experimental results.

The surface micropatterning with peptides provides opportunities to mimic and investigate the process of angiogenesis. The organization of ECs into tubular structures and the induction of sprouting angiogenesis are important towards the fabrication of vascularized tissues.

Paper II. Modulation of lumen formation by microgeometrical bioactive cues and migration mode of actin machinery

Small. 2012. Submitted.

Peptide micropatterning on polymer surfaces are designed to control the endothelial cell (EC) functions. EC morphogenesis into tubular structures is dependent on both microgeometrical cues of peptide micropatterns, and different migration mode of actin machinery on peptide micropatterns.

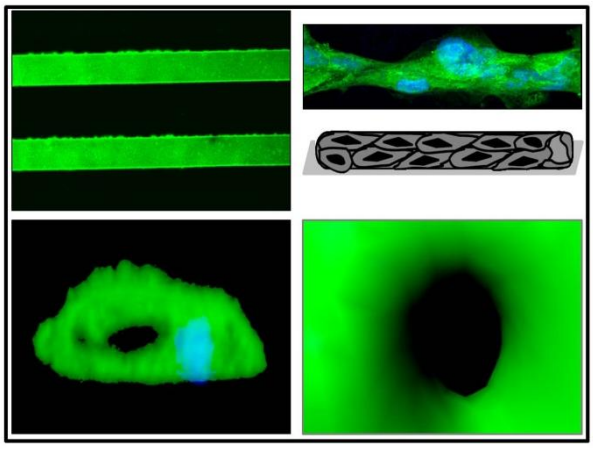

Figure 25. Endothelial cells align onto peptide micropatterns and form tubular structures with central lumen.

Submitted to small NANO MICRO

DOI: 10.1002/smll.((please add manuscript number))

Modulation of Lumen Formation by Microgeometrical Bioactive Cues and Migration Mode of Actin Machinery

Yifeng Lei[*], *Omar F. Zouani*[*+], *Murielle Rémy, Lila Rami, and Marie-Christine Durrieu*

[*] Dr. Y. Lei Corresponding-Author, Dr. O. F. Zouani Corresponding-Author [+], Dr. M.C. Durrieu
Université de Bordeaux 1-CNRS, UMR5248, Institut Européen de Chimie et Biologie,
2, rue Robert Escarpit, F-33607 Pessac, France
Université de Bordeaux 2, Inserm U1026, Bioingénierie Tissulaire,
146, rue Léo Saignat, F-33076 Bordeaux, France
E-mail: yifeng.lei@inserm.fr and omar.zouani@inserm.fr
[+] OFZ has supervised this work and is the principal investigator.

Dr. M. Rémy, L. Rami
Université de Bordeaux 2, Inserm U1026, Bioingénierie Tissulaire,
146, rue Léo Saignat, F-33076 Bordeaux, France

Keywords: Angiogenesis, filopodial migration, lamellipodial migration, surface functionalization, surface micropatterning

Abstract:

Study of how endothelial cells (ECs) express the particular filopodial or lamellipodial form of the actin machinery is critical to understanding EC functions such as angiogenesis and sprouting. It is not known how these mechanisms coordinately promote lumen formation of ECs. Here, adhesion molecule (RGD peptides) and inductor molecule (BMP-2 mimetic peptides) are micropatterned onto polymer surfaces by photolithographic technique to induce filopodial and lamellipodial migration mode, respectively. Firstly, the effects of peptide microgeometrical distribution on EC adhesion, orientation and morphogenesis are evaluated. Large micropatterns (100 μm) promote EC orientation without lumen formation, whereas small micropatterns (10-50 μm) elicit a collective cell organization and induce EC lumen formation, in the case of RGD peptides. Secondly, the correlation between EC actin machinery expression and EC self-assembly into lumen formation is addressed. We demonstrate that only filopodial migration mode (mimicked by RGD) but not lamellipodial

migration mode (mimicked by BMP-2) promotes EC lumen formation. This work gives a new concept for the design of biomaterials for tissue engineering and may provide new insight for angiogenesis inhibition on tumors.

1. Introduction

Angiogenesis, the formation of new capillary blood vessels by sprouting from pre-existing vessels, plays a critical role in tissue growth and homeostasis, as well as in pathogenesis of many diseases such as cancer.[1] Recent findings demonstrate that inhibition of angiogenesis can prevent the growth of tumors,[2] while the promotion of angiogenesis is essential to improve the vascularization in tissue engineering.[3] Despite their clinical importance, the mechanisms that regulate angiogenesis remain unclear. It is essential to understand the actin machinery that induces lumen formation in order to regulate the process of angiogenesis. The two forms of actin machinery coexist at the leading edge of motile cells: lamellipodia seem designed for persistent protrusion over a surface,[4] whereas filopodia appear to perform sensory and exploratory functions to steer cells depending on cues from the microenvironments.[4] The endothelial cells (ECs) in the process of angiogenesis take a certain form maintained by general organization of actin networks and focal adhesions (FAs), thus maintaining lumen structure by induced intracellular forces of ECs.[5]

The process of angiogenesis is orchestrated by the complex interaction between ECs and their neighboring mural cells and extracellular microenvironment.[6, 7] Different bioactive ligands have been used in angiogenesis research,[3] including Matrigel™ basement membrane matrix,[8] individual extracellular matrix (ECM) proteins (such as laminin (LN),[9] fibronectin (FN)[10] and gelatin[11]), or simply short peptide fragments (such as RGD[12] and SVVYGLR[13, 14] peptides).

In addition to chemical-biological modification by cell binding ligands (peptides, proteins, etc.),[15] another important conception to control cellular functions in the *in vitro*

culture systems is using micro-/nano-engineering to mimic the cellular microenvironments.[16-18] These micro-/nano-engineering techniques provide powerful tools to study *in vitro* cell-microenvironment interactions, they control the presentation of the biomolecules on biomaterial surfaces in defined sizes and shapes, thus influencing cell placement, orientation and cell functions.[17] Nanoscaled patterning of signaling molecules such as RGD peptides were developed on both inorganic and polymeric substrates for study the cellular responses to individual specific signaling molecules and their spatial ordering.[19-21] Previous studies in literature have also demonstrated that well-defined surfaces with biomolecule micropatterning are useful approaches to regulate the cell morphogenesis and to investigate the progress of angiogenesis.[10, 11]

Photolithography has attracted our attention and has been previously developed in our labs to create peptide micropatterns on polymer surfaces.[22] Previous results showed that the peptide micropatterns induced the selective assembly and orientation of pre-osteoblastic MC3T3-E1 cells.[22] In this work, we focus on the peptide micropatterned surface development in order to regulate EC functions. We aim to control *in vitro* microenvironments to understand biological mechanisms of EC lumen formation. Our work focuses on (i) the development of peptide micropatterned surfaces using photolithography; (ii) the study of the impact of peptide geometrical cues on EC orientation and morphogenesis into tube formation; and (iii) the understanding of the relationship between the migration mode of actin machinery (filopodial and lamellipodial migration) and EC lumen formation.

First, adhesion peptides (RGD) were micropatterned onto polymer surfaces by photolithography. And the effects of the RGD peptide geometrical distribution on EC adhesion, orientation and morphogenesis into tube formation were evaluated. We demonstrate with this culture system that ECs use filopodial migration mode to form a lumen structure. Subsequently, BMP-2 mimetic peptides were micropatterned onto the same surfaces to mimic

lamellipodial migration mode of ECs. In this configuration, no lumen formation has been detected whatever the geometrical distribution of peptide micropatterns. In this study, we demonstrate a robust correlation between EC migration mode and EC self-assembly into lumen formation.

2. Results and Discussion

2.1. Characterization of surface micropatterns

The roughness (Ra) of PET-COOH and PET-peptide (here referred to RGD) materials evaluated by AFM was 6.4 ± 0.6 nm and 7.0 ± 0.4 nm, respectively (**Table 1**). Statistical analysis of the data showed no significant difference in the roughness between the two substrates. No difference in mechanical properties was observed in PET-COOH and PET-peptide materials. Indeed, the elastic modulus was measured at 1.6 GPa (Table 1). The peptide densities were evaluated by indirect fluorescence microscopy measurement, and the results were shown in **Figure S1**. The quantitative analysis revealed that the average fluorescent peptide densities within the micropatterns were similar, and statistical analysis of the data showed no significant differences in peptide density among different conditions (Figure S1).

Photolithographic technique was developed in our laboratory to prepare the peptide micropatterns onto polymer surfaces (**Figure 1**a).[14, 22] Immobilization of fluorescent peptides (GRGDSK-FITC) onto polymer surfaces was used for validation of this process.[23] The surfaces with fluorescent peptide micropatterning with various geometries were shown in Figure 1b-c, which confirmed the successful micropatterning of peptides onto polymer surfaces. In this work, peptide stripes of three different sizes (10, 50, 100 μm) with same interspacing of 100 μm between the stripes (Figure 1d) were prepared for the purpose of cell culture. The micropatterned regions and unpatterned regions in Figure 1 were PET-RGD and PET-COOH, respectively.

Cellular developments were dramatically affected by ligands grafted onto the surfaces, the surface properties such as roughness and the surface mechanical properties can also affect cell functions.[24, 25] In our study, no differences in surface roughness and mechanical properties were observed in PET-COOH and PET-peptide (RGD) materials (Table 1), and similar peptide density was presented on the peptide micropatterns (Figure S1), we can therefore focus on comparing the effects of geometrical distribution of peptides onto EC behaviors.

In our previous work,[26] the results revealed that the homogeneous PET-RGD surfaces improved cell adhesion, spreading and migration of ECs as compared with PET-COOH surfaces. In the present work, the unpatterned regions and micropatterned regions on surfaces, *i.e.* PET-COOH and PET-RGD (Figure 1d), were served as cell non-adhesive and cell-adhesive substrates, respectively. Indeed, after several hours (4-6 h) of cell culture onto the surfaces, ECs adhered and aligned onto peptide stripes whatever the geometry of RGD micropatterns, as shown by the phase contrast images in Figure 1e. The fluorescent staining of cells also revealed EC alignment onto RGD micropatterns (**Figure 2**). ECs cultured on the surfaces recognized and attached on the peptide micropatterns rather than on PET-COOH mainly due to the ECs' affinity to the peptides via interaction of peptide-cell integrin receptors.

2.2. Cell spreading mediated by geometrical cues

Cell areas on different surfaces were represented in Figure 2e. ECs were spread most on the unpatterned RGD surfaces (mean projected cell areas: 2135 ± 717 μm^2). Cells seeded on 100 µm RGD micropatterns had a similar spreading level as compared with the unpatterned surfaces (mean cell area: 2031 ± 693 μm^2), while cell spreading was significantly

reduced on narrower stripes, with mean project cell areas of 1571 ± 639 μm^2 and 1278 ± 287 μm^2 for ECs on 50 μm and 10 μm RGD micropatterns, respectively.

2.3. Cell body orientation onto micropatterned polymer surfaces

Quantitative analyses of cell body orientation induced by RGD peptide micropatterns were represented in **Figure 3**. Cells on unpatterned surfaces displayed random orientation, the alignment angles of cell bodies were uniformly distributed between 0 to 90° (Figure 3a), with a mean value of 43.6 ± 25.8° (Figure 3e). As cells with alignment angle less than 10° were considered to be aligned (see "Materials and Methods" for more details), only 11% of the cells were aligned. For cells seeded on 100 μm RGD micropatterns (Figure 3b), mean cell body alignment angle was about of 25.9 ±15.8° (Figure 3e), and 27% of the cells were aligned in the direction of patterns (Figure 3b). The more the pattern width decreases, the more the mean alignment angles decrease: 15.2 ± 9.6° and 8.6 ± 6.1° for micropatterned surfaces of 50 μm and 10 μm RGD micropatterns, respectively (Figure 3e), and 42% and 73% of cells were considered to be aligned (Figure 3c-d). Cells exhibited a strong alignment onto the micropatterns, statistical analysis confirmed that there was a main effect of the micropattern width in driving cell body alignment angles ($p < 0.01$), and the alignment of cell body became more significant as the size became smaller ($p < 0.01$) (Figure 3e).

As shown by fluorescent images in Figure 2, most cells on patterned surfaces exhibited an elongated morphology. Quantitative analysis of cell body elongation on different surfaces was represented in Figure 3f. ECs on the unpatterned surface presented a mean cell body shape index of 0.66 ± 0.13. Cells on patterned surface showed decreased shape index as compared to the unpatterned controls, with mean cell body shape index of 0.58 ± 0.12, 0.44 ± 0.08 and 0.36 ± 0.07 for ECs on 100 μm, 50 μm and 10 μm RGD micropatterns, respectively. The decreasing in shape index showed that the cell bodies were more elongated on the

micropatterned surfaces. Statistical analysis showed that the elongation on 100 μm peptide stripes was more significant as compared with unpatterned surfaces ($p < 0.05$), and the elongation on smaller RGD micropatterns (50 μm and 10 μm) was more significant ($p < 0.01$) (Figure 3f).

The above analysis revealed a strong impact of RGD peptide geometrical distribution on cell morphology and orientation. The orientation of cell body was enhanced on patterned surface as compared with unpatterned surfaces, and the decrease of RGD stripe widths increased the alignment and elongation of cell body (Figure 3). These results were in well accordance with previous studies of cell-microengineered surface interaction, where reported the cell orientation parallel to the chemical micro-structure was increased on narrowed stripes.[27]

2.4. Orientation of cell focal contacts on micropatterned polymer surfaces

The quantification of orientation of cell focal contacts was shown in **Figure 4**. Similar to the cell body alignments, micropattern width showed a significant influence on focal contact alignment. The focal contacts on unpatterned surfaces appeared to fan out from the center of cells in all directions (Figure 2, vinculin), the focal contacts had random alignment as illustrated by the uniformly distributed data in Figure 4a, the mean alignment angle was 45.9 ± 26.1° (Figure 4e) and only 10% of focal contacts were aligned (Figure 4a). The cell focal contacts on RGD patterns were predominantly aligned to the direction of the patterns. As compared with the unpatterned controls, the alignment angle of cell focal contacts decreased to 30.0 ± 24.9°, 23.2 ± 19.1° and 14.3 ± 12.1° for the cells on 100 μm, 50 μm and 10 μm RGD micropatterns, respectively, and the amount of aligned focal contacts increased to 24%, 29% and 44%, respectively (Figure 4). Statistical analysis revealed a significant difference of cell focal contact alignment angle on micropatterned surfaces as compared with

the unpatterned controls ($p < 0.01$), and the focal contact alignment angles were significantly smaller as the RGD peptides width became smaller ($p < 0.01$) (Figure 4e).

The elongation of cell focal contacts was not significantly affected by the RGD patterns. Their mean value and standard deviations of shape index are similar (0.48 ± 0.16 for unpatterned surfaces, and 0.50 ± 0.18, 0.50 ± 0.19, 0.51 ± 0.17 for focal contacts of ECs on 100 μm, 50 μm and 10 μm RGD micropatterns, respectively) (Figure 4f). There was no significant change in elongation of cell focal contacts from the unpatterned surface to the patterned surfaces. These results were in accordance with the results of Charest *et al.*: they reported cell focal adhesion alignment, but no great effect of focal contact elongation on microgrooves.[28] Focal contacts are critical for cell adhesion, they also play a major role in cellular signaling and cell functions.[29] The dynamic assembly and disassembly of focal contacts plays a critical role in cell migration.[30] The orientations of focal contacts can guide the orientation of cell adhesion and migration.

2.5. Morphogenesis of ECs by geometrical cues

Micropatterning of RGD peptides showed regulation and guidance of the ECs. The results showed that the cell orientation and morphology are quite strongly regulated for pattern width in order of 50 μm or below. Furthermore, we investigated the EC morphogenesis on micropatterned surfaces.

After 28 h of cell culture in EGM®-2 medium, we observed that ECs on RGD micropatterned surfaces underwent morphogenesis and formed tubular structures depending on the width of RGD micropatterns (**Figure 5**). On 10 μm RGD micropatterns, ECs coalesced into highly organized tubular structures along the axis of the RGD patterns (Figure 5a), and vertical confocal image cross sections showed that ECs protruded their nuclei and cell bodies vertically upwards to form three dimentional (3D) tube-like structures with central lumen,

which appeared as a negatively stained central space when viewed from vertical cross section. For the cells cultured on 50 μm RGD micropatterns, multiple cells were stacked on top of each other (Figure 5b), the cell bodies were stretching around to form tubular like structure, and vertical cross section of such regions also revealed tube formation with central lumen. In contrast, ECs seeded on 100 μm RGD micropatterns remained spread on the RGD peptides micropatterns and failed to undergo morphogenesis, vertical cross section showed that the cells remained as monolayer close to the substrates (Figure 5c).

Normally, the ECs seeded on plastic culture dishes grow as a strict monolayer with a cobble stone appearance. In our study, ECs underwent morphogenesis and form 3D tube-like structures on micropatterned surfaces presenting RGD micropatterns. Our results revealed the feasibility of 3D tubular structures solely by optimization of size of functionalized micropatterns on two dimentional (2D) polymer surfaces. Cell spreading has been restricted on smaller RGD peptide patterns (10 or 50 μm), consequently altering cell-cell interaction.[31] The enhanced cell-cell interactions on the smaller RGD micropatterns switched on a tubular differentiation program of ECs. Cells seeded on micropatterned surface presenting larger RGD micropatterns failed to differentiate through cell-cell contacts to form tube-like structure.

Today, only few studied have reported the tubulogenesis of ECs by 2D microengineering of bioactive ligands. Dike *et al.* reported EC tube formation on 10 μm stripes of fibronectin, but not on 30 μm-lines of fibronectin.[10] Co *et al.* reported the ECs cultured on 20 μm lines of gelatin formed tube-like structures.[11] It seemed that tube-like structure could be formed only on 10-20 μm microstripes of proteins. However, in our study, tubulogenesis of ECs was induced not only on 10 μm RGD micropatterns, but also induced on 50 μm RGD micropatterns. The peptides are more stable, and the peptide density presented on material surfaces was more significant as compared with proteins used in previous works, this may explain the different results in our study from previous studies.

2.6. EC morphogenesis modulated by filopodial but not lamellipodial migration mode

The above results indicated the modulation of EC morphogenesis by geometrical distribution of adhesive RGD peptide. Are there only geometrical cues which regulate the lumen formation of ECs? We observed that ECs migrated with the filopodial mode in the cases of adhesive RGD micropatterning (Figure 2). Subsequently, we immobilized BMP-2 mimetic peptides on the same surfaces to mimic lamellipodial migration mode of ECs, and to study the effect of migration mode of actin machinery onto EC lumen formation.

ECs in culture express both lamellipodia and filopodia, as shown in **Figure 6**a. In our study, two microenvironments were created to induce different migration mode of ECs: in one case a microenvironment containing BMP-2 mimetic peptide for inducing lamellipodial mode machinery (Figure 6b), and in second case, a microenvironment containing RGD adhesion peptide for inducing filopodial mode machinery (Figure 6c). Phalloidin staining revealed an increase in the lamellipodia actin networks in the first case because of the absence of any component of cell focal adhesion (Figure 6b, *magnification*). In the second case, a significant decrease in the lamellipodia actin networks and an increase in actin staining in deeper lamellar regions were observed (Figure 6c, *magnification*). Morphometric analysis showed the absence of a certain percentage of lamellipodial perimeters on RGD substrates (Figure 6d); however, the number of filopodia extensions of ECs validated the expression of filopodial mode of actin machinery on RGD substrates (Figure 6e).

In our model consisting of surfaces with peptide micropatterns of defined sizes and shapes, ECs migrated with two different modes (lamellipodial or filopodial) to peptide micropatterns. In lamellipodial migration of ECs, the extreme leading edge of lamellipodia does not contain focal adhesions (**Figure 7**a-b, *left*); in turn, filopodial extensions end with focal adhesions (Figure 7a-b, *right*). On micropatterned surfaces containing adhesion

component (RGD), ECs spread with prominent, highly organized actin stress fibers and large total FA area and number (Figure 7c). In contrast, ECs on micropatterned surfaces containing non adhesive component (BMP-2) were spread with absence of actin stress fibers and small number of adhesion complexes (Figure 7c). The two different modes of actin machinery (lamellipodial or filopodial) were also maintained even during EC division (**Figure S2**). No lumen formation has been detected in the microenvironment promoting lamellipodial migration mode of ECs (Figure 7d), whatever the geometrical distribution of peptide micropatterns. Lumen formation was induced only in the microenvironment promoting filopodial mode of ECs migration (Figure 7e).

For the two aforementioned systems, we demonstrated that the engagement of integrins (filopodial migration mode) stimulated the process of lumen formation. The protein complexes within the machinery activation of the actin networks are dependent on the extracellular environment. The components of a mature FA are grouped into four basic processes: receptor/matrix binding; actin polymerization; intracellular signal transduction; and attachment to the internal actin cytoskeleton.[32, 33] Integrins not only structurally anchor cells, but they are also important bidirectional transmitters of force-induced signals across the plasma membrane.[32] This is instrumental for cell-ECM binding and subsequent mechano-transduction events.[32, 33] In our work, integrin-RGD binding immediately stimulates mechanical signals and signal transduction molecules (e.g. Rap1 GTPase) that drive subsequent integrin activation/clustering and talin recruitment.[34] Integrin clustering also increases the production of lipid second messengers that further influence signaling cascades.[35] Talin couples to actin,[36] and force-induced deformation of talin molecules reveals binding sites for vinculin.[37] Vinculin further augments integrin clustering and linkage of the complex to the actin cytoskeleton. However, it should be noted that Rho GTPases may promote vinculin binding to actin or actin-binding proteins independently of integrin

clustering; this association of vinculin may play a role in assembly of both stress fibers and focal adhesions.[38] Consequently, forces produced along the actin cytoskeleton by higher order factors such as stress fibers act both upstream and downstream to promote clustering of integrins which contributes to overall lumen structure. However, the lamellipodial machinery (induced by BMP-2) promotes softening of ECs, in turn inhibits the formation of lumen.

Regarding the mechanism of tubulogenesis in this study, we are in the context of cord hollowing process where cells assemble into a thin cylindrical cord to create a lumen between cells, whereas in the process of cell hollowing, the lumen forms within the cytoplasm from a single cell.[14, 39] Firstly, we investigated that the tube formation in our study supports the cord hollowing processes (Figure 5, 7d-e). Indeed, our system is a 2D culture system that explains the collective cells' behaviors. Secondly, we suggested that the cord hollowing process is depending on the nature of cell-cell interactions (adherens junctions, AJs[40]). We observed that the AJs between ECs on 50 μm stripes of BMP-2 are less concentrated than that on 50 μm stripes of RGD (**Figure S3**). However, the nature of AJs (PECAM-1) is the same. We suggest that the correct maturation of adherens junctions (AJs) and status of F-actin fiber stress are responsible for promoting tubulogenesis. With BMP-2 micropatterns, the cells possessed poor F-actin stress fibers (Figure 7) and low density of AJs (Figure S3), which consequently disturbed the process of tubulogenesis of endothelial cells.

There are today a number of studies concerning the impact of integrin engagement on EC response.[41] All these studies are conducted to achieve two points: the inhibition of angiogenesis in the cases of diseases, and the promotion of angiogenesis in the case of tissue repair with biomaterials. For example, in the case of bone repair, the aim was not only to differentiate osteoblasts to produce ECM and to enhance its mineralization, but also to vascularize this tissues with microvasculature networks that provide nutrients and oxygen.[42,

[43] The overall goal is to have a biomaterial with vascularization and compatibility with the implanted tissue.

3. Conclusion

In this study, we propose a model to study EC functions with microgeometrical composition. We have successfully applied a photolithographic technique to control EC functions through actin machinery expression. Large patterns (100 μm) promoted EC orientation without lumen formation, whereas small patterns (10-50 μm) elicited a collective cell organization and induced EC lumen formation, in the case of RGD peptides which induced filopodial migration mode of ECs. The disengagement of integrins inhibits lumen formation by the inhibition of filopodial structures, in the case of surfaces mimicked by BMP-2 peptides. Our understanding suggests that both the peptide microgeometrical cues and the engagement of integrins regulate the fate of ECs to form the structure of lumen. This gives a new concept for the design of biomaterials for tissue engineering and may provide new insight for angiogenesis inhibition on tumors.

4. Experimental Section

Materials: PET film (commercial bi-oriented film with thickness of 100 μm) is obtained from Goodfellow, France. Inorganic reagents (NaOH, $KMnO_4$, H_2SO_4 and HCl), acetone, acetonitrile, dimethylaminopropyl-3-ethylcarbodiimide hydrochloride (EDC), N-hydroxy Succinimide (NHS) and 2-(N-morpholino)-ethanesulfonic acid (MES) were purchased from Sigma-Aldrich, France. GRGDS, BMP-2 mimetic peptide (sequence: RKIPKASSVPTELSAISMLYL[23]) and GRGDSK-FITC peptides were synthesized by Genecust, France.

Preparation of micropatterned surface: Micropatterns on polymer surfaces were fabricated by photolithography as previously reported.[22] Briefly, the surface of materials were coated with S1818 photoresist (Rohm and Haas, USA) and spun at 1100 rpm for 30 s to obtain a uniform photoresist layer with thickness of approximately 2 µm. The surfaces were baked for 10 min at 110 °C. The films were then exposed to UV light (60 W) through a high-resolution Cr mask with predesigned pattern dimensions (Femto-St Sciences & Technologies, France) for 18 s. The films were then developed in Microposit Developer solution (Rohm and Haas, USA) to dissolve exposed photoresist, resulting in the desired pattern on polymer surface (Figure 1a).

Covalent grafting of peptides onto polymer surface: Polymer surfaces were modified according to Chollet *et al.* with some modifications.[15, 44] Briefly, PET films were hydrolyzed and oxidized to create COOH groups on the surfaces (named as "PET-COOH"). After this step, surfaces with micropatterns can be fabricated using photolithography as described in the above section. Then, the surfaces were immersed in a solution of EDC (0.2M) + NHS (0.1M) + MES (0.1M) in MilliQ water for surface activation. Finally, the surfaces were immersed in peptide solution (10^{-3} M in PBS) at room temperature for 16 h for peptide immobilization. After covalent immobilization, the surfaces were rinsed with MilliQ water for 1 week. Finally, the photoresist surrounding the peptide patterns was removed by acetone, resulting in micropatterned peptides on polymer surfaces. The peptide patterned and unpatterned regions on polymer surfaces were PET-peptide and PET-COOH, respectively. A schematic for peptide micropatterning onto polymer surfaces is presented in Figure 1a. Polymer surfaces micropatterned with 10, 50 and 100 µm RGD micropatterns with same interspaces of 100 µm were prepared. Immobilization of peptides onto non-patterned polymer surface was served as controls (named as "unpatterned" surfaces).

Surface characterizations: Fluorescent peptides were used to validate the peptide micropatterning onto PET surfaces.[23] GRGDS peptides were covalently conjugated to FITC fluochromes via Lysine (K) (GRGDSK-FITC), and the fluorescent peptides were grafted onto polymer surfaces as described in the above sections. Epifluorescence microscopy (Leica DM5500B, Germany) was employed for visualization of fluorescent peptide micropatterns.

Peptide density evaluation: The peptide densities on surfaces were evaluated by indirect fluorescence microscopy measurement.[26, 45] Briefly, FITC fluorochrome was covalently linked to the end of GRGDS peptides via Lysine (K) (labelled as GRGDSK–FITC). Then the fluorescent peptides were immobilized onto PET surfaces. Quantification of fluorescence intensity on surfaces with FITC-labelled peptides was performed with fluorescent microscopy (Leica DM5500B, Germany) and Leica MMAF software. Firstly, a calibration curve was established: a series of FITC with well-known quantities (from 1.1 to 18.4 nmol) was deposited on native surfaces and photographed with fluorescent microscopy, and the total fluorescence was quantified by Leica MMAF. Then the patterned or unpatterned surfaces grafted with FITC-labelled peptides were observed at the same magnification, and the fluorescence on each surface was quantified by Leica MMAF. Finally, the density of fluorescent peptide was determined according to the calibration curve (in nmol/cm^2).

The surface roughness of the PET-COOH and PET-peptide materials were characterized using atomic force microscopy (AFM) (Dimension 3100, Veeco) in tapping mode at a rate of 0.4 Hz at room temperature. The mechanical properties of PET-COOH and PET-peptide surfaces (RGD) were evaluated by nanoindentation technique as described by Zouani *et al.*.[46]

Cell culture: Human umbilical vein endothelial cells (HUVECs) were isolated from the human umbilical cord vein as described by Li *et al.*.[47] HUVECs were isolated and grown on gelatin coated culture flasks in a complete HUVEC culture medium (IMDM (Invitrogen, France) supplemented with 20% (v/v) fetal bovine serum (FBS) (PAA, France) and 0.4% (v/v) EC growth supplement/heparin kit (Promocell, France)). Cells were subcultured using trypsin/EDTA (Invitrogen, France) and maintained in a humidified atmosphere containing 5% CO_2 at 37 °C. Cells at passages 3 to 5 were used for experiments.

Cell adhesion: Different surfaces (unpatterned and patterned) were sterilized by 70% ethanol and fixed by the mean of glass rings. HUVECs were seeded on each surface at a density of 50000 cells/cm^2 for 4 h in serum free IMDM medium, which was used to avoid surface adsorption by proteins presented in serum, then in IMDM medium supplemented with 10% FBS for 20 h at 37 °C and 5% CO_2. The specimens were observed by phase-contrast microscopy (Zeiss Axiovert 25, Germany) during cell culture.

Cell staining: After 24 h in culture, cells were fixed by 4% (w/v) paraformaldehyde (PFA) at room temperature for 15 min, permeabilized with 0.5% Triton-X 100 and blocked with 1% bovine serum albumin, and then stained with primary and secondary antibodies. The primary antibodies used were mouse anti-vinculin antibody (Sigma, France), mouse anti-CD31 (PECAM-1) antibody (Invitrogen, France). Then samples were incubated with primary antibodies for 1 h at 37 °C, then coupled with Alexa Fluor® 568 goat anti-mouse IgG secondary antibody (Invitrogen, France) for 30 min at room temperature. Subsequently, cell actin was stained with Alexa Fluor® 488 phalloidin (Invitrogen, France) for 1 h at 37 °C. Nuclei were counterstained by DAPI (Sigma, France) for 10 min at room temperature. The

samples were mounted in Vectashield (Vector, USA) and observed by epifluorescence microscopy.

Determination of cell area: Cell areas were measured to evaluate the spreading level of ECs on different surfaces. ImageJ (NIH, http://rsb.info.nih.gov/ij/) was used for image analysis. The projected cell areas were determination by tracing the edges of actin cytoskeleton drawn from fluorescent images. At least twenty fields on each surface at lower magnification (10 X) were randomly photographed for this analysis.

Orientation of cell body: To study the effect of peptide micropatterning on cell orientation, fluorescent images of actin cytoskeleton at 40 X magnification were acquired and analyzed using ImageJ. Cell body alignment and elongation were evaluated as previously demonstrated.[28, 48] The cell body alignment angle, defined as the angle of the major axis of the cell body with respect to the direction of micropatterns,[28] was measured using ImageJ. For endothelial cells on unpatterned surfaces, the angle of the cell body major axis with respect to an arbitrary axis (here at 0°) was taken for cell alignment angle. A cell was aligned perfectly parallel to the direction of pattern when the alignment angle was 0° and perfectly perpendicular to the patterns when the alignment angle was 90°. For statistical analysis, alignment angles were subsequently grouped in 10° increments with respect to axis of micropatterns, cells with an alignment angle less than 10° were considered to be aligned.[28] For cell elongation analysis, cell body was fitted into an ellipse and cell area (s) and perimeter (l) were measured by ImageJ. The cell morphology was characterized by cell shape index (I) according to the following formula: $I = 4\pi s/l^2$.[48] Cells are round when I is equal to 1 and cells become infinitely elongated as I approaches 0. At least eighty cells for each surface were analyzed in this study.

Orientation of focal contacts: For analysis of orientation of cell focal contacts, fluorescent images of vinculin staining at 40 X magnification were converted to 8-bit file by ImageJ. After removing image background and smoothing, the resulting images appeared similar to the original photograph but with minimal background. Then the images were converted into a binary image by setting a threshold. Threshold values were determined empirically by selecting a setting which gave the most accurate binary image for a subset of randomly selected photograph. Then, the tool of "analyze particles" in ImageJ was employed to analyze the alignment angle, the area, perimeter, and shape index of focal contacts. Contact points less than 5 pixels were not taken into account. At least 30 cells per condition were analyzed in this study.

EC morphogenesis and visualization: To obtain a rapid morphogenesis, ECs were seeded at a density of 50000 cells/cm^2 in EGM®-2 medium (Lonza, France), which is a commercial medium containing the growth supplements in order that the ECs can have *in vivo*-like behaviors.[12, 49] The cells were photographed by phase contract microscopy and fixed when morphogenesis of ECs appeared after 28 h of culture. For visualization of EC tubular structures, ECs were labeled with 2 μM Cell Tracker Green (CMFDA, Invitrogen, France) for 30 minutes before fixation according to the technical protocol of product. Subsequently the cell nuclei were stained with DAPI. Confocal microscopy (Leica SP5, Germany) was used to access images of ECs in different z-stages. Imaris 7.0 software was used for three-dimensional (3D) reconstruction of confocal images.

Optical Profiling System (OPS): Wyko surface profiler systems (Veeco-NT1100, USA) are non-contact optical profilers that use two technique modes to measure a wide range

of surface heights. Phase-shifting interferometry (PSI) mode allows measuring smooth surfaces and small steps, while vertical scanning interferometry (VSI) mode allows measuring rough surfaces and steps up to several micrometers high. PSI mode was used to determine the nano-topography of surfaces. VSI mode was used to measure the thickness of the cells on the substrates. To achieve this, cells were fixed, dehydrated, metalized, and then measured under VSI mode. Wyko Vision V3.60 software was used for 3D reconstruction of OPS images.

Statistical analysis: Data were represented as mean values ± standard deviation. Statistical analysis was performed by one way analysis of variance (ANOVA). A *p*-value less than 0.05 was considered statistically significant.

Acknowledgements

The authors thank to Annie Zhe Cheng and Dr. Rajat K. Das for English language assistance, thank to Dr. Cédric Ayela, Céline Chollet, Christel Chanseau and Christine Labrugère for technical assistance, thank to Sébastien Marais (Bordeaux Image Center) for image analysis assistance. This work was supported by the "Région Aquitaine", the GIS "Advanced Materials in Aquitaine" as well as the "Agence Nationale pour la Recherche" (ANR).

References

[1] G. D. Yancopoulos, M. Klagsbrun, J. Folkman, *Cell* **1998,** *93* (5), 661-4.

[2] R. Kerbel, J. Folkman, *Nat Rev Cancer* **2002,** *2* (10), 727-39.

[3] E. A. Phelps, A. J. Garcia, *Curr Opin Biotechnol* **2010,** *21* (5), 704-9.

[4] M. R. Mejillano, S.-i. Kojima, D. A. Applewhite, F. B. Gertler, T. M. Svitkina, G. G. Borisy, *Cell* **2004,** *118* (3), 363-373.

[5] S. Huang, D. E. Ingber, *Cancer Cell* **2005,** *8* (3), 175-6.

[6] Z. K. Otrock, R. A. Mahfouz, J. A. Makarem, A. I. Shamseddine, *Blood Cells Mol Dis* **2007,** *39* (2), 212-20.

[7] R. K. Jain, *Nat Med* **2003,** *9* (6), 685-93.

[8] M. L. Ponce, *Methods Mol Biol* **2009,** *467*, 183-8.

[9] Y. Kubota, H. K. Kleinman, G. R. Martin, T. J. Lawley, *J Cell Biol* **1988,** *107* (4), 1589-98.

[10] L. E. Dike, C. S. Chen, M. Mrksich, J. Tien, G. M. Whitesides, D. E. Ingber, *In Vitro Cell Dev Biol Anim* **1999,** *35* (8), 441-8.

[11] C. C. Co, Y. C. Wang, C. C. Ho, *J Am Chem Soc* **2005,** *127* (6), 1598-9.

[12] J. J. Moon, M. S. Hahn, I. Kim, B. A. Nsiah, J. L. West, *Tissue Eng Part A* **2009,** *15* (3), 579-85.

[13] Y. Hamada, K. Nokihara, M. Okazaki, W. Fujitani, T. Matsumoto, M. Matsuo, Y. Umakoshi, J. Takahashi, N. Matsuura, *Biochem Biophys Res Commun* **2003,** *310* (1), 153-7.

[14] Y. Lei, O. F. Zouani, M. Rémy, C. Ayela, M.-C. Durrieu, *PLoS ONE* **2012,** *7* (7), e41163.

[15] C. Chollet, C. Chanseau, M. Remy, A. Guignandon, R. Bareille, C. Labrugere, L. Bordenave, M. C. Durrieu, *Biomaterials* **2009,** *30* (5), 711-20.

[16] D. Falconnet, G. Csucs, H. M. Grandin, M. Textor, *Biomaterials* **2006,** *27* (16), 3044-63.

[17] A. Khademhosseini, R. Langer, J. Borenstein, J. P. Vacanti, *Proc Natl Acad Sci U S A* **2006,** *103* (8), 2480-7.

[18] N. M. Alves, I. Pashkuleva, R. L. Reis, J. F. Mano, *Small* **2010,** *6* (20), 2208-2220.

[19] M. Arnold, E. A. Cavalcanti-Adam, R. Glass, J. Blümmel, W. Eck, M. Kantlehner, H. Kessler, J. P. Spatz, *ChemPhysChem* **2004,** *5* (3), 383-388.

[20] J. Huang, S. V. Grater, F. Corbellini, S. Rinck, E. Bock, R. Kemkemer, H. Kessler, J. Ding, J. P. Spatz, *Nano Lett* **2009,** *9* (3), 1111-6.

[21] S. Kruss, T. Wolfram, R. Martin, S. Neubauer, H. Kessler, J. P. Spatz, *Advanced Materials* **2010,** *22* (48), 5499-5506.

[22] C. Chollet, S. Lazare, F. Guillemot, M. C. Durrieu, *Colloids Surf B Biointerfaces* **2010,** *75* (1), 107-14.

[23] O. F. Zouani, C. Chollet, B. Guillotin, M. C. Durrieu, *Biomaterials* **2010,** *31* (32), 8245-53.

[24] D. R. Jung, R. Kapur, T. Adams, K. A. Giuliano, M. Mrksich, H. G. Craighead, D. L. Taylor, *Crit Rev Biotechnol* **2001,** *21* (2), 111-54.

[25] A. J. Engler, S. Sen, H. L. Sweeney, D. E. Discher, *Cell* **2006,** *126* (4), 677-89.

[26] Y. Lei, M. Rémy, C. Labrugère, M.-C. Durrieu, *Journal of Materials Science: Materials in Medicine* **2012**, 1-12.

[27] A. Magnani, A. Priamo, D. Pasqui, R. Barbucci, *Materials Science and Engineering: C* **2003,** *23* (3), 315-328.

[28] J. L. Charest, L. E. Bryant, A. J. Garcia, W. P. King, *Biomaterials* **2004,** *25* (19), 4767-75.

[29] M. D. Schaller, *J Cell Sci* **2010,** *123* (Pt 7), 1007-13.

[30] B. Wehrle-Haller, B. A. Imhof, *Int J Biochem Cell Biol* **2003,** *35* (1), 39-50.

[31] N. D. Gallant, K. E. Michael, A. J. Garcia, *Mol Biol Cell* **2005,** *16* (9), 4329-40.

[32] D. A. Calderwood, *J Cell Sci* **2004,** *117* (Pt 5), 657-66.

[33] E. Puklin-Faucher, M. Gao, K. Schulten, V. Vogel, *J Cell Biol* **2006,** *175* (2), 349-60.

[34] G. Giannone, B. J. Dubin-Thaler, H. G. Dobereiner, N. Kieffer, A. R. Bresnick, M. P. Sheetz, *Cell* **2004,** *116* (3), 431-43.

[35] K. L. Auer, B. S. Jacobson, *Mol Biol Cell* **1995,** *6* (10), 1305-13.

[36] G. Jiang, G. Giannone, D. R. Critchley, E. Fukumoto, M. P. Sheetz, *Nature* **2003,** *424* (6946), 334-7.

[37] A. del Rio, R. Perez-Jimenez, R. Liu, P. Roca-Cusachs, J. M. Fernandez, M. P. Sheetz, *Science* **2009,** *323* (5914), 638-41.

[38] L. M. Machesky, A. Hall, *J Cell Biol* **1997,** *138* (4), 913-26.

[39] B. Lubarsky, M. A. Krasnow, *Cell* **2003,** *112* (1), 19-28.

[40] Z. Liu, J. L. Tan, D. M. Cohen, M. T. Yang, N. J. Sniadecki, S. A. Ruiz, C. M. Nelson, C. S. Chen, *Proc Natl Acad Sci U S A* **2010,** *107* (22), 9944-9.

[41] K. Ghosh, D. E. Ingber, *Adv Drug Deliv Rev* **2007,** *59* (13), 1306-18.

[42] R. K. Jain, P. Au, J. Tam, D. G. Duda, D. Fukumura, *Nat Biotechnol* **2005,** *23* (7), 821-3.

[43] M. I. Santos, R. L. Reis, *Macromol Biosci* **2010,** *10* (1), 12-27.

[44] C. Chollet, C. Chanseau, B. Brouillaud, M. C. Durrieu, *Biomol Eng* **2007,** *24* (5), 477-82.

[45] L. Pichavant, G. Amador, C. Jacqueline, B. Brouillaud, V. Héroguez, M.-C. Durrieu, *Journal of Controlled Release* **2012,** *162* (2), 373-381.

[46] O. F. Zouani, C. Chanseau, B. Brouillaud, R. Bareille, F. Deliane, M.-P. Foulc, A. Mehdi, M.-C. Durrieu, *Journal of Cell Science* **2012,** *125*, 1-8. DOI 10.1242/jcs.093229.

[47] H. Li, R. Daculsi, M. Grellier, R. Bareille, C. Bourget, J. Amedee, *Am J Physiol Cell Physiol* **2010,** *299* (2), C422-30.

[48] S. S. Banerjee, D. Paul, S. G. Bhansali, N. D. Aher, A. Jalota-Badhwar, J. Khandare, *Small* **2012,** *8* (11), 1657-63.

[49] I. Arnaoutova, H. K. Kleinman, *Nat Protoc* **2010,** *5* (4), 628-35.

Received: ((will be filled in by the editorial staff))
Revised: ((will be filled in by the editorial staff))
Published online on ((will be filled in by the editorial staff))

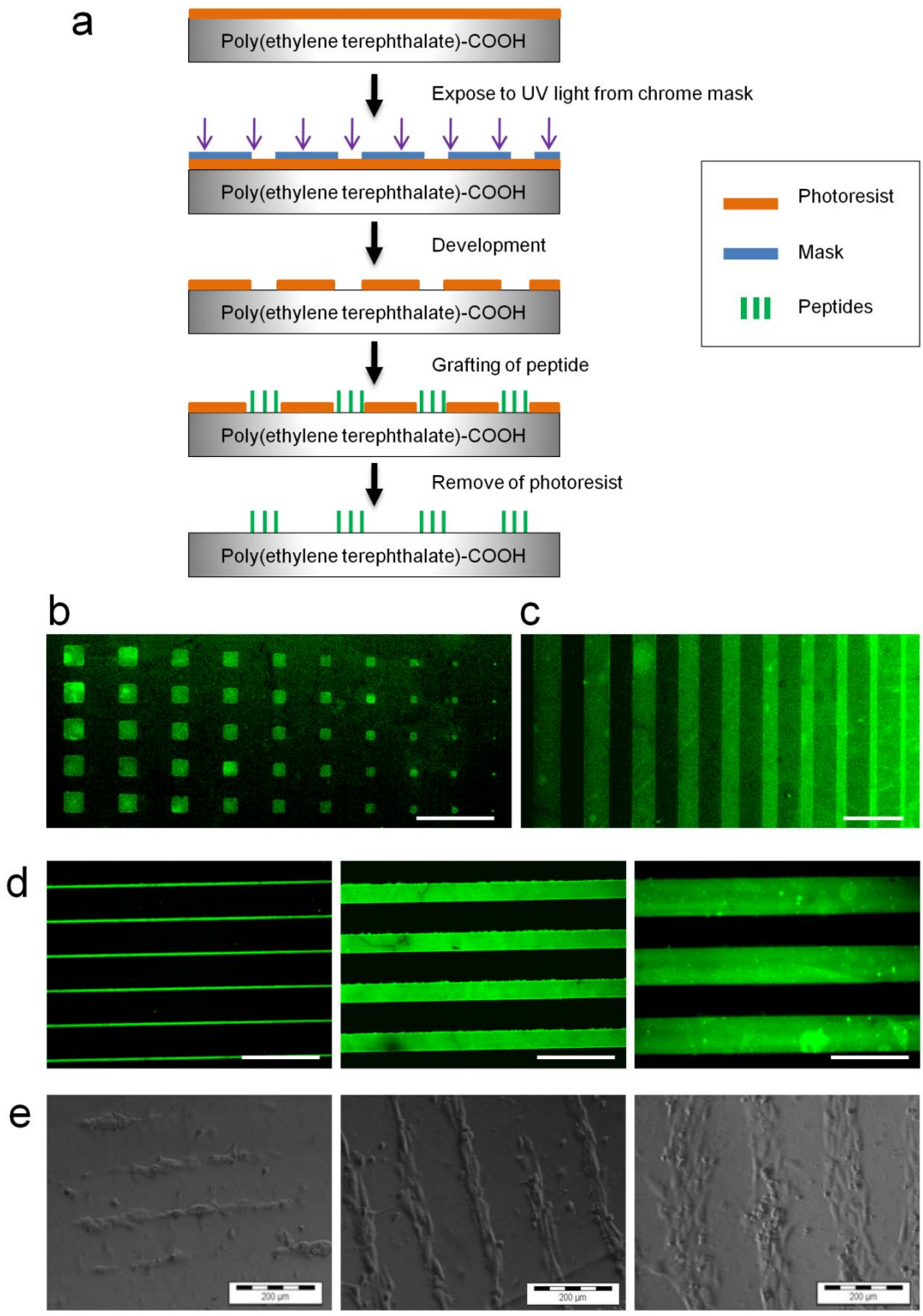

Figure 1. (a) Schematic of peptide micropatterning onto polymer surfaces using photolithography. (b) and (c) correspond to respective squares and lines from 100 µm to 10 µm with immobilization of fluorescent peptides (GRGDSK-FITC). (d) Surfaces micropatterned with 10, 50 and 100 µm stripes of fluorescent peptides, respectively. (e) EC alignment on 10, 50 and 100 µm RGD peptide stripes, respectively. Scale bars are 200 µm.

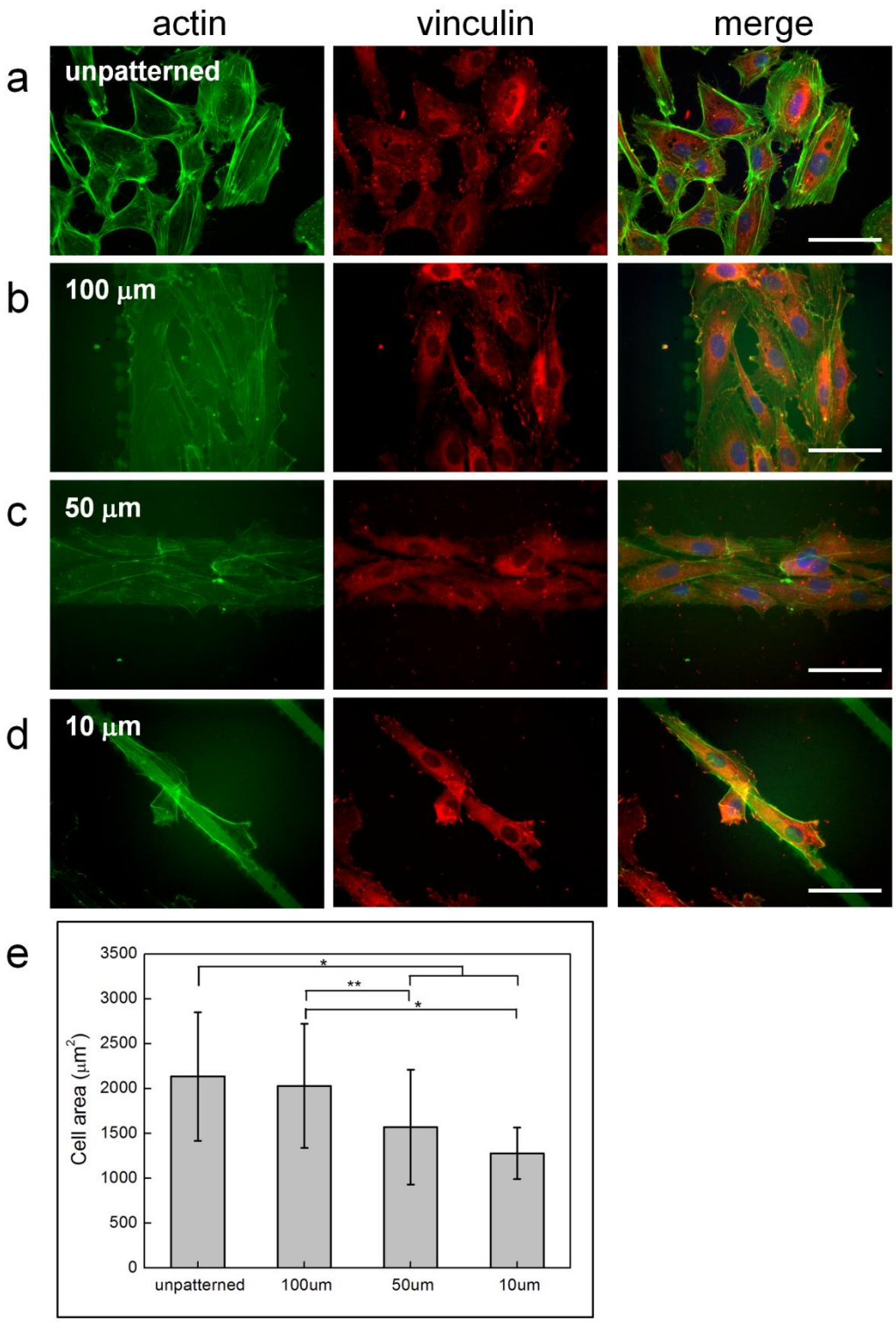

Figure 2. Representative images of ECs on (a) unpatterned surfaces, (b) 100 μm, (c) 50 μm and (d) 10 μm RGD micropatterns. Phalloidin and vinculin were stained in green and red, respectively. The merged channels (with DAPI staining in blue) were represented in the right column. Scale bars are 50 μm. (e) EC areas on different surfaces (* $p < 0.01$; ** $0.01 < p < 0.05$).

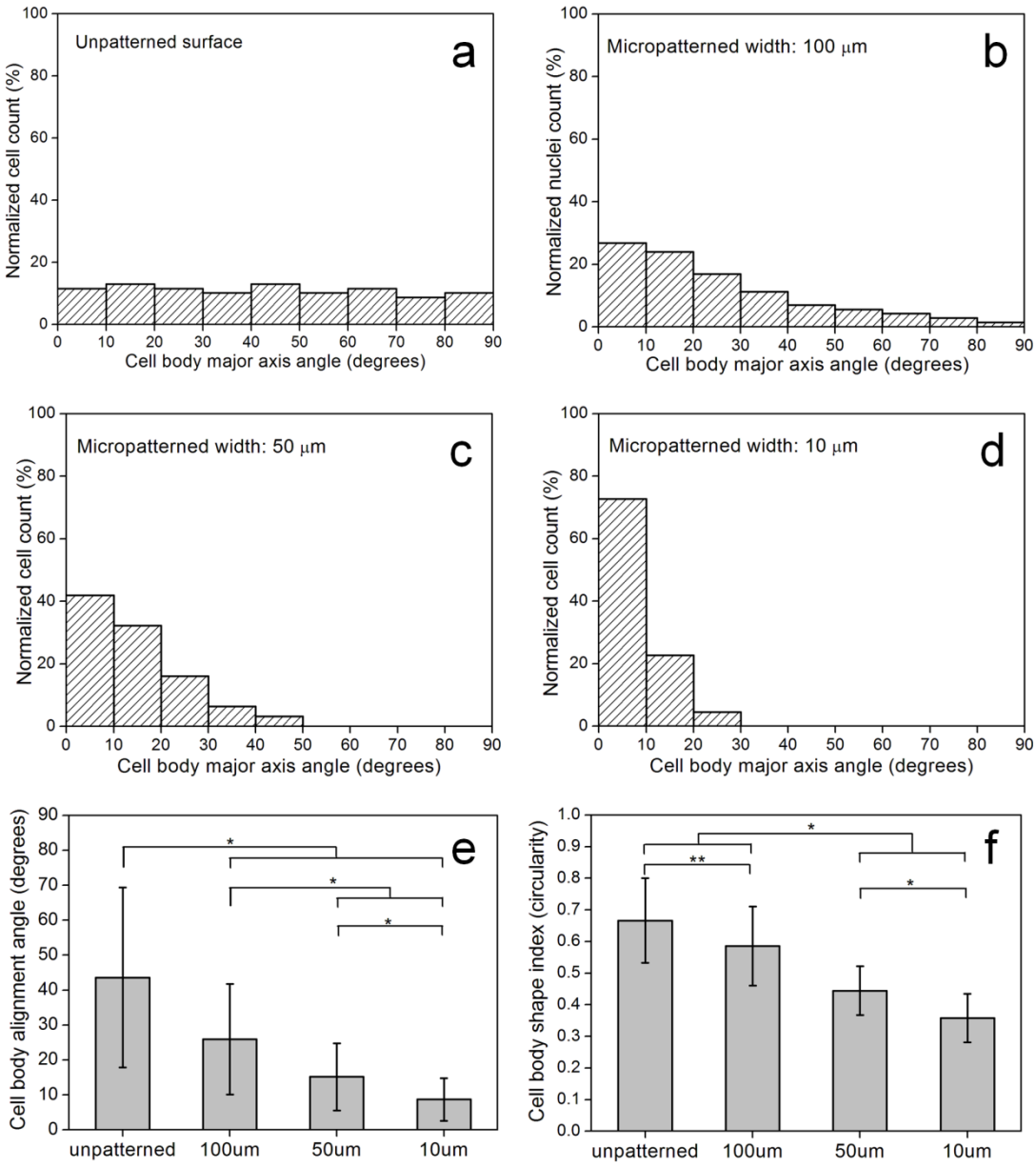

Figure 3. Histogram of alignment angle of cell body on (a) unpatterned surface, (b) 100 μm, (c) 50 μm and (d) 10 μm RGD micropatterns. The mean alignment angle and shape index of cell body were represented in (e) and (f), respectively (* $p < 0.01$; ** $0.01 < p < 0.05$).

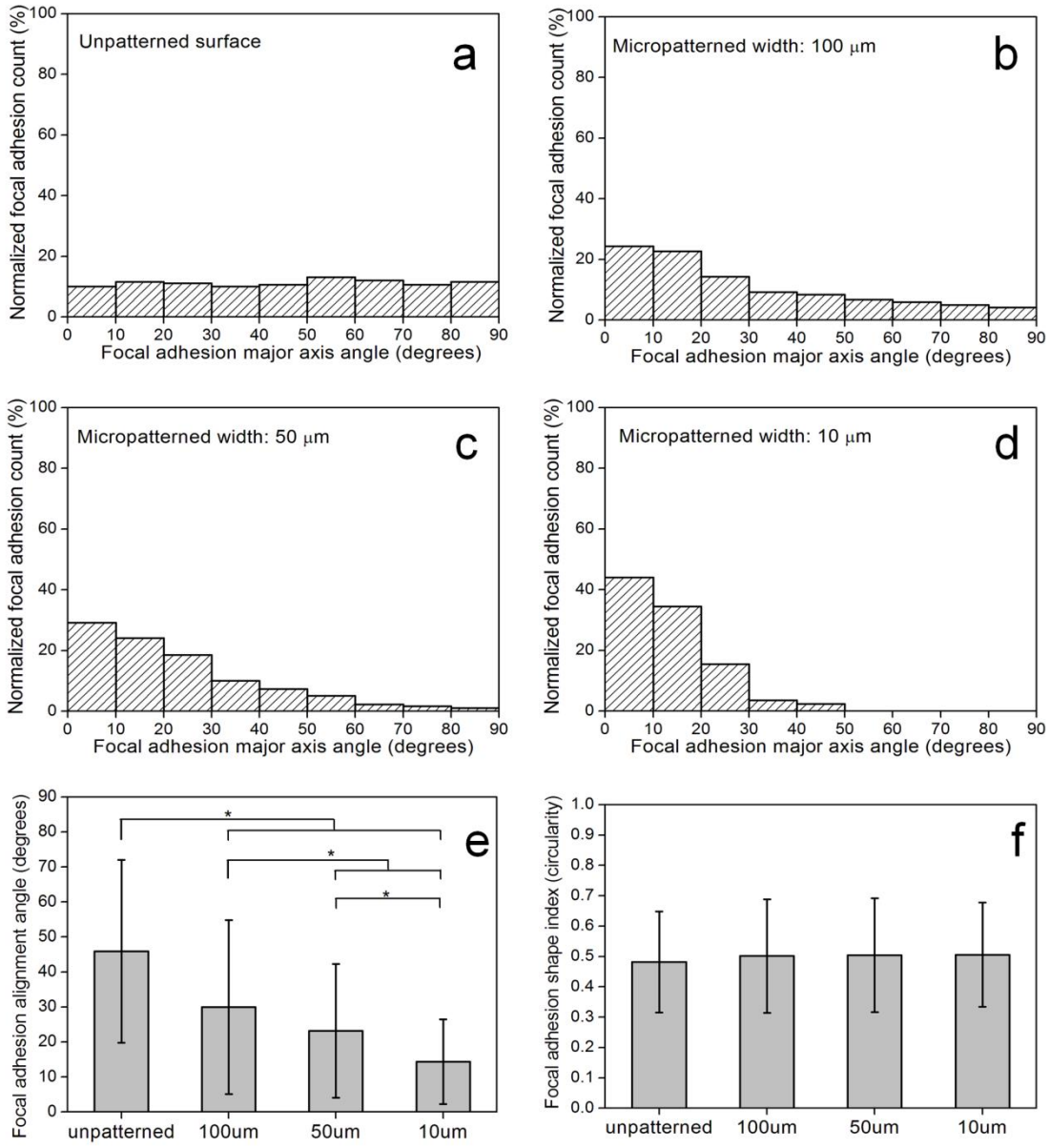

Figure 4. Histogram of alignment angle of cell focal contacts on (a) unpatterned surface, (b) 100 μm, (c) 50 μm and (d) 10 μm RGD micropatterns. The mean alignment angle and shape index of cell focal contacts were shown in (e) and (f), respectively (* $p < 0.01$; ** $0.01 < p < 0.05$).

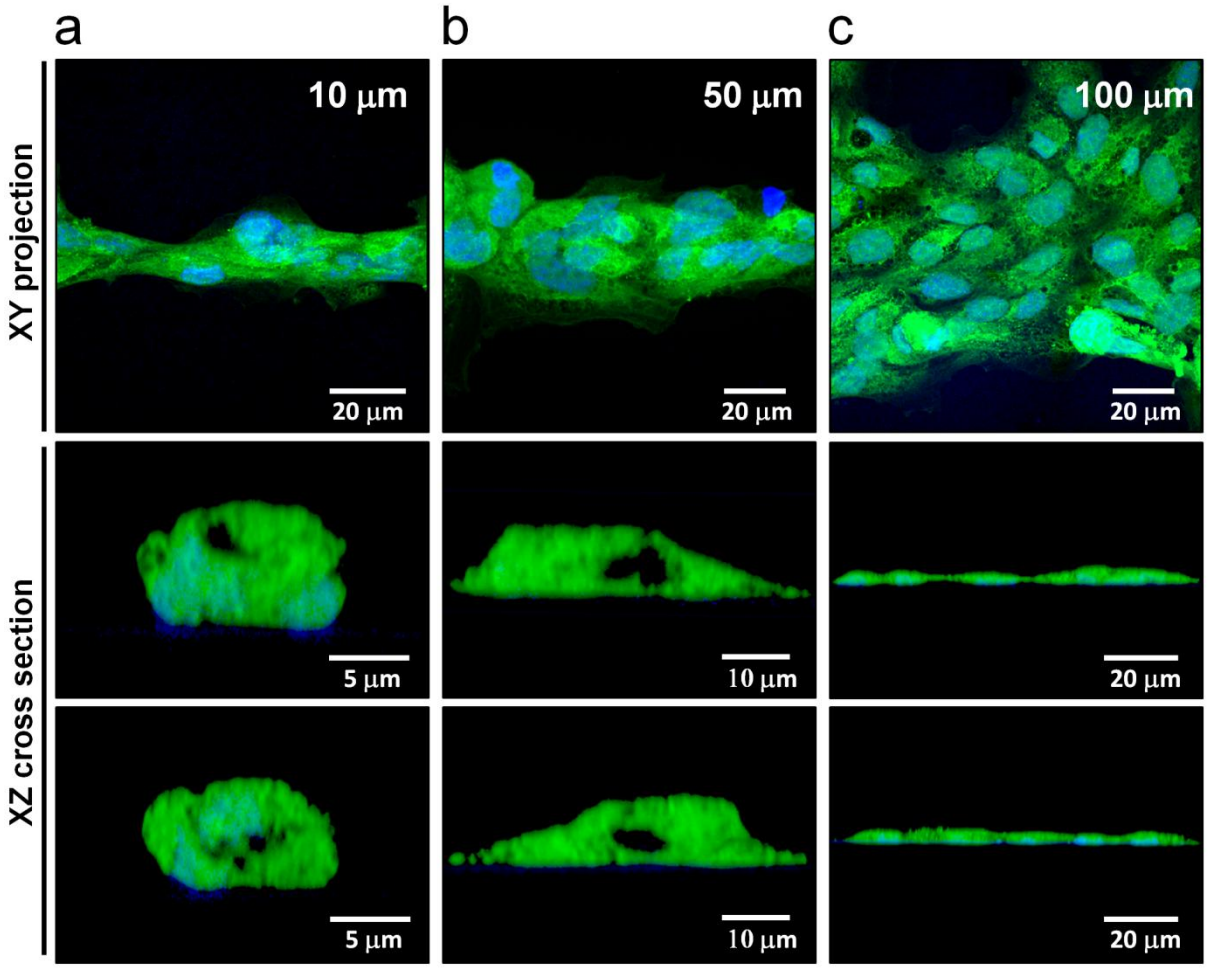

Figure 5. Confocal images of ECs on (a) 10 μm, (b) 50 μm and (c) 100 μm RGD micropatterns. Up: horizontal projections of ECs' confocal images; down: vertical confocal image cross sections of ECs. CMFDA and DAPI were represented in green and blue, respectively.

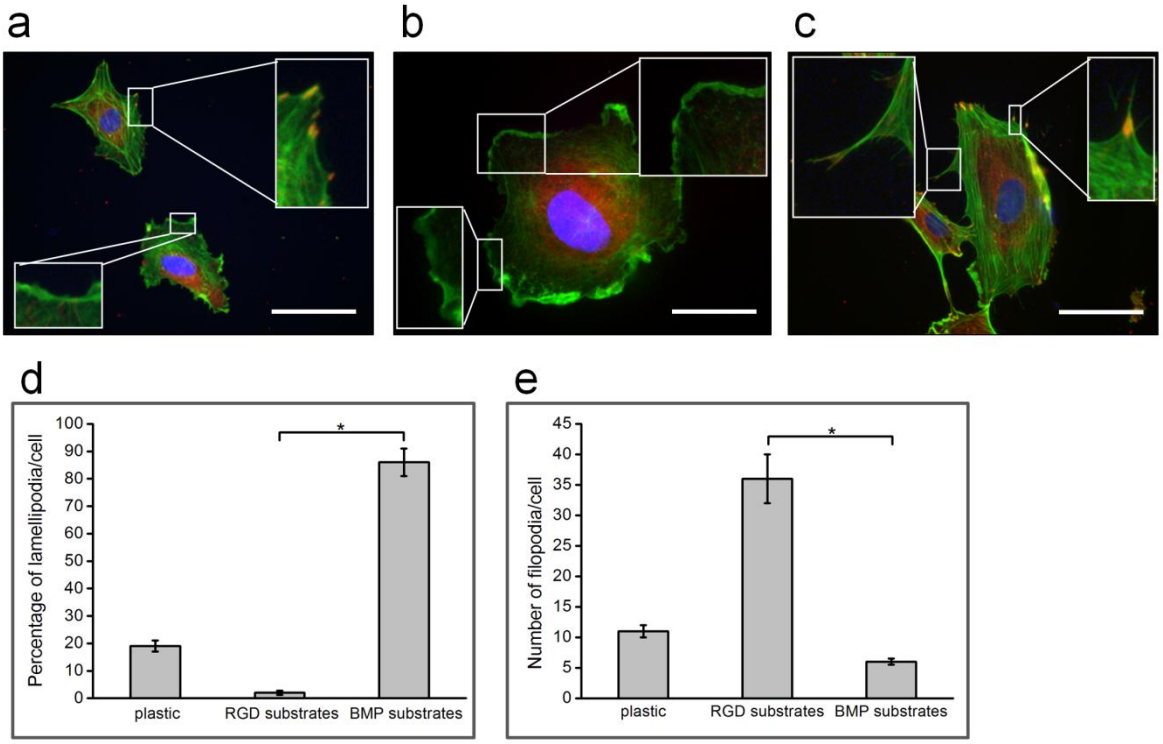

Figure 6. Induction of lamellipodial and filopodial mode of the actin machinery. (a) Distribution of actin and focal adhesions (FAs) in ECs cultured on plastic culture dish for 24h. Actin and FAs were revealed by staining of phalloidin (green) and vinculin (red), respectively. DAPI were shown in blue. Magnifications demonstrate that ECs express both lamellipodial and filopodial modes of actin machinery. (b, c) Fluorescent images of ECs on two culture systems: polymer surfaces homogeneously grafted with BMP-2 and RGD peptides, respectively. ECs express either lamellipodial or filopodial molecular machinery on the two culture systems, respectively. Scale bars are 50 µm. (d) and (e) present the quantification of lamellipodia perimeter and filopodia enrichment of ECs on the two culture substrates, respectively. Bars represent average (%) of cell perimeter occupied by lamellipodial network (d) or average number of filopodia (e) in ECs.

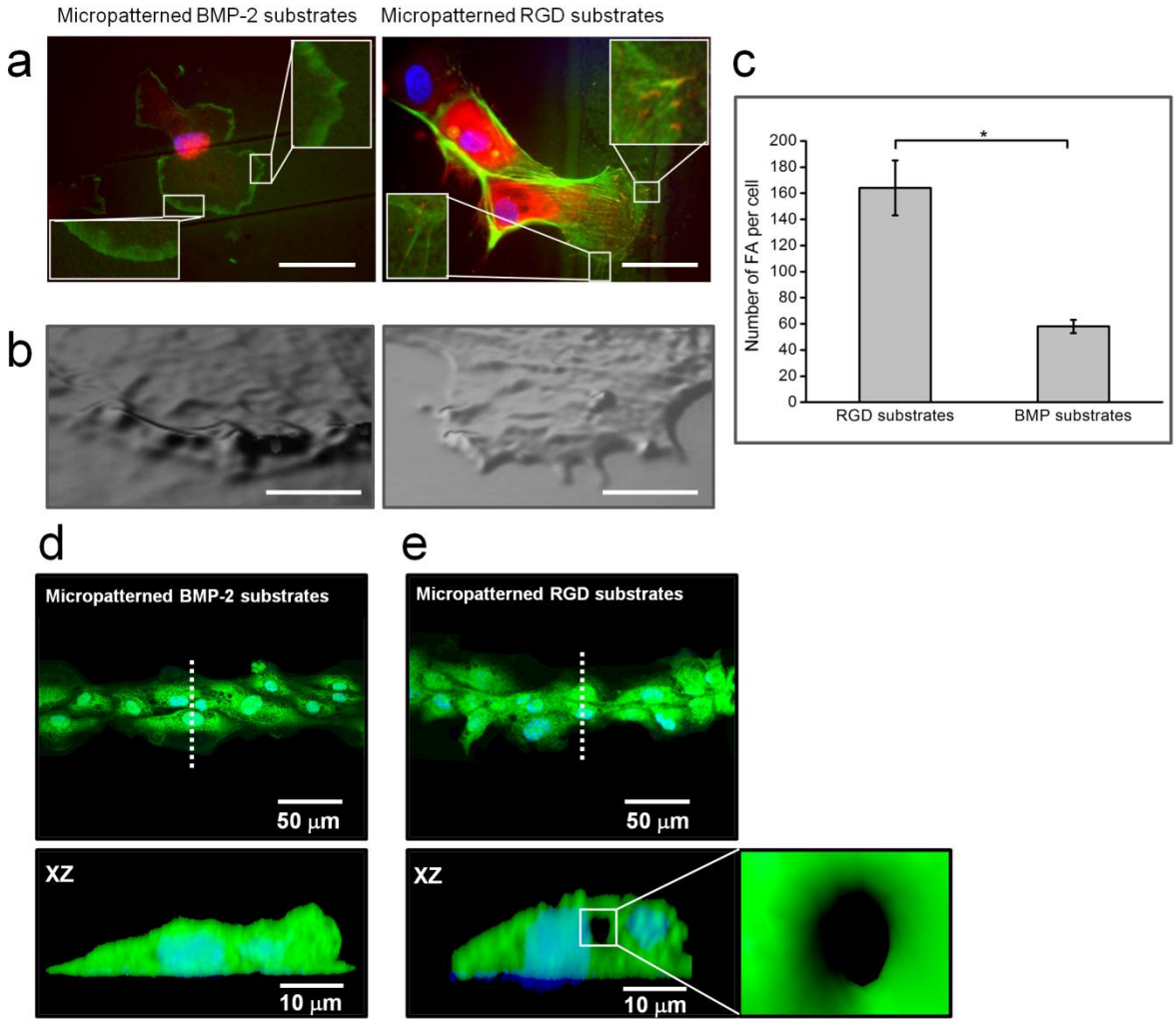

Figure 7. Filopodial but not lamellipodial migration mode of ECs promotes lumen formation. (a) Fluorescence images of ECs on two micropatterned culture systems (50 μm stripes of BMP-2 and 50 μm stripes of RGD) revealed the induction of EC lamellipodial and filopodial migration mode, respectively. EC staining with phalloindin, vinculin and DAPI were shown in green, red and blue, respectively. Scale bars are 50 μm. (b) OPS micrographs of cells revealed the protrusion of ECs on two respective micropatterned culture systems. Scale bars are 5 μm. (c) Quantification of total number of FAs per cell on two respective micropatterned substrates. (d) Confocal images showed that the ECs on 50 μm BMP-2 stripes were spread as a monolayer. (e) ECs underwent the lumen formation on 50 μm RGD micropatterns after 28 h in culture. ECs were labeled with CMFDA (green) and DAPI (blue).

Table 1. Chemical-physical characterization of materials

Materials	Roughness (Ra, nm)	Elastic modulis (*E*, GPa)
PET-COOH	6.4 ± 0.6	1.6 ± 0.1
PET-peptide (RGD)	7.0 ± 0.4	1.6 ± 0.2

Supplementary Information

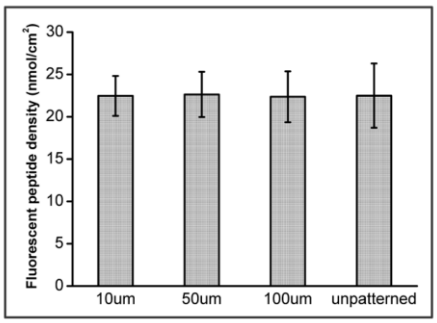

Figure S1. Fluorescent peptide density on unpatterned surfaces and within peptide micropatterns.

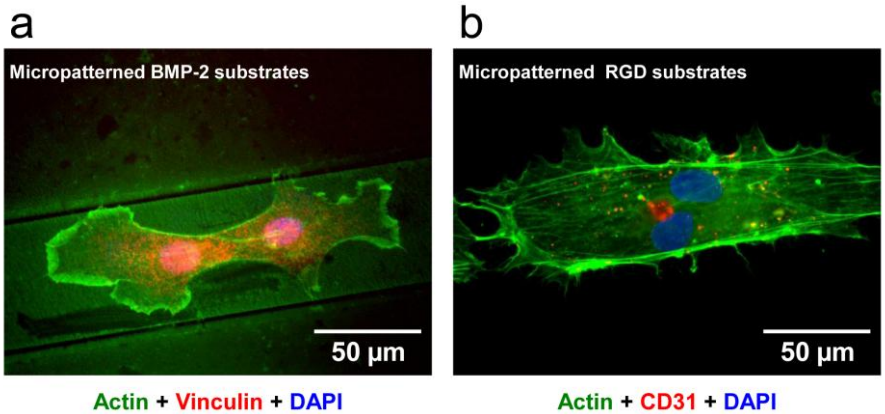

Figure S2. Lamellipodial and filopodial mode of actin machinery were induced by (a) 50 µm micropatterns of BMP-2 mimetic peptide and (b) 50 µm micropatterns of RGD peptide, respectively.

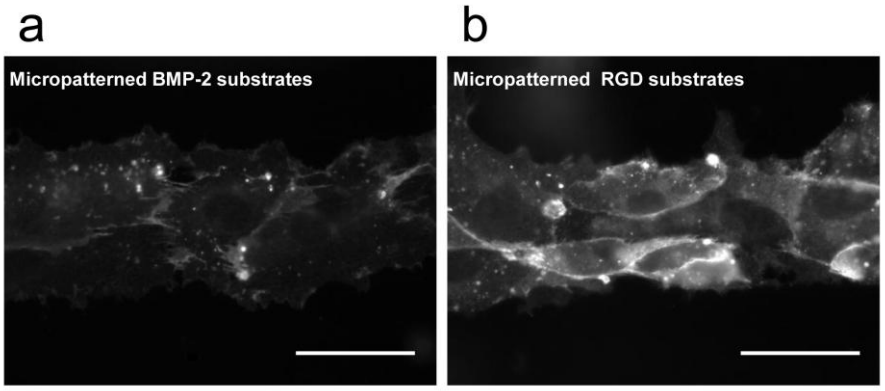

Figure S3. EC adherens junctions (AJs) were obtained from fluorescence staining with antibody against CD31. AJs on micropatterned surfaces with (a) 50 μm stripes of BMP-2 mimetic peptide and (b) 50 μm stripes of RGD peptide. Scale bars are 50 μm.

Peptide micropatterning on polymer surfaces are designed to control the endothelial cell (EC) functions. After cell seeding, ECs are aligned onto the peptide micropatterns, ECs' tubular structures with central lumen formation are regulated by both microgeometrical cues of peptide micropatterns, and the different migration mode of actin machinery on peptide micropatterns.

Keyword: Angiogenesis, filopodial migration, lamellipodial migration, surface functionalization, surface micropatterning

Yifeng Lei*, Omar F. Zouani*, Murielle Rémy, Lila Rami and Marie-Christine Durrieu

Modulation of Lumen Formation by Microgeometrical Bioactive Cues and Migration Mode of Actin Machinery

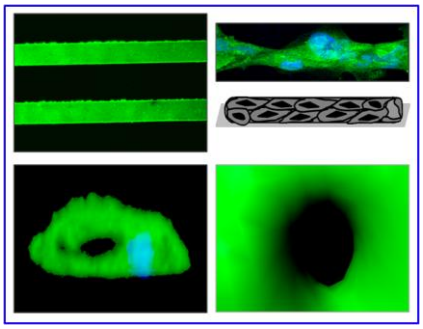

Page Headings
Left page: Y. Lei et al.
Right page: Lumen Formation by Microgeometrical Cues and Migration Mode of Actin Machinery

Paper III. Geometrical microfeature cues for directing tubulogenesis of endothelial cells

PLoS ONE. 2012, 7 (7): e41163.

EC tube-like formation and sprouting angiogenesis were induced by SVVYGLR peptide micropatterning. The central lumen of tubular structures can be formed by only single-to-four cells due to geometrical constraints applied on the micropatterns.

This work was carried out in close collaboration with the "Laboratoire de l'Intégration du Matériau au Système" (IMS) - Université de Bordeaux 1, and more precisely with Professor Claude Pellet and Dr. Cédric Ayela.

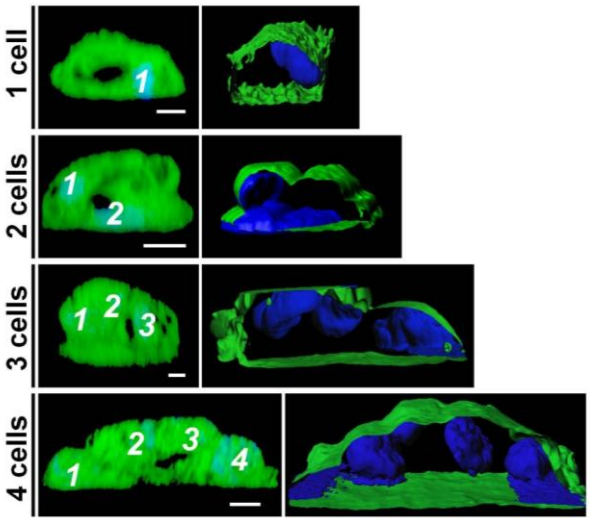

Figure 26. Endothelial cell lumen structure can be formed by one-to-four cells depending on the geometrical cues.

OPEN ACCESS Freely available online

PLoS one

Geometrical Microfeature Cues for Directing Tubulogenesis of Endothelial Cells

Yifeng Lei[1,2]*, Omar F. Zouani[1,2]*, Murielle Rémy[1], Cédric Ayela[3], Marie-Christine Durrieu[1,2]

1 INSERM U1026, Université Victor Segalen Bordeaux 2, Bordeaux, France, **2** CBMN, UMR CNRS 5248, Université Bordeaux 1, Pessac, France, **3** IMS, UMR CNRS 5218, Université de Bordeaux, Talence, France

Abstract

Angiogenesis, the formation of new blood vessels by sprouting from pre-existing ones, is critical for the establishment and maintenance of complex tissues. Angiogenesis is usually triggered by soluble growth factors such as VEGF. However, geometrical cues also play an important role in this process. Here we report the induction of angiogenesis solely by SVVYGLR peptide micropatterning on polymer surfaces. SVVYGLR peptide stripes were micropatterned onto polymer surfaces by photolithography to study their effects on endothelial cell (EC) behavior. Our results showed that the EC behaviors (cell spreading, orientation and migration) were significantly more guided and regulated on narrower SVVYGLR micropatterns (10 and 50 μm) than on larger stripes (100 μm). Also, EC morphogenesis into tube formation was switched on onto the smaller patterns. We illustrated that the central lumen of tubular structures can be formed by only one-to-four cells due to geometrical constraints on the micropatterns which mediated cell-substrate adhesion and generated a correct maturation of adherens junctions. In addition, sprouting of ECs and vascular networks were also induced by geometrical cues on surfaces micropatterned with SVVYGLR peptides. These micropatterned surfaces provide opportunities for mimicking angiogenesis by peptide modification instead of exogenous growth factors. The organization of ECs into tubular structures and the induction of sprouting angiogenesis are important towards the fabrication of vascularized tissues, and this work has great potential applications in tissue engineering and tissue regeneration.

Citation: Lei Y, Zouani OF, Rémy M, Ayela C, Durrieu M-C (2012) Geometrical Microfeature Cues for Directing Tubulogenesis of Endothelial Cells. PLoS ONE 7(7): e41163. doi:10.1371/journal.pone.0041163

Editor: Sharon Gerecht, Johns Hopkins University, United States of America

Received March 26, 2012; **Accepted** June 18, 2012; **Published** July 19, 2012

Copyright: © 2012 Lei et al. This is an open-access article distributed under the terms of the Creative Commons Attribution License, which permits unrestricted use, distribution, and reproduction in any medium, provided the original author and source are credited.

Funding: The work was financially supported by the "Région Aquitaine", the GIS "Advanced Materials in Aquitaine" (AMA) (www.ama-materials.com), and the "Agence nationale pour la Recherche" (ANR) (grant number ANR-09-ETEC-001-01) (www.agence-nationale-recherche.fr). The funders had no role in study design, data collection and analysis, decision to publish, or preparation of the manuscript.

Competing Interests: The authors have declared that no competing interests exist.

* E-mail: yifeng.lei@inserm.fr (YL); omar.zouani@inserm.fr (OFZ)

Introduction

Angiogenesis, the formation of new blood vessels by a process of sprouting from pre-existing ones [1], plays an important role in both normal developmental processes and numerous pathologies, ranging from tumor growth and metastasis to inflammation and ocular diseases [2]. It is also critical for the establishment and maintenance of large engineered tissues, and as known, vascularization is a critical challenge in tissue engineering [3]. Angiogenesis involves in multiple steps: degradation of the basement membrane, endothelial cell (EC) migration, proliferation, tube formation, and blood vessel maturation [4]. These steps are stimulated and controlled by a complex network of intracellular signaling mechanisms [5].

Ever since the introduction of the *in vitro* model of angiogenesis [1], many *in vitro* and *in vivo* assays have been developed to study and follow the sophisticated process of angiogenesis [6,7]. *In vitro*, angiogenesis is often studied by stimulating a monolayer of endothelial cells to assemble into tubes and sprouting [8]. Specific angiogenic molecules can initiate the process of angiogenesis and specific inhibitory molecules can stop it [5]. To promote local angiogenesis, one major theme is the delivery of angiogenic molecules. Numerous inducers of angiogenesis have been identified, such as extracellular matrix (ECM) proteins (laminin, collagen, etc) [9] and growth factors (VEGF, bFGF, etc) [5,10]. Conventional tissue engineering strategies utilized some biological molecules mentioned above to promote angiogenesis [11].

Vascular endothelial growth factor (VEGF, or VEGF-A) is the most potent angiogenic protein described to date [5]. VEGF plays a key role in most morphogenetic events during angiogenesis [12]. Many studies have demonstrated that VEGF enhanced proliferation, migration, sprouting [13,14] and tube formation of endothelial cells [12]. However, the design of VEGF therapy is costly, and one of the most critical problems associated with this therapy is the uncontrollable dose of VEGF delivered [15], which results in negative side effects in non-targeted tissues (hyperpermeable vessels, hypotension, stimulation of tumor growth, and uncontrolled neovascularization) [16].

Otherwise, sequence of angiogenic factors in ECM proteins can be mimicked closely in the process of angiogenesis. The main motivation for developing new synthetic mimicking culture systems is to minimize utilization of the above-mentioned natural ECM proteins and growth factors with the aim of reducing cost and avoiding biological challenges in purification and validation [17]. Numerous reports have described biological activities of ECM-derived peptides corresponding to active sites in proteins, thus using them for triggering angiogenesis [18,19]. Peptides offer advantages over the use of their parent ECM proteins: their chemical definition, accessibility, stability, practicality and sim-

plicity to be conjugated with materials in order to mimic *in vivo* microenvironment [17,20].

Among peptides investigated, a powerful candidate that induces angiogenesis is SVVYGLR peptide sequence. This peptide is a novel binding motif that was found adjacent to the RGD sequence in the osteopontin molecule following thrombin cleavage [21]. Previous studies reported that soluble SVVYGLR peptides activated adhesion, migration of endothelial cells *in vitro* [18], and induced angiogenesis *in vivo* in its soluble form [22]. SVVYGLR peptides are also shown to promote neovascularization in artificial bone marrow scaffold biomaterials [23]. It was reported to have much stronger angiogenic activity as compared with VEGF [18,23]. SVVYGLR presented in previous works were either coated on the surfaces or dissolved in solution for induction of local angiogenesis. However, the study of angiogenesis process and characteristics in these systems were still difficult because of the inaccessibility to this local microenvironment. To simply the complexity of numerous variables typical for ECs' native microenvironment, advanced synthetic systems could greatly facilitate the study of angiogenesis process.

Herein, our strategy consists in the use of microengineering tools to generate materials micropatterned with angiogenic biomolecules on their surfaces to control the cell behaviors. Microengineering technologies provide powerful tools to study *in vitro* cell-microenvironment interactions [24]. They allow the control of the presentation of angiogenic biomolecules on surfaces in pre-decided sizes and shapes, thus influencing cell placement, orientation, morphology, and cell functions on the surfaces [24]. Microengineered surfaces for cell-based assay were developed to control cell shape and behaviors as previously reported [19,25–30].

In this study, we focus on the covalent grafting of SVVYGLR peptides onto polymer surfaces with controlling geometries, and we aim to study their effect on EC behaviors as well as angiogenesis. Different micropatterns of SVVYGLR peptides on polymer surfaces were prepared by photolithographic technique. The EC behaviors, the induction of EC tube formation, and the vascular network formation on the micropatterned surfaces were addressed. We observe that the EC behaviors were significantly more guided and tube formation was switched on onto narrower micropatterns (10 and 50 μm) as compared with larger stripes (100 μm). We illustrate that the central lumen of tubular structure can be formed solely by geometrical cues. Then, we report that only single-to-four cells can form central lumen due to geometrical constraints on the micropatterns which mediated cell-substrate adhesion and generated a correct maturation of adherens junctions (AJs) [31]. In addition, sprouting angiogenesis of ECs and vascular networks were also induced by geometrical cues on surfaces micropatterned with SVVYGLR peptides. These findings serve to identify mechanism characteristics that alter EC lumen formation and sprouting in angiogenesis process, which may be utilized for innovating biomaterials and for application in tissue engineering.

Materials and Methods

Materials

Polyethylene terephthalate (PET) film is a commercial film obtained from Goodfellow, France. Inorganic reagents (NaOH, $KMnO_4$, H_2SO_4, and HCl), acetone, acetonitrile, dimethylaminopropyl-3-ethylcarbodiimide hydrochloride (EDC), N-hydroxy Succinimide (NHS) and 2-(N-morpholino)-ethanesulfonic acid (MES) were purchased from Sigma-Aldrich, France. GDSVVYGLR peptides and GDSVVYGLRK-FITC fluorescent peptides were synthesized by Genecust, France.

Covalent Grafting of Peptides onto PET Surface

PET surfaces were modified according to Chollet et al. [32] with some modifications. Briefly, PET was hydrolyzed and oxidized in order to create COOH groups on the surface (labelled as "PET-COOH"). Then, the surfaces were immersed in a solution of EDC (0.2 M) + NHS (0.1 M) + MES (0.1 M) in MilliQ water for activation. Subsequently, the surfaces were immersed in peptide solution (GDSVVYGLR peptides dissolved in PBS with a concentration of 10^{-3} M) for 16 h at room temperature for peptide immobilization onto PET surfaces (named as "SVVYGLR"). This peptide concentration was chosen after preliminary cell alignment tests on micropatterned surfaces with 50 μm peptide stripes (Fig. S1). After covalent immobilization, the surfaces were rinsed with MilliQ water for 1 week in order to remove the physically adsorbed peptides.

Preparation of Micropatterned Surfaces

Micropatterns on polymer surfaces were fabricated by photolithographic technique as previously developed [33]. Briefly, the surfaces of materials were coated with S1818 photoresist (Rohm and Haas, USA) and spun at 3000 rpm for 30 s to obtain a uniform photoresist layer with a thickness of approximately 2 μm. The surfaces were baked at 115°C for 1 min for drying. The surfaces were then exposed to UV light (60 W) through a high-resolution Cr mask with predesigned pattern dimensions (Femto-St Sciences & Technologies, France) for 18 s. Subsequently the surfaces were developed in Microposit Developer solution (Rohm and Haas, USA) for 40 s to dissolve the exposed photoresist, resulting in the desired pattern on material surfaces.

The micropatterns on surfaces were prepared after the "PET-COOH" step, subsequently the surface activation and peptide immobilization were realized as described in the above section. Finally, the photoresist surrounding the peptide micropatterns was removed by acetone, resulting in SVVYGLR peptide micropatterns on PET surfaces.

Surface Characterization

X-ray photoelectron spectroscopy (XPS) was used to characterize the surface chemical composition during the process of peptide immobilization. XPS was characterized on a VG Scientific ESCALAB photoelectron spectrometer, with an MgK X-ray source (1253.6 eV photons, 100W). Spectra were referenced by setting carbon pollution at 284.8 eV.

Fluorescent peptides were employed to facilitate the visualization of peptide micropatterns according to Zouani et al. [34]. In this case, GDSVVYGLR peptides were covalently conjugated to FITC fluochromes via lysine (labeled as "GDSVVYGLRK-FITC"), and immobilized onto micropatterned PET surfaces as described in the above sections. Epifluorescence microscopy (Leica DM5500B, Germany) was employed for visualization of fluorescent peptide patterns on polymer surfaces.

Cell Culture

Human umbilical vein endothelial cells (HUVECs) were obtained from the human umbilical cord vein according to the methods described previously [35,36]. HUVECs were isolated and grown on gelatin coated culture flasks in HUVEC complete culture medium (IMDM (Invitrogen, France) supplemented with 20% (v/v) fetal bovine serum (FBS) (PAA, France) and 0.4% (v/v) EC growth supplement/heparin kit (Promocell, France)). Cells

were subcultured using trypsin/EDTA (Invitrogen, France) and maintained in a humidified atmosphere containing 5% (v/v) CO_2 at 37°C. Cells at passages 3 to 5 were used for experiments.

Immobilization of SVVYGLR Peptides on EC Behaviors

To evaluate the effect of immobilization of SVVYGLR peptides on cell behaviors, cells were cultured on pristine PET surfaces (labeled as "PET") and PET grafted with SVVYGLR peptides (labeled as "Grafted SVV"). HUVECs were seeded at a density of 50000 cells/cm^2 in serum-free IMDM medium for 4 h on different surfaces (n = 6). Cells were allowed to adhere for 4 h, then IMDM medium was removed and ECs were cultured in IMDM medium containing 10% FBS for 1 and 3 days.

In competitive experiments, EC behaviors were also examined using soluble SVVYGLR peptides to ensure that improved EC adhesion and spreading were due to specific interaction with the SVVYGLR peptides that immobilized onto PET surfaces. ECs were seeded onto SVVYGLR peptides immobilized surfaces at 50000 cells/cm^2 in serum-free IMDM medium containing soluble SVVYGLR peptides at 10, 100, 1000 and 10000 ng/mL (labeled as "+10 SVV", "+100 SVV", "+1000 SVV", "+10000 SVV", respectively). EC adhesion and spreading were evaluated after 4 h incubation.

Immunofluorescent Staining

Immunofluorescent staining was performed to visualize the ECs on different surfaces. After cell culture, cells were fixed by 4% (w/v) paraformaldehyde (PFA), permeabilized with 0.5% Triton-X 100, blocked with 1% bovine serum albumin (BSA) in PBS solution, and stained with primary and secondary antibodies. The primary antibodies used were mouse anti-vinculin (Sigma, France), mouse anti-CD31 (PECAM-1) (Invitrogen, France). The secondary antibodies were anti-mouse antibodies conjugated with Alexa Fluor® 568 (Invitrogen, France). Cell actin cytoskeletons and nuclei were stained with Alexa Fluor® 488 phalloidin (Invitrogen, France) and DAPI (Sigma, France), respectively. The samples were mounted with ProLong® Gold antifade reagent (Invitrogen, France) and observed by fluorescence microscopy.

Cell adhesion and spreading were examined by ImageJ software (NIH, http://rsb.info.nih.gov/ij/). Cell nuclei were counted for evaluation of adherent cell number. The cell areas were determined by tracing the cell edges from actin cytoskeleton. At least 20 fields at low magnification (10 X) on each surface were analyzed for this study.

Micropatterning of SVVYGLR Peptides on EC Behaviors

To evaluate the effects of micropatterning of peptides on EC functions, polymer surfaces micropatterned with 10, 50 and 100 μm SVVYGLR peptide stripes with same interspaces of 100 μm were prepared by photolithography (the surfaces were labeled as "10 μm", "50 μm" and "100 μm", respectively). Immobilization of SVVYGLR peptides onto polymer surfaces homogenously without patterning served as controls (labeled as "unpatterned"). ECs were seeded onto different surfaces at a density of 50000 cells/cm^2 in EGM®-2 medium (Lonza, France), to study the effect of SVVYGLR peptide micropatterns on cellular functions.

Cell Spreading, Orientation and Migration

ECs on patterned and unpatterned surfaces were fixed after 26 h of culture and immunofluorescently stained as described previously. Cell areas were evaluated by ImageJ software.

Cell orientation (alignment and elongation) were evaluated as previously demonstrated [37,38]. The cell was fitted into an ellipse by ImageJ software. The cell body alignment angle, defined as the angle of the major axis of the cell body with respect to the direction of micropatterns [37], was measured using ImageJ. For cells on unpatterned surfaces, the angle of the cell body major axis with respect to an arbitrary axis (here fixed at 0°) was taken for cell alignment angle. A cell was aligned perfectly parallel to the direction of pattern when the alignment angle was 0° and perfectly perpendicular to the patterns when the alignment angle was 90°. Cell area (s) and perimeter (l) were measured by the "measure" tool in ImageJ, and cell morphology was characterized by cell shape index (I) which was calculated according to the following formula: $I = 4\pi s/l^2$ [38]. Cells are round when I is equal to 1 and cells become infinitely elongated as I approaches 0. About eighty cells for each surface were analyzed in this study.

For monitoring cell migration, HUVECs were seeded onto patterned and unpatterned surfaces at a density of 50000 cells/cm^2 and cultured in EGM®-2 medium at 37°C and 5% CO_2. ECs were allowed to adhere and align onto SVVYGLR peptide micropatterns in incubator for 4 h. Then the samples were transferred to time-lapse microscopy (Leica DM5500B) in a humidified atmosphere containing 5% CO_2 at 37°C, and cell migration on patterns was monitored by Leica MMAF software and automated stages. The images were photographed in intervals of every 6 min during 12 h. Then the videos were analyzed using the free software "Time Lapse Analyser" (TLA: http://www.informatik.uni-ulm.de/ni/staff/HKestler/tla/). For quantification of cell motility, cell trajectories, total distances and migration rate (μm/min) were calculated. A minimum of 30 cells per condition were analyzed. Experiments were done in duplicates for each surface.

Quantification of Focal Adhesions and Adherens Junctions

To quantify the number and size of focal adhesions (FAs), the fluorescent images of vinculin staining were analyzed using ImageJ [32,39]. The raw images were opened and converted into 8-bit file, smoothed by the unsharp mask feature (settings 1:0.2) and background removed (rolling ball radius 10). The resulting images were then converted to binary images by setting a same threshold. The threshold values were determined empirically by selecting a setting which gave most accurate binary images. The cell area was determined by manual delineation on raw fluorescent images. The number of focal contacts per cell and mean contact area per cell were calculated by "analyse particles" in ImageJ, and contacts smaller than 3 pixels were not taken into account. A minimum of 30 cells per condition were analyzed.

For quantification of cell-cell adherens junctions, the cells on different substrates were stained with antibody against platelet endothelial cell adhesion molecule (PECAM-1). The fluorescence images of PECAM staining were processed in ImageJ software. AJs of ECs were obtained from PECAM staining and were binarized with same thresholds on different surfaces. The AJ size and density on each surface was quantified by measuring respective cell-cell junction width and junction density with the "plot profile" tool in ImageJ software [31].

EC Morphogenesis into Tube-like Structure

HUVECs were seeded at a density of 50000 cells/cm^2 in EGM®-2 medium, cell growth was maintained at 37°C and 5% CO_2. The cells on surfaces were photographed by phase contrast microscopy (Zeiss Axiovert 25, Germany), and the cells were fixed

when morphogenesis of ECs seemed to appear after about 26 h of culture.

ECs were labelled with Cell Tracker Green (CMFDA, 5 μM) (Invitrogen, France) for 30 minutes prior to fixation, according to the technical protocol of the product. The cells were then fixed by 4% PFA, counterstained with actin and DAPI and mounted for observation. Confocal microscopy (Leica SP5, Germany) was used to access images of ECs in different z-stages. Imaris 7.0 software was employed for three-dimensional (3D) reconstruction of confocal images and for analysis of the tubular structure of ECs on micropatterned surfaces.

Statistical Analysis

Data were represented as mean values ± standard deviation (SD). Statistical analysis was performed by one-way analysis of variance (ANOVA) (OriginPro 8, OriginLab Corporation, USA), followed by LSD or Dunnett post-hoc test for multiple comparisons, where appropriate. A p-value less than 0.05 was considered statistically significant.

Results

Peptide Immobilization onto Polymer Surface

XPS was employed to determine the surface chemical compositions during PET surface modification. The pristine PET surfaces exhibit only C and O elements as expected (Fig. 1). As compared with PET surfaces, PET surfaces grafted with SVVYGLR peptides showed new N1s peaks which appeared at about 399.85 eV (3.9%), corresponding to the successful grafting of SVVYGLR onto the polymer surfaces. Details concerning XPS de-convolution during different steps of surface modification are referred to [32].

Peptide Micropatterning onto Polymer Surfaces

Photolithography was used for creating peptide micropatterns onto material surfaces [33]. In this present work, SVVYGLR peptide stripes of three different widths (10, 50 and 100 μm) with the same interspace of 100 μm between the stripes were micropatterned onto PET surfaces. To validate this process, fluorescent peptides (GDSVVYGLRK-FITC) were immobilized onto polymer surfaces for visualization. The polymer surfaces micropatterned with fluorescent peptides are represented in Fig. 2, which confirmed the successful micropatterning of SVVYGLR peptides onto polymer surfaces.

SVVYGLR Peptides Induced Cell Responses on Homogenous Polymer Surfaces

At the first step of biological evaluation, SVVYGLR peptides were homogenously grafted onto PET surfaces to study their effect on EC behaviors. The results of cell culture showed that the immobilization of SVVYGLR peptides onto PET induced significant EC adhesion and spreading as compared with pristine PET surfaces (Fig. 3A-C).

To ensure that improved cell adhesion and spreading were mediated by SVVYGLR specific cell receptors, competitive experiments of EC adhesion on SVVYGLR grafted surfaces were evaluated using soluble SVVYGLR peptides in culture medium for 4 h. EC adhesion on SVVYGLR peptide grafted surfaces was reduced in the presence of soluble SVVYGLR peptides over the entire ranges of the soluble peptide concentrations (10, 100, 1000 and 10000 ng/mL), as shown in Fig. 3D. Similar results were also observed in cell spreading levels (Fig. 3E). Similar to pristine PET surfaces, few cells adhered, and most cells were round in shape over the entire range of soluble peptide concentrations. These results suggest that the adhesion and spreading of ECs on the SVVYGLR immobilized surfaces are predominantly mediated by specific cell receptor-SVVYGLR peptide interactions.

The immobilization of SVVYGLR peptides onto PET surfaces induced significant EC adhesion and spreading. ECs on SVVYGLR grafted surfaces formed a confluent monolayer which appeared with typical cobble stone-like morphology after 3 days in culture (Fig. S2). However, neither EC tube formation nor angiogenesis was observed by this approach. Subsequently, the effects of SVVYGLR peptide micropatterning (10 to 100 μm) on EC behaviors as well as angiogenesis (central lumen formation and sprouting) were addressed.

Micropatterning of SVVYGLR Peptides onto ECs Responses

After 4 h in culture, ECs began to align onto the SVVYGLR peptide patterns regardless of the size of patterns. Fig. 4A illustrated the EC alignment on micropatterned surfaces after

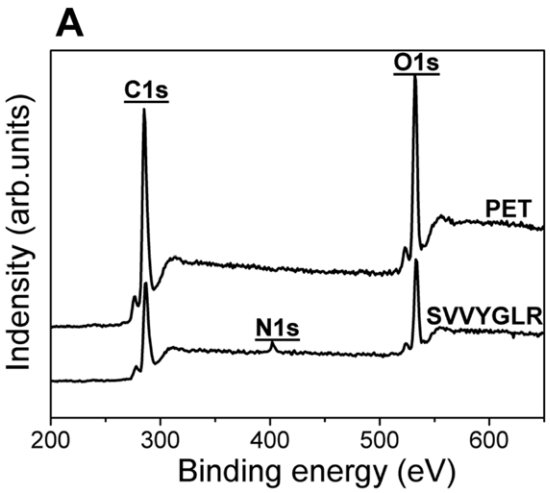

B

	C	O	N
PET	72,5	27,5	-
SVVYGLR	66,4	29,2	3,9

Figure 1. XPS characterization of surfaces. (A) XPS spectrum and (B) experimental atomic composition (%) of PET and PET surfaces grafted with SVVYGLR peptides.
doi:10.1371/journal.pone.0041163.g001

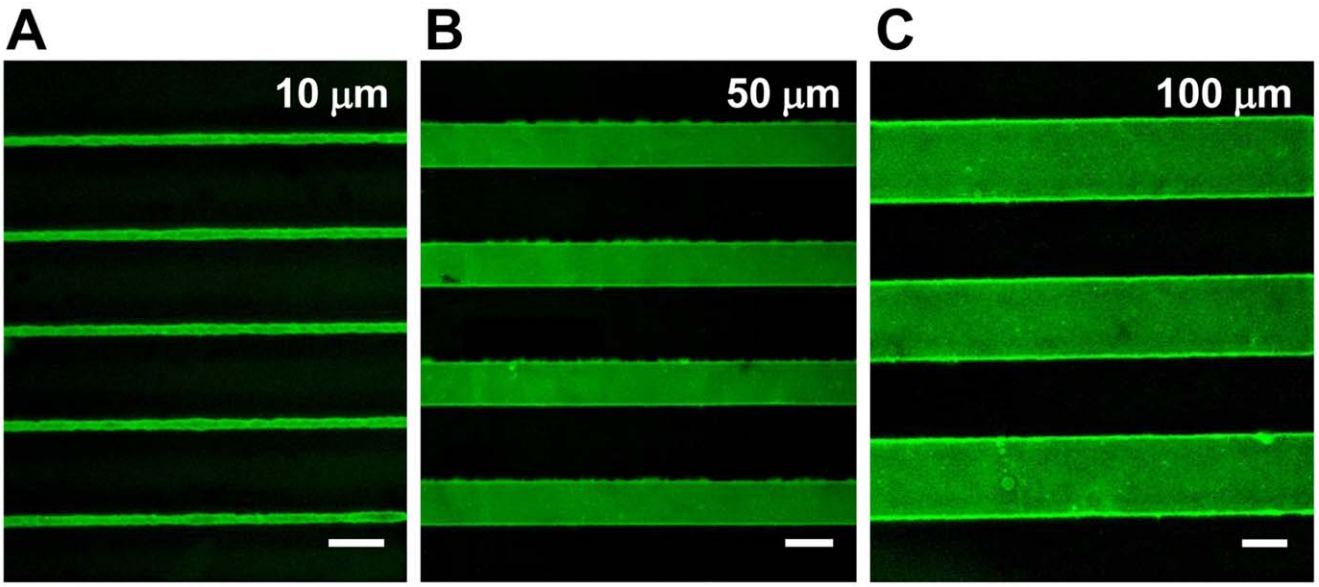

Figure 2. Fluorescent microscopy observation of polymer surfaces micropatterned with fluorescent peptides. The green lines correspond to (A) 10 μm, (B) 50 μm and (C) 100 μm stripes of GDSVVYGLRK-FITC peptides. Scale bars correspond to 50 μm.
doi:10.1371/journal.pone.0041163.g002

26 h in culture. However, the EC behaviors (cell spreading, alignment, elongation and cell migration) were significantly more regulated on smaller patterns (10 and 50 μm). The quantitative results of cell areas, cell orientation and cell migration on micropatterned and unpatterned surfaces were analyzed.

EC Spreading, Alignment and Elongation on SVVYGLR Micropatterned Surfaces

Cell areas on unpatterned surfaces and SVVYGLR micropatterns were represented in Fig. 4B. ECs were found to spread most on unpatterned surfaces (mean projected cell areas: 1854 ± 544 μm^2). Cells seeded on 100 μm SVVYGLR peptide stripes had a similar spreading level as compared with unpatterned surfaces (mean cell areas: 1825 ± 950 μm^2), while cell spreading was significantly reduced on narrower stripes, with mean projected cell areas of 1056 ± 377 μm^2 and 732 ± 370 μm^2 for ECs seeded on 50 μm and 10 μm SVVYGLR peptide stripes, respectively.

Quantitative analyses of cell alignment angles according to the direction of SVVYGLR micropatterns were represented in Fig. 4C. Cells on unpatterned surfaces displayed random orientation, the alignment angles of cell bodies were uniformly distributed, with a mean value of $44.06\pm22.74^\circ$. Cells on patterned SVVYGLR stripes exhibited a strong alignment to the direction of micropatterns ($p<0.01$). For ECs seeded on 100 μm SVVYGLR stripes, mean cell alignment angles decreased to $27.34\pm17.93^\circ$ as compared with unpatterned surfaces. The more the pattern width decreased, the more the mean alignment angles decreased: $17.75\pm12.44^\circ$ and $10.07\pm7.36^\circ$ for ECs on 50 μm and 10 μm SVVYGLR stripes, respectively. Statistical analysis confirmed that there was a main effect of peptide micropattern sizes in driving cell body alignment, and the alignment of cell body became more significant as the pattern size became smaller.

Quantitative analysis of cell body elongation on different surfaces was represented in Fig. 4D. ECs on the unpatterned surface presented a mean cell body shape index of 0.70 ± 0.19. Cells on patterned surfaces showed decreased shape index as compared to the unpatterned surfaces, with mean cell body shape index of 0.59 ± 0.15, 0.52 ± 0.14 and 0.44 ± 0.17 for ECs seeded on 100 μm, 50 μm and 10 μm stripes of SVVYGLR stripes, respectively. The decrease in shape index means that the cell bodies were more elongated on the peptide micropatterns. Statistical analysis showed that the cell elongation on peptide microstripes was more significant as compared with unpatterned surfaces ($p<0.01$), and the elongation on smaller SVVYGLR peptide stripes (50 μm and 10 μm) was more significant ($p<0.01$).

Geometrical Cues of SVVYGLR Micropatterns Decrease EC Migration

EC migration on different surfaces was monitored by time-lapse video microscopy. Fig. 5A–D illustrated the trajectories of cell migration on unpatterned and patterned surfaces during 12 h. ECs on unpatterned surfaces show random directional migration, while the ECs on SVVYGLR patterns exhibit guided migration along the direction of micropatterns. ECs on 10 and 50 μm SVVYGLR stripes have trajectories almost exclusively along the direction of micropatterns.

Total distances traveled by cells were calculated to determine the migration rate of ECs on different surfaces, and the result was summarized in Fig. 5E. There was no significant change in cell migration rate from the unpatterned surfaces to 100 μm SVVYGLR peptide stripes. However, the cell migration rate exhibited a significant decrease on 10 and 50 μm SVVYGLR peptide stripes ($p<0.01$). ECs exhibited a guidance response to micropatterns and restrictedly migrated on the region of micropatterns.

Geometrical Cues of SVVYGLR Micropatterns Induce Lumen Formation

Furthermore, we investigated the EC morphogenesis on SVVYGLR micropatterned surfaces. Formation of central lumen within these orientated cellular cords was analyzed by confocal microscopy with ECs labeled with a fluorescent cytoplasmic dye (CMFDA) and cell nuclei (DAPI).

The ECs seeded on 10 and 50 μm SVVYGLR peptide stripes underwent morphogenesis and formed capillary tube-like struc-

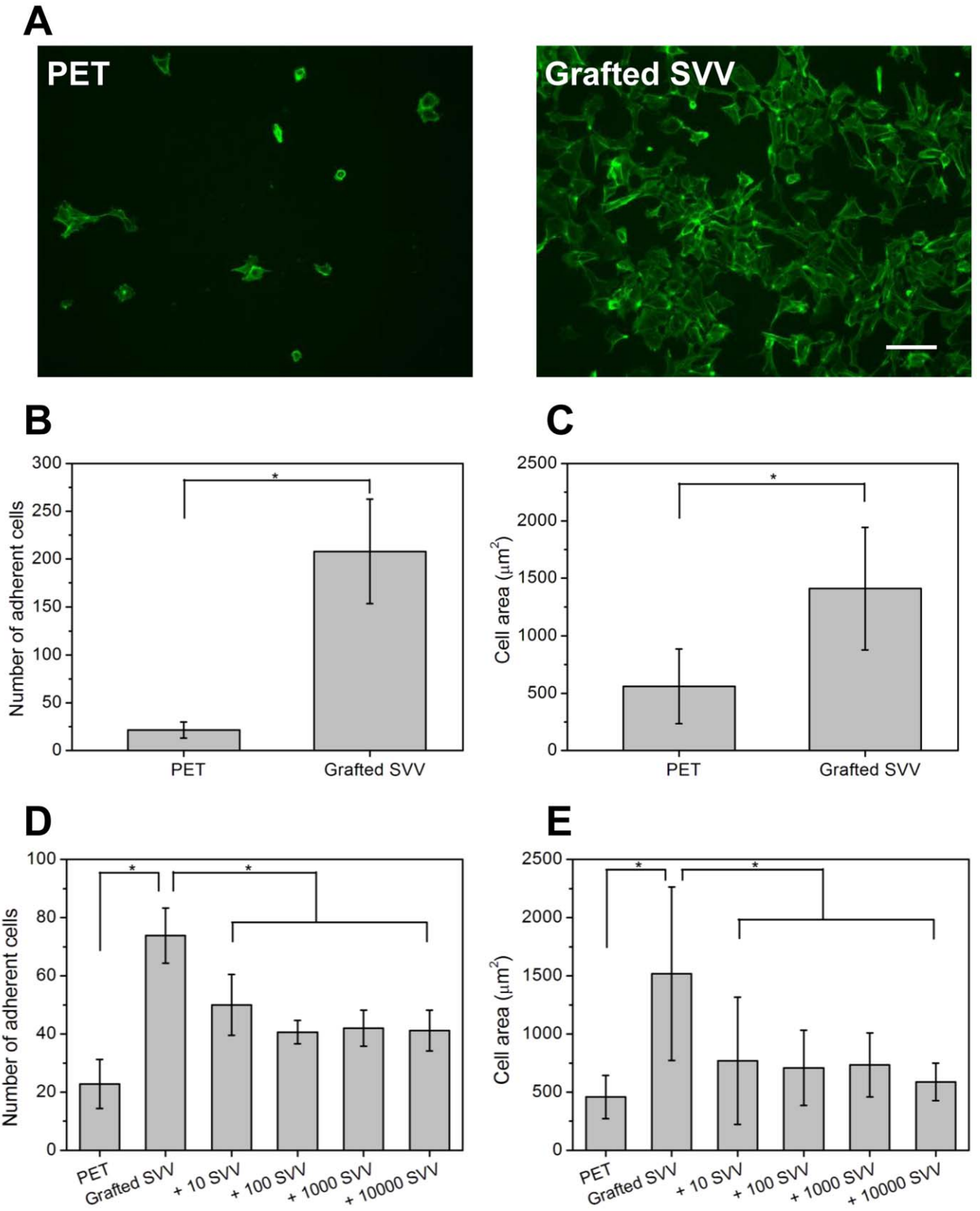

Figure 3. Cell responses induced by grafted and soluble SVVYGLR peptides. (A) EC actin skeleton on PET and PET surfaces grafted with SVVYGLR peptides after 24 h in culture, scale bars are 100 μm. (B) Number of adherent cells and (C) mean cell areas on different surfaces in (A). In competitive experiments, ECs were incubated on SVVYGLR peptides grafted surfaces with presentation of soluble SVVYGLR peptides at different concentrations (10, 100, 1000 and 10000 ng/mL) for 4 h incubation, (D) cell adhesion and (E) cell surface areas on different surfaces. (* $p<0.01$).
doi:10.1371/journal.pone.0041163.g003

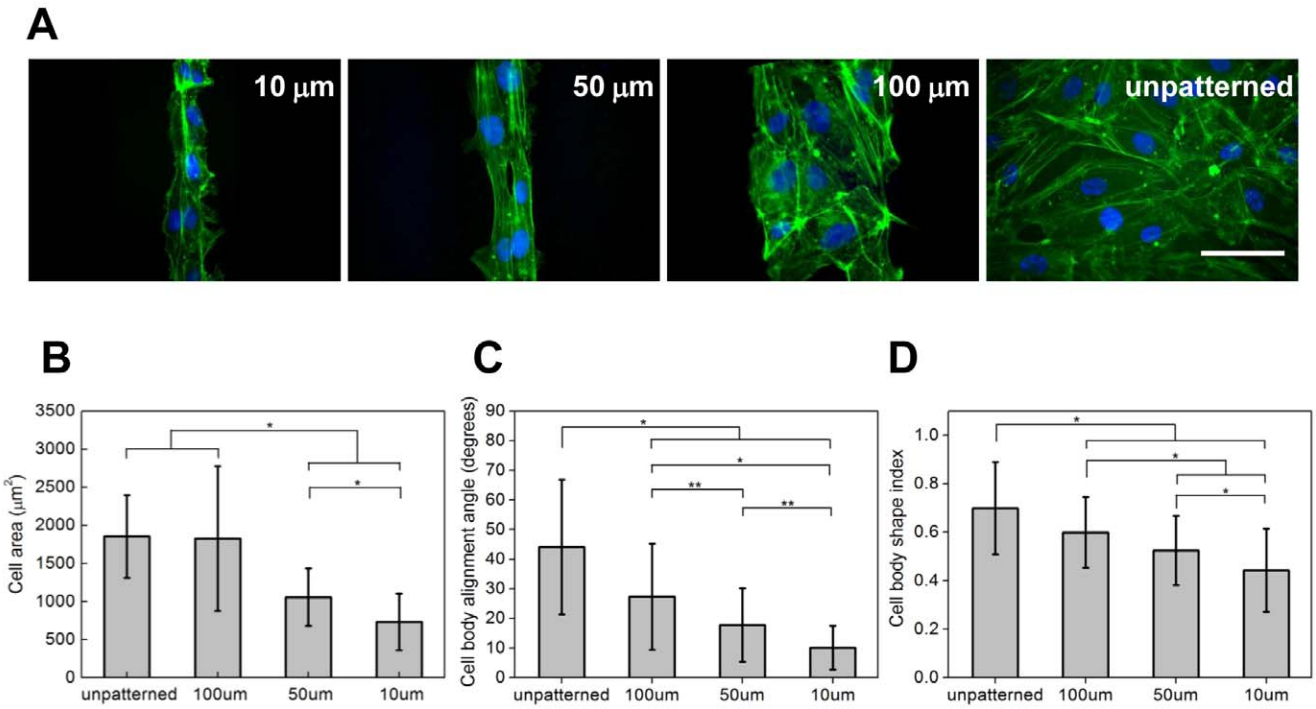

Figure 4. Cell responses induced by the micropatterning of SVVYGLR peptides. (A) ECs on 10 μm, 50 μm and 100 μm SVVYGLR peptide stripes and on unpatterned surfaces. Cells were labeled with phalloidin and nuclei which are represented in green and blue, respectively. Scale bars correspond to 100 μm. Quantification of (B) mean cell areas, (C) cell body alignment angles and (D) cell shape index of ECs on unpatterned surfaces, on 100 μm, 50 μm and 10 μm SVVYGLR peptide stripes (* $p<0.01$; ** $0.01<p<0.05$).
doi:10.1371/journal.pone.0041163.g004

tures (Fig. 6A, B). Confocal images of horizontal and vertical cross sections confirmed the existence of the central lumen, which appeared as a negatively stained central space extending along multiple cell lengths. The ECs also appeared to protrude their cell bodies vertically upwards so that the cytoskeleton system was no longer in a single focal plane characteristic of a spread cell in culture. In contrast, ECs on 100 μm SVVYGLR peptide stripes failed to generate morphogenesis and remained as an adherent, flattened monolayer (Fig. 6C). A vertical cross section of such region showed that ECs remained well spread as a monolayer close to the substrates of patterns. Confocal images in z-stacks also illustrated the cord-like structures of ECs on micropatterns (Fig. 6D for ECs on 50 μm SVVYGLR stripes and Fig. S3 for ECs on 10 μm SVVYGLR stripes).

Interestingly, vertical cross sections of confocal images showed that the central lumen could be induced by one, two, and three or up to four cells (Fig. 7A). The lumen could be formed by single-to-four cells in the case on 10 or 50 μm micropatterns, but not formed by more than four cells in the case on 100 μm micropatterns (Fig. 7B). Furthermore, we observed that the AJs between ECs cultured on 10 and 50 μm SVVYGLR micropatterns were smaller but more concentrated as compared with those on 100 μm SVVYGLR micropatterns (Fig. S4). Quantitatively, the AJ size was correlated with geometrical constraints applied to ECs by varying the pattern widths (Fig. 7C). Also, we observed a reduced number of focal contacts per cell on patterned surfaces (Fig. 7D). The smaller the micropatterns, the fewer the number of focal contacts per cell on micropatterns. The areas of focal contacts per cell on smaller patterns (10 and 50 μm) were also reduced as comparing with 100 μm micropatterns and unpatterned surfaces (Fig. 7E).

Tubulogenesis and Formation of Vascular Network

Aside from EC tube formation on SVVYGLR peptide micropatterns, immunofluorescent images also revealed ECs sprouting from the pre-formed tubular structure on SVVYGLR micropatterns (Fig. 8A). The sprout cells migrated via filopodial extensions and found receptive ECs from adjacent tubular structures and eventually lead to the formation of vascular networks based on the peptide micropatterned surfaces (Fig. 8B).

Discussion

Angiogenesis is essential towards the challenge of vascularization in tissue engineering [3]. Although some steps of the angiogenesis process have been identified, the exact mechanism involved in this process is complex and poorly understood. Mimicking angiogenesis will help us both in understanding the process and for its application in tissue engineering.

Many approaches have been developed to modulate angiogenesis with the use of scaffolds made of either natural fibers or polymer fibers [10,40]. Other assays have described the EC tube formation and promoted angiogenesis based on gel environment [6]. The term lumen is sometimes also used to describe features composed of cells forming circular structures in a nearly two-dimensional (2D) plane [41,42].

As reported previously, soluble SVVYGLR peptides displayed a similar level of angiogenic activity as VEGF [18,23]. Here in our work, the mimicking of angiogenesis, *i.e.*, tube formation as well as sprouting of ECs, was induced by micropatterning of SVVYGLR peptides grafted onto 2D polymer surfaces.

Cellular functions on material surfaces are controlled by a complex set of intercellular signaling events, originating from a variety of cell surface receptors. Some of these receptors

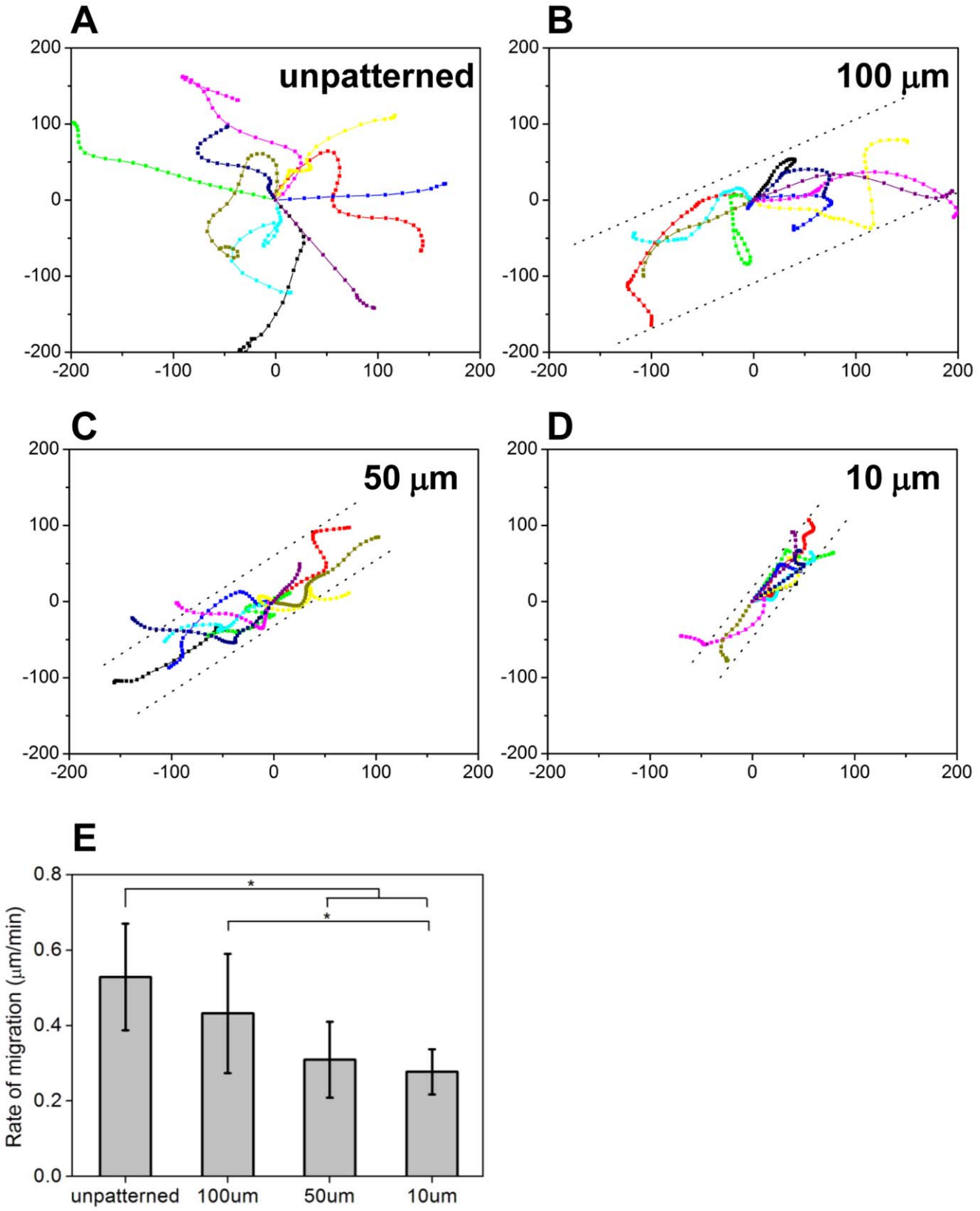

Figure 5. EC migration on micropatterned surfaces. Trajectories of ten ECs on (A) unpatterned surfaces, on (B) 100 μm, (C) 50 μm and (D) 10 μm SVVYGLR peptide stripes. The double dot lines illustrate the peptide micropatterns. (E) Mean rate of EC migration on surfaces of A–D (* $p<0.01$).
doi:10.1371/journal.pone.0041163.g005

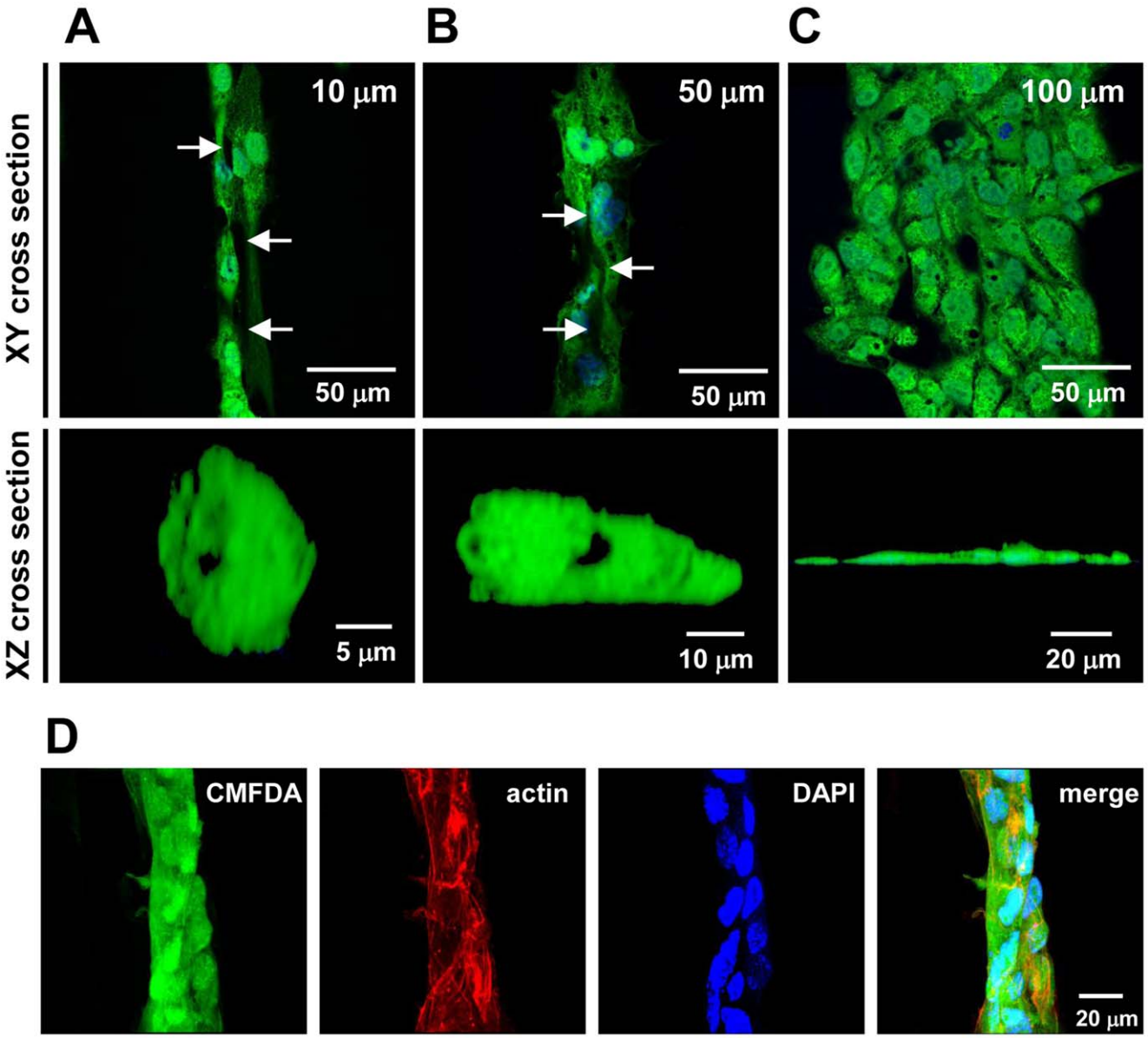

Figure 6. EC tube formation on SVVYGLR micropatterns. Confocal images of ECs seeded on (A) 10 μm and (B) 50 μm SVVYGLR peptide stripes showed a central cavity extending along several cell lengths. The lumen cavity appears as a negatively stained central space when viewed in horizontal (XY) and vertical (XZ) cross section. (C) ECs on 100 μm SVVYGLR stripes remained spread within an adherent monolayer and did not form tubes. Cell staining with Cell Tracker Green (CMFDA) and DAPI were represented in green and blue, respectively. (D) Confocal images of ECs' cord-like structures on 50 μm SVVYGLR peptide stripes.
doi:10.1371/journal.pone.0041163.g006

mediated ECM-cell or cell-cell interactions that are involved in angiogenesis [5,8]. As reported, the SVVYGLR motif binds the integrin receptors such as $\alpha_4\beta_1$ [43], $\alpha_4\beta_7$ [44], $\alpha_9\beta_1$ [21] and $\alpha_v\beta_3$ [45], and enhances EC adhesion and migration [18], which are two important processes in angiogenesis.

To ensure that the cell behaviors were mediated by SVVYGLR peptides grafted on PET surfaces, competitive experiments of the effects of soluble SVVYGLR peptides on EC responses were examined. The results showed that grafted SVVYGLR on PET surfaces significantly enhanced EC adhesion and spreading. However, the EC adhesion and spreading on SVVYGLR peptide grafted PET surfaces were reduced in the presence of soluble SVVYGLR peptides over the entire ranges of the soluble peptide density (10, 100, 1000 and 10000 ng/mL) (Fig. 3). These results revealed that the EC adhesion on SVVYGLR peptide immobilized surfaces is predominantly mediated by specific cell receptor-peptide interactions.

When SVVYGLR peptides were micropatterned onto polymer surfaces (Fig. 2), the ECs cultured on the surfaces recognized the micropatterns of SVVYGLR peptides via interaction with integrin receptors and induced EC attachment on the patterns. Subsequently, cell behaviors were guided and regulated by the micropatterned geometrical cues. Microengineered surfaces for cell-based assay were developed to control cell shape and function [25,26], and some studies reported EC morphogenesis on 2D substrates based on microengineering [19,27,28]. In our study, surface micropatterning with angiogenic SVVYGLR peptides was developed to regulate the cellular function and guide EC

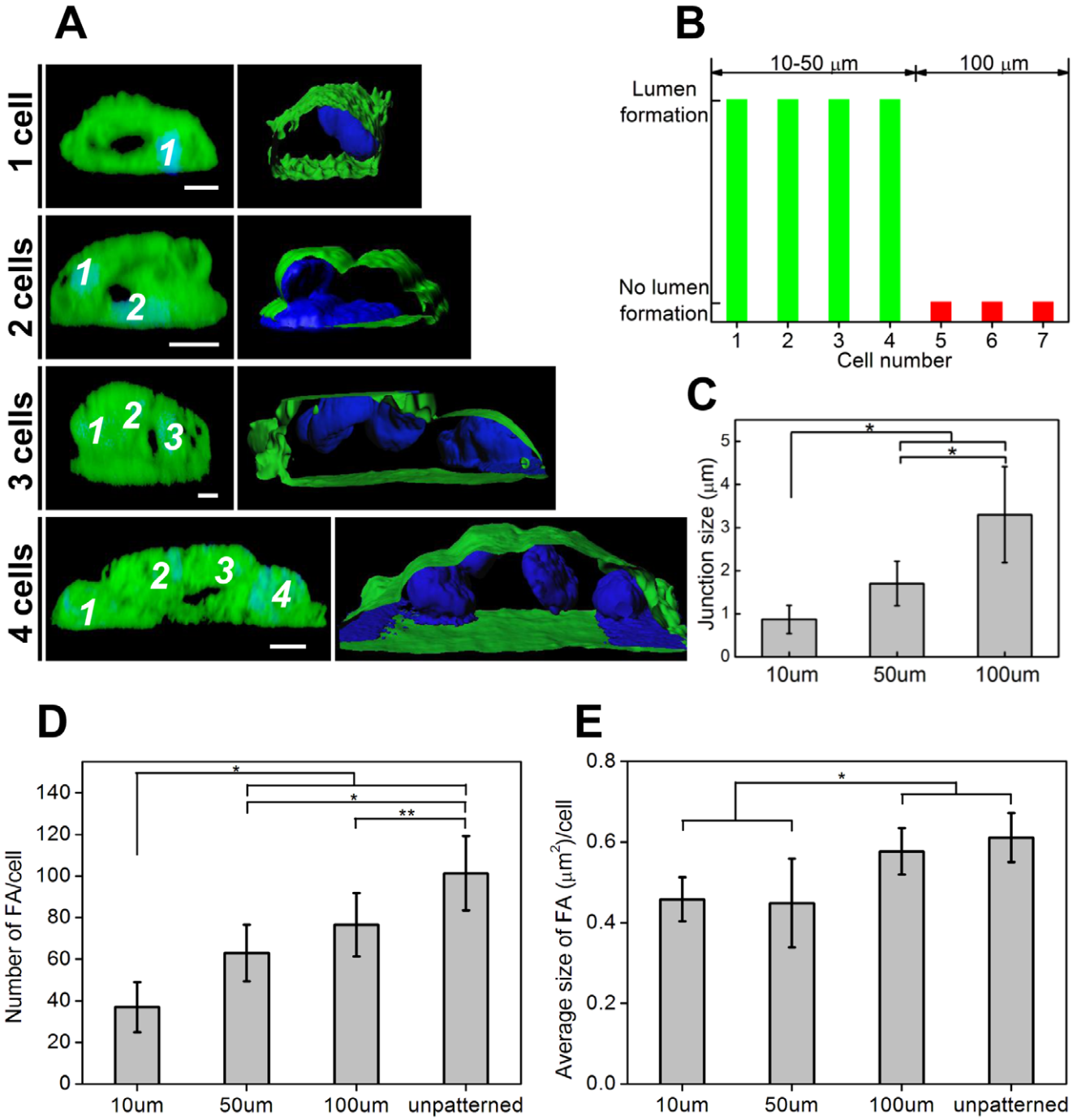

Figure 7. Lumen formation by geometrical cues. (A) Left: vertical confocal image cross sections revealed lumen formation by single-to-four cells, the numbers point out the position of cell nuclei. Right: XZ sections illustrate the lumen surfaces (CMFDA) and the position of cell nuclei (DAPI) corresponding to the images in the left column. Scale bars are 5 μm. (B) Lumen formations can be induced by single-to-four cells on 10 and 50 μm SVVYGLR peptide patterns, but there is no lumen structures formed on 100 μm SVVYGLR peptide patterns. In this last case, the patterns contained more than four cells which cannot support cell-cell reorganization and consequent central lumen formation. (C) Quantification of adherens junctions sizes of cell-cell contacts on SVVYGLR peptide patterns. (D) Number of focal contacts per cell and (E) average size of focal contacts per cell on different surfaces (* $p<0.01$; ** $0.01<p<0.05$).
doi:10.1371/journal.pone.0041163.g007

morphogenesis as well as to induce angiogenesis on polymer material surfaces. The peptide micropatterns described here had identical chemistry, and the ECs were cultured in the same medium. Therefore, the EC behaviors on these micropatterned surfaces differed only in a single parameter: geometrical cues of peptide micropatterns.

The tube-like structures were formed depending on the peptide micropattern sizes. As the results shown in Fig. 4 and Fig. 5, ECs remained in a similar state on larger SVVYGLR peptide stripes

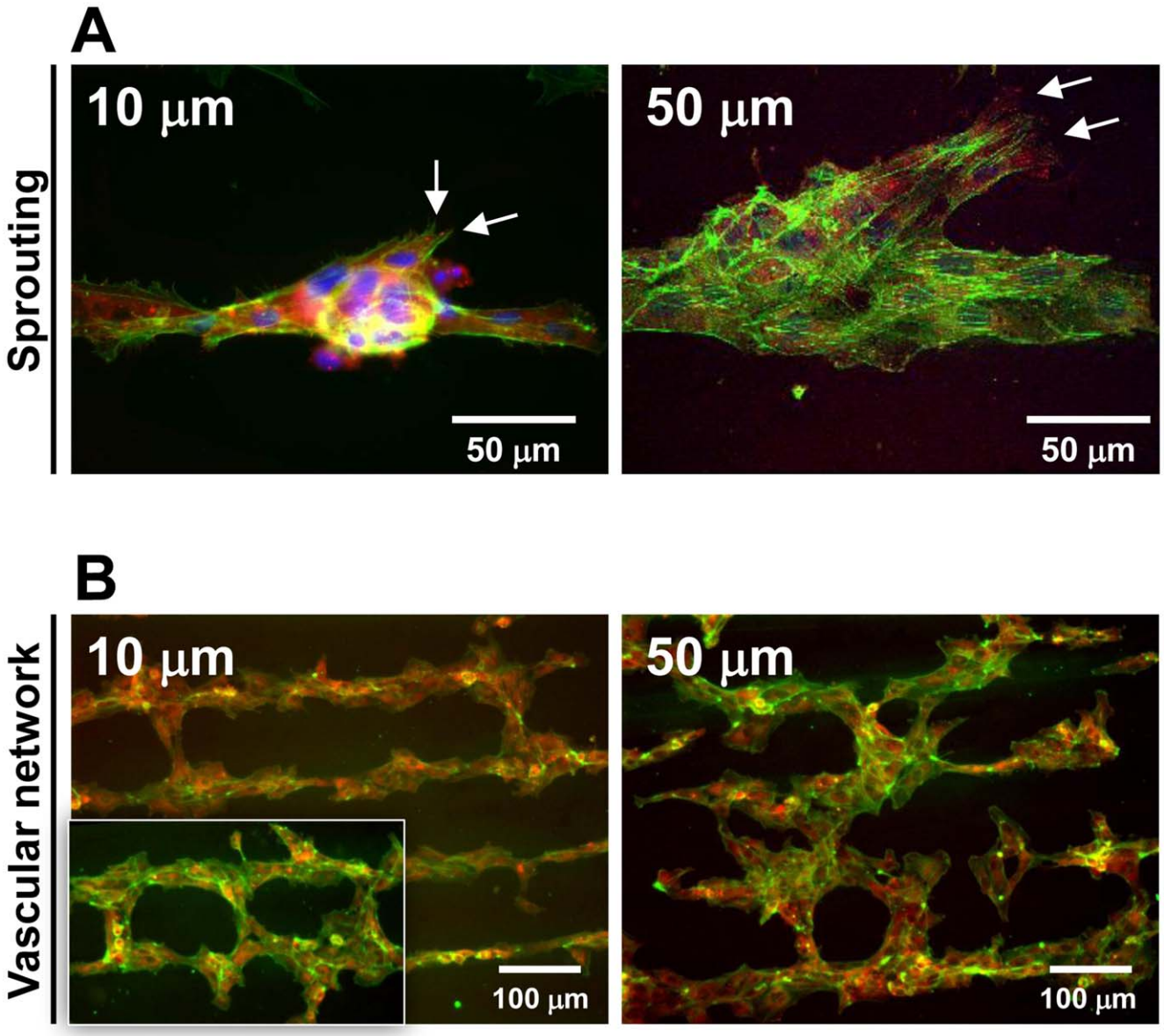

Figure 8. Sprouting and network formation on micropatterned surfaces. (A) Sprouting of ECs and (B) formation of vascular networks on surfaces micropatterned with SVVYGLR peptides. Phalloidin, vinculin and nuclei were stained in green, red and blue, respectively.
doi:10.1371/journal.pone.0041163.g008

(100 μm) as compared with on unpatterned surfaces. However, the cellular functions were significantly more regulated on SVVYGLR micropatterns composed of smaller widths (10 and 50 μm), ECs were restrictedly spread and the cell alignment and elongation were directionally regulated and more significant on narrower patterns (10 and 50 μm) as compared with on larger stripes (100 μm). We also found that ECs preferentially migrated along the direction of micropatterns but the migration rate of ECs was restricted on narrow patterns.

These significant EC responses on narrower micropatterns are important for the remodeling of extracellular matrix, promoting a significant cascade of events resulting in changes in cytoskeletal rearrangement and migration of cells which lead to the assembly of new vessels [8,19]. These restricted geometries send angiogenic cues to ECs and stimulate reorganization of the EC bodies into tubular structures.

Cell shape changes on the narrow patterns play a critical role in switching between growth and differentiation during angiogenesis [46]. Dike *et al.* showed that the differentiation program, which directs capillary tube formation, can be switched on geometrically [27]. In our study, the small geometry of SVVYGLR patterns (10 and 50 μm) promoted multicellular cell-cell interaction, turning on a tubular differentiation pathway. ECs on smaller patterns underwent vacuole formation by pinocytosis and phagocytosis [47,48], and these vacuoles coalesce to form lumen in long extensions of capillaries [8]. The vacuoles developed to form continuous tubular structures during several cell lengths along the direction of SVVYGLR peptide patterns (Fig. 6 A, B). In contrast, the ECs on larger patterns remained more spread, migrated and flattened on the patterns and failed to differentiate into tubes (Fig. 6 C).

The results of quantification of ECs' focal contacts on different surfaces demonstrated that the FA number and size per cell were

reduced on smaller patterns (10 and 50 μm) as compared with larger patterns (100 μm) and unpatterned surfaces (Fig. 7D–E). This revealed that the cell-surface adhesions decreased on smaller patterns. These phenomena were reminiscent of cell release from firm contact with the substrates, which is ultimately responsible for promoting tubulogenesis.

Furthermore, we observed that AJs were smaller but more concentrated on smaller peptide micropatterns (Fig. S4 and Fig. 7C). This change in AJ size is probably due to an increase of myosin activity [31]. AJ size and maturation are regulated by geometrical constraints and mechanically influence the ECs cultured on the smaller peptide stripes to form tube-like structure. In this study, we demonstrated that lumen formation is due to micro-geometrical constraints which affect both cell-substrate adhesion and cell-cell adhesion by modulating status of FAs and the correct maturation of AJs, respectively.

Our results suggest that geometrical cues are sufficient to switch ECs into a tubular differentiation program. We demonstrated that the ECs on small patterns self-organized into multi-cellular tubules, and we can adjust tube formation and tube dimensions through the patterns features on the surfaces.

For the first time, we illustrated here in this study the lumen formation by different cell organization on chemical micropatterns: the central lumen of tubular structure can be formed by one, two, and three or up to four cells (Fig. 7). One-cell self-organization into lumen structure was mostly observed on 10 μm SVVYGLR peptide patterns. The lumen formation by two cells is the most common observation during our study. On some SVVYGLR patterns (10 or 50 μm), multiple ECs were stacked on top of each other, two, three or four cells self-organized into the formation of a 3D tubular structure. Lumen structure cannot be observed by more than four cells, such is the case of ECs on larger peptide micropatterns of 100 μm (Fig. 7B).

As reported, the morphogenesis of endothelial cell tube formation can occur via at least two different mechanisms: cell hollowing and cord hollowing [49,50]. If the cells are arranged in a serial fashion, vacuoles are formed within the cells and coalesce. The fuse of vacuoles gives rise to an intracellular lumen (cell hollowing), and in this process, the lumen is formed by individual cells or chains of cells only one cell thick. We observed this process notably on 10 μm SVVYGLR peptide patterns. Alternatively, if cells are arranged in a paired fashion, they may form a lumen by cord hollowing. In this process, cells assembled into a thin cylindrical cord to create a lumen between cells by the formation and coalescence of vesicles. This tubulogenesis mechanism requires a cell cord two or more cells thick. We also observed this process of cord hollowing and postulate that it is possible to form lumen with 2–4 cells but not more in a 2D culture system. The confocal images presented in our study (Fig. 6–7) suggest that our system of peptide micropatterning supports tubulogenesis through both morphological processes of tube formation.

In our study, angiogenesis activities (tube-like formation and sprouting) were mimicked as the schematic illustrated in Fig. S5. The ECs aligned and restrictedly oriented on the SVVYGLR peptide patterns (Fig. 4, 5), ECs coalesced to form tube-like structures along the length of peptide patterns according to microfeature cues of angiogenic peptides (Fig. 6, 7). EC tube formation on the SVVYGLR peptide patterns played the role of pre-existing vessels, from which EC sprouting can occur and form connections between the adjacent patterns, and the sprouting occurred in parallel to form a vascular network (Fig. 8).

The sprouting angiogenesis requires the tip cells to migrate away from the pre-existing blood vessels [51–53]. The adjacent SVVYGLR peptide stripes served as angiogenic cues to each other and trigger the ECs to sprout from pre-formed tubular structures (Fig. 8). The filopodial mode on endothelial tip cells lead cell migration through RhoGTPase, Cdc42 and Rac 1 activation [53,54]. The stalk cells, comprising the length of the vascular sprout posterior to the tip cells, are highly proliferative and undergo a process of vacuole formation and fusion to form the vessel lumen [51,53]. The tip cells migrate and eventually find receptive ECs from adjacent vascular structures and eventually lead to the generation of a new vessel (Fig. 8). The angiogenic process occurring in parallel leads to the formation of a vascular network, which should be stabilized by recruitment of mural cells (pericytes and smooth muscle cells) in the future to ensure functional blood vessel network (Fig. S5) [55].

Our work presented here reported the micropattening of SVVYGLR peptides grafted onto polymer surfaces to mimic EC tube formation and vascular network formation, without the surface modification by exogenous growth factors. The EC tube formation can be regulated and guided by micropatterning of SVVYGLR peptides depending on geometrical cues of patterns. EC tubulogenesis and vascular network formation are important towards creating vascularization in tissue engineering and tissue regeneration. Scaffolds sufficiently pre-vascularized *in vitro* could be transplanted *in vivo* and encourage integration with host vasculature. The pre-existing endothelial networks may accelerate the vascularization of large engineered tissues, thus improving the survival of long-term implant of engineered tissues [56]. Modification of polymer surfaces could also be transferred to biodegradable materials for promoting vascularization of scaffold materials. In prospective studies, recruitment of other cell types such as pericytes or smooth muscle cells surrounding the EC tubular structure should be addressed.

Conclusions

In this study, we reported the EC tubulogeneis and vascular network formation by geometrical cues of angiogenic SVVYGLR peptides on polymer surfaces. It has been shown that EC morphogenesis can be regulated and guided by micropatterning of SVVYGLR peptides depending on the geometrical cues. EC behaviors were significantly more regulated on narrow SVVYGLR micropatterns, ECs were restrictedly spread and the cell orientation and migration were directionally regulated on narrower patterns (10 and 50 μm) as compared with larger stripes (100 μm), resulting in EC morphogenesis into tube formation on the smaller patterns. The central lumen of the tubular structure can be formed by single-to-four cells demonstrating two different processes of tubulogenesis: cell hollowing and cord hollowing. We suggest that EC focal adhesions, AJ size and maturation induced by geometrical constraints participate in the ECs self-assembly into tubular structures. In addition, sprouting of ECs and the formation of vascular network were induced on the surfaces micropatterned with SVVYGLR peptides. The micropatterning of SVVYGLR peptides here provides opportunities for mimicking angiogenesis by avoiding the surface modification by exogenous growth factors. The organization of ECs into tube-like structures and vascular network formation are important toward the fabrication of pre-vascularized tissues, which has great potential applications in tissue engineering and tissue regeneration.

Supporting Information

Figure S1 The effects of peptide concentration onto EC alignment. EC adhesion and alignment on surfaces micropatterned with 50 μm SVVYGLR peptide stripes after 24 h in

culture, the concentration of peptide solution was varied from 10^{-5} M, 10^{-4} M, 10^{-3} M to 10^{-2} M. Scale bar is 100 μm.
(TIF)

Figure S2 EC adhesion on PET and SVVYGLR grafted surfaces for 3 days. Cell actin skeletons were represented in green. Scale bar corresponds to 100 μm.
(TIF)

Figure S3 Confocal images of EC cord-like structure on 10 μm SVVYGLR peptide stripes.
(TIF)

Figure S4 EC adherens junctions (AJs) on SVVYGLR peptide micropatterns. (A) AJs of ECs were obtained from fluorescence staining with antibody against CD31. Scale bars are 20 μm. (B) The AJ size and density on each surface was analyzed by "plot profile" tool in ImageJ: the horizontal axis representing the AJ size and the vertical axis representing the AJ density, respectively.
(TIF)

Figure S5 Schematic of EC tube formation, sprouting, network formation on micropatterned surfaces and prospective work.
(TIF)

Acknowledgments

The authors gratefully thank Sébastien Marais (Bordeaux Image Center, France), Lila Rami (BioTis, Université de Bordeaux II, France), Christine Labrugère (ICMCB, Université de Bordeaux I, France) and Annie Zhe Cheng (IECB, Université de Bordeaux I, France) for image analysis assistance, technical assistance on confocal microscopy, X-ray photoelectron spectroscopy, and English language assistance, respectively.

Author Contributions

Conceived and designed the experiments: YL OFZ MCD. Performed the experiments: YL MR. Analyzed the data: YL OFZ. Contributed reagents/materials/analysis tools: CA MCD. Wrote the paper: YL OFZ MCD.

References

1. Folkman J, Haudenschild C (1980) Angiogenesis in vitro. Nature 288: 551–556.
2. Carmeliet P (2005) Angiogenesis in life, disease and medicine. Nature 438: 932–936.
3. Novosel EC, Kleinhans C, Kluger PJ (2011) Vascularization is the key challenge in tissue engineering. Adv Drug Deliv Rev 63: 300–311.
4. Risau W (1997) Mechanisms of angiogenesis. Nature 386: 671–674.
5. Otrock ZK, Mahfouz RA, Makarem JA, Shamseddine AI (2007) Understanding the biology of angiogenesis: review of the most important molecular mechanisms. Blood Cells Mol Dis 39: 212–220.
6. Arnaoutova I, Kleinman HK (2010) In vitro angiogenesis: endothelial cell tube formation on gelled basement membrane extract. Nat Protoc 5: 628–635.
7. Norrby K (2006) In vivo models of angiogenesis. J Cell Mol Med 10: 588–612.
8. Davis GE, Bayless KJ, Mavila A (2002) Molecular basis of endothelial cell morphogenesis in three-dimensional extracellular matrices. Anat Rec 268: 252–275.
9. Sottile J (2004) Regulation of angiogenesis by extracellular matrix. Biochim Biophys Acta 1654: 13–22.
10. Sukmana I, Vermette P (2010) The effects of co-culture with fibroblasts and angiogenic growth factors on microvascular maturation and multi-cellular lumen formation in HUVEC-oriented polymer fibre constructs. Biomaterials 31: 5091–5099.
11. Phelps EA, Garcia AJ (2010) Engineering more than a cell: vascularization strategies in tissue engineering. Curr Opin Biotechnol 21: 704–709.
12. Otrock ZK, Makarem JA, Shamseddine AI (2007) Vascular endothelial growth factor family of ligands and receptors: review. Blood Cells Mol Dis 38: 258–268.
13. Gerhardt H (2008) VEGF and endothelial guidance in angiogenic sprouting. Organogenesis 4: 241–246.
14. Ferrara N, Gerber HP, LeCouter J (2003) The biology of VEGF and its receptors. Nat Med 9: 669–676.
15. Davies N, Dobner S, Bezuidenhout D, Schmidt C, Beck M, et al. (2008) The dosage dependence of VEGF stimulation on scaffold neovascularisation. Biomaterials 29: 3531–3538.
16. Drake CJ, Little CD (1995) Exogenous vascular endothelial growth factor induces malformed and hyperfused vessels during embryonic neovascularization. Proc Natl Acad Sci U S A 92: 7657–7661.
17. Williams DF (2011) The role of short synthetic adhesion peptides in regenerative medicine; the debate. Biomaterials 32: 4195–4197.
18. Hamada Y, Nokihara K, Okazaki M, Fujitani W, Matsumoto T, et al. (2003) Angiogenic activity of osteopontin-derived peptide SVVYGLR. Biochem Biophys Res Commun 310: 153–157.
19. Moon JJ, Hahn MS, Kim I, Nsiah BA, West JL (2009) Micropatterning of poly(ethylene glycol) diacrylate hydrogels with biomolecules to regulate and guide endothelial morphogenesis. Tissue Eng Part A 15: 579–585.
20. Collier JH, Segura T (2011) Evolving the use of peptides as components of biomaterials. Biomaterials 32: 4198–4204.
21. Yokosaki Y, Matsuura N, Sasaki T, Murakami I, Schneider H, et al. (1999) The integrin alpha(9)beta(1) binds to a novel recognition sequence (SVVYGLR) in the thrombin-cleaved amino-terminal fragment of osteopontin. J Biol Chem 274: 36328–36334.
22. Hamada Y, Yuki K, Okazaki M, Fujitani W, Matsumoto T, et al. (2004) Osteopontin-derived peptide SVVYGLR induces angiogenesis in vivo. Dent Mater J 23: 650–655.
23. Hamada Y, Egusa H, Kaneda Y, Hirata I, Kawaguchi N, et al. (2007) Synthetic osteopontin-derived peptide SVVYGLR can induce neovascularization in artificial bone marrow scaffold biomaterials. Dent Mater J 26: 487–492.
24. Khademhosseini A, Langer R, Borenstein J, Vacanti JP (2006) Microscale technologies for tissue engineering and biology. Proc Natl Acad Sci U S A 103: 2480–2487.
25. Chen CS, Mrksich M, Huang S, Whitesides GM, Ingber DE (1998) Micropatterned surfaces for control of cell shape, position, and function. Biotechnol Prog 14: 356–363.
26. Kane RS, Takayama S, Ostuni E, Ingber DE, Whitesides GM (1999) Patterning proteins and cells using soft lithography. Biomaterials 20: 2363–2376.
27. Dike LE, Chen CS, Mrksich M, Tien J, Whitesides GM, et al. (1999) Geometric control of switching between growth, apoptosis, and differentiation during angiogenesis using micropatterned substrates. In Vitro Cell Dev Biol Anim 35: 441–448.
28. Co CC, Wang YC, Ho CC (2005) Biocompatible micropatterning of two different cell types. J Am Chem Soc 127: 1598–1599.
29. McBeath R, Pirone DM, Nelson CM, Bhadriraju K, Chen CS (2004) Cell shape, cytoskeletal tension, and RhoA regulate stem cell lineage commitment. Dev Cell 6: 483–495.
30. Kilian KA, Bugarija B, Lahn BT, Mrksich M (2010) Geometric cues for directing the differentiation of mesenchymal stem cells. Proc Natl Acad Sci U S A 107: 4872–4877.
31. Liu Z, Tan JL, Cohen DM, Yang MT, Sniadecki NJ, et al. (2010) Mechanical tugging force regulates the size of cell-cell junctions. Proc Natl Acad Sci U S A 107: 9944–9949.
32. Chollet C, Chanseau C, Remy M, Guignandon A, Bareille R, et al. (2009) The effect of RGD density on osteoblast and endothelial cell behavior on RGD-grafted polyethylene terephthalate surfaces. Biomaterials 30: 711–720.
33. Chollet C, Lazare S, Guillemot F, Durrieu MC (2010) Impact of RGD micropatterns on cell adhesion. Colloids Surf B Biointerfaces 75: 107–114.
34. Zouani OF, Chollet C, Guillotin B, Durrieu MC (2010) Differentiation of pre-osteoblast cells on poly(ethylene terephthalate) grafted with RGD and/or BMPs mimetic peptides. Biomaterials 31: 8245–8253.
35. Jaffe EA, Nachman RL, Becker CG, Minick CR (1973) Culture of human endothelial cells derived from umbilical veins. Identification by morphologic and immunologic criteria. J Clin Invest 52: 2745–2756.
36. Li H, Daculsi R, Grellier M, Bareille R, Bourget C, et al. (2010) Role of neural-cadherin in early osteoblastic differentiation of human bone marrow stromal cells cocultured with human umbilical vein endothelial cells. Am J Physiol Cell Physiol 299: C422–430.
37. Charest JL, Garcia AJ, King WP (2007) Myoblast alignment and differentiation on cell culture substrates with microscale topography and model chemistries. Biomaterials 28: 2202–2210.
38. Aubin H, Nichol JW, Hutson CB, Bae H, Sieminski AL, et al. (2010) Directed 3D cell alignment and elongation in microengineered hydrogels. Biomaterials 31: 6941–6951.
39. Zouani OF, Chanseau C, Brouillaud B, Bareille R, Deliane F, et al. (2012) Altered nanofeature size dictates stem cell differentiation. Journal of Cell Science 125: 1–8.
40. Santos MI, Tuzlakoglu K, Fuchs S, Gomes ME, Peters K, et al. (2008) Endothelial cell colonization and angiogenic potential of combined nano- and micro-fibrous scaffolds for bone tissue engineering. Biomaterials 29: 4306–4313.
41. Egginton S, Gerritsen M (2003) Lumen formation: in vivo versus in vitro observations. Microcirculation 10: 45–61.
42. Nakatsu MN, Sainson RC, Aoto JN, Taylor KL, Aitkenhead M, et al. (2003) Angiogenic sprouting and capillary lumen formation modeled by human

umbilical vein endothelial cells (HUVEC) in fibrin gels: the role of fibroblasts and Angiopoietin-1. Microvasc Res 66: 102–112.
43. Barry ST, Ludbrook SB, Murrison E, Horgan CM (2000) Analysis of the alpha4beta1 integrin-osteopontin interaction. Exp Cell Res 258: 342–351.
44. Green PM, Ludbrook SB, Miller DD, Horgan CM, Barry ST (2001) Structural elements of the osteopontin SVVYGLR motif important for the interaction with alpha(4) integrins. FEBS Lett 503: 75–79.
45. Egusa H, Kaneda Y, Akashi Y, Hamada Y, Matsumoto T, et al. (2009) Enhanced bone regeneration via multimodal actions of synthetic peptide SVVYGLR on osteoprogenitors and osteoclasts. Biomaterials 30: 4676–4686.
46. Ingber DE, Folkman J (1989) Mechanochemical switching between growth and differentiation during fibroblast growth factor-stimulated angiogenesis in vitro: role of extracellular matrix. J Cell Biol 109: 317–330.
47. Davis GE, Camarillo CW (1996) An alpha 2 beta 1 integrin-dependent pinocytic mechanism involving intracellular vacuole formation and coalescence regulates capillary lumen and tube formation in three-dimensional collagen matrix. Exp Cell Res 224: 39–51.
48. Kamei M, Saunders WB, Bayless KJ, Dye L, Davis GE, et al. (2006) Endothelial tubes assemble from intracellular vacuoles in vivo. Nature 442: 453–456.
49. Lubarsky B, Krasnow MA (2003) Tube Morphogenesis: Making and Shaping Biological Tubes. Cell 112: 19–28.
50. Ellertsdottir E, Lenard A, Blum Y, Krudewig A, Herwig L, et al. (2010) Vascular morphogenesis in the zebrafish embryo. Developmental Biology 341: 56–65.
51. Gerhardt H, Golding M, Fruttiger M, Ruhrberg C, Lundkvist A, et al. (2003) VEGF guides angiogenic sprouting utilizing endothelial tip cell filopodia. J Cell Biol 161: 1163–1177.
52. Jakobsson L, Franco CA, Bentley K, Collins RT, Ponsioen B, et al. (2010) Endothelial cells dynamically compete for the tip cell position during angiogenic sprouting. Nat Cell Biol 12: 943–953.
53. De Smet F, Segura I, De Bock K, Hohensinner PJ, Carmeliet P (2009) Mechanisms of vessel branching: filopodia on endothelial tip cells lead the way. Arterioscler Thromb Vasc Biol 29: 639–649.
54. Bayless KJ, Davis GE (2002) The Cdc42 and Rac1 GTPases are required for capillary lumen formation in three-dimensional extracellular matrices. J Cell Sci 115: 1123–1136.
55. Jain RK (2003) Molecular regulation of vessel maturation. Nat Med 9: 685–693.
56. Koike N, Fukumura D, Gralla O, Au P, Schechner JS, et al. (2004) Tissue engineering: creation of long-lasting blood vessels. Nature 428: 138–139.

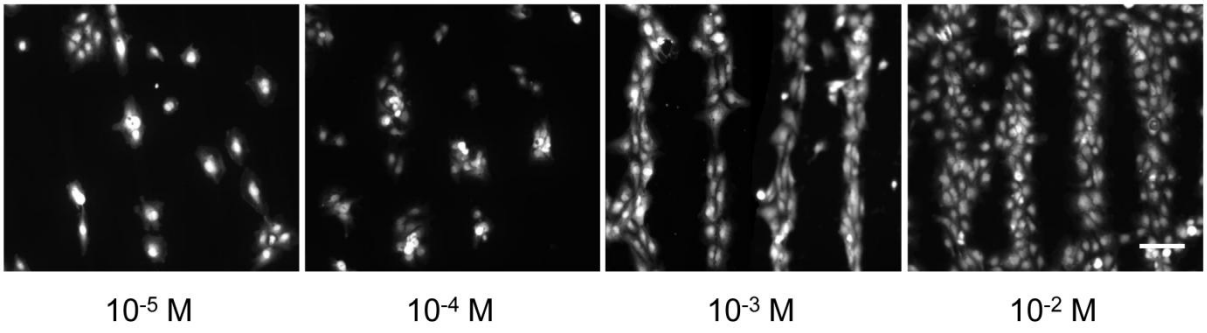

Figure S1

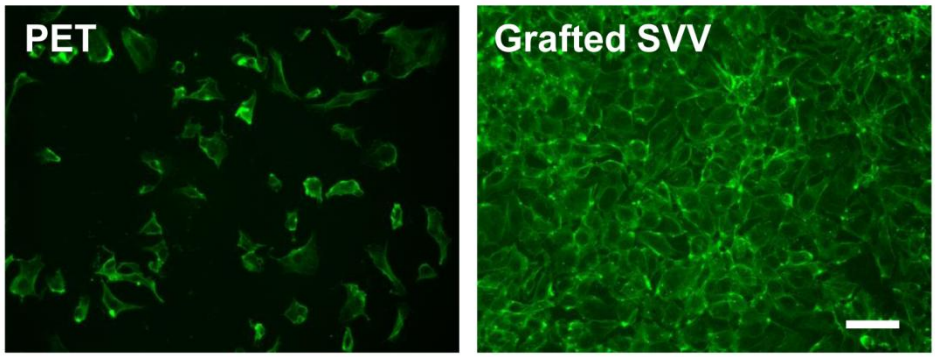

Figure S2

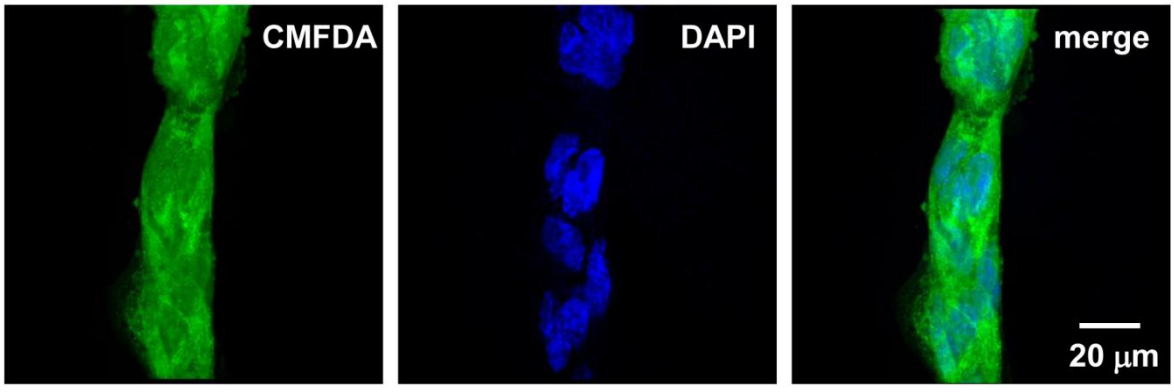

Figure S3

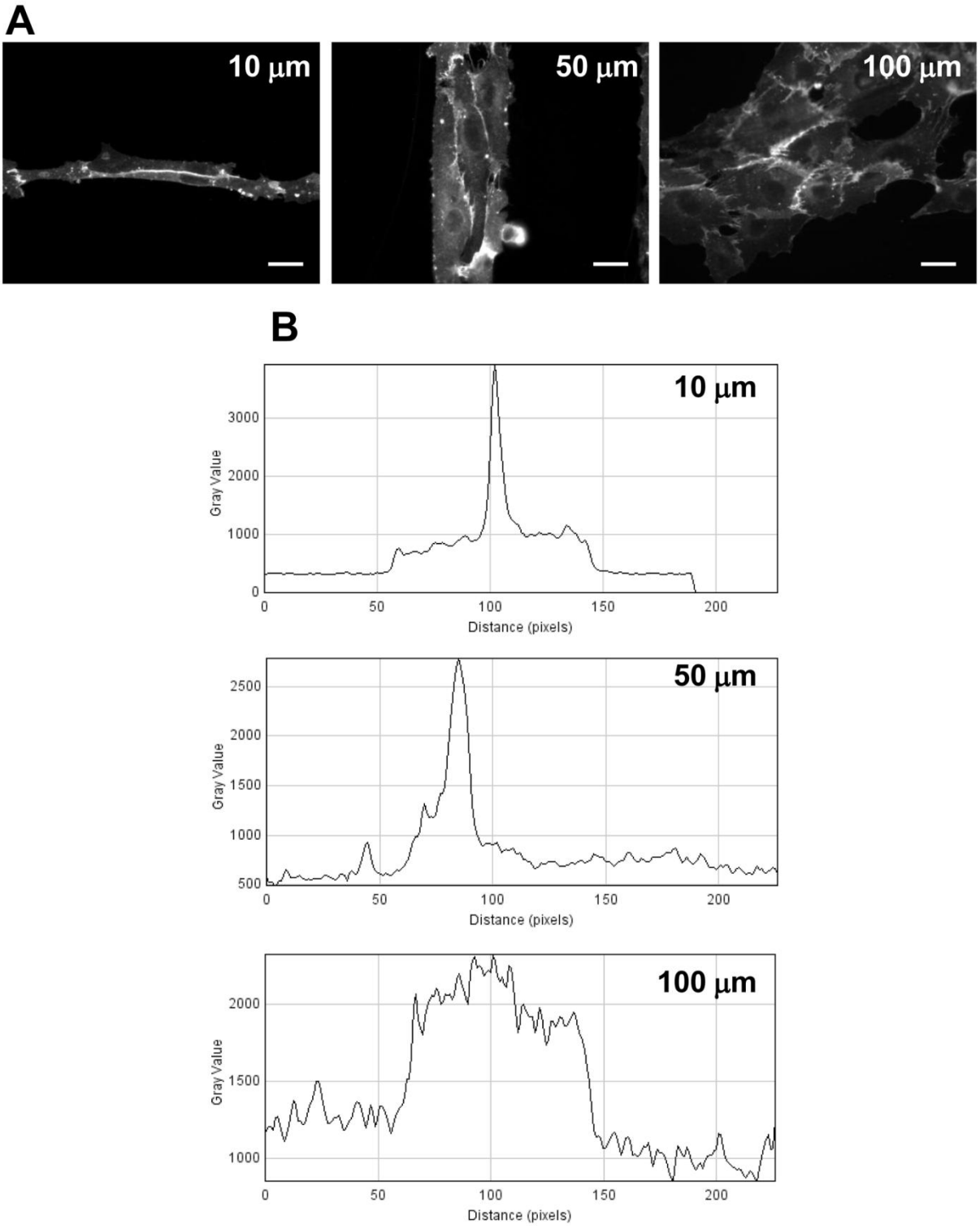
A
10 μm
50 μm
100 μm
B
10 μm
Gray Value
Distance (pixels)
50 μm
Gray Value
Distance (pixels)
100 μm
Gray Value
Distance (pixels)

Figure S4

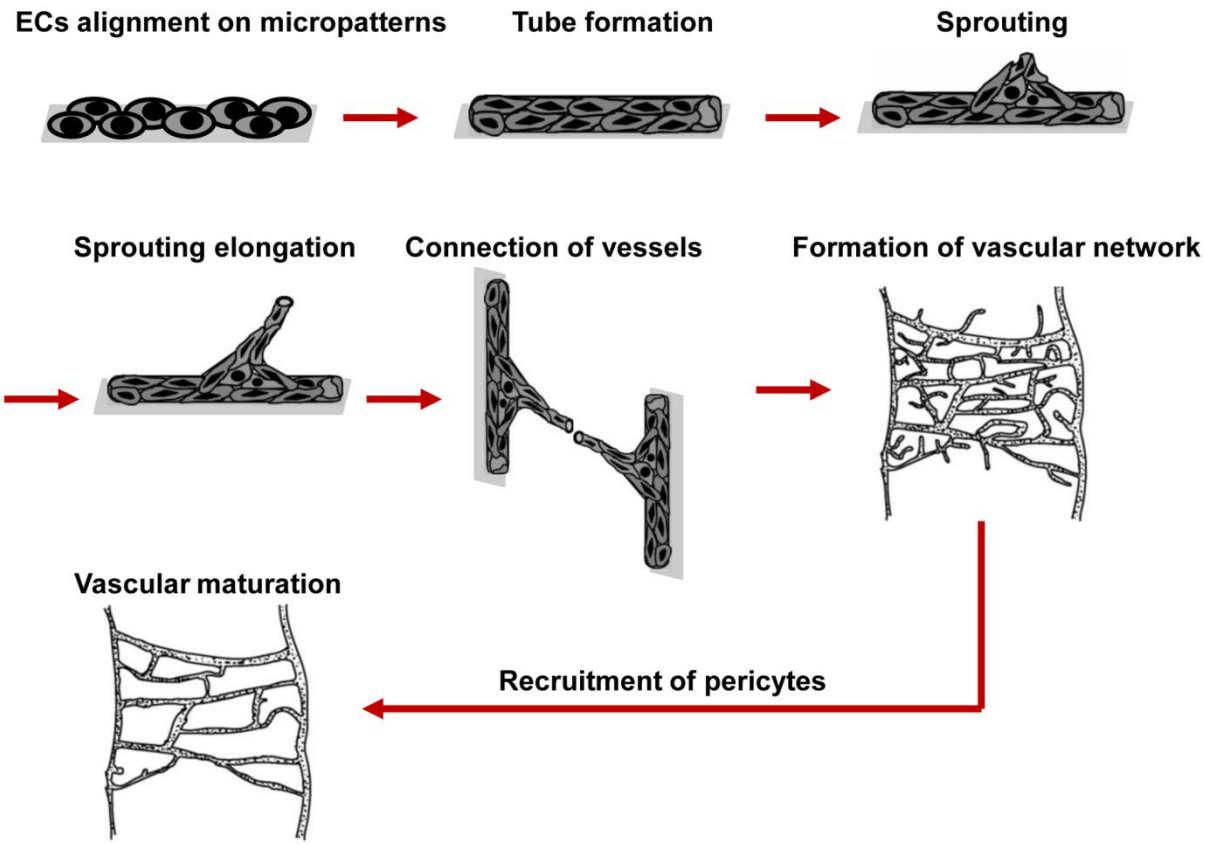
ECs alignment on micropatterns
Tube formation
Sprouting
Sprouting elongation
Connection of vessels
Formation of vascular network
Vascular maturation
Recruitment of pericytes

Figure S5

Paper IV. Modeling of the migration of endothelial cells on bioactive micropatterned polymers

Mathematical Biosciences and Engineering. 2012. Accepted.

Mathematical modeling was developed to study the endothelial cell migration on micropatterned surfaces. The numerical study showed that the model behaviors are in good agreement with the experimental results. Mathematical modeling offers good opportunity to study the influence of bioactive geometries onto endothelial cell migration

This work was carried out in close collaboration with the "Institut de Mathématique de Bordeaux" (IMB) - Université de Bordeaux 1, and more precisely with the team of Professor Thierry Colin.

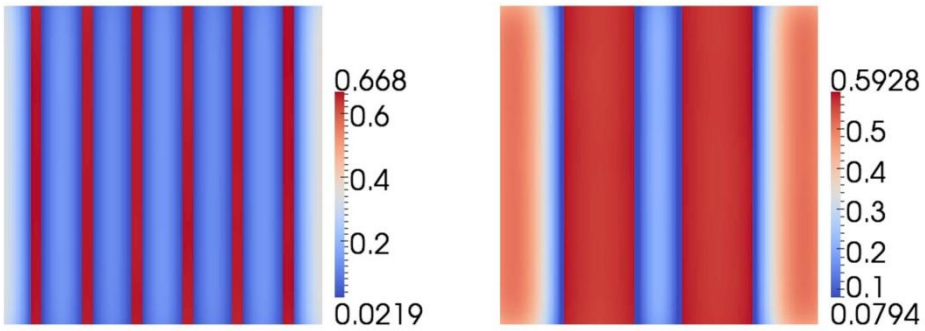

Figure 27. Endothelial cell density on small (left) and large (right) micropatterns by mathematical modeling.

MATHEMATICAL BIOSCIENCES
AND ENGINEERING
Volume **xx**, Number **0xx**, xx **20xx**

doi:10.3934/mbe.20xx.xx.xx

pp. **1–xx**

MODELING OF THE MIGRATION OF ENDOTHELIAL CELLS ON BIOACTIVE MICROPATTERNED POLYMERS

Thierry Colin

Univ. Bordeaux, IMB, UMR 5251,
F-33400 Talence, France.

Marie-Christine Durrieu

CNRS, IECB, UMR 5248,
F-33607 PESSAC, France

Julie Joie

Univ. Bordeaux, IMB, UMR 5251,
F-33400 Talence, France.

Yifeng Lei

Univ. Bordeaux, IECB, UMR 5248,
F-33607 PESSAC, France

Youcef Mammeri

INRIA
F-33400 Talence, France.

Clair Poignard

INRIA
F-33400 Talence, France.

Olivier Saut

CNRS, IMB, UMR 5251,
F-33400 Talence, France.

(Communicated by the associate editor name)

Abstract. In this paper, a macroscopic model describing endothelial cell migration on bioactive micropatterned polymers is presented. It is based on a system of partial differential equations of Patlak-Keller-Segel type that describes the evolution of the cell densities. The model is studied mathematically and numerically. We prove existence and uniqueness results of the solution to the differential system. We also show that fundamental physical properties such as mass conservation, positivity and boundedness of the solution are satisfied. The numerical study allows us to show that the model behaves in good agreement with the experiments.

2000 *Mathematics Subject Classification.* Primary:92B05, 92C17.

Key words and phrases. Tissue engineering, Keller-Segel type model, endothelial cells, migration.

The authors wish to thanks the GIS AMA "Advanced Materials in Aquitaine" (http://www.ama-materials.com/) for its financial support.

E-mail address: colin@math.u-bordeaux1.fr

1. **Introduction.** Tissue engineering is the use of combination of cells, engineering, materials, and suitable biochemical factors to improve or replace biological functions [26]. The main challenge of this scientific field consists in providing functional microvascular networks able to supply tissue with nutrients and oxygen and to remove metabolic wastes [18]. The lack of vascularization hampers the survival of engineered tissues after implantation [18]. Researchers rely on the increasing knowledge of angiogenic and vasculogenic processes to stimulate vascular network formation [32, 31]. This complex process of new blood vessel formation is orchestrated by the interaction between endothelial cells (ECs) and their neighboring mural cells via a complex network of intracellular signaling mechanisms [28, 17]. Ever since the introduction of the *in vitro* experimental models of angiogenesis [11], there has been an increasing research interest to understand the intricate process of tube formation. Although many efforts have been made, the mechanism associated with angiogenesis and vascularization is still poorly understood. A deeper comprehension of cells-biomaterials interaction is then required for basic understanding of angiogenesis and vascularization in tissue engineering [5].

One strategy in developing clinical implants consists of appropriate utilizations of bioactive materials: bioactive materials may induce *in vivo* regenerative response at the site of damage, whereas when used *in vitro*, they can stimulate the tissue growth for subsequent implantation [2, 23]. Different bioactive ligands have been used to study their effects on cell functions for a better understanding of vascularization [31]. In the aim of promoting angiogenesis in the case of tissue engineering or of inhibiting angiogenesis in the case of cancer, it is important to understand the mechanisms that regulate lumen formation. Successful micropatterning of cells is becoming a key component of this field [16]. Researchers are now interested in the behavior of cells on substrates that have been patterned by micro– or nano–fabrication [10, 27]. It is known that cell positioning and physiology can be controlled by the substrate on which the cells adhere [6]. Our experiments show that the use of cell adhesion peptides that are micropatterned onto material makes possible the formation of tube-like structures unlike the use of virgin or homogeneously grafted materials [22, 23].

Actually, experimental studies using micropatterned substrates revealed that the cell migration is governed by the geometry of patterns. Endothelial cells so cultured form extensive cell-cell interactions. In some configurations, accumulation of endothelial cell junctions implies that some cells form tube-like structures. The goal of the present paper is to provide a model that describes such experimental results.

Adhesive areas are composed of cell adhesion peptides or growth factor peptides that make the cells adhere. These areas are surrounded by non-adhesive areas [22]. We assume (and this is actually confirmed by experiments) that active principles (cell adhesion peptides or growth factors) do not diffuse. Therefore endothelial cells located outside the adhesive areas cannot straightforwardly "feel" the active principles. They find out the adhesive areas indirectly. We do not consider the influence of nutrients and assume that cells obtain enough nutrients from the material (due to grafted active principles onto material). Endothelial cells are seeded onto micropatterned bioactive materials during several hours, then they are washed out. Only the adhered endothelial cells remain on the material. The initial cell density is around 40 000 cells per cm^2. At the beginning of the experiments, during the migration phase, we observe that cells have a random motility and stop on adhesive areas. Moreover the attraction of endothelial cells on adhesive areas seems to be higher than the attraction of cells located outside these areas. Experiments show that endothelial cells are grouping together along the micropatterns. On bioactive materials composed of thin strips of tens of micrometers width, that is the order of magnitude of cell size, endothelial cells line their cytoskeleton to adjust it with the bioactive micropattern. Note also that tubes containing a central lumen may appear for such micropatterns[23, 7].In other words, blood vessels are created from an initial random density of endothelial cells. Such phenomenon is not observed with larger strips [7, 20, 25].

To illustrate these experiments, we present in Fig.1 pictures of the micropatterned bioactive materials at the end of the migration phase. Two different micropatterns are considered: on Fig.1(a) thin adhesive areas (bioactive pattern size: 10 μm and distance between patterns: 100 μm) have beed used, whereas Fig.1(b) shows the end of the migration on large strips (bioactive pattern size: 300 μm and distance between patterns: 100 μm). We refer the reader to [22, 23] for a detailed description of these experiments.

We observed that for the large adhesive areas, the adhered cell density is smaller than for thin strips. Therefore the geometry of the micropatterns is crucial in the endothelial cell migration and thus, in the formation of new vessels.

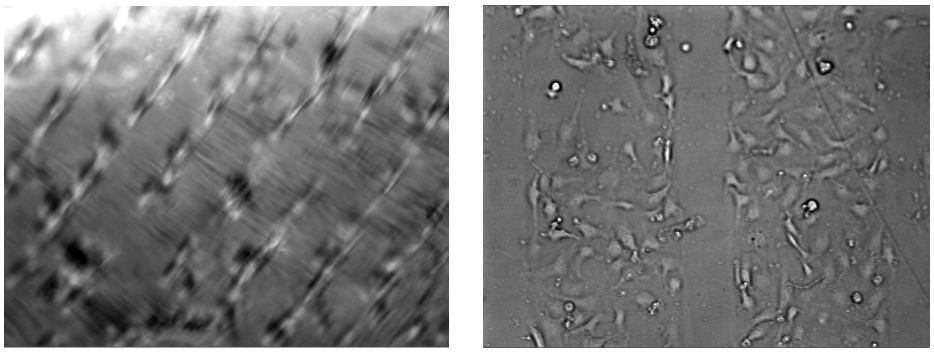

(a) thin areas (b) large areas

FIGURE 1. Endothelial cell alignment onto micropatterned polymer (PET) (10μm (A) and 300 μm (B) stripes of SVVYGLR peptides) [22]. The distance between bioactive patterns is 100 μm.

In this paper, we are interested in understanding how these patterns (size and spacing of the bioactive microfeatures) do influence endothelial cell migration. The model we present here is a Patlak-Keller-Segel type model [1, 13, 21, 30]. The chemotaxis term takes the cell-cell interactions into account instead of the cell-chemical attractant interactions. We show that this new model based on a system of coupled partial differential equations satisfies the mass conservation law and that existence and uniqueness results of weak solution hold. We also provide numerical results in accordance with the experiments, which ensures the validity of our model. Moreover, these numerical simulations make possible to obtain informations on the influence of the geometry and of the initial concentration of cells on the cell migration.

The outline of the article is the following. In section 2 we describe the mathematical model and we state the main result of global existence and uniqueness of the weak solution to the P.D.E system. Section 3 is devoted to the proof of the main theorem. We then provide numerical results in section 4 in order to compare the simulations to the experiments.

2. **Description of the model and main result.** In this section, we describe the Patlak-Keller-Segel type model we study throughout the paper. The model is composed of a diffusion term coupled with a reaction term, that describes the effect of the chemoattractants, which statisfy a diffusion equation.

Various continuous models of Patlak-Keller-Segel type have been used to describe cell motility [21, 30, 4, 14, 8, 33]. The governing equations of these models are written in the following general form, in a domain $\Omega \subset \mathbb{R}^n$:

$$\begin{aligned} \partial_t u &= \nabla.\left(D_1(u,v)\nabla u - \chi(u,v)u\nabla v\right) + f(u,v) \quad \text{on } \Omega, \\ \partial_t v &= \nabla.\left(D_2(u,v)\nabla v\right) + g(u,v) - h(u,v)v \qquad \text{on } \Omega, \end{aligned}$$

where u denotes the cells density, v is the chemical signal concentration. The diffusive terms take the random cell motility into account, whereas the advection describes the influence of the chemical signal on the cell motion. The two corresponding diffusion parameters are denoted by D_1 and D_2, while χ is the chemotaxis coefficient. The function f describes the growth and the death of cells, whereas the functions g and h describe respectively the production and the degradation of the chemotaxic signal. These equations have been theoretically studied for several years [3, 4, 8, 12, 14, 33]. Based on this extensive literature, we provide a slightly modified model to describe the cell migration on bioactive micropatterns.

2.1. **Statement of the equations.** According to the experiments, the behavior of the cells is drastically different on the adhesive areas and outside these areas. Actually, outside the adhesive strips, the cells seem to attract each other (probably thanks to the chemoattractant they produce) and also diffuse randomly in the domain, but as soon as they reach the adhesive strips the cells seem stuck on the strips and then they diffuse only on the bioactive material, ignoring the outer cells. Moreover, it seems that the cells located on the adhesive strips produce more chemoattractant than the outer cells.

Since there is no clear understanding of the way that endothelial cells communicate, we chose to consider the chemotaxis term as the attraction between endothelial cells (and we do not consider any gradient of concentration of the chemoattractant).

Based on these assumptions, we derive the following model. Consider a domain Ω splitted between adhesive areas, denoted by $\widetilde{\Omega}$, and non-adhesive areas denoted by $\Omega \setminus \widetilde{\Omega}$. We assume that all the domains are bounded domains with smooth boundary.

Two different types of endothelial cells are considered. We denote by $u_1(t,x,y)$ the density of endothelial cells, at any point (x,y) and at time t, that can freely move (*i.e.* they have yet to move over adhesion proteins). Cells that are adhering on the substrate are tracked through their density u_2. The function v represents the density of the chemoattractant. The equations governing the endothelial cell migration are given for $t>0$ by

$$\partial_t u_1 = d_1 \Delta u_1 - \lambda \mathbb{1}_{\widetilde{\Omega}} u_1(1-u_2) - \nabla.\left(\chi(u_1,v)u_1 \nabla v\right), \qquad \text{in } \Omega, \tag{1a}$$

$$\partial_t u_2 = d_2 \Delta u_2 + \lambda \mathbb{1}_{\widetilde{\Omega}} u_1(1-u_2), \qquad \text{in } \widetilde{\Omega}, \tag{1b}$$

$$\partial_t v = \Delta v - \eta v + \gamma_1 u_1 + \gamma_2 u_2, \qquad \text{in } \Omega, \tag{1c}$$

with the homogeneous boundary conditions on $\partial\Omega$ and $\partial\widetilde{\Omega}$:

$$\partial_{\mathbf{n}} u_1|_{\partial\Omega} = 0, \quad \partial_{\mathbf{n}} u_2|_{\partial\widetilde{\Omega}} = 0, \quad \partial_{\mathbf{n}} v|_{\partial\Omega} = 0, \tag{1d}$$

and with the initial conditions $(u_1^0, u_2^0, 0)$:

$$u_1|_{t=0} = u_1^0, \quad u_2|_{t=0} = u_2^0, \quad v|_{t=0} = 0. \tag{1e}$$

We then denote by u the total cell density:

$$u(t,x) = u_1(t,x) + u_2(t,x), \quad t \geq 0,\ x \in \Omega,$$

where u_2 is extended by 0 in $\Omega \setminus \widetilde{\Omega}$.

The parameters d_1, d_2, η, γ_1, γ_2 and λ are strictly positive and they will be fitted by the experiments in a forthcoming work, but we consider here that they are given constants. The coefficients d_1 and d_2 denote the diffusion coefficients of the cells u_1 and u_2 respectively. The coefficient $\eta > 0$ is the self-degradation rate of the chemoattractant produced by the cells, while the coefficients γ_1 and γ_2 are the coefficients of the production of the chemoattractant respectively for the cell u_1 and u_2. The parameter λ is the speed with which u_1 become u_2, when u_1 lies in the bioactive micropatterns $\widetilde{\Omega}$. The first two equations describe the cell migration in Ω. Outside the bioactive strips, the endothelial cells diffuse and attract the neighboring cells via the chemotaxis sensitivity function :

$$\chi(u_1,v) = \chi^0 \frac{v}{1+|v|}(1-u_1), \quad \text{with } \chi^0 > 0.$$

Here above, χ^0 is a chemotaxis parameter, and the term $(1-u_1)$ is settled to prevent the overcrowding of the cells u_1. Endothelial cells once they reach the adhesive area $\widetilde{\Omega}$ are captured and then diffuse only in the strip. This is handled by the penalty term $-\lambda \mathbb{1}_{\widetilde{\Omega}} u_1(1-u_2)$. Cells on the strips still have a random motility and their concentration grows up as the term $\lambda \mathbb{1}_{\widetilde{\Omega}} u_1(1-u_2)$, where $1-u_2$ prevents the blow-up of u_2 in equation (1b). The third equation (1c) describes the production of the chemoattractant by the cells. Since the cells on the strip seem to be more attractive, we suppose that the production coefficients satisfy $0 < \gamma_1 < \gamma_2$. We also add a degradation coefficient $\eta > 0$ describing the metabolization of the chemoattractant.

2.2. **Main theoretical result.** We have the following theorem which is a straightforward consequence of the results of section 3:

Theorem 2.1. *Let d_1, d_2, η, γ_1, γ_2 and λ be strictly positive constants. Suppose that the initial data $(u_1^0, u_2^0) \in L^\infty(\Omega) \times L^\infty(\widetilde{\Omega})$ are such that*

$$\forall x \in \Omega, \quad 0 \leq u_1^0(x) \leq 1, \quad \forall x \in \widetilde{\Omega}, \quad 0 \leq u_2^0(x) \leq 1.$$

There exists a unique weak solution (u_1, u_2, v) *to problem* (1) *such that*

$$(u_1, u_2, v) \in L^\infty\Big([0,+\infty); L^\infty(\Omega)\Big) \times L^\infty\Big([0,\infty); L^\infty(\widetilde{\Omega})\Big) \times L^\infty\Big([0,\infty); L^\infty(\Omega)\Big),$$

and for almost any $t > 0$

$$0 \le u_1(t,\cdot) \le 1, \quad 0 \le u_2(t,\cdot) \le 1, \quad \textit{and} \quad 0 \le v(t,\cdot) \le \frac{1}{\eta}\left(\gamma_1 + \gamma_2\right).$$

The next section is devoted to prove this theorem. The proof is based on Gaussian upper bounds for heat kernels [29]–[35].

3. **Theoretical study of the model .** In this section we study the mathematical properties of the model. Throughout this section we suppose that $\widetilde{\Omega}$ and Ω are smooth domains of $\mathbb{R}^2$. We remind that d_1, d_2 and η are strictly positive coefficients.

3.1. **Kernels of the operators.** The aim of this paragraph is to provide estimates satisfied by the kernels of the operators $\partial_t - \Delta + \eta$ and $\partial_t - d_1\Delta$ in Ω and by the kernel of $\partial_t - d_2\Delta$ in $\widetilde{\Omega}$, with homogeneous Neumann conditions imposed respectively on $\partial\Omega$ and $\partial\widetilde{\Omega}$.

Definition 3.1. The kernels $\mathcal{B}$, $\mathcal{G}$ and $\widetilde{\mathcal{G}}$ of the respective operators $\partial_t - \Delta + \eta$, $\partial_t - d_1\Delta$ on Ω, and $\partial_t - d_2\Delta$ on $\widetilde{\Omega}$, all with homogeneous Neumann conditions, are respectively defined by

$$\forall (x,y) \in \Omega, \quad \lim_{t\to 0^+} \mathcal{B}(t,x,y) = \delta_y(x),$$

and for any $(t,y) \in (0,\infty)\times\Omega$,

$$\begin{cases} \partial_t \mathcal{B}(t,x,y) = \Delta\mathcal{B}(t,x,y) - \eta\mathcal{B}(t,x,y), & \forall x \in \Omega, \\ \partial_{\mathbf{n}}\mathcal{B}(t,x_{\partial\Omega},y) = 0, & \forall x_{\partial\Omega} \in \partial\Omega, \end{cases} \tag{2a}$$

for $\mathcal{B}$, while $\mathcal{G}$ is given by

$$\forall (x,y) \in \Omega, \quad \lim_{t\to 0^+} \mathcal{G}(t,x,y) = \delta_y(x), \tag{3a}$$

and for any $(t,y) \in (0,\infty)\times\Omega$,

$$\begin{cases} \partial_t \mathcal{G}(t,x,y) = d_1\Delta\mathcal{G}(t,x,y), & \forall x \in \Omega, \\ \partial_{\mathbf{n}}\mathcal{G}(t,x_{\partial\Omega},y) = 0, & \forall x_{\partial\Omega} \in \partial\Omega, \end{cases} \tag{3b}$$

and $\widetilde{\mathcal{G}}$ is the solution to

$$\forall (x,y) \in \widetilde{\Omega}, \quad \lim_{t\to 0^+} \widetilde{\mathcal{G}}(t,x,y) = \delta_y(x), \tag{4a}$$

and for any $(t,y) \in (0,\infty)\times\widetilde{\Omega}$,

$$\begin{cases} \partial_t \widetilde{\mathcal{G}}(t,x,y) = d_2\Delta\widetilde{\mathcal{G}}(t,x,y), & \forall x \in \widetilde{\Omega}, \\ \partial_{\mathbf{n}}\widetilde{\mathcal{G}}(t,x_{\partial\widetilde{\Omega}},y) = 0, & \forall x_{\partial\widetilde{\Omega}} \in \partial\widetilde{\Omega}. \end{cases} \tag{4b}$$

Note that the above kernels are symmetric in their second and third variables.

Proposition 1. *For any* $y \in \Omega$ *(respectively for any* $y \in \widetilde{\Omega}$*), we have the following estimates for positive constants* C_Ω *and* $C_{\widetilde{\Omega}}$*, which depend on the domain* Ω *and* $\widetilde{\Omega}$ *respectively:*

$$\|\mathcal{G}(t,\cdot,y)\|_{L^1(\Omega)} \le C_\Omega, \tag{5a}$$

$$\left\|\widetilde{\mathcal{G}}(t,\cdot,y)\right\|_{L^1(\Omega)} \le C_{\widetilde{\Omega}}, \tag{5b}$$

$$\|\mathcal{B}(t,\cdot,y)\|_{L^1(\Omega)} \le C_\Omega, \tag{5c}$$

and gradient estimates hold too:

$$\|\nabla_x \mathcal{G}(t,\cdot,y)\|_{L^1(\Omega)} \leq C_\Omega \max(1, t^{-3/4}), \tag{6a}$$

$$\left\|\nabla_x \widetilde{\mathcal{G}}(t,\cdot,y)\right\|_{L^1(\Omega)} \leq C_{\widetilde{\Omega}} \max(1, t^{-3/4}), \tag{6b}$$

$$\|\nabla_x \mathcal{B}(t,\cdot,y)\|_{L^1(\Omega)} \leq C_\Omega \max(1, t^{-3/4}). \tag{6c}$$

In addition due to the boundedness of Ω*, we also have*

$$\|\nabla_y \mathcal{G}(t,\cdot,y)\|_{L^1(\Omega)} \leq C_\Omega \max(1, t^{-3/4}), \tag{7a}$$

$$\left\|\nabla_y \widetilde{\mathcal{G}}(t,\cdot,y)\right\|_{L^1(\Omega)} \leq C_{\widetilde{\Omega}} \max(1, t^{-3/4}), \tag{7b}$$

$$\|\nabla_y \mathcal{B}(t,\cdot,y)\|_{L^1(\Omega)} \leq C_\Omega \max(1, t^{-3/4}). \tag{7c}$$

Proof. Obviously the diffusion coefficients d_1 and d_2, since they are strictly positive constants, do not play a crucial role, and can be supposed to be equal to 1, after an appropriate rescaling of the time variable t. Moreover it is sufficient to prove the above estimates for the heat kernel $\mathcal{G}$, since

$$\mathcal{B} = \mathrm{e}^{-\eta t}\mathcal{G}.$$

For $t \geq 1$, estimates (3.2)–(3.3) of [35] straightforwardly provide the result. Suppose that $0 < t \leq 1$. Estimates (5) easily come from Theorem 6.10 pp 171 of [29], since for any $x \in \Omega$,

$$0 \leq \frac{1}{\sqrt{t}} \int_\Omega \mathrm{e}^{-|x-y|^2/t}\, dy \leq 2\pi.$$

Estimates (6) are consequences of the section 6.6 entitled Weighted Gradient Estimates and in particular of Theorem 6.19 p 185 [29]. Actually by Cauchy-Schwarz inequality

$$\begin{aligned}
\|\nabla_x \mathcal{G}(t,\cdot,y)\|^2_{L^1(\Omega)} &\leq \int_\Omega |\nabla_x \mathcal{G}(t,\cdot,y)|^2\, \mathrm{e}^{2\beta|x-y|^2/t}\, dy \int_\Omega \mathrm{e}^{-2\beta|x-y|^2/t}\, dy \\
&\leq Ct^{-2}\mathrm{e}^{ct} \int_\Omega \mathrm{e}^{-2\beta|x-y|^2/t}\, dy, \\
&\leq 2\pi C t^{-3/2}\mathrm{e}^{ct} \leq Ct^{-3/2},
\end{aligned}$$

hence the estimates (6).

Now let $\phi \in L^\infty(\Omega)$, by estimates (6) and since the measure $|\Omega|$ of Ω is bounded we infer

$$\begin{aligned}
\int_\Omega |\phi(y)| \int_\Omega |\nabla_y \mathcal{G}(t,x,y)|\, dx\, dy &= \int_{\Omega\times\Omega} |\phi(y)|\, |\nabla_y \mathcal{G}(t,x,y)|\, dy\, dx, \\
&\leq \|\phi\|_{L^\infty(\Omega)} \int_\Omega \|\nabla_y \mathcal{G}(t,x,\cdot)\|_{L^1(\Omega)}\, dx, \\
&\leq |\Omega| C t^{-3/4} \|\phi\|_{L^\infty(\Omega)},
\end{aligned}$$

hence estimates (7), which ends the proof of the proposition. □

Remark 1. The above estimates are probably not optimal, since for the half-plane the heat kernel writes:

$$\mathcal{G}(t,x,y) = \frac{1}{4\pi t}\left(\mathrm{e}^{|x-y|^2/(4t)} + \mathrm{e}^{|x-y^c|^2/(4t)}\right), \quad \text{where } y^c = (y_1, -y_2),$$

and therefore the power $t^{-3/4}$ has to be replaced by $t^{-1/2}$ similarly to the heat kernel of the whole plane $\mathbb{R}^2$. However these results are sufficient to prove existence and uniqueness of the solution to problem (1).

Corollary 1. *In particular, for* $T > 0$*, and for any* $\phi \in L^\infty([0,T]; L^\infty(\Omega))$ *the solution to the following problem:*

$$\begin{cases} \partial_t u = \Delta u - \eta u + \phi(t,\cdot), & \text{in } \Omega, \\ \partial_{\mathbf{n}} u|_{\partial\Omega} = 0, \quad u|_{t=0} = 0, \end{cases} \tag{8}$$

satisfies almost everywhere in $(0,T)\times\Omega$*:*

$$|\nabla u(t,\cdot)| \le C_\Omega t^{1/4} \sup_{s\in(0,T)} \|\phi(s,\cdot)\|_{L^\infty(\Omega)}. \tag{9}$$

Proof. Since

$$u(t,\cdot) = \int_0^t \int_\Omega \mathcal{B}(t-s,\cdot,y)\phi(s,y)\,dy,$$

and thus

$$\begin{aligned}|\nabla u(t,x)| &\le \int_0^t \int_\Omega |\nabla_x \mathcal{B}(t-s,x,y)\phi(s,y)|\ dy,\\ &\le \sup_{s\in(0,T)} \|\phi(s,\cdot)\|_{L^\infty(\Omega)} \int_0^t \|\nabla_x \mathcal{B}(t-s,x,\cdot)\|_{L^1(\Omega)},\end{aligned}$$

inequality (9) holds. □

3.2. **Local existence.** Using the above appropriate kernels, we deduce that a weak solution to problem (1) writes:

$$\begin{aligned}u_1(t,x) &= \int_\Omega \mathcal{G}(t,x,y)u_1^0(y)\,dy - \lambda\int_0^t\int_{\widetilde\Omega} \widetilde{\mathcal{G}}(t-s,x,y)u_1(s,y)(1-u_2)(s,y)\,dy\,ds\\ &\quad + \int_0^t\int_\Omega u_1(s,y)\chi(u_1,v)(s,y)\nabla_y\mathcal{G}(t-s,x,y)\cdot\nabla v(s,y)\,dy\,ds,\end{aligned} \tag{10a}$$

$$u_2(t,x) = \int_{\widetilde\Omega} \widetilde{\mathcal{G}}(t,x,y)u_2^0(y)\,dy + \lambda\int_0^t\int_{\widetilde\Omega} \widetilde{\mathcal{G}}(t-s,x,y)u_1(s,y)(1-u_2)(s,y)\,dy\,ds, \tag{10b}$$

$$v(t,x) = \int_0^t\int_\Omega \mathcal{B}(t-s,x,y)\left(\gamma_1 u_1(s,y)+\gamma_2 u_2(s,y)\right)\,dy\,ds. \tag{10c}$$

In this paragraph we aim at proving a local-existence result.

3.2.1. *Definition of the appropriate functional space* $\mathcal{X}_M^T$. Let M be a strictly positive constant, and let $T>0$ that will be chosen later. We define the functional space $\mathcal{X}_M^T$ as

$$\mathcal{X}_M^T = \left\{\Lambda\in L^\infty\left([0,T];L^\infty(\Omega)\right)\ :\ \sup_{t\in[0,T]}\|\Lambda(t,\cdot)\|_{L^\infty(\Omega)}\le M\right\}.$$

Let $\mathcal{L}$ be the linear operator defined on $\mathcal{X}_M^T\times\mathcal{X}_M^T$ by

$$\mathcal{L}\ :\ (\nu_1,\nu_2)\mapsto \int_0^t\int_\Omega \mathcal{B}(t-s,\cdot,y)\left(\gamma_1\nu_1(s,y)+\gamma_2\nu_2(s,y)\right)\,dy\,ds.$$

Using estimates (5)–(6) we infer that for any $(\nu_1,\nu_2)\in\mathcal{X}_M^T\times\mathcal{X}_M^T$:

$$\begin{aligned}&\|\mathcal{L}(\nu_1,\nu_2)(t,\cdot)\|_{L^\infty(\Omega)} \le C_\Omega(\gamma_1+\gamma_2)M,\\ &\|\nabla\mathcal{L}(\nu_1,\nu_2)(t,\cdot)\|_{L^\infty(\Omega)} \le C_\Omega(\gamma_1+\gamma_2)Mt^{1/4}.\end{aligned} \tag{11}$$

Define now the operator $\mathcal{T}$ on $\mathcal{X}_M^T\times\mathcal{X}_M^T$ by

$$\mathcal{T}\ :\ (\nu_1,\nu_2)\mapsto\Big(\big(\mathcal{T}_1-\mathcal{T}_2\big)(\nu_1,\nu_2)\,,\,\mathcal{T}_2(\nu_1,\nu_2)\Big),$$

where $\mathcal{T}_1$ is the operator defined on $\mathcal{X}_M\times\mathcal{X}_M^T$ by

$$\mathcal{T}_1(\nu_1,\nu_2) = \int_0^t\int_\Omega \nu_1\chi\left(\nu_1,\mathcal{L}(\nu_1,\nu_2)\right)\nabla_y\mathcal{G}(t-s,\cdot,y)\cdot\nabla_y\mathcal{L}(\nu_1,\nu_2)\,dy\,ds,$$

and $\mathcal{T}_2$ is defined by

$$\mathcal{T}_2(\nu_1,\nu_2) = \lambda\int_0^t\int_{\widetilde\Omega}\widetilde{\mathcal{G}}(t-s,x,y)\nu_1(s,y)(1-\nu_2)(s,y)\,dy\,ds.$$

Remark 2. Proving that $\mathcal{T}$ is a contraction mapping from $\mathcal{X}_M^T \times \mathcal{X}_M^T$ onto itself for small enough time T will then ensure the local existence of the weak solution given by (10) to problem (1).

3.2.2. *Contraction mappings.*

Proposition 2. *The operator $\mathcal{T}$ is a contraction mapping from $\mathcal{X}_M^T \times \mathcal{X}_M^T$ onto itself for T small enough.*

Proof. The proof is based on the properties of the kernels $\mathcal{B}$, $\mathcal{G}$ and $\widetilde{\mathcal{G}}$ given by Proposition 1. Thanks to estimates (5) we deduce for any $(\nu_1, \nu_2) \in \mathcal{X}_M^T \times \mathcal{X}_M^T$:

$$\|\mathcal{T}_2(\nu_1, \nu_2)\|_{L^\infty(\widetilde{\Omega})} \leq C_\Omega \lambda M(1+M)T,$$

hence for T small enough $\mathcal{T}_2$ maps $\mathcal{X}_M^T \times \mathcal{X}_M^T$ onto $\mathcal{X}_M^T$. Moreover using inequality:

$$|\nu_1(1-\nu_2) - \mu_1(1-\mu_2)| \leq (1+|\nu_2|)|\nu_1 - \mu_1| + |\nu_2||\mu_1 - \mu_2|,$$

we infer for T small enough the operator $\mathcal{T}_2$ is a contraction mapping from $\mathcal{X}_M^T \times \mathcal{X}_M^T$ onto $\mathcal{X}_M^T$.

Prove now that $\mathcal{T}_1$ is a contraction mapping from $\mathcal{X}_M^T \times \mathcal{X}_M^T$ onto $\mathcal{X}_M^T$. First observe that for any $s \in \mathbb{R}$, $|s|/(1+|s|) \leq 1$ hence for any $\nu_1 \in \mathcal{X}_M^T$, for any $s \in \mathbb{R}$,

$$\|\chi_1(\nu_1, s)(t,\cdot)\|_{L^\infty(\Omega)} \leq \chi^0(1+M), \quad \text{for almost any } t \in (0,T),$$

hence for any $(\nu_1, \nu_2) \in \mathcal{X}_M^T \times \mathcal{X}_M^T$

$$\|\chi_1(\nu_1, \mathcal{L}(\nu_1, \nu_2))(t,\cdot)\|_{L^\infty(\Omega)} \leq \chi^0(1+M), \quad \text{for almost any } t \in (0,T),$$

and thanks to estimates (6)–(11)

$$|\mathcal{T}_1(\nu_1, \nu_2)(t,\cdot)| \leq C_\Omega\,(\gamma_1 + \gamma_2)\,\chi^0(1+M)M^2\sqrt{T}.$$

This implies that for T small enough $\mathcal{T}_1$ maps $\mathcal{X}_M^T \times \mathcal{X}_M^T$ onto $\mathcal{X}_M^T$. In addition observe that for two couples (ν_1, ν_2) and (μ_1, μ_2) belonging to $\mathcal{X}_M^T \times \mathcal{X}_M^T$ we have

$$\begin{aligned}
\mathcal{T}_1(\nu_1, \nu_2) - \mathcal{T}_1(\mu_1, \mu_2) = &\int_0^t \int_\Omega (\nu_1 - \mu_1)\chi^{\nu_1,\nu_2} \nabla_y \mathcal{G}(t-s,\cdot,y) \cdot \nabla_y \mathcal{L}(\nu_1, \nu_2)\, dy\, ds \\
&+ \int_0^t \int_\Omega \mu_1 \chi^{\nu_1,\nu_2} \nabla_y \mathcal{G}(t-s,\cdot,y) \cdot \nabla_y \mathcal{L}(\nu_1 - \mu_1, \nu_2 - \mu_2)\, dy\, ds \\
&+ \int_0^t \int_\Omega \mu_1 \left(\chi^{\nu_1,\nu_2} - \chi^{\mu_1,\mu_2}\right) \nabla_y \mathcal{G}(t-s,\cdot,y) \cdot \nabla_y \mathcal{L}(\mu_1, \mu_2)\, dy\, ds,
\end{aligned}$$

where to simplify notations we have denoted by χ^{ν_1,ν_2} the function

$$\chi^{\nu_1,\nu_2} = \chi(\nu_1, \mathcal{L}(\nu_1, \nu_2)),$$

and similarly for χ^{μ_1,μ_2}. According to estimates (6) and thanks to the definition of $\mathcal{L}$ we infer

$$\|\nabla_y \mathcal{L}(\nu_1 - \mu_1, \nu_2 - \mu_2)\| \leq C_\Omega(\gamma_1 + \gamma_2)t^{1/4}\left(\|\nu_1 - \mu_1\|_{L^\infty(\Omega)} + \|\nu_2 - \mu_2\|_{L^\infty(\Omega)}\right).$$

Moreover, observing that

$$\begin{aligned}
\chi^{\nu_1,\nu_2} - \chi^{\mu_1,\mu_2} = &\chi^0 \frac{\mathcal{L}(\nu_1, \nu_2)}{1 + |\mathcal{L}(\nu_1, \nu_2)|}\,(\mu_1 - \nu_1) \\
&+ \chi^0(1-\mu_1)\left(\frac{\mathcal{L}(\nu_1, \nu_2)}{1 + |\mathcal{L}(\nu_1, \nu_2)|} - \frac{\mathcal{L}(\mu_1, \mu_2)}{1 + |\mathcal{L}(\mu_1, \mu_2)|}\right),
\end{aligned}$$

we deduce from estimates (5)–(6)–(7) and (11) that there exists a constant $C > 0$ which depends on M, and on the parameters χ^0, γ_1, γ_2, λ such that

$$\|\mathcal{T}_1(\nu_1, \nu_2) - \mathcal{T}_1(\mu_1, \mu_2)\|_{L^\infty(\Omega)} \leq C\sqrt{T},$$

which ensures the strict contractility of $\mathcal{T}_1$ for T small enough, and therefore $\mathcal{T}$ is a strict contraction from $\mathcal{X}_M^T \times \mathcal{X}_M^T$ onto itself. □

The Picard fixed point theorem straightforwardly implies the following theorem of existence and uniqueness for small time.

Theorem 3.2. *Let $(u_1^0, u_2^0) \in L^\infty(\Omega)\times L^\infty(\widetilde{\Omega})$. Then for T small enough there exists a unique weak solution (u_1, u_2, v) to (1) such that*

$$(u_1, u_2, v) \in L^\infty\left([0,T]; L^\infty(\Omega)\right) \times L^\infty\Big([0,T]; L^\infty(\widetilde{\Omega})\Big) \times L^\infty\Big([0,T]; L^\infty(\Omega)\Big).$$

3.3. **Mass conservation and global existence.** We first observe that the total mass of cells is conserved.

Proposition 3. *Let $(u_1^0, u_2^0) \in L^\infty(\Omega) \times L^\infty(\widetilde{\Omega})$ and let T small enough so that a weak solution (10) to (1) exists. Then for any $t \in [0,T]$*

$$\int_\Omega u(t,x)\,dx = \int_\Omega (u_1 + \mathbb{1}_{\widetilde{\Omega}}\, u_2)(t,x)\,dx = \int_\Omega u_1^0\,dx + \int_{\widetilde{\Omega}} u_2^0\,dx$$

Proof. Actually integrating (1a) and (1b) respectively and summing the integrands imply, since $\partial_{\mathbf{n}} u_1|_{\partial\Omega}$, $\partial_{\mathbf{n}} u_2|_{\partial\widetilde{\Omega}}$ and $\partial_{\mathbf{n}} v|_{\partial\Omega}$ vanish

$$\partial_t \int_\Omega u(x)\,dx = \partial_t \int_\Omega (u_1(x) + u_2(x))\,dx = 0.$$

□

We now show that if u_1^0 and u_2^0 are positive and bounded by 1 then u_1 and u_2 stay positive and bounded by 1 on $[0,T]$.

Proposition 4. *Let $(u_1^0, u_2^0) \in L^\infty(\Omega) \times L^\infty(\widetilde{\Omega})$ and let T small enough so that a weak solution given by (10) to problem (1) exists. If (u_1^0, u_2^0) are such that*

$$0 \le u_1^0 \le 1, \quad 0 \le u_2^0 \le 1,$$

then for almost any $t \in [0,T]$

$$0 \le u_1(t,x) \le 1, \quad 0 \le u_2(t,x) \le 1.$$

In addition

$$0 \le v(t,x) \le \frac{1}{\eta}\left(\gamma_1 + \gamma_2\right), \quad \text{for } x \in \Omega.$$

Therefore the weak solution (10) exists for almost any $t \in (0, +\infty)$.

Proof. First observe that if u_1 is positive then since u_2^0 is positive the function u_2 is positive almost everywhere. Actually multiplying (1b) by $u_2^- = \max(0, -u_2)$ and integrating by parts implies

$$\frac{1}{2}\partial_t \|u_2^-(t,\cdot)\|^2_{L^2(\widetilde{\Omega})} = -d_2 \|\nabla u_2^-\|^2_{L^2(\widetilde{\Omega})} - \lambda \int_{\widetilde{\Omega}} u_1 u_2^- + \lambda u_1 (u_2^-)^2 \le \lambda M \|(u_2^-)^2\|_{L^2(\widetilde{\Omega}},$$

hence u_2^- equal zero by Gronwall's lemma. Similarly, if u_1 is positive, then since u_2 is therefore also positive we infer that v is positive by multiplying (1c) by v^- and integrating by parts.

Prove now that $u_1^- = \max(0, -u_1)$ vanishes too. Multiply (1a) by u_1^- and integrate by parts to obtain for almost any $t \in [0,T]$:

$$\begin{aligned}\frac{1}{2}\partial_t \|u_1^-(t,\cdot)\|^2_{L^2(\Omega)} &\le -d_1 \|\nabla u_1^-(t,\cdot)\|^2_{L^2(\Omega)} + \lambda(1+M)\|u_1^-(t,\cdot)\|^2_{L^2(\widetilde{\Omega})} \\ &\quad + \chi^0 \left| \int_\Omega u_1^- \frac{v}{1+|v|}(1-u_1^-)\nabla v \nabla u_1^-\,dx \right|.\end{aligned}$$

Moreover applying estimates (9) to v implies

$$\begin{aligned}\left| \int_\Omega u_1^-(1-(u_1+u_2))\nabla v \nabla u_1^-\,dx \right| &\le C_\Omega t^{1/4} \|\gamma_1 u_1(t,\cdot) + \gamma_2 \mathbb{1}_{\widetilde{\Omega}} u_2(t\cdot)\|_{L^\infty(\Omega)} \\ &\quad \times \int_\Omega u_1^-(t,x)|1-u_1^-|(t,x)\nabla u_1^-(t,x)\,dx, \\ &\le C_\Omega T^{1/4} M(\gamma_1+\gamma_2)(1+2M) \int_\Omega \left|u_1^-(t,x)\nabla u_1^-(t,x)\right|\,dx, \\ &\le \widetilde{C} T^{1/4}\left(\frac{1}{4\alpha}\|\nabla u_1^-\|^2_{L^2(\Omega)} + \alpha \|u_1^-\|^2_{L^2(\Omega)}\right),\end{aligned}$$

by Cauchy-Schwarz estimates and the well-known Peetre's inequality with $\alpha > 0$ large enough. Thus, since $|s|/(1+|s|) \leq 1$ for any $s \in \mathbb{R}$, we infer

$$\partial_t \|u_1^-(t,\cdot)\|^2_{L^2(\Omega)} \leq \alpha \widetilde{C} T^{1/4} \|u_1^-(t,\cdot)\|^2_{L^2(\Omega)}.$$

Gronwall's lemma implies therefore that

$$\|u_1^-(t,\cdot)\|^2_{L^2(\Omega)} = 0,$$

since $u_1^-(0,\cdot)$ equals zero.

Prove now that $u_2 \leq 1$. Let $U_2 = u_2 - 1$:

$$\partial_t U_2 = \Delta U_2 - \lambda u_1 U_2,$$

hence, multiplying by $U_2^+ = \max(0, U_2)$ the above equation and since $U_2^+(0,\cdot)$ equals 0, we infer that U_2 vanishes everywhere thanks to Gronwall's lemma, and therefore $u_2 \leq 1$.

Similarly let

$$U_1 = u_1 - 1.$$

Then U_1 satisfies

$$\partial_t U_1 = d_1 \Delta U_1 - \lambda \mathbb{1}_{\widetilde{\Omega}} (1-u_2)(U_1+1) + \chi^0 \nabla . \left((U_1+1) \frac{v}{1+|v|} U_1 \nabla v \right), \quad \text{in } \Omega. \tag{12}$$

Once again, multiply (12) by $U_1^+ = \max(U_1, 0)$ and integrate by parts to obtain

$$\begin{aligned} \frac{1}{2}\partial_t \left(\|U_1^+\|^2_{L^2(\Omega)} \right) &= -d_1 \|\nabla U_1^+\|^2_{L^2(\Omega)} - \lambda \int_{\widetilde{\Omega}} (1-u_2) U_1^+ (U_1^+ + 1)\, dx \\ &\quad - \chi^0 \int_\Omega (U_1^+ + 1) \frac{v}{1+|v|} U_1^+ \nabla v \cdot \nabla U_1^+ \, dx. \end{aligned}$$

Since $1 - u_2$ is positive and using Cauchy-Schwarz estimate and Peetre inequality for α large enough (as used above to prove that $u_1 \geq 0$) implies that

$$\partial_t \left(\|U_1^+\|^2_{L^2(\Omega)} \right) \leq \alpha\, C \|U_1^+\|^2_{L^2(\Omega)}.$$

Therefore Gronwall lemma implies that U_1^+ vanishes almost everywhere in $(0,T) \times \Omega$ hence $u_1 \leq 1$.

To obtain the positivity of v, first multiply (1c) by v^- and integrate by part to infer, since u_1 and u_2 are positive that:

$$\partial_t \|v^-\|^2_{L^2(\Omega)} \leq 0.$$

Then the function $V = v - \eta^{-1}(\gamma_1 + \gamma_2)$ satisfies

$$\partial_t V = \Delta V - \eta V + \gamma_1(u_1 - 1) + \gamma_2(u_2 - 1).$$

Since $\gamma_1(u_1-1) + \gamma_2(u_2-1) \leq 0$, we infer that V^+ identically vanishes after multiplication and integration by parts, hence

$$0 \leq v \leq \eta^{-1}(\gamma_1 + \gamma_2).$$

From the implicit representation integral of u_1 and u_2 we deduce easily that if T_M is the maximal time of existence, then there exists a sequence $(t_n)_{n\in\mathbb{N}}$ tending to T_M, with $t_n < T_M$ such that

$$\lim_{n \to +\infty} \|u_1(t_n,\cdot)\|_{L^\infty} = +\infty,$$

hence u_1 and u_2 exists for almost any $t \in (0, +\infty)$ by contraposition. □

Theorem 2.1 is an easy consequence of the above results.

The following result is a straightforward consequence of proposition 4. It ensures that the mass of the cells tends to concentrate on the micropatterns.

Corollary 2. *Let* $(u_1^0, u_2^0) \in L^\infty(\Omega) \times L^\infty(\widetilde{\Omega})$ *such that*

$$0 \leq u_1^0 \leq 1, \quad 0 \leq u_2^0 \leq 1,$$

and let (u_1, u_2) *the weak solution to problem* (1). *Then*

$$0 \leq \int_\Omega u_1(t,x)\,dx \leq \int_\Omega u_1(0,x)\,dx,$$
$$\int_{\widetilde{\Omega}} u_2(0,x)\,dx \leq \int_{\widetilde{\Omega}} u_2(t,x)\,dx \leq |\widetilde{\Omega}|.$$

4. **Numerical results.** We now describe the numerical schemes that are used to compute problem (1), and then we show the simulations that corroborate the experimental results.

4.1. **Approximation of the problem.** We consider a cartesian mesh (composed by quadrilaterals). We discretize the model using the finite volume method [9] and we use an implicit Crank-Nicolson scheme for the time discretization. We solve the model using a decoupled approach [15]. In particular, the first equation is split into advection and diffusion parts. Let us recall the expression of this equation :

$$\partial_t u_1 = d_1 \Delta u_1 - \lambda \mathbb{1}_{\widetilde{\Omega}} u_1(1-u_2) - \nabla.\left(\chi(u_1,v) u_1 \nabla v\right) \text{ in } \Omega. \tag{13}$$

To simplify the notations we define A and B as:

$$A(u_1,u_2) = d_1\Delta u_1 - \lambda \mathbb{1}_{\widetilde{\Omega}} u_1(1-u_2), \quad \text{and} \quad B(u_1,v) = \nabla.\left(\chi(u_1,v)u_1\nabla v\right).$$

Let us denote the time step by Δt, set $t^n = n\Delta t$ and let (u_1^n, u_2^n, v^n) be the solution at the time t^n. At each time step we first solve the diffusive part :

$$\frac{\tilde{u}_1^{n+1} - u_1^n}{\Delta t} = \frac{1}{2}\left(A(\tilde{u}_1^{n+1}, u_2^{n+1}) + A(u_1^n, u_2^n)\right).$$

For all the diffusive terms, the spatial discretization is handled by a centered finite volume scheme, all the species being computed at the centre of each element of the mesh. We then solve the advection part :

$$\frac{u_1^{n+1} - \tilde{u}_1^{n+1}}{\Delta t} = \frac{1}{2}\left(B(u_1^{n+1}, v^{n+1}) + B(\tilde{u}_1^{n+1}, v^n)\right).$$

The high order WENO 5 (Weighted Essentially Non-Oscillatory) finite difference scheme introduced in [24] and improved in [19] has been used to handle the convective term. These solvers are implemented in the academic library eLYSe[1].

In the following the initial conditions write

$$u_1^0 = \mathbb{1}_{\Omega\setminus\widetilde{\Omega}}\, u^0, \quad u_2^0 = \mathbb{1}_{\widetilde{\Omega}}\, u^0, \tag{14}$$

where u^0 is a function of $x \in \Omega$. Hence the supports of u_1 and u_2 are disjoint at the initial time.

4.2. **Mathematical behavior of the model.** In this paragraph, we present the numerical results, that corroborate the mathematical results of the previous section. We want to check the properties of the model, when the maximal cell density on the adhesive area is reached. The domain Ω is the unit square $\Omega = [0,1]\times[0,1]$. The cartesian grid is composed by 100×100 quadrilaterals. The domain $\widetilde{\Omega}$ is the strip of width 0.08 located at the middle of Ω (cf Fig. 2).

At the initial time the cells are uniformly distributed meaning u^0 of (14) is constant. We consider two different values of u^0:

$$u^0 = \begin{cases} 0.08, \\ 0.25. \end{cases}$$

We plot the results along the axis $\{y = 0.5\}$ in order to have the profile of the distribution of u_1 and u_2. The densities u_1 along the axis at different time steps are given by Fig. 3 and the densities u_2 at the same time steps are given by Fig. 4.

When considering $u^0 = 0.08$, the maximal density on the adhesive area is never reached. We observe that u_1 is decreasing, while u_2 is increasing with respect to the time. In the second case, for $u^0 = 0.25$, the maximal density of u_2 is reached at $t = 0.3$ therefore after this time the cells u_1 cannot become u_2.

[1] http://www.math.u-bordeaux1.fr/~osaut/

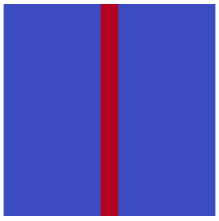

FIGURE 2. Geometry of the micropattern.

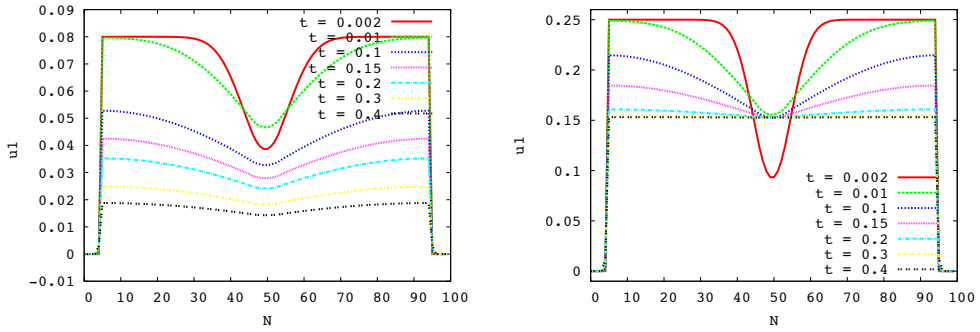

(a) Profiles of u_1 for $u^0 = 0.08$ (b) Profiles of u_1 for $u^0 = 0.25$

FIGURE 3. Profiles of $u_1(t, x, y = 0.5)$ at different time steps for two different initial conditions.

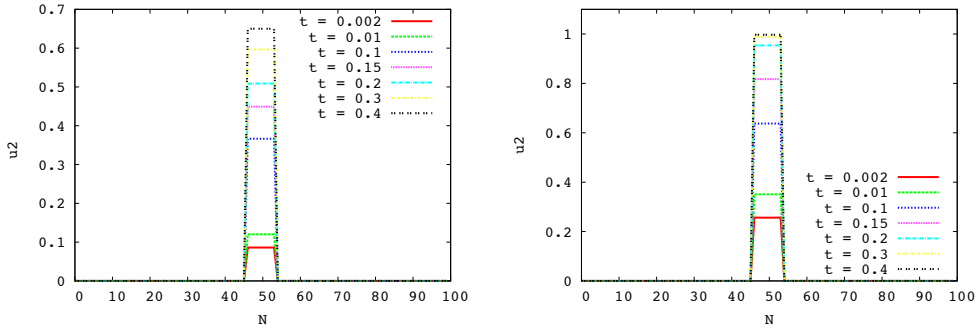

(a) Profiles of u_2 for $u^0 = 0.08$ (b) Profiles of u_2 for $u^0 = 0.25$

FIGURE 4. Behavior of $u_2(t, x, y = 0.5)$ at different time steps.

As expected, the migration stops. These simulations show that a minimum amount of endothelial cells is required at the initial time in order to reach the maximal concentration on the strips at the end of the experiment. If this initial concentration is too small the final density of endothelial cells is suboptimal.

4.3. **Behavior on realistic benchmarks.** We now provide simulations in realistic setups: throughout this subsection the initial data u^0 of (14) is a normal random distribution (between 0 and 1).

4.3.1. *Behavior on the thin strips.* We first consider a bioactive micropattern composed by six adhesive thin strips (in red on Fig.5(b)).

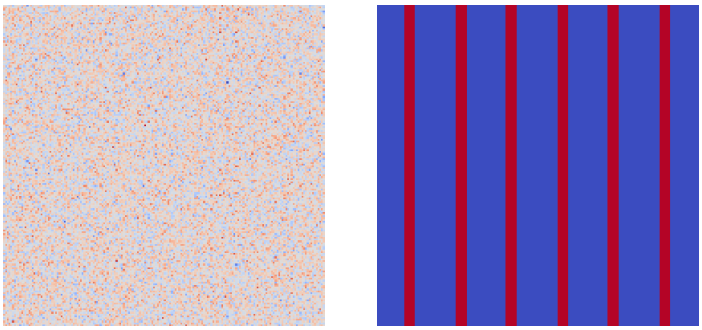

(a) The initial random distribution of endothelial cells

(b) The micropattern. Width strips = 0.05

FIGURE 5. Initial setup: endothelial cells (left) and adhesion substrate (right).

The simulation Fig. 6, represents the total density of endothelial cells ($u = u_1 + u_2$) at time $t = 0.3$ (in Fig 6(a)) and 1.0 (in Fig 6(b)) obtained for the following set of parameters: $d_1 = d_2 = \chi^0 = \gamma_2 = 1, \gamma_1 = 0.5, \lambda = 100$.

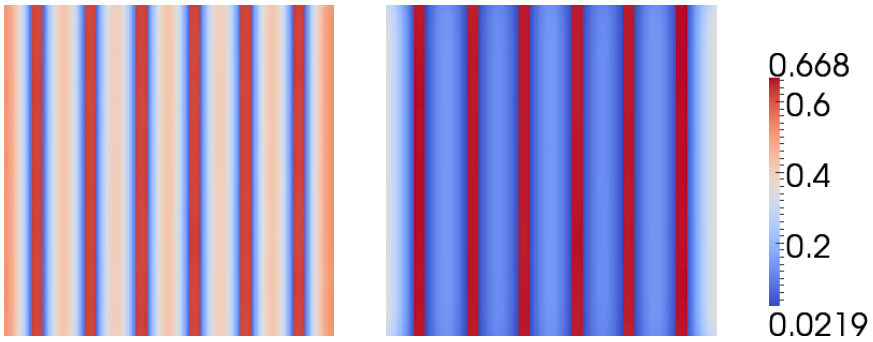

(a) t = 0.3

(b) t = 1.0

FIGURE 6. The total density of endothelial cells u at two different time steps.

Fig. 7 shows the behavior of v for the same set of parameters.

The numerical results are in good agreement with the expected evolutions. Indeed, the cell density u_2 on the adhesive areas increases with the time variable, whereas outside u_1 becomes very small. Cells are stucked on the strips and stop moving once they are over them. As a consequence the density of the attractant on the strips also increases.

4.3.2. *Behavior on large strips.* We now consider a domain $\Omega = [0, 1] \times [0, 1]$ composed by two large strips of length 0.2. The geometry is presented in Fig.8(b)

In Fig. 9, we present the total density of endothelial cells ($u = u_1 + u_2$) at times 0.3 (in Fig. 9(a)) and 1.0 (in Fig. 9(b)) obtained for the choice of parameters : $d_1 = d_2 = \chi^0 = \gamma_2 = 1, \gamma_1 = 0.5, \lambda = 100$.

In Fig. 10, we present the behavior of the chemoattractant v for the same set of parameters at the times $t = 0.3$ and $t = 0.6$.

As previously we observe a behavior in good agreement with the experiments. When considering two large adhesive areas the velocity of the migration is smaller than for a large number of thin strips. Indeed at the time step $t = 1.0$ we observe that with thin strips the migration seems to be more advanced than in

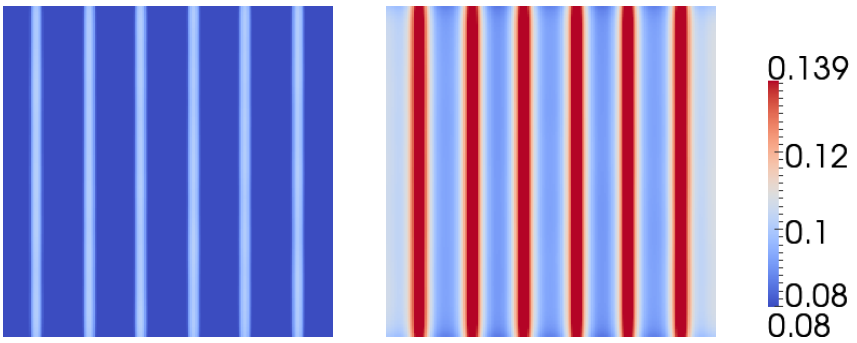

(a) t = 0.3 (b) t = 0.6

FIGURE 7. The density v at two different time steps.

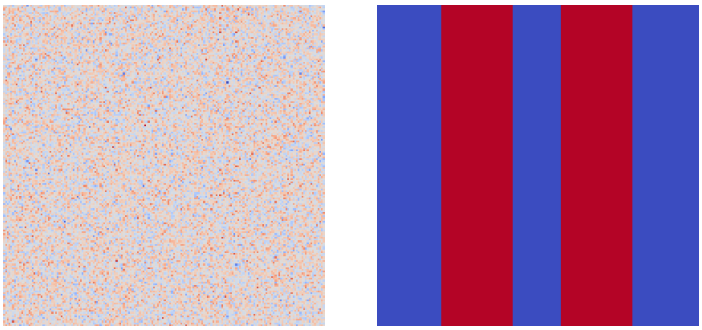

(a) The initial random distribution of endothelial cells

(b) The micropattern. Width strip = 0.2

FIGURE 8. Initial setup: endothelial cells (left) and patterns (right).

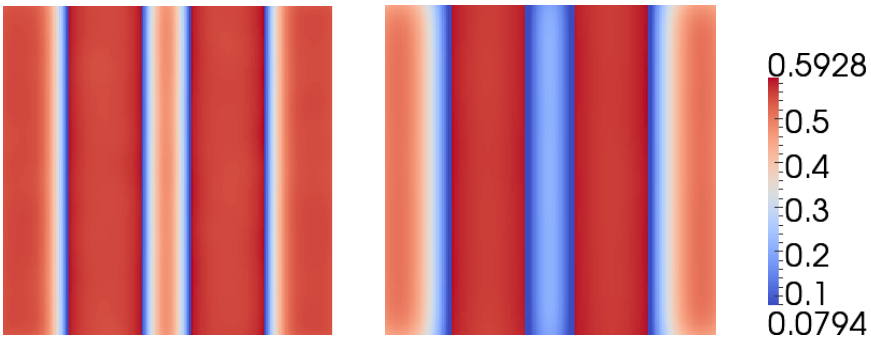

(a) t = 0.3 (b) t = 1.0

FIGURE 9. The density of endothelial cells u at two different time steps.

the case with large strips. This could be explained by the fact that some cells are far away from a strip and their migration toward the strips takes more time.

4.3.3. *Influence of the number of strips on the migration.* We want to study the influence of the pattern spacing on the cell migration.We set the surface of the adhesive domain, and let the number of strips, N_s, vary. The average of u_2 in term of the time for $N_s = 1$, 2, and 4 is presented in Fig. 11 .

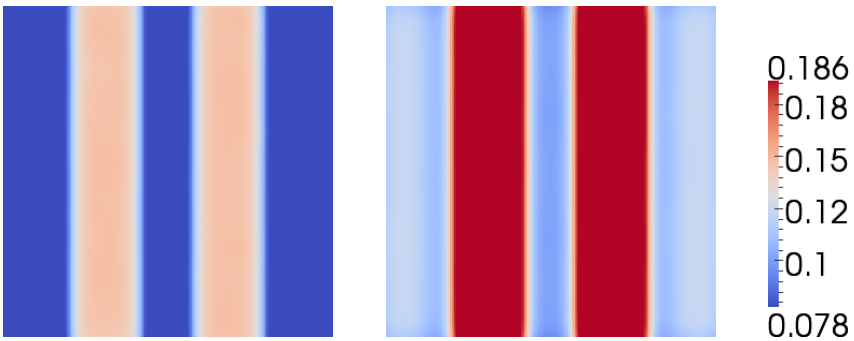

(a) t = 0.3 (b) t = 0.6

FIGURE 10. The density of the signal v at two different time steps.

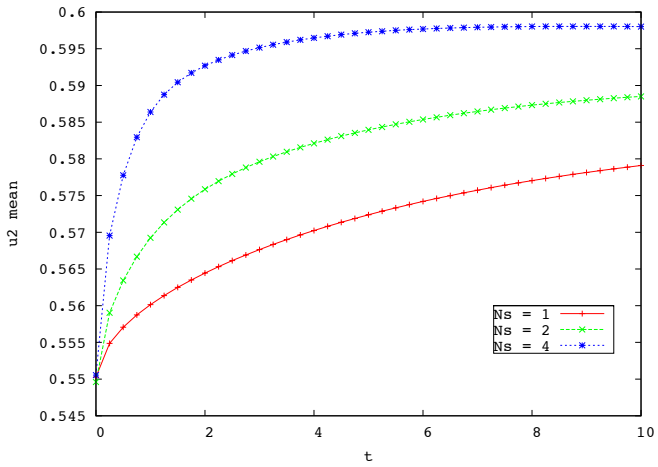

FIGURE 11. The average of the density u_2 with respect to the time for different number of strips.

We observe that when considering four strips the migration is quicker. Moreover the mean density reached is higher, which corroborates the experiments.

5. **Conclusion.** In this paper a macroscopic model describing the endothelial cell migration on bioactive micropatterns is presented. Its major biological assumption is that the cells produce a chimical subtance so as to gather, but the bioactive chemical substance does not diffuse any chemoattractant: it just sticks the cells located on it.

Mathematically, mass conservation, global existence and uniqueness results are shown. Numerically, the model behaves in good agreement with the biological experiments. Despite the lack of direct attraction of the bioactive patterns, the non-washed out endothelial cells end up on the patterns since the cells stuck on the micropattern produce more chemoattractant than the cells outside the bioactive material. We have observed two facts that have been reported by the experiments:

1. For a given surface of bioactive material, the process of cell migration is more efficient with a large number of thin strips than with a small number of large strips.
2. There exists a minimum value of the initial density of endothelial cells to be imposed in order to have an optimal cell migration towards the bioactive pattern.

We therefore believe that this model is a first step towards better understanding of cell migration on micropatterns, the long-term goal being optimal designing of patterns in order to build biological tissues.

REFERENCES

[1] A. Anderson and M. Chaplain. Continuous and discrete mathematical models of tumor-induced angiogenesis. Bulletin of Mathematical Biology, 60(5) : 857–899, 1998.

[2] K. Anselme, P. Davidson, A.M. Popa, M. Giazzon, M. Liley, L. Ploux, The interaction of cells and bacteria with surfaces structured at the nanometre scale, Acta Biomaterialia, 6: 3824–3846, 2010

[3] P. Biler and T. Nadzieja. Existence and nonexistence of solutions for a model of gravitational interaction of particles. I. Colloq. Math. 66 : 319–334, 1993.

[4] A. Blanchet, J. Dolbeault and B. Perthame. Two dimensional Keller–Segel model : optimal critical mass and qualitative properties of the solution. Electron. J. Differential Equations, 44 : 1–33, 2006.

[5] P. Carmeliet and M. Tessier–Lavigne, Common mechanisms of nerve and blood vessel wiring. Nature, 436 : 193–200, 2005

[6] C.S Chen, M. Mrksich, S. Huang, G.M. Whitesides and D.E. Ingber, Geometric control of cell life and death. Science 276(5317):1425–1428, 1997.

[7] L.E. Dike, C.S. Chen, M. Mrksich, J. Tien, G.M. Whitesides, D.E. Ingber, Geometric control of switching between growth, apoptosis, and differentiation during angiogenesis using micropatterned substr'ates. In Vitro Cell. Dev. Biol., 35 : 441–448, 1999.

[8] J. Dolbeault and B. Perthame. Optimal critical mass in the two dimensional Keller-Segel model in $\mathbb{R}^2$. C. R. Math. Acad. Sci. Paris, 339(9) : 611–616, 2004.

[9] R. Eymard, T. Gallouet, R. Herbin, *Finite Volume Methods*, Handbook of Numerical Analysis, P.G Ciarlet, J.L Lions eds, 2007.

[10] A. Folch, M. Toner, Microengineering of cellular interactions. Annu. Rev. Biomed. Eng., 2:227–256, 2000.

[11] J. Folkman and C. Haudenschild . Angiogenesis *in vitro*. Nature, 288 : 551–6, 1980.

[12] H. Gajewski and K. Zacharias, Global behavior of a reaction-diffusion system modelling chemotaxis. Math. Nachr., 195(1) : 77–114, 1998.

[13] T. Hillen and K.J. Painter, A user's guide to PDE models for chemotaxis. J. Math. Biol, 58(1–2) : 183–217, 2008.

[14] D. Horstmann, The nonsymmetric case of the Keller-Segel model in chemotaxis: some recent results. Nonlinear differ. equ. appl. 8(4) : 399–423, 2001.

[15] W. Hundsdorfer and J.G. Verwer, *Numerical solution of time-dependent advection-diffusion-reaction equations*. Springer Series in Comput. Math. 33, Springer, 2003.

[16] Y. Ito, Surface micropatterning to regulate cell functions. Biomaterials, 20:(23/24) 2333–2342, 1999

[17] R.K. Jain, Molecular regulation of vessel maturation. Nat Med, 9:685–93, 2003.

[18] R.K. Jain, P. Au, J. Tam, D.G. Duda, D. Fukumura, Engineering vascularized tissue. Nat Biotechnol, 23 : 821–3, 2005

[19] G.S. Jiang and C.W Shu, Efficient implementation of weighted ENO schemes, J. of Computational Physics, 126 : 202–228, 1996.

[20] M. Kamei, W.B. Saunders, K.J. Bayless, L. Dye, G.E. Davis and B.M. Weinstein, Endothelial tubes assemble from intracellular vacuoles *in vivo*, Nature 442 : 453–456, 2006.

[21] E.F. Keller, L.A. Segel, Traveling band of chemotactic bacteria: a theoretical analysis, Journal of Theo. Biol., 30(2) : 235–248, 1971.

[22] Y. Lei, M. Rémy, O. Zouani, C. Chollet; L. Ramy, C. Chanseau, and M.C. Durrieu, Micropatterning of polyethylene terephthalate with RGD peptides for induction of endothelial cell alignment and morphogenesis, Biomaterials, submitted.

[23] Y. Lei, O. Zouani, M .Remy, C. Ayela, M.C. Durrieu, Mimicking angiogenesis by SVVYGLR peptide micropatterning, Biomaterials, submitted 2012

[24] X.D. Liu, S. Osher, and T. Chan. Weighted essentially non-oscillatory schemes. Journal of Computational Physics, 115(1):200–212, 1994.

[25] B. Lubarsky and M.A. Krasnow. Tube morphogenesis: making and shaping biological tubes. Cell 112 : 19–28, 2003.

[26] R.M. Nerem Tissue engineering: the hope, the hype, and the future. Tissue Eng 12 : 1143–50, 2006.

[27] D.V. Nicolau, T. Taguchi, H. Taniguchi, H. Tanigawa and S. Yoshikawa, Patterning neuronal and glia cells on light-assisted functionalized photoresists. Biosens. Bioelectron, 14(3): 317–325, 1999.

[28] Z.K. Otrock, R.A. Mahfouz, J.A. Makarem and A.I. Shamseddine. Understanding the biology of angiogenesis: review of the most important molecular mechanisms. Blood Cells Mol Dis, 39 : 212–20, 2007.

[29] E.M Ouhabaz. Analysis of heat equations on domains. London Math. Soc. Monographs Series, Princeton University Press. 31, 2005.

[30] C.S. Patlak, Random walk with persistence and external bias, Bull. Math. Biophys., 15 : 311–338, 1953.

[31] E.A. Phelps and A.J.Garcia, Engineering more than a cell: vascularization strategies in tissue engineering. Curr Opin Biotechnol, 21 : 704–709, 2010.

[32] M.I. Santos and R.L. Reis. Vascularization in bone tissue engineering: physiology, current strategies, major hurdles and future challenges. Macromol Biosci, 10 : 12–27, 2010.

[33] T. Senba and T. Suzuki, Chemotactic collapse in a parabolic-elliptic system of mathematical biology. Adv. Differential Equations 6 : 21–50, 2001.

[34] Y. Y. Li and M. S. Vogelius, Gradient Estimates for Solutions to Divergence Form Elliptic Equations with Discontinuous Coefficients. Arch. Rational Mech. Anal., 153:91–151, 2000.

[35] F.Y Wang and L.Yan, Gradient Estimate on Convex Domains and Application. To appear in AMS. Proc., 2012. (avalaible on arxiv: http://arxiv.org/abs/1009.1965v2)

Discussion

Angiogenesis, the formation of new blood vessels, is essential for the development of vascularized tissues. However, the mechanism of the angiogenesis process is still not clearly, the details of conditions which govern angiogenesis are to be delineated. In this thesis, we focused on the mechanism understanding of angiogenesis from different aspects: geometrical factors of peptides, effects of different peptide motifs, and density of peptides, etc...

The geometrical cues on lumen formation

As discussed in Paper II and III, the geometrical cues of peptide micropatterns are predominant during the process of tubulogenesis. EC tubular structures were formed due to the sizes of peptide micropatterns.

The smaller peptide micropatterns (10-50 μm) significantly more regulated EC orientation and migration, and induced EC morphogenesis into tube formation (either RGD or SVVYGLR peptides). Larger peptide micropatters (100 μm) facilitated EC adhesion and spreading but without lumen formation (Figure 28).

The significant EC responses on smaller micropatterns are important for the remodeling of extracellular matrix, promoting a significant cascade of events resulting in changes in cytoskeletal rearrangement and migration of cells which lead to the assembly of new vessels [87, 224]. These restricted geometries send angiogenic cues to ECs and stimulate reorganization of the EC bodies into tubular structures.

To understand the mechanism of tubulogenesis, we quantified the cell-ECM adhesions by analyzing of focal adhesions (FAs) of ECs on different substrates. We found that both FA number and size per cell were reduced on smaller patterns (10 or 50 μm) as compared with ECs on 100 μm or on unpatterned surfaces (Paper III). This revealed that the cell-substrate adhesions decreased on smaller patterns. These phenomena were reminiscent of cell release from firm contact with the substrates, which is ultimately responsible for promoting the tubulogenesis program. On larger patterns, the cells had strong FAs with substrates, which consequently disturbed the process of tubulogenesis of ECs.

Furthermore, we observed that adherens junctions (AJs) were smaller but more concentrated on smaller peptide micropatterns (Paper III). AJ size and maturation are

regulated by geometrical constraints and mechanically influence the ECs cultured on the smaller peptide stripes to form tube-like structures.

We demonstrated that lumen formation is due to micro-geometrical constraints, which affect both cell-substrate adhesion and cell-cell adhesion by modulating status of FAs and the correct maturation of AJs, respectively.

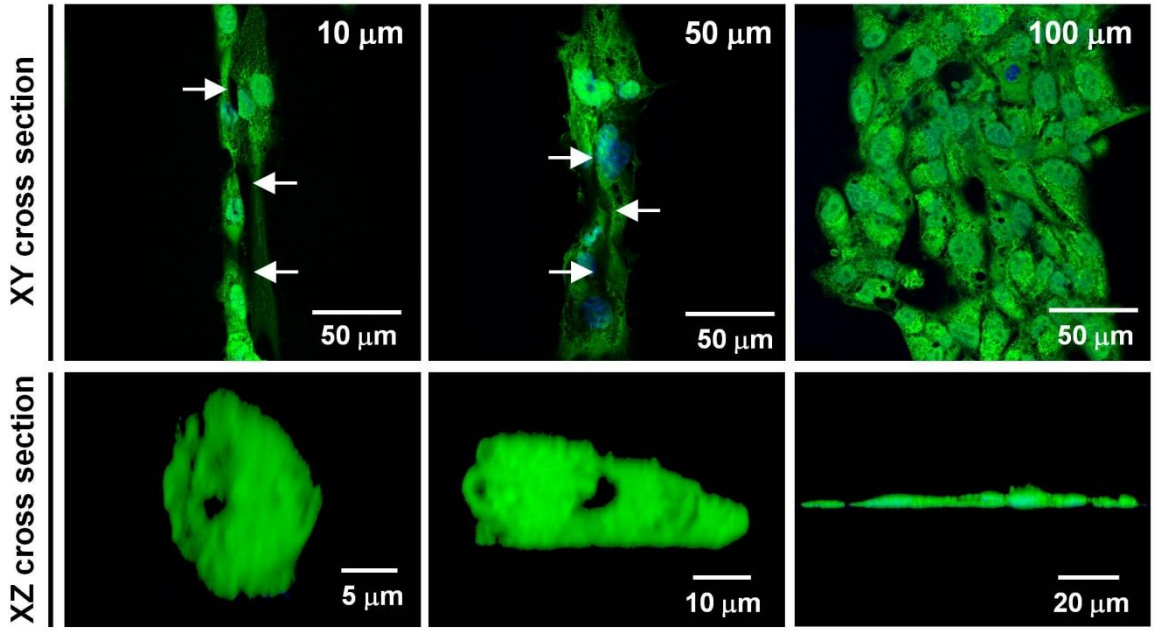

Figure 28. EC tube formation is dependent on geometrical cues of peptide micropatterns. ECs seeded on (A) 10 μm and (B) 50 μm SVVYGLR peptide stripes underwent morphogenesis into lumen formation with a central cavity. (C) ECs on 100 μm SVVYGLR stripes remained spread and did not form tubes.

The peptide motifs on lumen formation

Previous results suggest that geometrical factors are sufficient to switch ECs into a tubular differentiation program. At this stage, we may wonder are there only geometrical cues which regulate the tubulogenesis of ECs?

Therefore, we addressed the correlation between EC actin machinery expression and EC self-assembly into lumen formation (Paper II). Adhesion molecule (RGD peptides) and inductor molecule (BMP-2 mimetic peptides) are micropatterned onto PET surfaces to induce filopodial and lamellipodial migration mode of ECs, respectively. No lumen formation has been detected in the microenvironment promoting lamellipodial migration mode of ECs, whatever the geometrical distribution of BMP-2 peptide micropatterns. We demonstrated that only filopodial migration mode (mimicked by RGD) but not lamellipodial migration mode (mimicked by BMP-2) promotes EC lumen formation (Figure 29). We also investigated that the engagement of integrins (filopodial migration mode) stimulated the process of lumen formation. However, the lamellipodial machinery (induced by BMP-2) promotes softening of ECs, in turn inhibits the formation of lumen (Paper II).

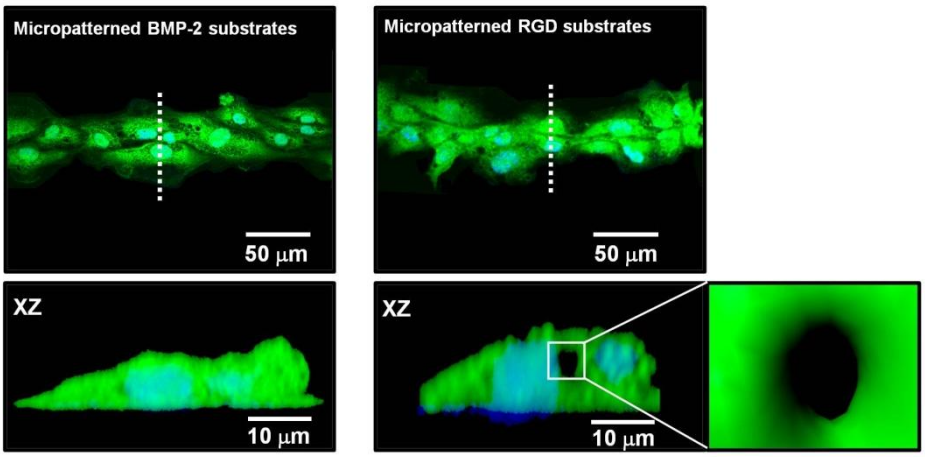

Figure 29. Lumen formation is dependent on the peptide motifs: BMP-2 mimetic peptides mimicked lamellipodial migration mode of ECs but cannot induce tubular structures; whereas RGD adhesion peptides induced filopodial migration mode of ECs and promoted lumen formation.

Moreover, we proved that the sprouting process of angiogenesis is dependent on peptide motifs (Figure 30). Sprouting of ECs and vascular network formation were induced on surfaces micropatterned with SVVYGLR peptides, but not with RGD peptides (Figure 30).

SVVYGLR sequence was reported to be the strongest angiogenic peptide, and it was reported to possess much stronger angiogenic activity than VEGF [174, 176]. This peptide might be expected to stimulate angiogenesis in scientific research because of its advantages. In this study, according to microfeature cues, ECs coalesced to form tube-like structures along the length of peptide micropatterns, either with RGD or SVVYGLR peptides. However, only in the case of SVVYGLR micropatterns, the adjacent SVVYGLR peptide stripes served as angiogenic cues to each other and triggered the ECs to sprout from pre-formed tubular structures (Figure 30B). EC tube formation on the SVVYGLR peptide patterns played the role of pre-existing vessels, from which ECs sprouted and formed connections between the adjacent patterns. The sprouting occurred in parallel to form a vascular network (Figure 30B).

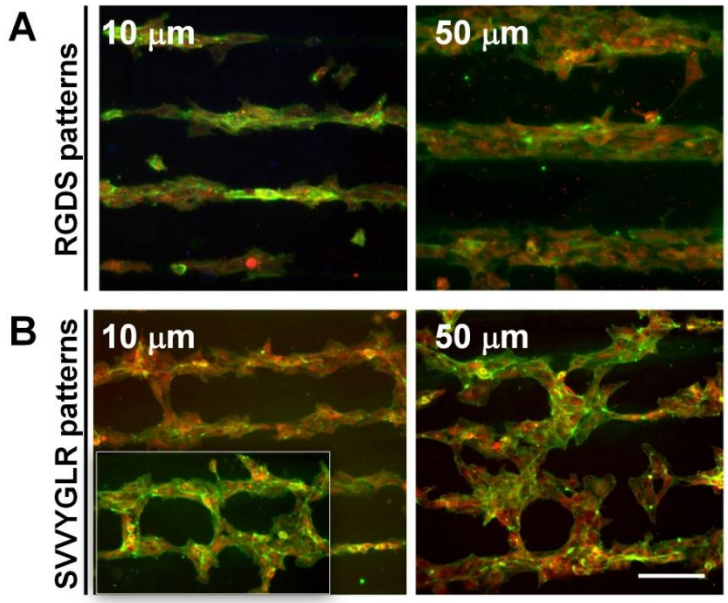

Figure 30. Sprouting of endothelial cells and vascular network formation are dependent on peptide motifs. ECs on surfaces micropatterned with (A) RGDS and (B) SVVYGLR peptides. Scale bar is 100 μm.

The peptide density onto EC morphogenesis

In previous results of our group, RGD peptide density on the surface is shown important to influence cell adhesion and focal contact formation for endothelial cells or osteoblast cells [159]. In this study, we continue to research with various peptide concentrations on micropatterned surfaces, in order to examine the effect of peptide concentration onto EC angiogensis.

The surfaces with 50 μm SVVYGLR peptide micropatterns were prepared, with the concentrations of the peptide solution varied from 10^{-5} M, 10^{-4} M, 10^{-3} M to 10^{-2} M. The results of EC alignment after 24 h in culture were shown in Figure 31 (Paper IV). In the case of lower concentrations (10^{-5} M and 10^{-4} M), few cells adhered and aligned onto the peptide micropatterns. ECs seeded on micropatterned surfaces at 10^{-3} M aligned and underwent morphogenesis on the peptide stripes. Oppositely, ECs cultured on stripes with higher concentration at 10^{-2} M adhered and spread on the micropatterned substrates (Paper IV).

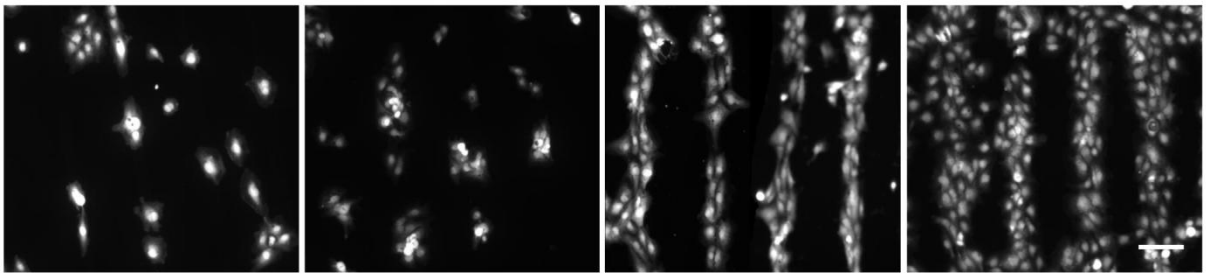

Figure 31. The effects of peptide concentration onto EC morphogenesis. EC culture for 24 h on surfaces with 50 μm SVVYGLR peptide micropatterns, the concentration of peptide solution was varied from 10^{-5} M, 10^{-4} M, 10^{-3} M to 10^{-2} M. Scale bar is 100 μm. ([227])

There have been several studies examined the effect of ligand concentration on angiogenesis. A seminal paper published in 1989 by Ingber and Folkman showed that modulating the density of the adhesive fibronectin could induce changes in EC shape and morphogenesis [86]. Capillary ECs were cultured on culture dishes which were precoated with varying concentrations of fibronectin. Cell spreading and growth were either stimulated or inhibited on highly adhesive (> 500 ng/cm^2) and nonadhesive (< 100 ng/cm^2) ECM substrate, respectively [86]. Interestingly, intermediate fibronectin coating densities (100–500 ng/cm^2) promoted formation of EC tube networks within 1–2 days [86]. Moon *et al.* also

manipulated EC tubulogenesis on hydrogels micropatterned with cell adhesive ligand (RGDS) in desired concentrations, and concluded that endothelial cord formation was stimulated on intermediate concentration of RGDS at 20 mg/cm^2 [95].

Deriving from these previous studies, this study also found the optimal concentration for cell adhesion ligands (10^{-3} M), at which EC morphogenesis can be promoted and guided in pre-designed geometries.

EC cord formation was promoted at intermediate concentration of peptides. A logical explanation for these results can be like this: the lower concentration of peptides are non-adhesive for ECs; the higher concentration of peptides promoted a strong adhesion of ECs with the substrate; however, intermediate concentration of peptides support a relatively reduced cell-substrate adhesions, the reduced adhesion is ultimately responsible for promoting the tubulogenic program.

3. Stabilization of Tubulogenesis by Co-culture of Cells

Paper V. Pericytes, stem cell-like cells, but not mesenchymal stem cells are recruited to support vasculogenic tube stabilization

Blood. 2012. In preparation

Co-culture of endothelial cells with pericytes/mesenchymal stem cells was developped to induce a stabilized and functional vascularization.

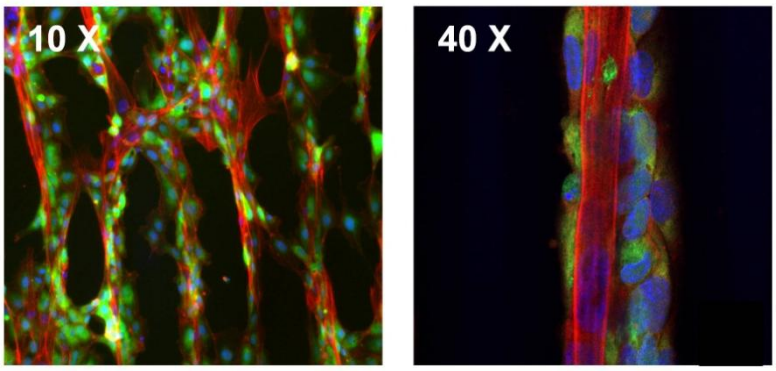

Figure 32. Interaction of endothelial cells (green) and pericytes (red) as the two types of cells were co-cultured on micropatterned surfaces.

Brief Reports

Pericytes, stem cell-like cells, but not mesenchymal stem cells are recruited to support vasculogenic tube stabilization

Yifeng Lei, Omar F. Zouani* and Marie-Christine Durrieu

Institut Européen de Chimie et Biologie (IECB), CNRS, UMR 5248, Université de Bordeaux I.
2, rue Robert Escarpit, 33607, Pessac, France.

***** Author for correspondence (*E-mail:* **omar.zouani@inserm.fr**)

ABSTRACT

During recent years, different studies report that a subpopulation of human perivascular cells expresses both pericyte and mesenchymal stem cell (MSC) markers *in situ*. In this communication, we report the essential role of these two cell populations in vasculogenic tube stabilization. We induce endothelial cell (EC) tubulogenesis after 24 hours incubation on polymer surfaces micropatterned with 50 µm SVVYGLR peptides. From 36 hours, these vasculogenic tubes lose tubular structures and endothelial cells proliferate rapidly to form a homogeneous monolayer of cells. To avoid this perturbation of vasculogenic tubes, we add different components to this initial system. First, at 24 hours incubation of ECs, pericytes or human MSCs (hMSCs) are added separately to the system. The results reveal that only pericytes have an affinity to ECs and stabilize the EC tubular structures. In a second step, at 24 hours incubation of ECs, two components mimicking basement membrane: type IV collagen or Matrigel are added to the initial system, respectively. Then, pericytes or hMSCs are directly added to the system. Only pericytes migrate through these mimetic basement membrane and support EC lumen structures.

Keywords: tubulogenesis, pericyte, mesenchymal stem cell, surface micropatterning

INTRODUCTION

Blood vessels are composed of two interacting cell types. Endothelial cells (ECs) form the inner lining of the vessel wall and perivascular cells, referred to as pericytes, vascular smooth muscle cells (vSMCs), or mural cells, envelop the surface of the vascular tubes[1]. Recent interesting studies suggest that there is a link between these perivascular cells (referred to pericytes) and multipotent stem cells and/or progenitor cells such as adult human mesenchymal stem cells (hMSCs)[2-4], white adipocyte progenitors[5,6], muscle stem cells[7], and even neural stem cells[8]. Otherwise, cultured pericytes were shown to differentiate *in vitro* into osteoblasts, adipocytes, chondrocytes, vSMCs and skeletal muscle[7,9-11].

Several molecular markers for pericytes are listed in different reviews[12], such as PDGFRβ (platelet-derived growth factor receptor-beta), desmin, NG2 (chondroitin sulfate proteoglycan 4), and α-SMA (alpha-smooth muscle actin). Human MSCs don't express these markers. However, pericytes sometimes express MSCs markers such as CD73, CD105, and CD90[2,12]. Moreover, the perivascular cells that express MSC markers are surrounding vasculogenic tubes[13,14]. Here, we want to distinguish the specific role of human pericytes and human MSCs in vasculogenic tube stabilization. We want to study whether hMSCs can play the vasculogenic tube stabilization function of pericytes.

RESULTS AND DISCUSSION

First, we created an *in vitro* experimental model. It consisted of micropatterned polymer surfaces with 50 µm stripes of angiogenic SVVYGLR peptides[15]. Micropatterns on polymer surfaces were fabricated by photolithographic techniques as previously reported[15]. Fluorescent peptides (GDSVVYGLRK-FITC) were immobilized onto polymer surfaces for visualization (Figure 1). Then, we seeded ECs onto this modified surfaces. After 4 h in culture, ECs began to align onto the SVVYGLR peptide micropatterns[15]. Fig. 2A (top) illustrated the EC alignment on micropatterned surfaces after 24 h in culture. The cell bodies were more elongated

on the peptide micropatterns as compared with unpatterned controls[15]. The ECs seeded on 50µm SVVYGLR peptide stripes underwent morphogenesis and formed capillary tube-like structures after 24 h in culture (Fig. 2A, middle and bottom). Confocal images of horizontal and vertical cross sections confirmed the existence of the central lumen, which appeared as a negatively stained central space extending along multiple cell lengths. From 36 h, vasculogenic tubes lost the tubular structures, and ECs proliferate rapidly to form a homogeneous monolayer of cells (Figure 2B, C, and D). This is an interesting experimental model which we can use to reveal if pericytes or hMSCs can stabilize the vasculogenic lumen.

Interestingly, direct co-cultures of ECs/pericytes but not ECs/hMSCs on glass coverslips show interactions between cells. In fact, hMSCs remain away from ECs (Figure 3A). Pericytes interact clearly with ECs to form vascular like structures. (Figure 3B).

Then, after 24 h incubation of ECs on micropatterned surfaces, we added pericytes or hMSCs for 16 h to our experimental model (Figure 4). Vasculogenic lumens are stabilized only with pericytes but not with hMSCs (Figure 4A, B). We also show that hMSCs did not affect EC proliferation (Figure 4C). On the other hand, pericytes can have different locations as shown in 3D reconstruction of confocal images in Figure 4D. The most visualized location is pericytes beneath ECs. In this *in vitro* 2D system, it reveals that pericytes are points of adhesion supporting vasculogenic lumen stabilization.

In order to further validate the distinct roles of pericytes and hMSCs, we added to our experimental model a mimicking basement membrane with type IV collagen (a major component of basement membrane[16]) (Figure 5A). Then, above this mimicking matrix, we added respective pericytes and hMSCs to the system. We show that only pericytes migrated through type IV collagen and interacted with ECs (Figure 5B, C). However, the vasculogenic tubes were not conserved. In fact, 3D reconstruction of confocal images shows the loss of lumen structures despite the presence of pericytes (Figure 5C). These results *in vitro* suggest that hMSCs did not interact with ECs as pericytes which were located near ECs.

To overcome the problem of the loss of vasculogenic lumen structure, we changed type IV collagen with Matrigel. This latter is known to induce vasculogenic lumen intensively[17]. Interestingly, vacuoles were observed after Matrigel addition to the experimental model (Figure 6A). In this case, we observed that only pericytes but not hMSCs migrated through the Matrigel to stabilize vasculogenic tubes (Figure 6B, C).

Our results suggest that hMSCs don't have affinity to ECs. However, pericytes are sensitive to EC status. Contrary to the results shown in the case of hMSCs, the migration of pericytes towards ECs is systematic regardless of their status.

CONCLUSIONS

In summary, we show that only pericytes, stem cell-like cells but not hMSCs have an affinity to ECs and stabilize the EC tubular structures. The presence of stem cell markers in pericytes can probably explain their roles. By demonstrating the multipotency of pericytes, they can play a greater role in bone and muscle tissue regeneration. In the future, the use of these cells in tissue engineering becomes critical.

EXPERIMENTAL

Fabrication and preparation of micropatterned surfaces

Micropatterns on polymer surfaces were fabricated by photolithographic techniques as previously developed[15]. Briefly, the surfaces of materials were coated with S1818 photoresist (Rohm and Haas, USA) and spun at 3000 rpm for 30 s to obtain a uniform photoresist layer with a thickness of approximately 2 µm. The surfaces were baked at 115 °C for 1 min for drying. The surfaces were then exposed to UV light (60 W) through a high-resolution Cr mask with predesigned pattern dimensions (Femto-St Sciences & Technologies, France) for 18 s. Subsequently the surfaces were developed in Microposit Developer solution (Rohm and Haas, USA) for 40 s to dissolve the exposed photoresist, resulting in the desired pattern on material surfaces. Subsequently, the GDSVVYGLR peptides (Genecust, France) were

functionalized onto the micropatterns by covalent immobilization as previously reported[15,18]. Finally, the photoresist surrounding the peptide micropatterns was removed by acetone, resulting in SVVYGLR peptide micropatterns on polymer surfaces.

Fluorescent peptides were employed to validate the peptide micropatterning according to Zouani et al.[19]. In this case, GDSVVYGLR peptides were covalently conjugated to FITC fluochromes via Lysine (named as "GDSVVYGLRK-FITC") (Genecust, France), and immobilized onto micropatterned polymer surfaces for observation with fluorescence microscopy (Leica DM5500B, Germany).

Cell culture

Human umbilical vein endothelial cells (HUVECs) and human pericytes were purchased from Promocell, France (C-12203 and C-12980, respectively). HUVECs are vWF positive, CD31 positive and smooth muscle alpha-actin (α-SMA) negative; pericytes are revealed to be CD146 positive. Human (Bone Marrow) Mesenchymal Stem Cells were obtained from LONZA, Switzland (PT-2501).

HUVECs were grown in HUVEC culture medium (IMDM (Invitrogen, France) supplemented with 20% (v/v) fetal bovine serum (FBS) (PAA, France) and 0.4% (v/v) EC growth supplement/heparin kit (Promocell))[15]. Pericytes were maintained in pericyte growth medium (Promocell). Human MSCs were cultured in Minimum Essential Medium (Alpha-MEM, GIBCO) supplemented with 10% (v/v) FBS and 1% penicillin/streptomycin (GIBCO)[20]. These cells were incubated in a humidified atmosphere containing 5% (v/v) CO_2 at 37 °C. The cells were subcultured using trypsin/EDTA. HUVECs at passages 3 to 5, pericytes at passages 4 to 5 and hMSCs at passage 2 were used for experiments.

Cell functions on micropatterned surfaces

In direct co-culture of HUVECs and pericytes, 25000 cells/cm^2 HUVECs and 25000 cells/cm^2 pericytes were mixed in EGM®-2 medium and seeded onto glass

coverslips at 37 °C and 5% CO_2 for 24 h. Same conditions were employed for direct co-culture of HUVECs with hMSCs.

Subsequent co-culture of cells was developed on micropatterned surfaces in this study. In the first case, 50000 cells/cm^2 HUVECs in EGM®-2 medium were seeded onto the micropatterned surfaces. After 24 h culture of ECs on the surfaces, medium was aspirated from the cells, and 50000 cells/cm^2 hMSCs or pericytes were added onto the surfaces and further cultured for 16 h, respectively. In another case, basement membrane components were used to mimic the physiological condition of EC tubulugenesis. After 24 h culture of ECs, medium on the surfaces was removed, and 500 µl of 4 °C Matrigel (1:4) (v/v) (BD Bioscience, France) or 500 µl of room temperature type IV collagen (Sigma, France) were added onto the surfaces and incubated for 1 h at 37 °C, respectively. Then the medium was removed, and 50000 cells/cm^2 hMSCs or pericytes in EGM®-2 medium were added to the surfaces and further cultured for 16 h.

In controlled condition, 50000 cells/cm^2 HUVECs were seeded on the micropatterned surfaces in EGM®-2 medium and incubated for 24 h, 36 h, 48 h and 72 h, respectively.

Immunohistochemistry and fluorescent microscopy

In some cases, HUVECs were labeled with cell tracker green (CMFDA, Invitrogen) before cell seeding onto materials. Pericytes and hMSCs were labeled with cell tracker red (CMTPX, Invitrogen) before cell seeding.

Immunofluorescence staining was also performed to visualize the cells in different conditions. After cell culture, the samples were fixed with 4% (w/v) paraformaldehyde (PFA), permeabilized with 0.5 % triton X-100 in PBS (v/v) and stained with primary and secondary antibodies. The primary antibodies used were: anti-smooth muscle α-actin (α-SMA, Sigma), anti-chondroitin sulfate proteoglycan (NG2, Millipore), anti-CD31 (R&D Systems), anti-von Willebrand Factor (Invitrogen). Cells were washed twice with PBS and incubated with Alexa Fluor® 568- or 488-conjugated secondary antibodies (Invitrogen). Cell nuclei were counterstained with

DAPI. Then the samples were mounted with ProLong® Gold antifade reagent (Invitrogen) for observation. Imaging was performed using confocal microscopy (Leica SP5, Germany), and Imaris 7.0 software was employed for three-dimentinal (3D) reconstructions of confocal images of cells on micropatterned surfaces

STATISTICS

All observations of morphology and proliferation were based on three populations for each condition, and experiments were performed in triplicates. Data were displayed as mean values ± standard deviation (SD). Statistical analysis was performed by one-way analysis of variance (ANOVA) (OriginPro 8, USA). *P*-values less than 0.05 were considered statistically significant.

ACKNOWLEDGMENTS

This work was supported by the "Région Aquitaine" and the "Agence Nationale pour la Recherche" (ANR).

AUTHORSHIP

Contributions: Y.L. performed the experiments, collected and analyzed the data. M.C.D. designed the experiments. O.F.Z. designed the experiments, analyzed the data and wrote the paper.

Conflict-of-interest disclosure: The authors state that they have no conflicts of interest.

REFERENCES

1. Bergers G, Song S. The role of pericytes in blood-vessel formation and maintenance. Neuro Oncol. 2005;7:452-464.
2. Crisan M, Yap S, Casteilla L, et al. A perivascular origin for mesenchymal stem cells in multiple human organs. Cell Stem Cell. 2008;3:301-313.
3. Davidoff MS, Middendorff R, Enikolopov G, Riethmacher D, Holstein AF, Muller D. Progenitor cells of the testosterone-producing Leydig cells revealed. J Cell Biol. 2004;167:935-944.
4. Feng J, Mantesso A, De Bari C, Nishiyama A, Sharpe PT. Dual origin of mesenchymal stem cells contributing to organ growth and repair. Proc Natl Acad Sci U S A. 2011;108:6503-6508.
5. Olson LE, Soriano P. PDGFRbeta signaling regulates mural cell plasticity and inhibits fat development. Dev Cell. 2011;20:815-826.
6. Tang W, Zeve D, Suh JM, et al. White fat progenitor cells reside in the adipose vasculature. Science. 2008;322:583-586.
7. Dellavalle A, Sampaolesi M, Tonlorenzi R, et al. Pericytes of human skeletal muscle are myogenic precursors distinct from satellite cells. Nat Cell Biol. 2007;9:255-267.
8. Dore-Duffy P, Katychev A, Wang X, Van Buren E. CNS microvascular pericytes exhibit multipotential stem cell activity. J Cereb Blood Flow Metab. 2006;26:613-624.
9. Collett G, Wood A, Alexander MY, et al. Receptor tyrosine kinase Axl modulates the osteogenic differentiation of pericytes. Circ Res. 2003;92:1123-1129.
10. Doherty MJ, Ashton BA, Walsh S, Beresford JN, Grant ME, Canfield AE. Vascular pericytes express osteogenic potential in vitro and in vivo. J Bone Miner Res. 1998;13:828-838.
11. Farrington-Rock C, Crofts NJ, Doherty MJ, Ashton BA, Griffin-Jones C, Canfield AE. Chondrogenic and adipogenic potential of microvascular pericytes. Circulation. 2004;110:2226-2232.
12. Armulik A, Genove G, Betsholtz C. Pericytes: developmental, physiological, and pathological perspectives, problems, and promises. Dev Cell. 2011;21:193-215.
13. Bianco P, Robey PG, Simmons PJ. Mesenchymal stem cells: revisiting history, concepts, and assays. Cell Stem Cell. 2008;2:313-319.
14. Caplan AI. All MSCs are pericytes? Cell Stem Cell. 2008;3:229-230.
15. Lei Y, Zouani OF, Rémy M, Ayela C, Durrieu M-C. Geometrical Microfeature Cues for Directing Tubulogenesis of Endothelial Cells. PLoS ONE. 2012;7:e41163.
16. Liotta LA, Tryggvason K, Garbisa S, Hart I, Foltz CM, Shafie S. Metastatic potential correlates with enzymatic degradation of basement membrane collagen. Nature. 1980;284:67-68.
17. Ponce ML. In vitro matrigel angiogenesis assays. Methods Mol Med. 2001;46:205-209.
18. Chollet C, Chanseau C, Remy M, et al. The effect of RGD density on osteoblast and endothelial cell behavior on RGD-grafted polyethylene terephthalate surfaces. Biomaterials. 2009;30:711-720.
19. Zouani OF, Chollet C, Guillotin B, Durrieu MC. Differentiation of pre-osteoblast cells on poly(ethylene terephthalate) grafted with RGD and/or BMPs mimetic peptides. Biomaterials. 2010;31:8245-8253.
20. Zouani OF, Chanseau C, Brouillaud B, et al. Altered nanofeature size dictates stem cell differentiation. Journal of Cell Science. 2012;125:1-8.

FIGURE AND FIGURE LEGENDS

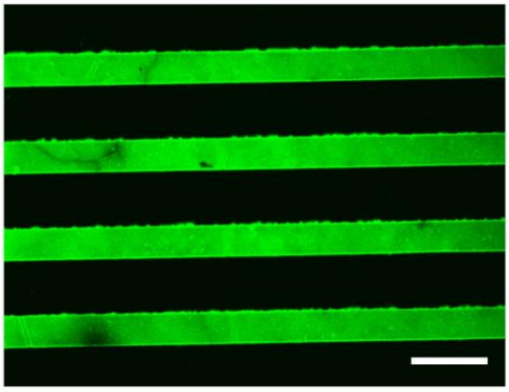

Figure 1. Fluorescent microscopy observation of polymer surfaces micropatterned with fluorescent peptides. The green lines correspond to 50 µm stripes of GDSVVYGLRK-FITC peptides with interspaces of 100 µm between them. Scale bar is 100 µm.

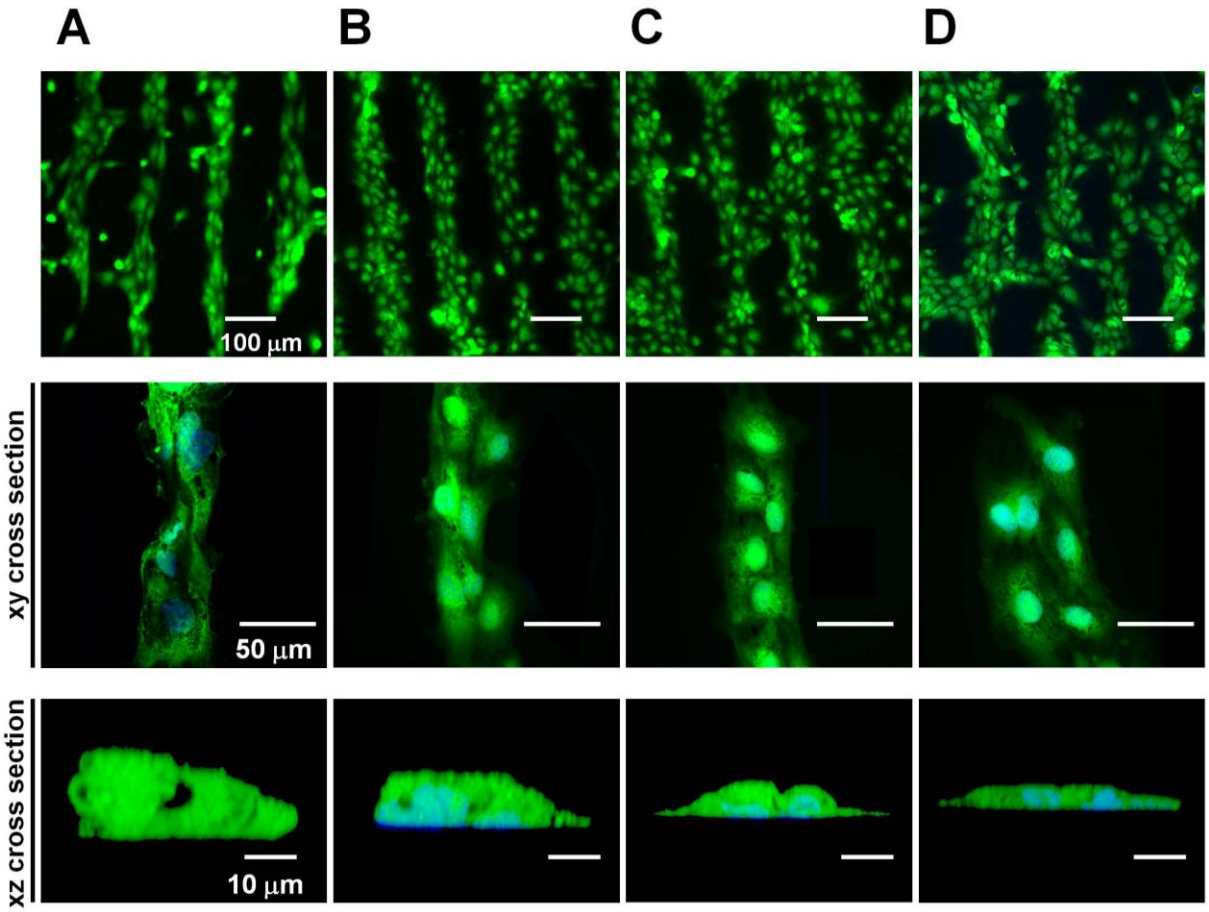

Figure 2. Confocal images of ECs seeded on 50 μm SVVYGLR peptide micropatterned surfaces for (A) 24 h, (B) 36h, (C) 48 h and (D) 72h. ECs formed tubular structure at 24 h of culture. However, after 36 h of culture, ECs lost their lumen structures and formed a monolayer of cells. Cell staining with Cell Tracker Green (CMFDA) and DAPI were represented in green and blue, respectively.

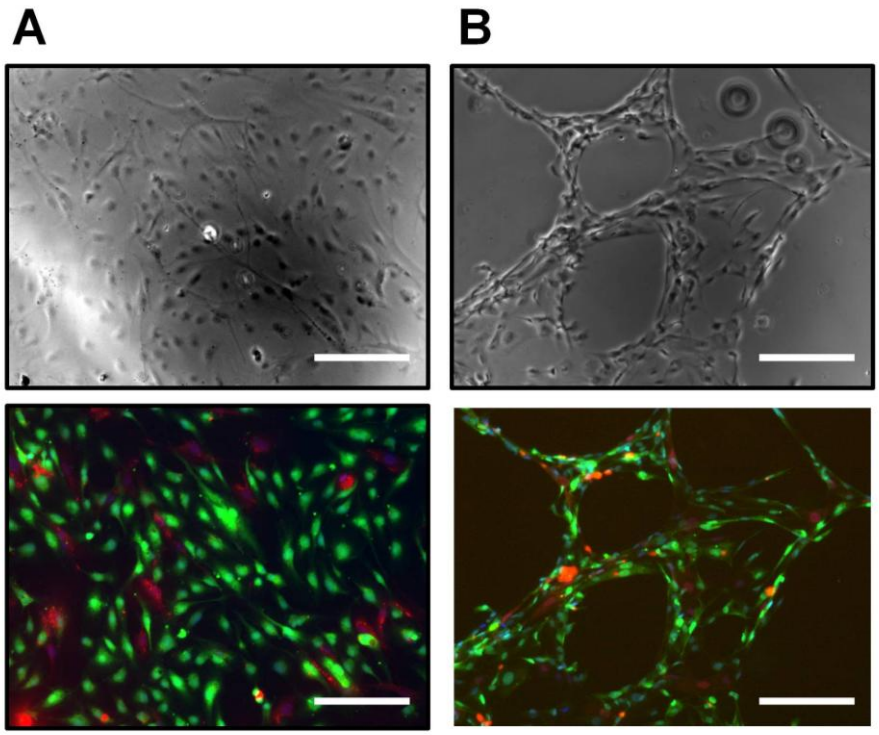

Figure 3. Direct co-culture of cells: (A) HUVECs with hMSCs and (B) HUVECs with pericytes on glass coverslips for 24 h. Top: Phase contrast image of cells. Down: fluorescence microscopy observation of cells, HUVECs were labeled with Cell Tracker Green (CMFDA), hMSCs and pericytes were both labeled with Cell Tracker Red (CMTPX), and cell nuclei were stained with DAPI. Scale bars are 200 µm.

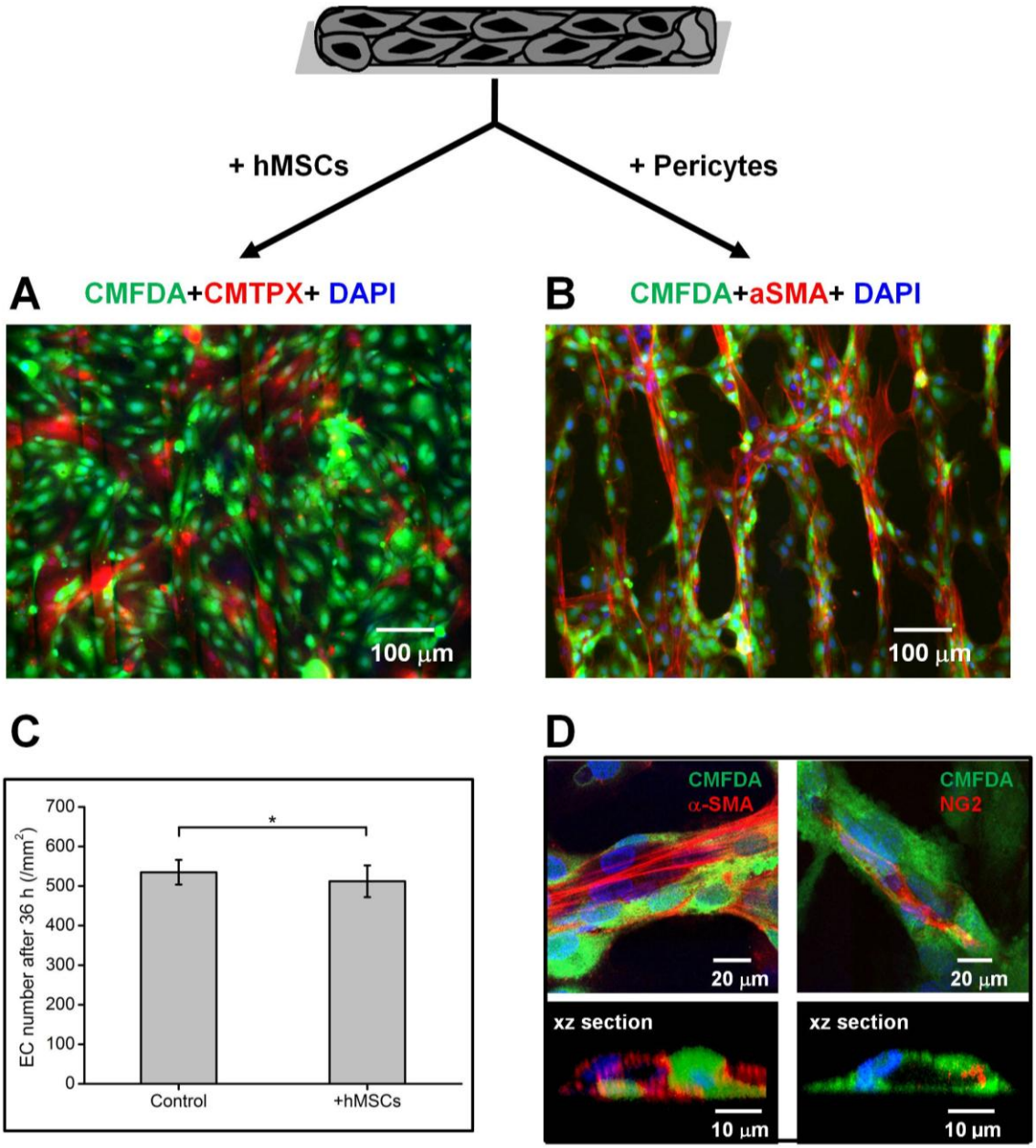

Figure 4. Subsequent co-cultures of cells. ECs were cultured for 24 h on micropatterned surfaces, followed by the addition of (A) hMSCs and (B) pericytes for 16 h to the initial system. (C) EC proliferation on Control (ECs seeded on peptide micropatterned surfaces for 36 h) and on co-culture system of ECs with hMSCs. * $P > 0.05$. (D) Confocal images of location of ECs (green) and pericytes (red) in the co-culture system of ECs with pericytes for 16 h.

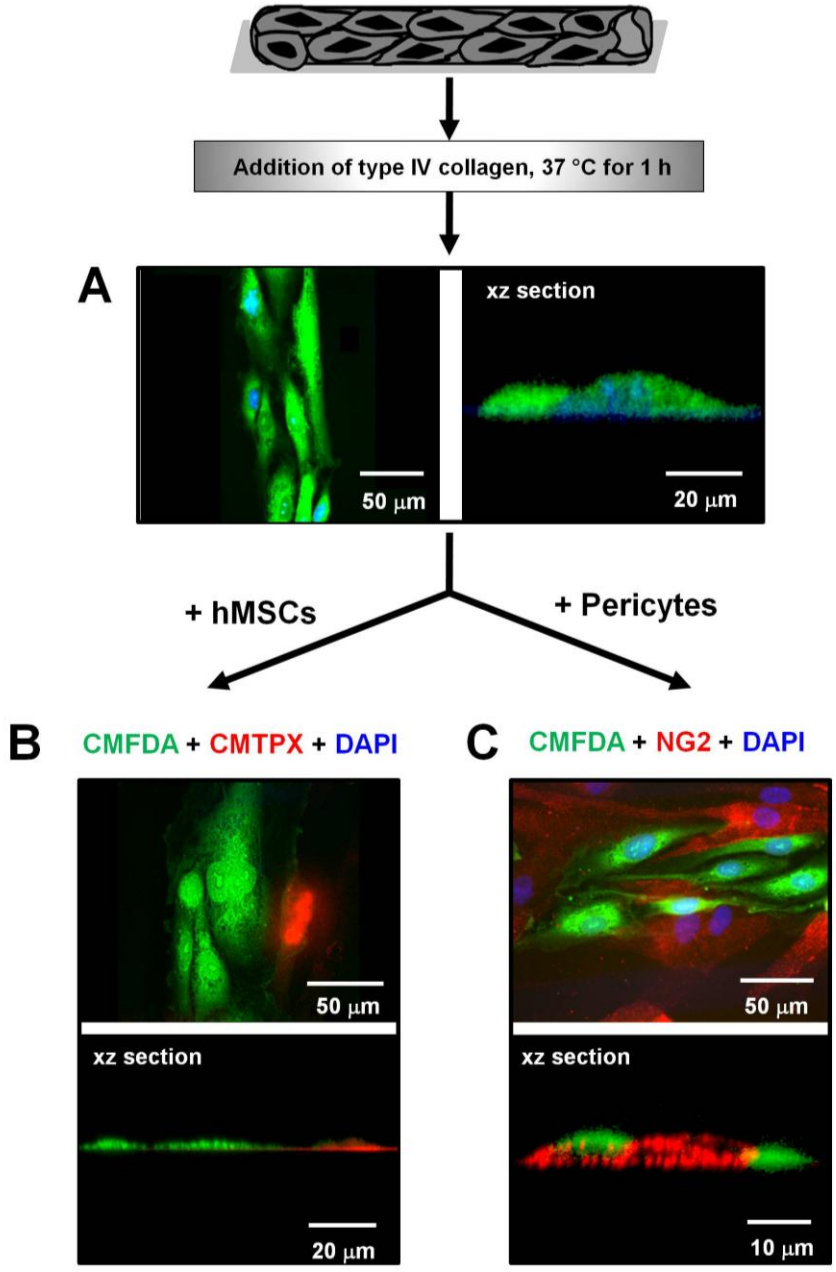

Figure 5. Subsequent co-cultures of cells with the recruitment of type IV collagen. ECs were seeded for 24 h on micropatterned surfaces, added and incubated with type IV collagen for 1 h(A), and followed by the addition of (B) hMSCs and (C) pericytes for 16 h.

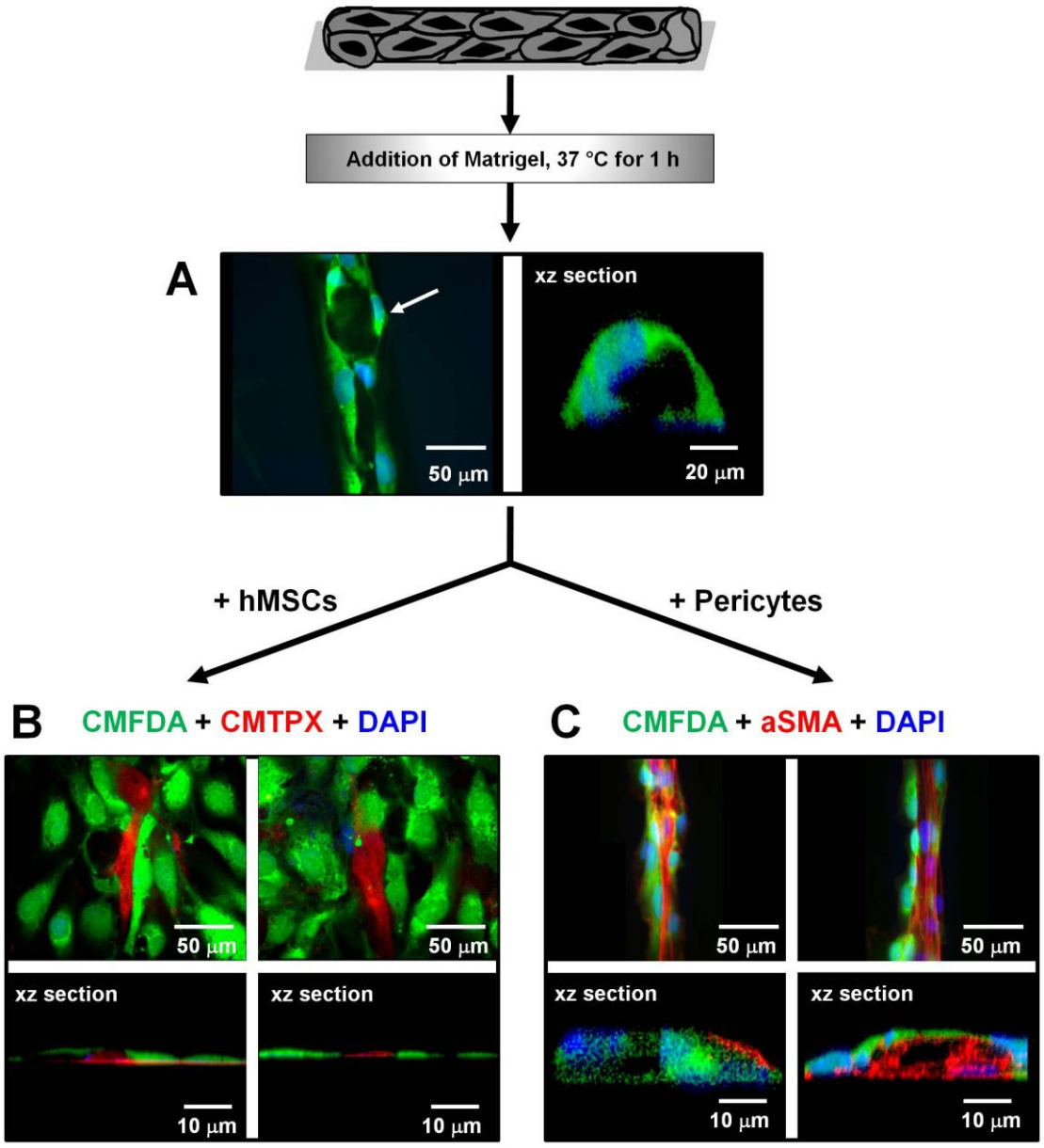

Figure 6. Subsequent co-cultures of cells with the recruitment of Matrigel. ECs were seeded for 24 h on micropatterned surfaces, added and incubated with Matrigel for 1 h (A), and followed by the addition of (B) hMSCs and (C) pericytes for 16 h.

Conclusions and Perspectives

Conclusions

Vascular engineering remains a major concern in advancing the field of tissue engineering. In this study, we developed several models of *in vitro* cell culture combining materials and endothelial cells to understand the process of angiogenesis.

The objective of this work is the control of both the biochemical ligands and micro-geometrical distribution of ligands on biomaterials surfaces which mimic the microenvironment of the extracellular matrix. We developed bioactive biomaterials (polymers functionalized with different peptides, and controlled their distribution at the micrometer scale) which may mimic a physiological situation of ECs. Three parts were developed in this thesis:

- Biochemical modification of materials with peptides for studying endothelial cell functions
- Microscale modification of materials with peptide micropatterning for inducing endothelial cell angiogenesis
- Co-culture of endothelial cells with pericytes/hMSCs for induction of stabilized vascularization.

Concerning the biochemical modification with peptides

In this part, we covalently immobilized the cell adhesive RGDS, EC specific REDV and YIGSR, angiogenic SVVYGLR sequences as well as combination of peptides onto polyethylene terephthalate (PET) surfaces, to study their specific effects on EC functions.

The surface functionalization by peptides was validated by physical-chemical characterization (XPS, AFM, fluorescence microscopy, contact angle measurement). The peptide density on PET surfaces evaluated by fluorescence microscopy was similar with each surface.

Biological evaluation revealed that these peptides can give bioactivity to polymer surfaces, and enhance the EC adhesion, spreading and migration. Specifically, the RGDS peptides induced more cell adhesion, while the YIGSR and SVVYGLR sequences induced more cell spreading and cell migration.

These results indicate that the surface functionalization by peptides specific for ECs has potential applications in promoting endothelialization of vascular prostheses and for construction of vascularized tissues in tissue engineering.

Concerning the microscale modification with peptide micropatterning

The surfaces micropattening with peptides were developed to modulate the angiogenesis of endothelial cells. Photolithography was used to prepare peptide micropatterns on polymer surfaces for the purpose of cell culture.

After cell culture, ECs were adhered and aligned onto peptides micropatterns whatever the size of peptide micropatterns.

EC behaviors (cell spreading, orientation and migration) were significantly more regulated on smaller micropatterns (10 and 50 μm) than on larger stripes (100 μm).

EC morphogenesis into tube formation can switch onto the smaller micropatterns (10 and 50 μm) with either RGD or SVVYGLR peptides.

The central lumen of tubular structures can be formed by single-to-four cells due to geometrical constraints applied on the micropatterns.

Sprouting angiogenesis of ECs and vascular network formation can be induced on surfaces micropatterned with angiogenic SVVYGLR peptides.

Mathematical modeling revealed the numerical simulation was in well accordance with experimental results.

Our results revealed the induction of angiogenesis is multi-parametric, which is dependent on biochemical constituents and their micro-distribution.

The surface micropatterning with peptides provides opportunities to mimic and investigate the process of angiogenesis. The organization of ECs into tubular structures and the induction of sprouting angiogenesis are important towards the fabrication of vascularized tissues.

Concerning coculture of cells to induce stabilized vascularization

The co-cultures of ECs with pericytes/hMSCs as well as recruitment of basement membrane components were developed in order to enhance capillary structures' stabilization.

EC tubular structures on peptide micropatterned surfaces were not stable, and ECs proliferated rapidly to form a homogeneous monolayer after 36 h in culture.

The addition of pericytes to this initial system can stabilize the vasculogenic tube structures, but not with hMSCs.

The addition of Matrigel to the initial system can induce vacuole formation. Only pericytes (but not hMSCs) can migrate through the mimetic basement membrane layer and support endothelial cell lumen structures.

In summary, our work in this thesis highlights that bioactive micropatterning of polymer is effective to stimulate angiogenesis and to construct functional vascularization. This work helps us to understand the fundamental biology of angiogenesis, and has great potential for application in tissue engineering.

Perspectives

There are lots of perspectives and suggestions which should be investigated in future studies.

Concerning the 2D micropatterning

There are clearly many other parameters that would be of interest on the 2D micropatterning, such as the distance between the peptide micro-stripes, the induction of vascular network, and study their effects onto EC vascularization.

We need also develop the study of the effect of different peptide principles, as well as different peptide densities onto EC angiogenesis.

Another perspective of the work would be the multi-functionalization of peptides on the micropatterned surfaces in order to mimic more complex ECM environment. For example, grafting of BMP-2 mimetic peptides and SVVYGLR angiogenic peptides on the micropatterned surfaces hence to promote both osteogenesis and angiogenesis of engineered products, respectively.

Investigation for 3D vascularization

The lack of a 3D vascularization remains a major challenge for 3D tissue culture [216]. In future work, we propose to develop the investigation for 3D vascularization by conjugation with the results in present thesis work, for examples:

Carry out the peptide micropatterning in 3D gels to induce the endothelial tubulogenesis [212].

Develop the 3D micropatterning of bioactive hydrogels, for example via laser scanning lithography, to guide 3D endothelial cell angiogenesis [211], or to develop branching capillary networks [96].

Control the microscaled chemical environment by microfluidic structures in order to aid in engineering complex tissues [216].

Annexes

Structures and symbols of amino acids

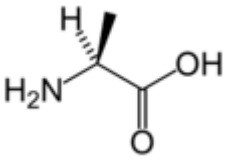

L-Alanine
(Ala / A)

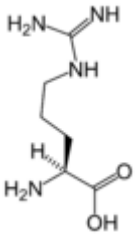

L-Arginine
(Arg / R)

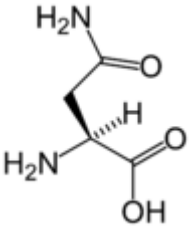

L-Asparagine
(Asn / N)

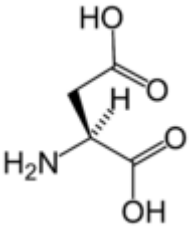

L-Aspartic acid
(Asp / D)

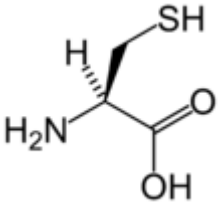

L-Cysteine
(Cys / C)

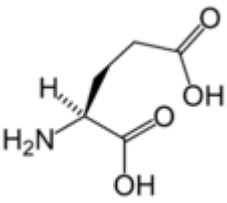

L-Glutamic acid
(Glu / E)

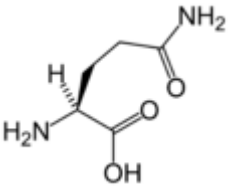

L-Glutamine
(Gln / Q)

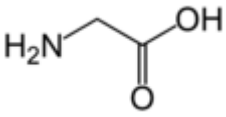

Glycine
(Gly / G)

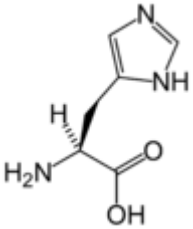

L-Histidine
(His / H)

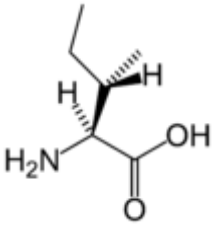

L-Isoleucine
(Ile / I)

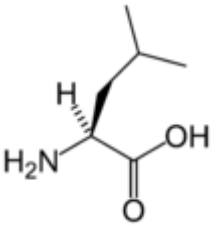

L-Leucine
(Leu / L)

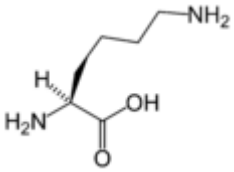

L-Lysine
(Lys / K)

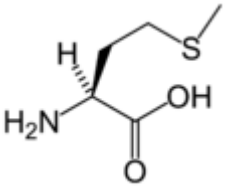

L-Methionine
(Met / M)

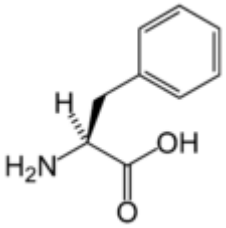

L-Phenylalanine
(Phe / F)

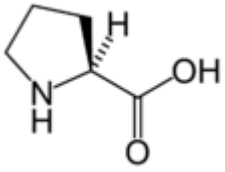

L-Proline
(Pro / P)

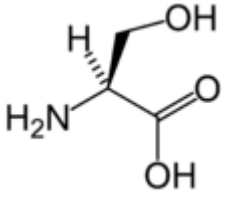

L-Serine
(Ser / S)

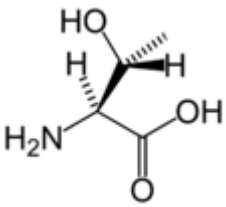

L-Threonine
(Thr / T)

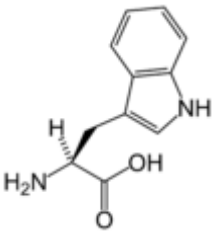

L-Tryptophan
(Trp / W)

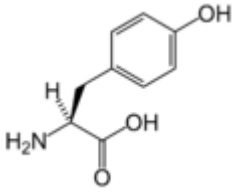

L-Tyrosine
(Tyr / Y)

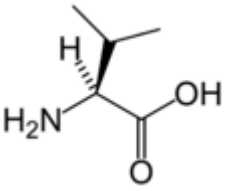

L-Valine
(Val / V)

Structures and symbols of fluorochrome

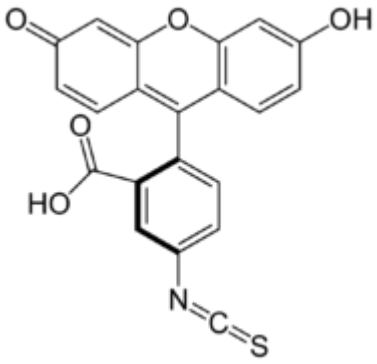

Fluorescein isothiocyanate

FITC

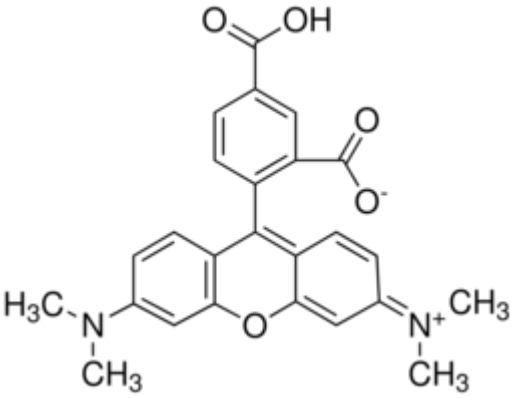

Carboxytetramethylrhodamine

TAMRA

Scientific Communications

Publications

Y. Lei, M. Rémy, O.F. Zouani, C. Labrugère, M.C. Durrieu. Surface functionalization of polyethylene terephthalate by peptides to study specific endothelial cell adhesion, spreading and migration. **Journal of Materials Science: Materials in Medicine**. 2012. Accepted.

Y. Lei, O.F. Zouani, M. Rémy, L. Rami, M.C. Durrieu. Modulation of Lumen Formation by Microgeometrical Bioactive Cues and Migration Mode of Actin Machinery. **Small**. 2012. In Revision.

Y. Lei, O. F. Zouani, M. Rémy, C. Ayela, M.C. Durrieu. Geometrical Microfeature Cues for Directing Tubulogenesis of Endothelial Cells. **PLoS ONE.** 2012, 7 (7): e41163.

T. Colin, M.C. Durrieu, J. Joie, Y. Lei, Y. Mammeri, C. Poignard, O. Saut. Modeling of the migration of endothelial cells on bioactive micropatterned polymers. **Mathematical Biosciences and Engineering**. 2012. Accepted.

Y. Lei, O.F. Zouani, M.C. Durrieu. Pericytes, stem cell-like cells, but not mesenchymal stem cells are recruited to support vasculogenic tube stabilization. 2012. In preparation.

Oral Communication

Y. Lei, O.F. Zouani, M. Rémy, M.C. Durrieu. Mimicking the angiogenic role of VEGF by peptides micropatterning. **9th World Biomaterials Congress**. June 2012. Chengdu, China. ("**Young scientist award**", 4% award acceptance rate).

Y. Lei, M. Rémy, O.F. Zouani, C. Chollet, C. Chanseau, M.C. Durrieu. Micropatterning of polyethylene terephthalate (PET) with peptides for induction of vascularization. **TERMIS 2011**. June 2011. Granada, Spain.

Y. Lei, C. Chollet, M. Remy, O.F. Zouani, L. Bordenave, M. C. Durrieu. Micropatterning of poly(ethylene terephthalate) with peptides to enhance angiogenesis. **The European Society for Biomaterials (ESB)**. September 2010. Tampere, Finland.

Poster

Y. Lei, O.F. Zouani, C. Chollet, M. Rémy, M.C. Durrieu. Micropatterning of poly(ethylene terephthalate) with YIGSR peptide for inducing endothelial cell migration. **Young Scientists Days**. May 2010. Bordeaux, France.

Y. Lei, O. F. Zouani, M. Rémy, C. Ayela, M.C. Durrieu. Geometrical Microfeature Cues for Directing Tubulogenesis of Endothelial Cells. **GDR MNS-MNF**. July 2012. Bordeaux, France.

Training Workshop

Cells on chips: From single cell studies towards tissue engineering. September 2012. Bordeaux, France.

Around the Stem Cell. March 2010. Bordeaux, France.

References

[1] Langer R, Vacanti JP. Tissue engineering. Science 1993;260(5110):920-6.
[2] Jain RK, Au P, Tam J, Duda DG, Fukumura D. Engineering vascularized tissue. Nat Biotechnol 2005;23(7):821-3.
[3] Vacanti JP, Langer R. Tissue engineering: the design and fabrication of living replacement devices for surgical reconstruction and transplantation. Lancet 1999;354 Suppl 1SI32-4.
[4] Nerem RM. Tissue engineering: the hope, the hype, and the future. Tissue Eng 2006;12(5):1143-50.
[5] Griffith LG, Naughton G. Tissue engineering--current challenges and expanding opportunities. Science 2002;295(5557):1009-14.
[6] Rouwkema J, Rivron NC, van Blitterswijk CA. Vascularization in tissue engineering. Trends Biotechnol 2008;26(8):434-41.
[7] Mansbridge J. Skin substitutes to enhance wound healing. Expert Opin Investig Drugs 1998;7(5):803-9.
[8] Place ES, Evans ND, Stevens MM. Complexity in biomaterials for tissue engineering. Nat Mater 2009;8(6):457-70.
[9] Ko HC, Milthorpe BK, McFarland CD. Engineering thick tissues-the vascularisation problem. Eur Cell Mater 2007;141-19.
[10] Kannan RY, Salacinski HJ, Sales K, Butler P, Seifalian AM. The roles of tissue engineering and vascularisation in the development of micro-vascular networks: a review. Biomaterials 2005;26(14):1857-75.
[11] Novosel EC, Kleinhans C, Kluger PJ. Vascularization is the key challenge in tissue engineering. Adv Drug Deliv Rev 2011;63(4-5):300-11.
[12] Atala A, Bauer SB, Soker S, Yoo JJ, Retik AB. Tissue-engineered autologous bladders for patients needing cystoplasty. Lancet 2006;367(9518):1241-6.
[13] http://www.graphicshunt.com/health/images/blood_vessel-635.htm.
[14] Wight TN. The extracellular matrix and atherosclerosis. Curr Opin Lipidol 1995;6(5):326-34.
[15] Ratcliffe A. Tissue engineering of vascular grafts. Matrix Biol 2000;19(4):353-7.
[16] http://en.wikipedia.org/wiki/Artery.
[17] Bergers G, Song S. The role of pericytes in blood-vessel formation and maintenance. Neuro Oncol 2005;7(4):452-64.
[18] Bicknell RJ. Endothelial Cell Culture. New York: Cambrige University Press; 1996.
[19] Garlanda C, Dejana E. Heterogeneity of Endothelial Cells : Specific Markers. Arteriosclerosis, Thrombosis, and Vascular Biology 1997;17(7):1193-202.
[20] Wu KK, Thiagarajan P. Role of endothelium in thrombosis and hemostasis. Annu Rev Med 1996;47315-31.
[21] Palmer RM, Ferrige AG, Moncada S. Nitric oxide release accounts for the biological activity of endothelium-derived relaxing factor. Nature 1987;327(6122):524-6.
[22] Seifalian AM, Tiwari A, Hamilton G, Salacinski HJ. Improving the clinical patency of prosthetic vascular and coronary bypass grafts: the role of seeding and tissue engineering. Artif Organs 2002;26(4):307-20.
[23] Risau W, Flamme I. Vasculogenesis. Annu Rev Cell Dev Biol 1995;1173-91.
[24] Risau W. Mechanisms of angiogenesis. Nature 1997;386(6626):671-4.
[25] Moon JJ, West JL. Vascularization of engineered tissues: approaches to promote angio-genesis in biomaterials. Curr Top Med Chem 2008;8(4):300-10.
[26] Folkman J. Angiogenesis: initiation and control. Ann N Y Acad Sci 1982;401212-27.

[27] Ausprunk DH, Folkman J. Migration and proliferation of endothelial cells in preformed and newly formed blood vessels during tumor angiogenesis. Microvasc Res 1977;14(1):53-65.
[28] Gerhardt H, Golding M, Fruttiger M, Ruhrberg C, Lundkvist A, Abramsson A, et al. VEGF guides angiogenic sprouting utilizing endothelial tip cell filopodia. J Cell Biol 2003;161(6):1163-77.
[29] Laschke MW, Harder Y, Amon M, Martin I, Farhadi J, Ring A, et al. Angiogenesis in tissue engineering: breathing life into constructed tissue substitutes. Tissue Eng 2006;12(8):2093-104.
[30] Phelps EA, Garcia AJ. Update on therapeutic vascularization strategies. Regen Med 2009;4(1):65-80.
[31] Lovett M, Lee K, Edwards A, Kaplan DL. Vascularization strategies for tissue engineering. Tissue Eng Part B Rev 2009;15(3):353-70.
[32] Xia Y, Whitesides GM. Soft Lithography. Angewandte Chemie International Edition 1998;37(5):550-75.
[33] Druecke D, Langer S, Lamme E, Pieper J, Ugarkovic M, Steinau HU, et al. Neovascularization of poly(ether ester) block-copolymer scaffolds in vivo: long-term investigations using intravital fluorescent microscopy. J Biomed Mater Res A 2004;68(1):10-8.
[34] Cao Y, Mitchell G, Messina A, Price L, Thompson E, Penington A, et al. The influence of architecture on degradation and tissue ingrowth into three-dimensional poly(lactic-co-glycolic acid) scaffolds in vitro and in vivo. Biomaterials 2006;27(14):2854-64.
[35] Hutmacher DW, Sittinger M, Risbud MV. Scaffold-based tissue engineering: rationale for computer-aided design and solid free-form fabrication systems. Trends Biotechnol 2004;22(7):354-62.
[36] Hutmacher DW. Scaffold design and fabrication technologies for engineering tissues--state of the art and future perspectives. J Biomater Sci Polym Ed 2001;12(1):107-24.
[37] Hollister SJ. Porous scaffold design for tissue engineering. Nat Mater 2005;4(7):518-24.
[38] Malda J, Woodfield TB, van der Vloodt F, Wilson C, Martens DE, Tramper J, et al. The effect of PEGT/PBT scaffold architecture on the composition of tissue engineered cartilage. Biomaterials 2005;26(1):63-72.
[39] Hutmacher D, Hurzeler MB, Schliephake H. A review of material properties of biodegradable and bioresorbable polymers and devices for GTR and GBR applications. Int J Oral Maxillofac Implants 1996;11(5):667-78.
[40] Raeber GP, Lutolf MP, Hubbell JA. Molecularly engineered PEG hydrogels: a novel model system for proteolytically mediated cell migration. Biophys J 2005;89(2):1374-88.
[41] Lee SH, Miller JS, Moon JJ, West JL. Proteolytically degradable hydrogels with a fluorogenic substrate for studies of cellular proteolytic activity and migration. Biotechnol Prog 2005;21(6):1736-41.
[42] Miller JS, Shen CJ, Legant WR, Baranski JD, Blakely BL, Chen CS. Bioactive hydrogels made from step-growth derived PEG-peptide macromers. Biomaterials 2010;31(13):3736-43.
[43] Gafni Y, Zilberman Y, Ophir Z, Abramovitch R, Jaffe M, Gazit Z, et al. Design of a filamentous polymeric scaffold for in vivo guided angiogenesis. Tissue Eng 2006;12(11):3021-34.
[44] Nomi M, Miyake H, Sugita Y, Fujisawa M, Soker S. Role of growth factors and endothelial cells in therapeutic angiogenesis and tissue engineering. Curr Stem Cell Res Ther 2006;1(3):333-43.
[45] Presta M, Dell'Era P, Mitola S, Moroni E, Ronca R, Rusnati M. Fibroblast growth factor/fibroblast growth factor receptor system in angiogenesis. Cytokine Growth Factor Rev 2005;16(2):159-78.

[46] Otrock ZK, Mahfouz RA, Makarem JA, Shamseddine AI. Understanding the biology of angiogenesis: review of the most important molecular mechanisms. Blood Cells Mol Dis 2007;39(2):212-20.
[47] Ferrara N, Gerber HP, LeCouter J. The biology of VEGF and its receptors. Nat Med 2003;9(6):669-76.
[48] Breier G, Risau W. The role of vascular endothelial growth factor in blood vessel formation. Trends Cell Biol 1996;6(12):454-6.
[49] Shweiki D, Itin A, Neufeld G, Gitay-Goren H, Keshet E. Patterns of expression of vascular endothelial growth factor (VEGF) and VEGF receptors in mice suggest a role in hormonally regulated angiogenesis. J Clin Invest 1993;91(5):2235-43.
[50] Jakeman LB, Armanini M, Phillips HS, Ferrara N. Developmental expression of binding sites and messenger ribonucleic acid for vascular endothelial growth factor suggests a role for this protein in vasculogenesis and angiogenesis. Endocrinology 1993;133(2):848-59.
[51] Carmeliet P, Ferreira V, Breier G, Pollefeyt S, Kieckens L, Gertsenstein M, et al. Abnormal blood vessel development and lethality in embryos lacking a single VEGF allele. Nature 1996;380(6573):435-9.
[52] Jain RK. Molecular regulation of vessel maturation. Nat Med 2003;9(6):685-93.
[53] Folkman J, Langer R, Linhardt RJ, Haudenschild C, Taylor S. Angiogenesis inhibition and tumor regression caused by heparin or a heparin fragment in the presence of cortisone. Science 1983;221(4612):719-25.
[54] DeLong SA, Moon JJ, West JL. Covalently immobilized gradients of bFGF on hydrogel scaffolds for directed cell migration. Biomaterials 2005;26(16):3227-34.
[55] Heldin CH, Westermark B. Mechanism of action and in vivo role of platelet-derived growth factor. Physiol Rev 1999;79(4):1283-316.
[56] Andrae J, Gallini R, Betsholtz C. Role of platelet-derived growth factors in physiology and medicine. Genes Dev 2008;22(10):1276-312.
[57] Carmeliet P. Angiogenesis in health and disease. Nat Med 2003;9(6):653-60.
[58] Carmeliet P. Mechanisms of angiogenesis and arteriogenesis. Nat Med 2000;6(4):389-95.
[59] Thurston G, Suri C, Smith K, McClain J, Sato TN, Yancopoulos GD, et al. Leakage-resistant blood vessels in mice transgenically overexpressing angiopoietin-1. Science 1999;286(5449):2511-4.
[60] Davies N, Dobner S, Bezuidenhout D, Schmidt C, Beck M, Zisch AH, et al. The dosage dependence of VEGF stimulation on scaffold neovascularisation. Biomaterials 2008;29(26):3531-8.
[61] Drake CJ, Little CD. Exogenous vascular endothelial growth factor induces malformed and hyperfused vessels during embryonic neovascularization. Proc Natl Acad Sci U S A 1995;92(17):7657-61.
[62] Zisch AH, Lutolf MP, Hubbell JA. Biopolymeric delivery matrices for angiogenic growth factors. Cardiovasc Pathol 2003;12(6):295-310.
[63] Ehrbar M, Djonov VG, Schnell C, Tschanz SA, Martiny-Baron G, Schenk U, et al. Cell-demanded liberation of VEGF121 from fibrin implants induces local and controlled blood vessel growth. Circ Res 2004;94(8):1124-32.
[64] Ehrbar M, Metters A, Zammaretti P, Hubbell JA, Zisch AH. Endothelial cell proliferation and progenitor maturation by fibrin-bound VEGF variants with differential susceptibilities to local cellular activity. J Control Release 2005;101(1-3):93-109.
[65] Harvey K, Welch Z, Kovala AT, Garcia JG, English D. Comparative analysis of in vitro angiogenic activities of endothelial cells of heterogeneous origin. Microvasc Res 2002;63(3):316-26.

[66] Vailhe B, Vittet D, Feige JJ. In vitro models of vasculogenesis and angiogenesis. Lab Invest 2001;81(4):439-52.
[67] Luttun A, Carmeliet G, Carmeliet P. Vascular progenitors: from biology to treatment. Trends Cardiovasc Med 2002;12(2):88-96.
[68] Hristov M, Erl W, Weber PC. Endothelial progenitor cells: isolation and characterization. Trends Cardiovasc Med 2003;13(5):201-6.
[69] Miller-Kasprzak E, Jagodzinski PP. Endothelial progenitor cells as a new agent contributing to vascular repair. Arch Immunol Ther Exp (Warsz) 2007;55(4):247-59.
[70] Chen X, Aledia AS, Popson SA, Him L, Hughes CC, George SC. Rapid anastomosis of endothelial progenitor cell-derived vessels with host vasculature is promoted by a high density of cotransplanted fibroblasts. Tissue Eng Part A 2010;16(2):585-94.
[71] Riha GM, Lin PH, Lumsden AB, Yao Q, Chen C. Review: application of stem cells for vascular tissue engineering. Tissue Eng 2005;11(9-10):1535-52.
[72] Yamahara K, Itoh H. Potential use of endothelial progenitor cells for regeneration of the vasculature. Ther Adv Cardiovasc Dis 2009;3(1):17-27.
[73] Thébaud N-B, Pierron D, Bareille R, Le Visage C, Letourneur D, Bordenave L. Human endothelial progenitor cell attachment to polysaccharide-based hydrogels: A pre-requisite for vascular tissue engineering. Journal of Materials Science: Materials in Medicine 2007;18(2):339-45.
[74] Matsumoto T, Mifune Y, Kawamoto A, Kuroda R, Shoji T, Iwasaki H, et al. Fracture induced mobilization and incorporation of bone marrow-derived endothelial progenitor cells for bone healing. J Cell Physiol 2008;215(1):234-42.
[75] Seebach C, Henrich D, Kahling C, Wilhelm K, Tami AE, Alini M, et al. Endothelial progenitor cells and mesenchymal stem cells seeded onto beta-TCP granules enhance early vascularization and bone healing in a critical-sized bone defect in rats. Tissue Eng Part A 2010;16(6):1961-70.
[76] Lee DY, Cho TJ, Kim JA, Lee HR, Yoo WJ, Chung CY, et al. Mobilization of endothelial progenitor cells in fracture healing and distraction osteogenesis. Bone 2008;42(5):932-41.
[77] Kirkpatrick CJ, Fuchs S, Unger RE. Co-culture systems for vascularization - Learning from nature. Advanced Drug Delivery Reviews 2011;63(4-5):291-9.
[78] Hurley JR, Balaji S, Narmoneva DA. Complex temporal regulation of capillary morphogenesis by fibroblasts. Am J Physiol Cell Physiol 2010;299(2):C444-53.
[79] Unger RE, Ghanaati S, Orth C, Sartoris A, Barbeck M, Halstenberg S, et al. The rapid anastomosis between prevascularized networks on silk fibroin scaffolds generated in vitro with cocultures of human microvascular endothelial and osteoblast cells and the host vasculature. Biomaterials 2010;31(27):6959-67.
[80] Borges J, Muller MC, Momeni A, Stark GB, Torio-Padron N. In vitro analysis of the interactions between preadipocytes and endothelial cells in a 3D fibrin matrix. Minim Invasive Ther Allied Technol 2007;16(3):141-8.
[81] Chung S, Sudo R, Mack PJ, Wan CR, Vickerman V, Kamm RD. Cell migration into scaffolds under co-culture conditions in a microfluidic platform. Lab Chip 2009;9(2):269-75.
[82] Folkman J, Haudenschild C. Angiogenesis in vitro. Nature 1980;288(5791):551-6.
[83] Kubota Y, Kleinman HK, Martin GR, Lawley TJ. Role of laminin and basement membrane in the morphological differentiation of human endothelial cells into capillary-like structures. J Cell Biol 1988;107(4):1589-98.
[84] Haralabopoulos GC, Grant DS, Kleinman HK, Maragoudakis ME. Thrombin promotes endothelial cell alignment in Matrigel in vitro and angiogenesis in vivo. Am J Physiol 1997;273(1 Pt 1):C239-45.

[85] Maciag T, Kadish J, Wilkins L, Stemerman MB, Weinstein R. Organizational behavior of human umbilical vein endothelial cells. J Cell Biol 1982;94(3):511-20.
[86] Ingber DE, Folkman J. Mechanochemical switching between growth and differentiation during fibroblast growth factor-stimulated angiogenesis in vitro: role of extracellular matrix. J Cell Biol 1989;109(1):317-30.
[87] Dike LE, Chen CS, Mrksich M, Tien J, Whitesides GM, Ingber DE. Geometric control of switching between growth, apoptosis, and differentiation during angiogenesis using micropatterned substrates. In Vitro Cell Dev Biol Anim 1999;35(8):441-8.
[88] Matsuda T, Kurumatani H. Surface induced in vitro angiogenesis: surface property is a determinant of angiogenesis. ASAIO Trans 1990;36(3):M565-8.
[89] Shakado S, Sakisaka S, Noguchi K, Yoshitake M, Harada M, Mimura Y, et al. Effects of extracellular matrices on tube formation of cultured rat hepatic sinusoidal endothelial cells. Hepatology 1995;22(3):969-73.
[90] Co CC, Wang YC, Ho CC. Biocompatible micropatterning of two different cell types. J Am Chem Soc 2005;127(6):1598-9.
[91] Bettinger CJ, Zhang Z, Gerecht S, Borenstein JT, Langer R. Enhancement of In Vitro Capillary Tube Formation by Substrate Nanotopography. Adv Mater 2008;20(1):99-103.
[92] Chalupowicz DG, Chowdhury ZA, Bach TL, Barsigian C, Martinez J. Fibrin II induces endothelial cell capillary tube formation. J Cell Biol 1995;130(1):207-15.
[93] Montesano R, Orci L, Vassalli P. In vitro rapid organization of endothelial cells into capillary-like networks is promoted by collagen matrices. J Cell Biol 1983;97(5 Pt 1):1648-52.
[94] Saik JE, Gould DJ, Keswani AH, Dickinson ME, West JL. Biomimetic hydrogels with immobilized ephrinA1 for therapeutic angiogenesis. Biomacromolecules 2011;12(7):2715-22.
[95] Moon JJ, Hahn MS, Kim I, Nsiah BA, West JL. Micropatterning of poly(ethylene glycol) diacrylate hydrogels with biomolecules to regulate and guide endothelial morphogenesis. Tissue Eng Part A 2009;15(3):579-85.
[96] Leslie-Barbick JE, Shen C, Chen C, West JL. Micron-scale spatially patterned, covalently immobilized vascular endothelial growth factor on hydrogels accelerates endothelial tubulogenesis and increases cellular angiogenic responses. Tissue Eng Part A 2011;17(1-2):221-9.
[97] Santos MI, Tuzlakoglu K, Fuchs S, Gomes ME, Peters K, Unger RE, et al. Endothelial cell colonization and angiogenic potential of combined nano- and micro-fibrous scaffolds for bone tissue engineering. Biomaterials 2008;29(32):4306-13.
[98] Montano I, Schiestl C, Schneider J, Pontiggia L, Luginbuhl J, Biedermann T, et al. Formation of human capillaries in vitro: the engineering of prevascularized matrices. Tissue Eng Part A 2010;16(1):269-82.
[99] Dickinson LE, Moura ME, Gerecht S. Guiding endothelial progenitor cell tube formation using patterned fibronectin surfaces. Soft Matter 2010;6(20):5109-19.
[100] Fuchs S, Hofmann A, Kirkpatrick CJ. Microvessel-like structures from outgrowth endothelial cells from human peripheral blood in 2-dimensional and 3-dimensional co-cultures with osteoblastic lineage cells. Tissue Eng 2007;13(10):2577-88.
[101] Vo E, Hanjaya-Putra D, Zha Y, Kusuma S, Gerecht S. Smooth-muscle-like cells derived from human embryonic stem cells support and augment cord-like structures in vitro. Stem Cell Rev 2010;6(2):237-47.
[102] Unger RE, Halstenberg S, Sartoris A, Kirkpatrick CJ. Human endothelial and osteoblast co-cultures on 3D biomaterials. Methods Mol Biol 2011;695229-41.
[103] Unger RE, Sartoris A, Peters K, Motta A, Migliaresi C, Kunkel M, et al. Tissue-like self-assembly in cocultures of endothelial cells and osteoblasts and the formation of

microcapillary-like structures on three-dimensional porous biomaterials. Biomaterials 2007;28(27):3965-76.
[104] Hofmann A, Ritz U, Verrier S, Eglin D, Alini M, Fuchs S, et al. The effect of human osteoblasts on proliferation and neo-vessel formation of human umbilical vein endothelial cells in a long-term 3D co-culture on polyurethane scaffolds. Biomaterials 2008;29(31):4217-26.
[105] Fuchs S, Ghanaati S, Orth C, Barbeck M, Kolbe M, Hofmann A, et al. Contribution of outgrowth endothelial cells from human peripheral blood on in vivo vascularization of bone tissue engineered constructs based on starch polycaprolactone scaffolds. Biomaterials 2009;30(4):526-34.
[106] Fuchs S, Jiang X, Schmidt H, Dohle E, Ghanaati S, Orth C, et al. Dynamic processes involved in the pre-vascularization of silk fibroin constructs for bone regeneration using outgrowth endothelial cells. Biomaterials 2009;30(7):1329-38.
[107] Santos MI, Unger RE, Sousa RA, Reis RL, Kirkpatrick CJ. Crosstalk between osteoblasts and endothelial cells co-cultured on a polycaprolactone-starch scaffold and the in vitro development of vascularization. Biomaterials 2009;30(26):4407-15.
[108] Santos MI, Reis RL. Vascularization in bone tissue engineering: physiology, current strategies, major hurdles and future challenges. Macromol Biosci 2010;10(1):12-27.
[109] Ghanaati S, Fuchs S, Webber MJ, Orth C, Barbeck M, Gomes ME, et al. Rapid vascularization of starch-poly(caprolactone) in vivo by outgrowth endothelial cells in co-culture with primary osteoblasts. J Tissue Eng Regen Med 2011;5(6):e136-43.
[110] Fuchs S, Motta A, Migliaresi C, Kirkpatrick CJ. Outgrowth endothelial cells isolated and expanded from human peripheral blood progenitor cells as a potential source of autologous cells for endothelialization of silk fibroin biomaterials. Biomaterials 2006;27(31):5399-408.
[111] Yu H, Vandevord PJ, Gong W, Wu B, Song Z, Matthew HW, et al. Promotion of osteogenesis in tissue-engineered bone by pre-seeding endothelial progenitor cells-derived endothelial cells. J Orthop Res 2008;26(8):1147-52.
[112] Steffens L, Wenger A, Stark GB, Finkenzeller G. In vivo engineering of a human vasculature for bone tissue engineering applications. J Cell Mol Med 2009;13(9B):3380-6.
[113] Frerich B, Lindemann N, Kurtz-Hoffmann J, Oertel K. In vitro model of a vascular stroma for the engineering of vascularized tissues. Int J Oral Maxillofac Surg 2001;30(5):414-20.
[114] Dente CJ, Steffes CP, Speyer C, Tyburski JG. Pericytes augment the capillary barrier in in vitro cocultures. J Surg Res 2001;97(1):85-91.
[115] Hirschi KK, D'Amore PA. Pericytes in the microvasculature. Cardiovasc Res 1996;32(4):687-98.
[116] Sims DE. Diversity within pericytes. Clin Exp Pharmacol Physiol 2000;27(10):842-6.
[117] Carmeliet P, Conway EM. Growing better blood vessels. Nat Biotechnol 2001;19(11):1019-20.
[118] Thomas WE. Brain macrophages: on the role of pericytes and perivascular cells. Brain Res Brain Res Rev 1999;31(1):42-57.
[119] Gerhardt H, Betsholtz C. Endothelial-pericyte interactions in angiogenesis. Cell Tissue Res 2003;314(1):15-23.
[120] Abramsson A, Lindblom P, Betsholtz C. Endothelial and nonendothelial sources of PDGF-B regulate pericyte recruitment and influence vascular pattern formation in tumors. J Clin Invest 2003;112(8):1142-51.
[121] Tremblay PL, Hudon V, Berthod F, Germain L, Auger FA. Inosculation of tissue-engineered capillaries with the host's vasculature in a reconstructed skin transplanted on mice. Am J Transplant 2005;5(5):1002-10.

[122] Levenberg S, Rouwkema J, Macdonald M, Garfein ES, Kohane DS, Darland DC, et al. Engineering vascularized skeletal muscle tissue. Nat Biotechnol 2005;23(7):879-84.
[123] Casabona F, Martin I, Muraglia A, Berrino P, Santi P, Cancedda R, et al. Prefabricated engineered bone flaps: an experimental model of tissue reconstruction in plastic surgery. Plast Reconstr Surg 1998;101(3):577-81.
[124] Pelissier P, Villars F, Mathoulin-Pelissier S, Bareille R, Lafage-Proust MH, Vilamitjana-Amedee J. Influences of vascularization and osteogenic cells on heterotopic bone formation within a madreporic ceramic in rats. Plast Reconstr Surg 2003;111(6):1932-41.
[125] Scheufler O, Schaefer DJ, Jaquiery C, Braccini A, Wendt DJ, Gasser JA, et al. Spatial and temporal patterns of bone formation in ectopically pre-fabricated, autologous cell-based engineered bone flaps in rabbits. J Cell Mol Med 2008;12(4):1238-49.
[126] Kneser U, Polykandriotis E, Ohnolz J, Heidner K, Grabinger L, Euler S, et al. Engineering of vascularized transplantable bone tissues: induction of axial vascularization in an osteoconductive matrix using an arteriovenous loop. Tissue Eng 2006;12(7):1721-31.
[127] Kneser U, Schaefer DJ, Polykandriotis E, Horch RE. Tissue engineering of bone: the reconstructive surgeon's point of view. J Cell Mol Med 2006;10(1):7-19.
[128] Hubbell JA. Biomaterials in tissue engineering. Biotechnology (N Y) 1995;13(6):565-76.
[129] Phelps EA, Garcia AJ. Engineering more than a cell: vascularization strategies in tissue engineering. Curr Opin Biotechnol 2010;21(5):704-9.
[130] Hay ED. Cell Biology of Extracellular Matrix. 2 ed. New York: Plenum Press; 1991.
[131] Kleinman HK, McGarvey ML, Liotta LA, Robey PG, Tryggvason K, Martin GR. Isolation and characterization of type IV procollagen, laminin, and heparan sulfate proteoglycan from the EHS sarcoma. Biochemistry 1982;21(24):6188-93.
[132] Ponce ML. Tube formation: an in vitro matrigel angiogenesis assay. Methods Mol Biol 2009;467183-8.
[133] Fukuda J, Khademhosseini A, Yeh J, Eng G, Cheng J, Farokhzad OC, et al. Micropatterned cell co-cultures using layer-by-layer deposition of extracellular matrix components. Biomaterials 2006;27(8):1479-86.
[134] Wittmer CR, Phelps JA, Saltzman WM, Van Tassel PR. Fibronectin terminated multilayer films: protein adsorption and cell attachment studies. Biomaterials 2007;28(5):851-60.
[135] Gomes ME, Azevedo HS, Moreira AR, Ella V, Kellomaki M, Reis RL. Starch-poly(epsilon-caprolactone) and starch-poly(lactic acid) fibre-mesh scaffolds for bone tissue engineering applications: structure, mechanical properties and degradation behaviour. J Tissue Eng Regen Med 2008;2(5):243-52.
[136] Kidd KR, Dal Ponte D, Stone AL, Hoying JB, Nagle RB, Williams SK. Stimulated endothelial cell adhesion and angiogenesis with laminin-5 modification of expanded polytetrafluoroethylene. Tissue Eng 2005;11(9-10):1379-91.
[137] Straface G, Aprahamian T, Flex A, Gaetani E, Biscetti F, Smith RC, et al. Sonic hedgehog regulates angiogenesis and myogenesis during post-natal skeletal muscle regeneration. J Cell Mol Med 2009;13(8B):2424-35.
[138] Pola R, Ling LE, Silver M, Corbley MJ, Kearney M, Blake Pepinsky R, et al. The morphogen Sonic hedgehog is an indirect angiogenic agent upregulating two families of angiogenic growth factors. Nat Med 2001;7(6):706-11.
[139] Lawson ND, Vogel AM, Weinstein BM. sonic hedgehog and vascular endothelial growth factor act upstream of the Notch pathway during arterial endothelial differentiation. Dev Cell 2002;3(1):127-36.
[140] Fietz MJ, Concordet JP, Barbosa R, Johnson R, Krauss S, McMahon AP, et al. The hedgehog gene family in Drosophila and vertebrate development. Dev Suppl 199443-51.

[141] Dohle E, Fuchs S, Kolbe M, Hofmann A, Schmidt H, Kirkpatrick CJ. Sonic hedgehog promotes angiogenesis and osteogenesis in a coculture system consisting of primary osteoblasts and outgrowth endothelial cells. Tissue Eng Part A 2010;16(4):1235-7.
[142] Zisch AH, Zeisberger SM, Ehrbar M, Djonov V, Weber CC, Ziemiecki A, et al. Engineered fibrin matrices for functional display of cell membrane-bound growth factor-like activities: study of angiogenic signaling by ephrin-B2. Biomaterials 2004;25(16):3245-57.
[143] Moon JJ, Lee SH, West JL. Synthetic biomimetic hydrogels incorporated with ephrin-A1 for therapeutic angiogenesis. Biomacromolecules 2007;8(1):42-9.
[144] Williams DF. The role of short synthetic adhesion peptides in regenerative medicine; the debate. Biomaterials 2011;32(18):4195-7.
[145] Elbert DL, Hubbell JA. Conjugate addition reactions combined with free-radical cross-linking for the design of materials for tissue engineering. Biomacromolecules 2001;2(2):430-41.
[146] Fields GB, Lauer JL, Dori Y, Forns P, Yu YC, Tirrell M. Protein-like molecular architecture: biomaterial applications for inducing cellular receptor binding and signal transduction. Biopolymers 1998;47(2):143-51.
[147] Horbett TA, Lew KR. Residence time effects on monoclonal antibody binding to adsorbed fibrinogen. J Biomater Sci Polym Ed 1994;6(1):15-33.
[148] Hersel U, Dahmen C, Kessler H. RGD modified polymers: biomaterials for stimulated cell adhesion and beyond. Biomaterials 2003;24(24):4385-415.
[149] Collier JH, Segura T. Evolving the use of peptides as components of biomaterials. Biomaterials 2011;32(18):4198-204.
[150] Ito Y, Kajihara M, Imanishi Y. Materials for enhancing cell adhesion by immobilization of cell-adhesive peptide. J Biomed Mater Res 1991;25(11):1325-37.
[151] Boxus T, Touillaux R, Dive G, Marchand-Brynaert J. Synthesis and evaluation of RGD peptidomimetics aimed at surface bioderivatization of polymer substrates. Bioorg Med Chem 1998;6(9):1577-95.
[152] Neff JA, Caldwell KD, Tresco PA. A novel method for surface modification to promote cell attachment to hydrophobic substrates. J Biomed Mater Res 1998;40(4):511-9.
[153] Ruoslahti E. RGD and other recognition sequences for integrins. Annu Rev Cell Dev Biol 1996;12697-715.
[154] Arnaout MA, Mahalingam B, Xiong JP. Integrin structure, allostery, and bidirectional signaling. Annu Rev Cell Dev Biol 2005;21381-410.
[155] Bellis SL. Advantages of RGD peptides for directing cell association with biomaterials. Biomaterials 2011;32(18):4205-10.
[156] Hynes RO. Integrins: bidirectional, allosteric signaling machines. Cell 2002;110(6):673-87.
[157] Plow EF, Haas TA, Zhang L, Loftus J, Smith JW. Ligand binding to integrins. J Biol Chem 2000;275(29):21785-8.
[158] Zamir E, Geiger B. Molecular complexity and dynamics of cell-matrix adhesions. J Cell Sci 2001;114(Pt 20):3583-90.
[159] Chollet C, Chanseau C, Remy M, Guignandon A, Bareille R, Labrugere C, et al. The effect of RGD density on osteoblast and endothelial cell behavior on RGD-grafted polyethylene terephthalate surfaces. Biomaterials 2009;30(5):711-20.
[160] Porte-Durrieu MC, Guillemot F, Pallu S, Labrugere C, Brouillaud B, Bareille R, et al. Cyclo-(DfKRG) peptide grafting onto Ti-6Al-4V: physical characterization and interest towards human osteoprogenitor cells adhesion. Biomaterials 2004;25(19):4837-46.
[161] Durrieu MC, Pallu S, Guillemot F, Bareille R, Amedee J, Baquey CH, et al. Grafting RGD containing peptides onto hydroxyapatite to promote osteoblastic cells adhesion. J Mater Sci Mater Med 2004;15(7):779-86.

[162] Hubbell JA, Massia SP, Desai NP, Drumheller PD. Endothelial cell-selective materials for tissue engineering in the vascular graft via a new receptor. Biotechnology (N Y) 1991;9(6):568-72.
[163] Massia SP, Hubbell JA. Vascular endothelial cell adhesion and spreading promoted by the peptide REDV of the IIICS region of plasma fibronectin is mediated by integrin alpha 4 beta 1. J Biol Chem 1992;267(20):14019-26.
[164] Plouffe BD, Njoka DN, Harris J, Liao J, Horick NK, Radisic M, et al. Peptide-mediated selective adhesion of smooth muscle and endothelial cells in microfluidic shear flow. Langmuir 2007;23(9):5050-5.
[165] Monchaux E, Vermette P. Bioactive microarrays immobilized on low-fouling surfaces to study specific endothelial cell adhesion. Biomacromolecules 2007;8(11):3668-73.
[166] Boateng SY, Lateef SS, Mosley W, Hartman TJ, Hanley L, Russell B. RGD and YIGSR synthetic peptides facilitate cellular adhesion identical to that of laminin and fibronectin but alter the physiology of neonatal cardiac myocytes. Am J Physiol Cell Physiol 2005;288(1):C30-8.
[167] Maeda T, Titani K, Sekiguchi K. Cell-adhesive activity and receptor-binding specificity of the laminin-derived YIGSR sequence grafted onto Staphylococcal protein A. J Biochem 1994;115(2):182-9.
[168] Massia SP, Rao SS, Hubbell JA. Covalently immobilized laminin peptide Tyr-Ile-Gly-Ser-Arg (YIGSR) supports cell spreading and co-localization of the 67-kilodalton laminin receptor with alpha-actinin and vinculin. J Biol Chem 1993;268(11):8053-9.
[169] Jun HW, West JL. Modification of polyurethaneurea with PEG and YIGSR peptide to enhance endothelialization without platelet adhesion. J Biomed Mater Res B Appl Biomater 2005;72(1):131-9.
[170] Kouvroukoglou S, Dee KC, Bizios R, McIntire LV, Zygourakis K. Endothelial cell migration on surfaces modified with immobilized adhesive peptides. Biomaterials 2000;21(17):1725-33.
[171] Fittkau MH, Zilla P, Bezuidenhout D, Lutolf MP, Human P, Hubbell JA, et al. The selective modulation of endothelial cell mobility on RGD peptide containing surfaces by YIGSR peptides. Biomaterials 2005;26(2):167-74.
[172] Grant DS, Tashiro K-I, Segui-Real B, Yamada Y, Martin GR, Kleinman HK. Two different laminin domains mediate the differentiation of human endothelial cells into capillary-like structures in vitro. Cell 1989;58(5):933-43.
[173] Yokosaki Y, Matsuura N, Sasaki T, Murakami I, Schneider H, Higashiyama S, et al. The integrin alpha(9)beta(1) binds to a novel recognition sequence (SVVYGLR) in the thrombin-cleaved amino-terminal fragment of osteopontin. J Biol Chem 1999;274(51):36328-34.
[174] Hamada Y, Nokihara K, Okazaki M, Fujitani W, Matsumoto T, Matsuo M, et al. Angiogenic activity of osteopontin-derived peptide SVVYGLR. Biochem Biophys Res Commun 2003;310(1):153-7.
[175] Hamada Y, Yuki K, Okazaki M, Fujitani W, Matsumoto T, Hashida MK, et al. Osteopontin-derived peptide SVVYGLR induces angiogenesis in vivo. Dent Mater J 2004;23(4):650-5.
[176] Hamada Y, Egusa H, Kaneda Y, Hirata I, Kawaguchi N, Hirao T, et al. Synthetic osteopontin-derived peptide SVVYGLR can induce neovascularization in artificial bone marrow scaffold biomaterials. Dent Mater J 2007;26(4):487-92.
[177] Wilson CJ, Clegg RE, Leavesley DI, Pearcy MJ. Mediation of biomaterial-cell interactions by adsorbed proteins: a review. Tissue Eng 2005;11(1-2):1-18.
[178] Sydor JR, Nock S. Protein expression profiling arrays: tools for the multiplexed high-throughput analysis of proteins. Proteome Sci 2003;1(1):3.

[179] Krijgsman B, Seifalian AM, Salacinski HJ, Tai NR, Punshon G, Fuller BJ, et al. An assessment of covalent grafting of RGD peptides to the surface of a compliant poly(carbonate-urea)urethane vascular conduit versus conventional biological coatings: its role in enhancing cellular retention. Tissue Eng 2002;8(4):673-80.
[180] de Mel A, Jell G, Stevens MM, Seifalian AM. Biofunctionalization of biomaterials for accelerated in situ endothelialization: a review. Biomacromolecules 2008;9(11):2969-79.
[181] Thery M. Micropatterning as a tool to decipher cell morphogenesis and functions. J Cell Sci 2010;123(Pt 24):4201-13.
[182] Falconnet D, Csucs G, Grandin HM, Textor M. Surface engineering approaches to micropattern surfaces for cell-based assays. Biomaterials 2006;27(16):3044-63.
[183] Khademhosseini A, Langer R, Borenstein J, Vacanti JP. Microscale technologies for tissue engineering and biology. Proc Natl Acad Sci U S A 2006;103(8):2480-7.
[184] Borenstein JT, Weinberg EJ, Orrick BK, Sundback C, Kaazempur-Mofrad MR, Vacanti JP. Microfabrication of three-dimensional engineered scaffolds. Tissue Eng 2007;13(8):1837-44.
[185] Kane RS, Takayama S, Ostuni E, Ingber DE, Whitesides GM. Patterning proteins and cells using soft lithography. Biomaterials 1999;20(23-24):2363-76.
[186] Jeong DA, Markle G, Owen F, A. P, Von Bunau Grenville R. The future of optical lithography. Solid State Technol 1994;3739-47.
[187] Yap FL, Zhang Y. Protein and cell micropatterning and its integration with micro/nanoparticles assembly. Biosens Bioelectron 2007;22(6):775-88.
[188] Miura Y, Sato H, Ikeda T, Sugimura H, Takai O, Kobayashi K. Micropatterned carbohydrate displays by self-assembly of glycoconjugate polymers on hydrophobic templates on silicon. Biomacromolecules 2004;5(5):1708-13.
[189] Healy KE, Thomas CH, Rezania A, Kim JE, McKeown PJ, Lom B, et al. Kinetics of bone cell organization and mineralization on materials with patterned surface chemistry. Biomaterials 1996;17(2):195-208.
[190] Chollet C, Lazare S, Guillemot F, Durrieu MC. Impact of RGD micro-patterns on cell adhesion. Colloids Surf B Biointerfaces 2010;75(1):107-14.
[191] Xia Y, Kim E, Zhao XM, Rogers JA, Prentiss M, Whitesides GM. Complex Optical Surfaces Formed by Replica Molding Against Elastomeric Masters. Science 1996;273(5273):347-9.
[192] Xia Y, Whitesides GM. SOFT LITHOGRAPHY. Annual Review of Materials Science 1998;28(1):153-84.
[193] Kumar A, Whitesides GM. Features of gold having micrometer to centimeter dimensions can be formed through a combination of stamping with an elastomeric stamp and an alkanethiol ink followed by chemical etching Appl Phys Lett 1993;63(14):2002-4.
[194] Singhvi R, Kumar A, Lopez GP, Stephanopoulos GN, Wang DI, Whitesides GM, et al. Engineering cell shape and function. Science 1994;264(5159):696-8.
[195] Kumar A, Biebuyck HA, Whitesides GM. Patterning Self-Assembled Monolayers: Applications in Materials Science. Langmuir 1994;10(5):1498-511.
[196] Qin D, Xia Y, Whitesides GM. Soft lithography for micro- and nanoscale patterning. Nat Protoc 2010;5(3):491-502.
[197] Graber DJ, Zieziulewicz TJ, Lawrence DA, Shain W, Turner JN. Antigen Binding Specificity of Antibodies Patterned by Microcontact Printing. Langmuir 2003;19(13):5431-4.
[198] Mrksich M, Chen CS, Xia Y, Dike LE, Ingber DE, Whitesides GM. Controlling cell attachment on contoured surfaces with self-assembled monolayers of alkanethiolates on gold. Proc Natl Acad Sci U S A 1996;93(20):10775-8.

[199] Mrksich M, Dike LE, Tien J, Ingber DE, Whitesides GM. Using microcontact printing to pattern the attachment of mammalian cells to self-assembled monolayers of alkanethiolates on transparent films of gold and silver. Exp Cell Res 1997;235(2):305-13.
[200] Chen CS, Mrksich M, Huang S, Whitesides GM, Ingber DE. Geometric control of cell life and death. Science 1997;276(5317):1425-8.
[201] Thery M, Racine V, Pepin A, Piel M, Chen Y, Sibarita JB, et al. The extracellular matrix guides the orientation of the cell division axis. Nat Cell Biol 2005;7(10):947-53.
[202] Thery M, Piel M. Adhesive micropatterns for cells: a microcontact printing protocol. Cold Spring Harb Protoc 2009;2009(7):pdb prot5255.
[203] Bietsch A, Michel B. Conformal contact and pattern stability of stamps used for soft lithography J Appl Phys 2000;88(7):4310-8.
[204] Sharp KG, Blackman GS, Glassmaker NJ, Jagota A, Hui C-Y. Effect of Stamp Deformation on the Quality of Microcontact Printing: Theory and Experiment. Langmuir 2004;20(15):6430-8.
[205] Kim E, Xia Y, Whitesides GM. Polymer microstructures formed by moulding in capillaries. Nature 1995;376(6541):581-4.
[206] Folch A, Ayon A, Hurtado O, Schmidt MA, Toner M. Molding of deep polydimethylsiloxane microstructures for microfluidics and biological applications. J Biomech Eng 1999;121(1):28-34.
[207] Kim E, Xia Y, Whitesides GM. Micromolding in Capillaries: Applications in Materials Science. Journal of the American Chemical Society 1996;118(24):5722-31.
[208] Delamarche E, Bernard A, Schmid H, Michel B, Biebuyck H. Patterned delivery of immunoglobulins to surfaces using microfluidic networks. Science 1997;276(5313):779-81.
[209] Bernard A, Michel B, Delamarche E. Micromosaic immunoassays. Anal Chem 2001;73(1):8-12.
[210] Folch A, Toner M. Cellular micropatterns on biocompatible materials. Biotechnol Prog 1998;14(3):388-92.
[211] Lee SH, Moon JJ, West JL. Three-dimensional micropatterning of bioactive hydrogels via two-photon laser scanning photolithography for guided 3D cell migration. Biomaterials 2008;29(20):2962-8.
[212] Raghavan S, Nelson CM, Baranski JD, Lim E, Chen CS. Geometrically controlled endothelial tubulogenesis in micropatterned gels. Tissue Eng Part A 2010;16(7):2255-63.
[213] Ling Y, Rubin J, Deng Y, Huang C, Demirci U, Karp JM, et al. A cell-laden microfluidic hydrogel. Lab Chip 2007;7(6):756-62.
[214] King KR, Wang CCJ, Kaazempur-Mofrad MR, Vacanti JP, Borenstein JT. Biodegradable Microfluidics. Advanced Materials 2004;16(22):2007-12.
[215] Lim D, Kamotani Y, Cho B, Mazumder J, Takayama S. Fabrication of microfluidic mixers and artificial vasculatures using a high-brightness diode-pumped Nd:YAG laser direct write method. Lab on a Chip 2003;3(4):318-23.
[216] Choi NW, Cabodi M, Held B, Gleghorn JP, Bonassar LJ, Stroock AD. Microfluidic scaffolds for tissue engineering. Nat Mater 2007;6(11):908-15.
[217] Miller JS, Stevens KR, Yang MT, Baker BM, Nguyen D-HT, Cohen DM, et al. Rapid casting of patterned vascular networks for perfusable engineered three-dimensional tissues. Nat Mater 2012;11(9):768-74.
[218] Bettinger CJ, Zhang Z, Gerecht S, Borenstein JT, Langer R. Enhancement of In Vitro Capillary Tube Formation by Substrate Nanotopography. Advanced Materials 2008;20(1):99-103.
[219] Ford MC, Bertram JP, Hynes SR, Michaud M, Li Q, Young M, et al. A macroporous hydrogel for the coculture of neural progenitor and endothelial cells to form functional vascular networks in vivo. Proc Natl Acad Sci U S A 2006;103(8):2512-7.

[220] Bouhadir KH, Mooney DJ. Promoting angiogenesis in engineered tissues. J Drug Target 2001;9(6):397-406.
[221] Chow D, Nunalee ML, Lim DW, Simnick AJ, Chilkoti A. Peptide-based Biopolymers in Biomedicine and Biotechnology. Mater Sci Eng R Rep 2008;62(4):125-55.
[222] Rezania A, Healy KE. Biomimetic peptide surfaces that regulate adhesion, spreading, cytoskeletal organization, and mineralization of the matrix deposited by osteoblast-like cells. Biotechnol Prog 1999;15(1):19-32.
[223] Zouani OF, Chollet C, Guillotin B, Durrieu MC. Differentiation of pre-osteoblast cells on poly(ethylene terephthalate) grafted with RGD and/or BMPs mimetic peptides. Biomaterials 2010;31(32):8245-53.
[224] Davis GE, Bayless KJ, Mavila A. Molecular basis of endothelial cell morphogenesis in three-dimensional extracellular matrices. Anat Rec 2002;268(3):252-75.
[225] Sottile J. Regulation of angiogenesis by extracellular matrix. Biochim Biophys Acta 2004;1654(1):13-22.
[226] Sukmana I, Vermette P. The effects of co-culture with fibroblasts and angiogenic growth factors on microvascular maturation and multi-cellular lumen formation in HUVEC-oriented polymer fibre constructs. Biomaterials 2010;31(19):5091-9.
[227] Lei Y, Zouani OF, Rémy M, Ayela C, Durrieu M-C. Geometrical Microfeature Cues for Directing Tubulogenesis of Endothelial Cells. PLoS ONE 2012;7(7):e41163.

Abstract

The creation of a functional vascular network is a major concern to ensure the perfect vitality of tissue engineered products. Understanding the mechanism of angiogenesis is essential for the vascularization in tissue engineering. In this work, we aimed to characterize the microenvironment responsible for angiogenesis of endothelial cells (ECs). To achieve this request, we developed bioactive biomaterials (polymers functionalized mainly with peptides, and controlled their distribution at micrometer scale) to mimic a physiological microenvironment of ECs. Our results demonstrate that the induction of angiogenesis is multi-parametric. This is dependent on biochemical constituents and their micro-distribution. Our results show that the central lumen of tubular structures can be formed by single-to-four cells due to geometrical constraint applied. This work helps us to understand the fundamental biology of angiogenesis and may help its application in tissue engineering.

Résumé

La création d'un réseau vasculaire fonctionnel est une préoccupation importante afin d'assurer la parfaire vitalité des produits d'ingénierie tissulaire. Dans ce travail, nous avons visé à caractériser le microenvironnement responsable de l'angiogenèse des cellules endothéliales. Pour cela, nous avons élaboré des biomatériaux bioactifs (polymères fonctionnalisés principalement par des peptides d'adhésion, des facteurs angiogènes, distribués de façon contrôlée à l'échelle micrométrique) susceptible de mimer une situation physiologique. Nos résultats démontrent que l'induction de l'angiogenèse est multiparamétrique. Celle-ci est dépendante de constituants biochimiques et de leur micro-distribution. Nos résultats montrent que la formation de vaisseaux peut être constituée d'une à quatre cellules selon la contrainte géométrique appliquée. Enfin, ce travail a permis de comprendre la biologie de l'angiogenèse et pourra aider à son application dans l'ingénierie tissulaire.